The effect of organic molecules on magnesium degradation

Dissertation

zur Erlangung des akademischen Grades

Doktor der Ingenieurwissenschaften

(Dr.-Ing.)

der Technischen Fakultät

der Christian-Albrechts-Universität zu Kiel

vorgelegt von

Ruiqing Hou

Kiel 2019

Erstgutachterin: Prof. Dr. Regine Willumeit-Römer

Zweitgutachter: Prof. Dr. Rainer Adelung

Termin der Disputation: 15.02.2019

Eidesstattliche Erklärung

Hiermit erkläre ich, dass die beigefügte Dissertation, abgesehen von der Beratung durch die Betreuerin, nach Inhalt und Form meine eigene Arbeit ist.

Die Arbeit, ganz oder zum Teil, wurde nie schon einer anderen Stelle im Rahmen eines Prüfungsverfahrens vorgelegt und ist abgesehen, von den im Anhang angegebenen Veröffentlichungen, nicht anderweitig zur Veröffentlichung vorgelegt worden.

Außerdem ist die Arbeit unter Einhaltung der Regeln guter wissenschaftlicher Praxis der Deutschen Forschungsgemeinschaft entstanden.

Geesthacht, den 12. 11. 2018

Table of contents

Abstract

Magnesium (Mg) and its alloys have been widely investigated as biomaterials due to their remarkable biodegradability and bioresorbability. However, the discrepancy of degradation results between *in vitro* and *in vivo* observations demands a much better understanding for the mechanism of the degradation processes. Although lots of studies have been performed to investigate the effect of physiological parameters, the roles of organic molecules in Mg degradation remain unclear. In this thesis, several typical organic components, L-ascorbic acid (L-AA), L-glutamine (L-Gln), L-alanyl-L-glutamine (L-Ala-L-Gln), bovine serum albumin (BSA), fibrinogen (Fib) and fetal bovine serum (FBS) were chosen to elucidate the effects of organic components on the degradation of pure Mg under cell culture conditions. The degradation rate of pure Mg was determined by mass loss after different immersion time. The degradation products were analysed by X-ray diffraction (XRD), X-ray photoelectron spectroscopy (XPS), infrared reflection microspectroscopy (IR) as well as chemical mappings. The results reveal that the influence of organic components on the degradation of pure Mg is time- and medium-dependent. Small organic molecules increase the degradation rate of pure Mg after relatively long-term immersion, while proteins generally reduce the degradation of Mg. On the other hand, they play an important role in the formation of the degradation products. The addition of organic components favours the precipitation of crystalline nesquehonite rather than hydromagnesite in the 'outer' layer with an 'inner' layer composed by carbonate, phosphate and magnesium hydroxide in HBSS. Whereas, in HBSSCa and DMEM organic components accelerate the formation of Ca/P-rich products in the top of degradation layer, accompanied by an 'inner' layer mainly composed by carbonate and magnesium hydroxide, presenting an *in vivo*-like degradation layer. Moreover, proteins seem to stabilize the top of Ca/P-rich layer and protect the integrity of degradation layer, which are of importance to Mg degradation. The formation of Ca/P-rich products on Mg surface reduces the surface roughness and changes the surface chemistry and charge, eventually weakening the adsorption of proteins. More importantly, macromolecules / organic mixtures exhibit larger influence than small organic molecules / single organic molecule on Mg degradation. The interactions between organic molecules should be taken into considerations when organic mixtures are applied. For example, when both Fib and BSA are present in DMEM, the degradation rate of Mg significantly increase due to the interplay between BSA and Fib. A promising result is that the addition of organic molecules, especially FBS, can weaken the difference of Mg degradation caused by the different conditions used, such as the composition of media, the ratio of medium volume to sample and the static or semi-static conditions, which enables the results more comparable.

Zusammenfassung

Magnesium und seine Legierungen sind wegen ihrer besonderen Eigenschaften – gute biologische Verträglichkeit und Resorbierbarkeit – von großem Interesse für die Forschung. Von besonderem Interesse ist das mechanistische Verständnis des Degradationsverhaltens, da hier deutliche Unterschiede zwischen in vitro und in vivo Studien zu beobachten sind. Trotz einer Vielzahl an Studien, die die physiologischen Parameter beleuchten, ist der Einfluss organischer Substanzen auf die Magnesiumdegradation noch nicht verstanden. In dieser Arbeit wurden daher verschiedene organische Moleküle (L-Ascorbinsäure (L-AA), L-Glutamin (L-Gln), L-Alanyl-L-Glutamin (L-Ala-L-Gln), bovines Serumalbumin (BSA), Fibrinogen (Fib) und fötales Kälberserum (FBS)), ausgewählt, um deren Einfluss auf die Degradation von Magnesium unter physiologischen Bedingungen zu untersuchen. Hierzu wurde die Degradationsrate durch Massenverlust bestimmt, und die Degradationsprodukte mittels Röntgenstreuung (XRD), Röntgenphotoelektronenspektroskopie (XPS), Infrarotspektrometrie (IR) und chemische Analyse identifiziert. Es zeigt sich, dass der Einfluss organischer Moleküle Zeit- und Mediumabhängig ist. Kleine organische Moleküle erhöhen die Degradationsrate im späteren Zeitverlauf, während Proteine zu einer generellen Reduzierung führen. Darüber hinaus haben spielen sie eine wichtige Rolle bei der Bildung von Degradationsprodukten. Unter ihrem Einfluss wird in Hank‘ Lösung (HBSS) bevorzugt Nesquehonit anstatt Hydormagnesit in der äußeren Degradationsschicht präzipitiert, und die innere Schicht setzt sich aus Carbonat, Phosphat und Magnesiumhydroxid zusammen. Im Gegensatz dazu werden bei Zugabe von Calcium und in Zellkulturmedium (DMEM) bevorzugt Calciumphosphatverbindungen in der äußeren Schicht gebildet, während die innere Schicht überwiegend aus Carbonat und Magnesiumhydroxid besteht. Diese Schichtung entspricht dem Degradationsverhalten in vivo. Proteine stabilisieren die äußere Calciumphosphatschicht und die Integrität der Degradationsschicht. Durch die Calciumphosphatverbindungen wird die Oberflächenrauigkeit reduziert, sowie die Oberflächenchemie und –ladung, was zu einer Verminderung der Proteinadsorption führt. In diesem Zusammenhang ist wichtig zu erwähnen, dass der Einfluss von Makromolekülen bzw. Mischung organischer Substanzen deutlich größer ist, als bei Betrachtung kleiner bzw. einzelner organischer Moleküle. Daher sollte die Interaktion zwischen den einzelnen Molekülen weiter untersucht werden. Als Beispiel führt die Interaktion von Fibrinogen und Serumalbumin in Zellkulturmedium zu einem deutlichen Anstieg der Degradationsrate. Ein weiteres wichtiges Ergebnis ist, dass die Zugabe von Kälberserum zu einheitlicheren Ergebnissen in unterschiedlichen experimentellen Umgebungen führt.

1. Introduction

1.1. Mg as biomaterials

Magnesium (Mg) and its alloys as one kind of degradable metallic materials drawn much attentions and were developed due to their excellent biodegradability and bioresorbability. Mg is an extraordinarily light metal with a density of 1.74 g/cm^3, which is close to the density of bone (cortical bone: 1.8-2.0 g/cm^3, cancellous bone: 1.0-1.4 g/cm^3) [1]. Moreover, the Young's modulus of Mg and its alloys (41-46 GPa) is closer to bone (0.01-23 GPa) than other metallic materials, such as titanium alloys (79-114 GPa), iron alloys (189-205 GPa), indicating a weak stress shielding effect [1-3]. Mg is one of the abundant cations in the human body [4], with around 25 grams in adult human body, and about two-thirds of the body's magnesium is present in the skeleton and the rest is in soft tissues [5]. It is essential to regulate numerous cellular functions and enzymatic systems in human body, and stabilize the structures of DNA and RNA [6, 7]. The concentration of Mg^{2+} in plasma and extracellular fluid is approximately 1.2-1.4 mM, one-third of which is bound by extracellular proteins (e.g. albumin) or other biochemical molecules [6]. The intake of Mg for a normal adult is recommended to 300-400 mg per day [8], excessive Mg can be rapidly excreted in the urine [5]. During times of deprivation, Mg can be conserved in the kidney [9]. Mg depletion remarkably disturbs calcium homeostasis and induces some cardiovascular diseases [9-11]. More importantly, Mg has been found to have stimulatory effects on the growth of new bone tissue [12, 13]. The degradability of Mg can avoid repeated surgery, decreases the costs and further morbidity to the patient. All of these characteristics result in promising prospects for Mg-based implanted materials.

The positive therapeutic effect of Mg used as biomaterials has already been displayed by the early clinical applications and animal experiments. The details were reviewed in [14]. Some valuable experience and knowledge can be gained from these studies. For example, Erwin Payr, one of the most influential pioneers, found that the degradation of Mg *in vivo* is mainly determined by the surrounding environment, e.g. water content, carbon dioxide, dissolved salts, and so on. Although some successful treatments were reported [15], many surgeons still waived Mg products as biomaterials after the middle of last century since the corrosion of Mg *in vivo* could not be sufficiently controlled.

With the development of metallurgy and recent advances in material science and engineering, the availability of ultra-high purity Mg and the surface modification of Mg-based devices have enabled corrosion rates and mechanical properties to be controlled [4, 16, 17]. Additionally, increasing life expectancy and improving life quality encourage the development of

degradable biomaterials, which should be degradable, biocompatible and do not affect tissue healing after surgical implantation. This situation has led to a renaissance of Mg as degradable metallic materials (Fig. 1.1).

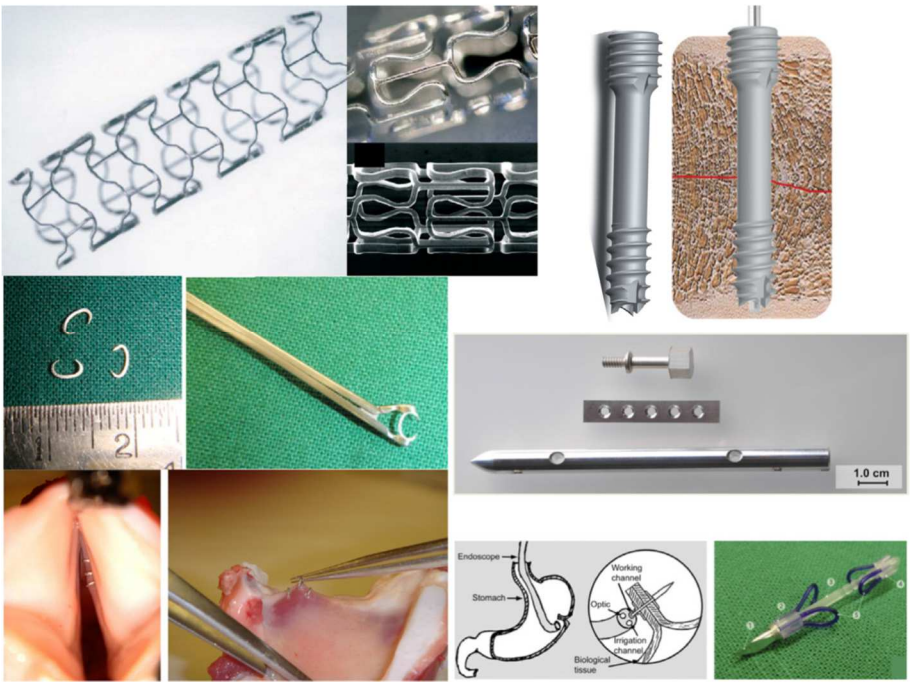

Figure 1.1: Real/possible applications of biodegradable magnesium implants: (a) cardiovascular stents (BIOTRONIK, Berlin, Germany, received CE mark in Europe), (b) MAGNEZIX screw (Syntellix, Hannover, Germany, received CE mark in Europe), (c) microclip for laryngeal microsurgery (pure magnesium), (d) biodegradable orthopedic implants, (e) wound-closing devices (WZ21) [18] (reproduced with permission from Elsevier).

To improve the mechanical properties and corrosion resistance of Mg, various Mg alloys including binary Mg series alloys (e.g. Mg-Sr, Mg-Ag, Mg-Ca, Mg-Zn, etc.), ternary and quaternary series alloys (Mg-Ca-Zn, Mg-Zn-Mn, Mg-Nd-Zn-Zr, etc.) were developed in the last decades [18, 19]. Furthermore, the biological and degradation performance of selected alloys has been assessed by numerous animal studies, which has been reviewed in the literature [19-21]. Considering the excellent performance, some of degradable Mg-based implants also start the clinical trials and get access to the medical device market, such as AMS stents made of WE43 systems [22-25], the first Mg-Y-RE-Zr screw in Germany [21] [26], Mg-5Ca-1Zn (wt%) screw approved by the Korea Food and Drug Administration (KFDA) in 2015 [27], and high-purity Mg screws in China [28].

The encouraging and promising results for the degradable Mg-based implants have been obtained from *in vitro* and *in vivo* evaluations, even clinical performances. They have already largely encouraged surgeons and scientists to accelerate the translation of their novel Mg-

based implants into clinical application. However, prior to their application, it is essential to evaluate the new developed Mg-based implants. This evaluation helps not only to avoid the failure of implant during clinical application (possibly caused by the uncontrollable degradation, mechanical integrity, etc.), but also to promote the use of Mg-based medical devices.

1.2. Evaluation of Mg as biodegradable materials

During the process from intensive research to clinical reality, many different complex considerations need to be addressed for the clinical translation of degradable Mg-based implant materials. How to evaluate the potential Mg-based implants became an important part for the process from research to clinical application.

1.2.1. Safety

Biosafety should be the general consideration for the development of degradable biomaterials. The released metallic ions and the formed degradation products generated by the gradual degradation of Mg or its alloys may disturb the local physiological equilibrium at the implantation site, inducing systemic toxicity to human and localised toxicity to the peri-implant cells. Therefore, the choice of alloying elements is of importance to control the release of potentially toxic metallic elements. The alloying element released in the body should be kept at very low concentration below its threshold level to avoid such adverse effects. For example, excessive amounts of Zn (daily allowance: 15 mg) can induce neurotoxicity, cramps and diarrhoea [19, 29]. *In vitro* cytotoxicity of rare earth elements containing Nd, Gd, La, Ce, Dy, etc. often used to improve the mechanical properties of Mg alloys, has been evaluated for different cell lines [30]. La and Ce exhibit the highest cytotoxicity, Gd and Dy with high solubility in Mg seem to be more suitable than Y due to the better inflammatory and toxicity performance [30]. Moreover, the concentration of the released metal ions into tissue varies with the tissue type, the implanting time, the distance to the implants and the local micro environments (e.g. local pH, local osmolality, local blood supply), which affect the diffusion and transfer of the released metal ions and the adsorption of tissue to metal ions [31]. Therefore, the amount of the alloying elements in Mg-alloys implants needs to be optimised according to the degradation rate of Mg-based implants and the physiological environment at the implantation site.

To estimate the potential hazards of new Mg-based implants, *in vitro* cytotoxicity tests and cell culture assays are suitable tools to give insights into the effect of Mg-based materials and their degradation products on cell viability and proliferation prior to *in vivo* testing. Many different cell lines including fibroblasts, osteoblasts, osteoclasts and endothelial cells have been used to evaluate the degradable Mg alloys with respect to different applications. For example,

osteoblasts and osteoclasts are used to evaluate orthopaedic implant materials [32, 33], while endothelial cells are applied to test biodegradable Mg-based stents [34]. Normally used cytotoxicity tests contains MTT assays, XTT assays, LDH assays, cell count, cell attachment, DNA content and cell proteins [35]. MTT and XTT assays are in accordance with EN ISO 10993-5, which describes the *in vitro* cytotoxicity tests for the evaluation of medical devices. Determination of LDH activity is frequently used as a good indicator of cellular damage for cytotoxicity studies [36]. Cell count is determined by staining cells via different dyes, such as DAPI, calcein-AM and propidium iodide (PI) [37-39]. Furthermore, the cell morphology on the surface of Mg materials can be analysed [32, 40]. Cell proteins and DNA contents are sometimes assessed to get more accurate results in view of the genetic level, it can provide more details about the mechanisms [33]. However, when applying these experiments for degradable Mg materials, some improvements or problems should be carefully noticed to obtain reasonable *in vitro* results for specific motivations. For example, the diluted extraction medium should be used to conduct MTT assays for the degradable Mg materials [41], which is not consistent with the ISO standard.

1.2.2. Mechanical integrity

Besides the biosafety, Mg-based materials as degradable implants must also have sufficient mechanical strength and stable biomechanical function over implantation time. The degeneration of mechanical integrity of Mg and its alloys with time should match the healing process of tissues during the implantation (Fig. 1.2).

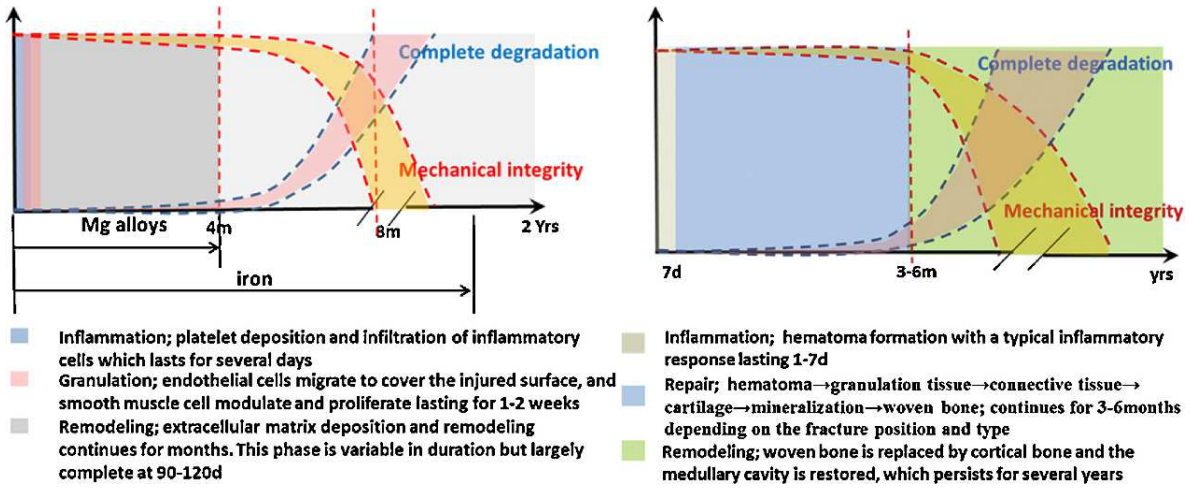

Figure 1.2: The schematic diagram of degradation behaviour and the change of mechanical integrity of biodegradable Mg during the vascular healing process (a) and during the bone healing process (b) [19] (reproduced with permission from Elsevier).

Normally, the mechanical properties of Mg-based materials are examined before degradation to evaluate the initial mechanical properties. However, this approach cannot satisfy the

demands for the mechanical evaluation of the degradable Mg-based materials. One of the reasons is that the stability of Mg-based materials is largely influenced by the corrosion and stress, which leads to materials cracking (stress corrosion cracking (SCC) and corrosion fatigue). Some investigations have already evaluated the stability of the Mg-based materials via three-point bending [42-46], four-point bending [47, 48], tensile and compression tests [49, 50] after *in vitro* [42, 46-50] or *in vivo* [43-45, 51] experiments and slow strain rate test (SSRT) method [52-54]. A general reduction of mechanical properties can be observed for the Mg-based materials, which relates to the degradation rate and degradation type (localised or uniform) [42, 48, 49]. For example, pitting corrosion largely decrease the performance of Mg-based materials due to the formation of defects during immersion.

1.2.3. Degradability

The degradability of Mg-based materials is not only one of the critical advantages as biomaterials, but also a challenge for the clinical applications. As mentioned above, the degradation of Mg-based materials affects the mechanical integrity of materials during service period, also controls the release of metal ions into the human body. Too fast degradation will have an adverse influence on mechanical integrity, and the toxicity to tissues due to the higher concentration of metal ions, higher local pH and the formation of gas cavities. Therefore, the evaluation of the degradation for potential Mg-based implants including degradation type (localised or uniform) is essential prior to their application.

In vitro degradation rate of Mg-based implant materials can be determined by different methods, such as mass loss, hydrogen evolution, electrochemical methods and ion release. Each method has its advantages and limitations for the determination of degradation rate, which has been reviewed in literature [55]. For example, mass loss can simply provide accurate, clearly defined data, but it needs multiple samples for accuracy and offers little information on corrosion mechanisms. Recently, a new degradation expression based on mass loss, mean degradation depth, has developed since it has a higher probability in predicting long term degradation behaviour of Mg [56, 57]. It can be calculated as follows:

$$h = \frac{10000 \cdot \Delta m}{A \cdot \rho} \qquad (1.1)$$

where A is the surface area in cm^2, ρ is the density of material and Δm is the observed mass loss in gram. Volume loss of Mg-based materials is a prominent tool to calculate the *in vivo* degradation rate by using micro-tomography [58, 59]. Based on the *in vivo* results [60], compared with the degradation rate of AZ91D alloys, a hydrogen evolution rate 0.01 $mL/cm^2/day$ (0.02 mm $year^{-1}$) is proposed to be acceptable for medical implant applications

[61, 62]. It should be noted that this value is just a simple reference, since the degradation rate of Mg-based materials varies with the *in vitro* conditions used and the *in vivo* implantation sites [63]. Moreover, although Mg alloys typically corrode faster than this value, even under *in vivo* conditions, some of them still give a good performance *in vivo*. [18, 59, 64]. Therefore, for the success reliable evaluation for Mg-based materials, a systematic approach is needed for *in vitro* tests and it should be able to simulate the desired implantation site and its local environment to help screen the suitable Mg-based implants.

At present, there are several available standards for *in vitro* tests: the European standard ISO 10993 [65] and the standards outlined by the American Society for Testing and Materials (ASTM G31-72) [66, 67]. The ISO 10993 standards mainly focuses on the biological evaluation of materials including the safety and risk management. It still has some limitations for testing degradable or corroding biomaterials [1, 41]. The ASTM standard highlights the importance of the sample volume to surface area ratio and the immersion time. However, the recommended solution volumes are thought to be too small to accommodate the pH change [55]. A new standard ISO/TR 37137:2014 [68] (Cardiovascular biological evaluation of medical devices – Guidance for absorbable implants) has been published to provide interim part-by-part guidance on potential adjustments to various test methods within the 10993 series.

To predict the *in vivo* behaviour of Mg-based biomaterials, reliable and reproducible *in vitro* results are of utmost importance. However, the truth is that sometimes the degradation data obtained from different literatures are not comparable, even for the same alloy, due to the different *in vitro* conditions used. Staiger et al. have summarised the key aspects of the entire discussion and structured the main topics, concerns and comments during the 2nd Symposium on Biodegradable Metals [69]. The poor correlation between *in vitro* and *in vivo* behaviour over time is one of the major challenges in developing degradable metallic implants for applications in humans [69]. Initial studies [14, 60, 69, 70] indicate very low relationship between degradation behaviour *in vitro* and *in vivo*. Sometimes, even opposite degradation properties are obtained, such as for LA442 and AZ91D [70]. Walker et al. [71] have compared the degradation rate of pure Mg and five alloys (AZ31, Mg-0.8Ca, Mg-1Zn, Mg-1Mn, Mg-1.34Ca-3Zn) under *in vivo* conditions (in a subcutaneous environment in Lewis rats) with different *in vitro* media buffered by CO_2/HCO_3^-. The degradation rate of samples in Earle's Balanced Salt Solution (EBSS) is more comparable to *in vivo* conditions, and the addition of bovine serum albumin (BSA) to Minimum Essential Media (MEM) increases the degradation rate of Mg and Mg alloys in this study. Sanchez et al. have reviewed the comparison between *in vitro* and *in vivo* results (Fig. 1.3, [20]). It shows that the corrosion factors for Mg alloys are

below 3 for EBSS and simulated body fluid (SBF), while it is in the range between 1.5 and 3.5 for MEM. When BSA is added, the corrosion factor increases to a range between 4 and 7.

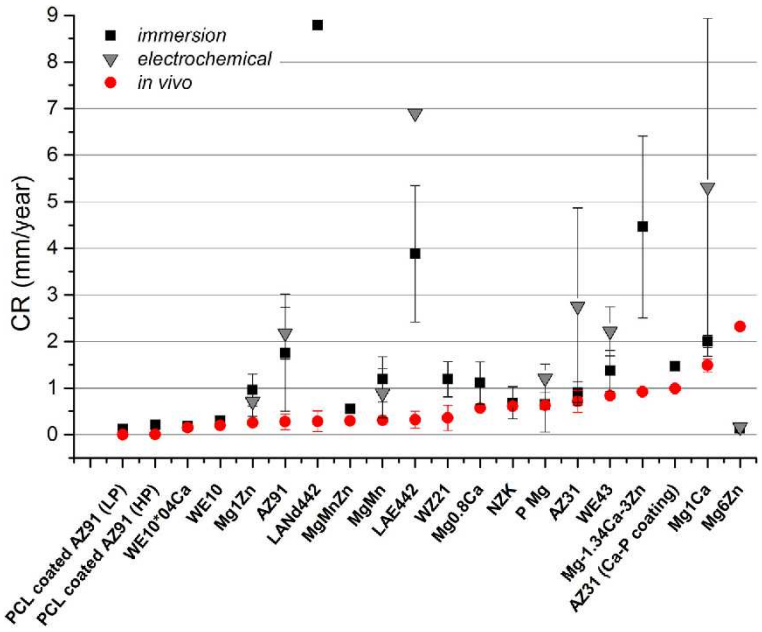

Figure 1.3: Comparison of the averaged *in vitro* and *in vivo* corrosion rates of 20 different materials (CR: corrosion rate) [20] (reproduced with permission from Elsevier).

For a valid comparison between *in vitro* and *in vivo* tests and to improve the mechanistic understanding, besides degradation rate, the degradation mechanism must be the same. The general degradation of Mg-based materials can be described as following:

$$Mg + H_2O \rightarrow Mg^{2+} + OH^- + H_2 \uparrow \qquad (1.1)$$

Due to the release of Mg^{2+} and the local alkalization, the degradation products including $Mg(OH)_2$, $Mg_3(PO_4)_2$ form on the Mg surface. $MgCO_3$, $CaCO_3$ and Ca-P salts also can form on surface due to the existence of Ca^{2+} and the CO_2/HCO_3^- buffering *in vivo* [72, 73]. Furthermore, interactions with organic molecules shift the reaction equilibrium towards new pathways [72], and the adsorption of organic matters affects the resistance of the formed degradation layer [74] and enables cells to grow on the materials [75]. The formation of different products on Mg-based implant materials indicates different degradation process and possible different mechanism. For example, $Mg(OH)_2$ is found to be the main product on Mg surface in simple sodium chloride (NaCl) solution in air, in SBF the main product is amorphous carbonated calcium phosphate [76], while under cell culture conditions (5% CO_2) crystalline nesquehonite ($MgCO_3 \cdot 3H_2O$) also is formed on Mg surface in SBF [77]. Some conditions, e.g. low ratio of medium volume to sample or fast degradation, will result in the severe deposition of precipitates on the Mg surface, resulting in two sections of the degradation layer: loosely

"outer" crystalline layer and "inner" amorphous layer [78]. I. Marco et al. [79] have investigated the degradation behaviour of pure Mg, Mg-10Gd and Mg-2Ag in HBSS, PBS and DMEM under cell culture conditions. Compared with *in vivo* tests, DMEM as testing medium, not only maintains a physiological pH level and produces a comparable degradation rate to *in vivo* conditions, but also generates the degradation layer similar to that formed *in vivo*. This comparable degradation layer to *in vivo* contains two layers: the first layer, next to the alloy surface, contained $Mg(OH)_2$ and (Mg,Ca)-CO_3; the second layer is a thin (Mg,Ca)-PO_4 layer on top of the first one [79-81], indicating similar degradation mechanism compared to *in vivo*. Therefore, it is reasonable to mimic the *in vivo* situations, such as simulated body fluids, the ratio of medium volume to sample surface, flow rate, to deduce reliable predictions from laboratory tests.

One of the major reasons for the miscorrelation between *in vitro* and *in vivo* results is the difference of the flow conditions. The commonly used *in vitro* method is the static test, which is performed in a certain medium volume during the whole duration. However, it is hard to illustrate the *in vivo* conditions, especially for long-term tests, due to the lack of the consideration of dynamic equilibrium in human body. To simulate the conditions *in vivo*, some investigations have been conducted by entirely or partially replacing the fluid by fresh one after certain testing intervals (semi-static conditions) [32, 71, 82, 83], because an average adult human has about 2.75 L of blood plasma and excretes 1.5 L of urine per day [84, 85]. The semi-static conditions can present more physiological conditions (stable pH, low osmolality and fresh medium) for Mg-based material during *in vitro* experiments. To control the flow rate of medium upon material surface accurately, different setups have been built for the *in vitro* tests (dynamic conditions) [29, 86-91]. General results shows faster degradation of Mg alloys under dynamic conditions than static conditions due to the faster mass transfer process and the increased mechanical force [88, 92]. Moreover, flow conditions also change the degradation type (localised or uniform), degradation products and local pH change [86, 93].

1.3. Simulated body fluid

Choosing a suitable physiological solution is a critical point to evaluate the degradation of Mg alloys and to obtain comparable *in vitro* results to *in vivo* trials. Simulated physiological solutions with increasing complexity were used to determine the degradation of Mg: from 0.9% NaCl solution, Hanks balanced salt solution (HBSS), simulated body fluid (SBF), to cell culture medium. Different simulated solutions used result not only in different degradation rates of Mg [94], but also different degradation products [76, 82], suggesting different degradation chemistry and degradation mechanism. Therefore, the choice of a suitable solution for the evaluation of Mg degradation is of utmost importance.

Table 1.1: the compositions of common simulated physiological solutions. Addition of organic components are highlighted in bold. (reused from published review [66])

Ingredient	SBP	SBF	Hanks	EBSS	KBM	DMEM	E-MEM	MEM	Plasma
Na^+	120.9	142	142	151	120	155	151	144	142
K^+	5.37	5	5.4	5.4	5	5.3	5.4	5.3	5
Ca^{2+}	1.8	1.6-2.5	1.3-2.5	1.8	2.5	1.8	1.8	1.8	2.5 (1.3)
Mg^{2+}	0.87	1.0-1.5	0.75-0.87	0.4	0.5	0.8	0.8	0.8	1.5 (1.0)
Cl^-	125.2	103-148.8	144-147	135	103	116	125	126	103
HCO_3^-	2.6	4.2-27	4.2	26	26.2	44.1	26	26.2	22-30
HPO_4^{2-}	1.14	1	0.3	1	0.9	0.9	0.9	1	1
$H_2PO_4^-$			0.4						
SO_4^{2-}	0.87	0.5	0.26-0.8	0.4	0.5	0.8	0.8	0.4	0.5
Amino acids	**-**	**-**	**-**	**-**	**-**	**10.6**	**0.9(mg/L)**	**8.54**	**unknown**
Vitamins	**-**	**-**	**-**	**-**	**-**	**0.15**	**-**	**0.32**	**unknown**
Proteins (g/L)	**-**	**-**	**-**	**-**	**-**	**-**	**-**	**-**	**63-80**
Dex/glucose (g/L)	**-**	**-**	**5.6**	**5.5**	**5**	**25**	**1**	**5.5**	**3.6-5.2**
Phenol red (g/L)	**-**	**-**	**-**	**-**	**-**	**0.04**	**0.1**	**0.03**	**-**
Reference	[94]	[96, 100, 103-106]	[61, 90, 94, 101, 102]	[95, 100]	[95]	[39, 79, 99]	[82]	[16, 98]	[82, 95-97]

Note: All concentrations in mmol/L unless otherwise stated. SBP: simulated blood plasma; SBF: simulated body fluid; EBSS: Earle's Balanced Salt Solution; KBM: Kirkland's biocorrosion medium; DMEM: Dulbecco's Modified Eagle's Medium; E-MEM: Eagle's Minimum Essential Medium; MEM: Minimum Essential Medium.

A suitable simulated solution should contain three important parts: i) appropriate inorganic ingredients, ii) applicable buffering system and iii) organic components. The detailed compositions of several common simulated physiological solutions are compared to the blood plasma composition (Table 1.1). There are some reports to study the degradation of Mg in physiological saline (0.9% NaCl) solution [107, 108], but they will not be discussed, as the results obtained with physiological saline solutions are far away or even contradictory from that obtained under physiological conditions [109].

1.3.1. Inorganic ions

To gain closer physiological conditions results, simulated body fluids (SBF) and Hanks' solution are widely used to determine the degradation rate of Mg, as they have a similar inorganic ion composition compared to blood plasma. SBF was developed as a solution for *in vitro* measurement of apatite-forming ability on implant materials and several improved recipes are available (Technical Committee ISO/TC150) [96, 110]. Compared to other solutions shown in Table 1, SBF has a closer composition to blood plasma. However, a large amount of Ca and Mg ions present in plasma is bound to organic molecules, which should be taken into consideration due to the absence of inorganic compounds in SBF. Moreover, Ca^{2+} with a high concentration of HCO_3^- and/or PO_4^{3-} can largely reduce the degradation rate of Mg due to the enhancement of Mg/Ca-P salts and/or $CaCO_3$ precipitation [83, 94, 106, 111]. Cl^- is one of the most concerned factors to magnesium alloy, which promotes the corrosion of Mg in aqueous solutions due to the accelerated breakdown of the surface film caused by the competitive adsorption of Cl^- and OH^- on the Mg surface [112-114]. The deleterious effect of Cl^- can be significantly improved by F^- addition to the Cl^- containing solution [115]. SO_4^{2-} also attacks Mg and stimulates Mg dissolution, but it is not as severe as that by Cl^- [112, 116]. However, under cell culture conditions the increase of SO_4^{2-} in HBSS+10% FBS showed no significant influence on degradation rate of Mg but increased the heterogeneity of the degradation layer [111]. Therefore, it is of utmost importance to investigate these factors under more physiological conditions and to state the exact composition as a guide for the readers.

1.3.2. Buffering

A good simulated body fluid should possess similar buffering capability to that of body plasma. Body blood pH is regulated by (a) the open system HCO_3^-/CO_2 adjusted by the respiration via lungs, (b) plasma protein buffers and (c) a low concentration of phosphate [96]. However, the most common buffers for simulated body fluids used are (a) 4-(2-hydroxyethyl)-1-piperazineethanesulfonic acid (HEPES), (b) Tris-HCl, (c) $CO_2/NaHCO_3$ and (d) phosphate. HEPES and Tris were introduced in the 1960's by Good et al. [117] for systems without CO_2-buffering.

Phosphate

The phosphate buffering contribution in human body is low and only significant in the urine and in the intracellular fluid, due to its low concentration. The too high concentration of phosphate alters the chemical properties of the degradation layer, as they can produce insoluble salts with magnesium ions and eventually precipitate on the surface, thereby leading to a different degradation performance compared to *in vivo* conditions [97, 118]. As already found, the degradation behaviour of Mg alloys in PBS shows a large difference to that in blood

[118]. Mg alloys in PBS showed a weight gain due to generation of a microscopically visible degradation layer, while a more or less distinct weight loss was observed in the blood test system [118]. Therefore, PBS is not suitable to simulate or predict degradation behaviour of Mg alloys under *in vivo* conditions.

HEPES

Under same conditions, HEPES increases the corrosion rate of pure Mg by a factor of up to four times compared with $NaHCO_3$ buffering alone in not only simply salt solution but also in EBSS and DMEM [71, 82, 95, 119, 120]. For WZ21 alloy, this factor increased to approximately 60 in SBF buffered with HEPES (100 mmol/L) compared to that buffered with CO_2/$NaHCO_3$ [121]. Moreover, HEPES in testing solutions also reduces the formation of calcium phosphate and carbonate in degradation layer by influencing the nucleation processes, thereby accelerating the degradation of Mg [95, 119]. The interaction between HEPES and Mg is also a possible reason for the effect of HEPES on the degradation of Mg [95]. HEPES destabilizes the protective layer, generating a less dense degradation layer and allowing the progressive diffusion of aggressive ions like Cl^- [122].

Tris-HCl

Tris is also one common buffering used in simulated body fluid, which also accelerates the corrosion rate of pure Mg by a factor of ten during earlier stage exposure due to the consumption of OH^- [123]. Moreover, when Tris-HCl is present in SBF, pure Mg is more sensitive to pitting corrosion behaviour [103]. Similar to HEPES, it was shown for AZ31 alloys that Tris-HCl prevents the formation of precipitates and degradation products due to the lower local pH [124]. For WZ21 alloy, the corrosion rate is five times faster in SBF buffered with 50 mmol/L Tris than that buffered with CO_2/HCO_3^- [105]. Even the CO_2/HCO_3^- buffered SBF shows a lower pH than Tris or HEPES buffered SBF, the degradation rate of pure Mg in SBF buffered with CO_2/HCO_3^- is the lowest compared to the other buffered SBFs [105]. This indicates an increase of Mg degradation caused by the addition of HEPES or Tris (as a pH buffer) results not only from the lower pH on Mg surface, but also from possible unidentified interactions between HEPES/Tris and Mg.

CO_2/HCO_3^-

It is not surprising that CO_2/HCO_3^- is preferable for *in vitro* tests instead of HEPES and Tris due to the similarity to the human pH regulation system. The presence of this buffering system causes the shift of equilibrium towards HCO_3^-, leading to a more stable pH via the equilibrium of HCO_3^-/CO_2. The presence of HCO_3^- (27 mmol/L) induce the rapid passivation of AZ91 in a simple salt solution due to the fast precipitation of insoluble magnesium carbonate on Mg

surface, followed by an accelerated degradation during the early immersion stage [116]. Similarly, increase of bicarbonate concentration in Tris-HCl buffered SBF from 4 to 27 mmol/L is proven to increase the passivity of the degradation layer and reduce corrosion [106]. However, when the bicarbonate concentration increases above 40 mmol/L in SBF without other buffer (Tris-HCl, HEPES), the degradation shows a reversed trend [125]. At absence of other ions (eg. Ca^{2+}) in solution, the increasing HCO_3^- concentration (0.5 - 50 mmol/L) accelerates the overall degradation rate of AZ31B alloy [83]. This phenomenon possibly relates to the formed surface film, since the precipitation of calcium carbonate, the further ionization of HCO_3^- and the incorporation of calcium and phosphate affect the resistance of surface film.

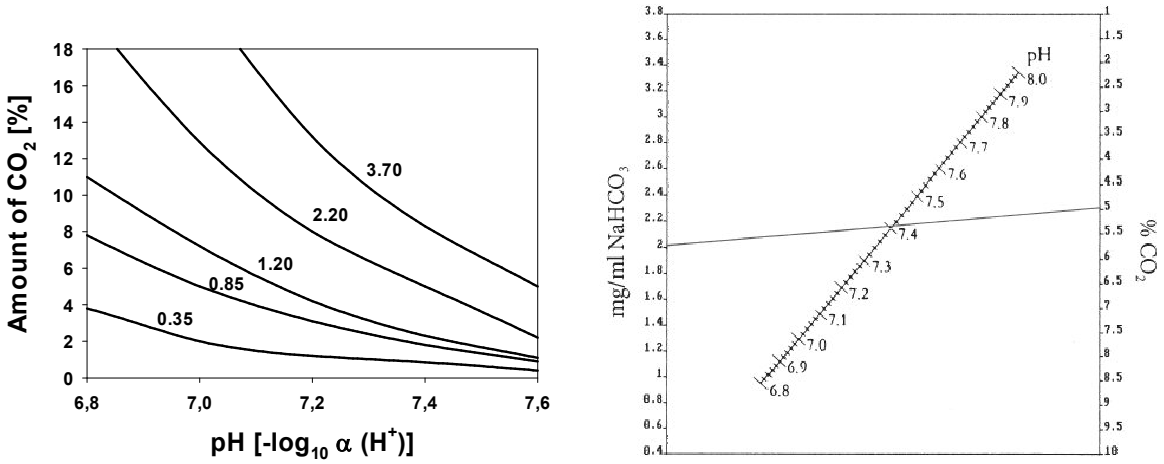

Figure 1.4: Left: Dependence of buffering pH on the amount of $NaHCO_3$ (in mg/mL, inserts) under cell culture conditions at different CO_2 regimes (adapted from [126]). Right: simplified nomogram for the determination of CO_2 according to the concentration of $NaHCO_3$ in the medium based on acid-base calculations [127]. The line depicts as an example the normal range of CO_2 and $NaHCO_3$ concentrations in a cell culture conditions (reused under creative commons license CC BY-NC-ND 4.0 [66]).

Only HCO_3^-, like Tris and HEPES, is not able to remain a stable pH as body blood pH (7.4±0.05) during long-term Mg degradation. Thus, the use of HCO_3^- assisted with CO_2 is a relatively simple, yet powerful method to control the pH value of the testing solution in degradation tests. Under aqueous conditions, the presence of CO_2 results in the formation of a carbonated film, which is thicker than magnesium hydroxide film formed in the absence of CO_2, resulting in a slower corrosion [128]. The most used approach is to perform the experiments under cell culture conditions (21% O_2, 5% CO_2 in a humidified atmosphere). The partial pressure of CO_2 above the solution establishes the HCO_3^-/ H_2CO_3 buffer system, hence indirectly regulates the pH of the testing solution. At present, many studies were performed under cell culture conditions, which also was discussed as physiological environment [39, 99]. Agha et al found

that $NaHCO_3$ (4.2, 22, 44 mmol/L) alone does not influence significantly the degradation rate of pure Mg in HBSS+10% FBS under cell culture conditions, indicating an equilibrium of HCO_3^- /CO_2 buffering system [111]. To ensure a good dissolution of the CO_2 in the testing solution, a setup with flow conditions for CO_2 in the testing container was used for degradation tests [61, 90, 102, 105]. The inflow of CO_2 enhance their contact with the testing solution, thereby increasing the dissolution. Zainal Abidin et al. stressed the importance of the partial pressure of CO_2 used according to the concentration of HCO_3^- in testing solution, to maintain the pH in the testing solution constant [61]. The resulting pH under cell culture conditions is directly correlated to the amount of HCO_3^- and the partial pressure of CO_2 in the incubator (Fig. 1.4).

1.3.3. Organic components

Organic components play a considerable role in the degradation of Mg, especially for the biological performance of Mg materials and magnesium metabolism in organisms. For example, a huge part of Mg^{2+} is present in the form of a complex with ATP, phosphonucleotides and phosphometabolites [6]. Moreover, there is a variety of organic components in organisms, such as vitamins, amino acids, glucose, lipids, fatty acids and proteins. Contact with these substances is inevitable for Mg-based materials after implantation. For a full understanding of Mg degradation process under physiological conditions, organic components are essential constituents to include in test solution for *in vitro* investigations. At present, the studies upon the effect of organic components on Mg degradation mainly focus on amino acids and proteins due to their relatively high concentration.

Vitamins and Amino acids

Actually, due to the environmental issues, varieties of vitamins and amino acids have already been investigated as green corrosion inhibitor for metallic corrosion [129-132]. For instance, the maximum inhibitor efficiency of L-ascorbic acid (AA) can reach 69% for mild steel in 0.04 mol/L H_2SO_4 solutions due to the adsorption on the surface [133], similar results also were obtained on carbon steel [134]. The amino acids also showed a positive corrosion inhibition for the Mg–Al–Zn alloy in chloride free neutral solutions (Fig. 1.5, [135]), which also was verified by the results that L-cysteine (6 mg/L) could inhibit the corrosion of pure Mg in 0.9 wt.% NaCl solution due to its adsorption [136]. However, under physiological conditions, the mixture of vitamins and amino acids in cell culture medium encourages the dissolution of Mg [71, 82]. Although the detailed and clear mechanism is still undefined, these results indicate that the *in vitro* investigations about the effect of organic molecules on Mg degradation should be performed under physiological conditions to obtain comparable results to *in vivo*.

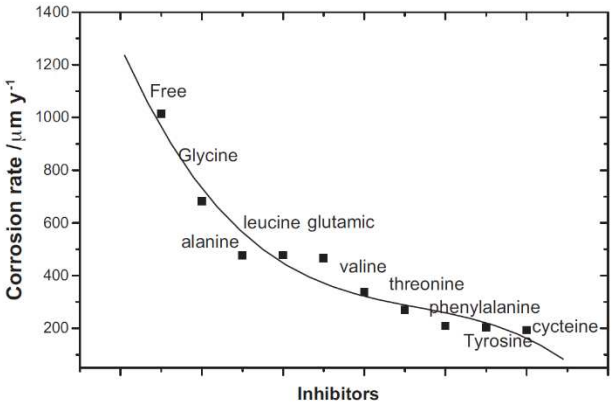

Figure 1.5: Effect of different amino acids at constant concentration of 1 × 10^{-3} mol/dm^3 on the corrosion rate of Mg-Al-Zn alloy in chloride free, stagnant, naturally aerated solutions of pH 7 at 25 °C (reproduced with permission from Elsevier [135]).

Proteins

Proteins, consisting of amino acid residues, are macromolecules. They widely exist and perform various functions within organisms, including catalysing metabolic reactions, DNA replication, responding to stimuli, and transport for ions and small molecules. The plasma proteins was found to be a vital part for physiologic pH [137]. They can help to keep the blood at a stable pH by binding excess H^+ ions due to the existence of carboxylic and amino groups. It is estimated that plasma may contain up to 10000 different proteins [138], and at least 490 proteins have been revealed by proteomic approaches [139].

As shown in table 1.2, albumin is the most abundant class of plasma proteins. It consists of a single polypeptide chain of 610 amino acids synthesized in liver and has a molecular weight of 66 kDa with a heart-like shape [140]. It comprises three helical domains, each comprising two subdomains (Fig. 1.6a) [140]. It is rich in some essential amino acids, such as aspartic acid and glutamic acid. The presence of these residues makes the molecule highly charged with positive and negative charged regions [141]. One important role of albumin is in the maintenance of osmotic pressure and fluid distribution between blood and tissues. It has a nutritive role as a transport carrier for various biomolecules including fatty acids, hormones, lipoproteins, amino acids and drugs by the binding effect [140, 142]. Fibrinogen (Fib) is another important rod-like plasma protein with a molecular weight of around 340 kDa. It is a disulfide-linked dimer composed of three pairs of non-identical polypeptide chains, two terminal globular regions and a compact central domain (Fig. 1.6a) [143]. The major function of Fib is to form fibrin clots that prevent the loss of blood upon vascular injury [143]. The molecular characteristics between different proteins can lead to different influence on Mg degradation due to the different interaction between Mg surface and proteins. For example, BSA and Fib adsorb on the same surface with different conformation and different affinity [144, 145].

Therefore, the detailed information on proteins used should be stated during the study about effect of proteins on Mg degradation.

Table 1.2: The main protein composition of plasma [146]

Protein	Amount in Normal Plasma (mg/mL)
Albumin	35 - 50
Fibrinogen	2.00 - 4.50
Fibronectin	0.25 - 0.40
Transferrin	2.00 - 3.20
Antithrombin III	0.20 - 0.40
Hemopexin	0.50 - 1.15
Immunoglobulin A	0.90 - 4.50
Immunoglobulin G	8.00 - 18.00
Immunoglobulin M	0.60 - 2.50
Haptoglobin	3.80 - 7.80
α1-Antitrypsin	2.00 - 4.00
α1-Acid glycoprotein	0.55 - 1.40
α1-Antichymotrypsin	0.30 - 0.60
GC Globulin	0.20 - 0.55
Ceruloplasmin	0.15 - 0.60

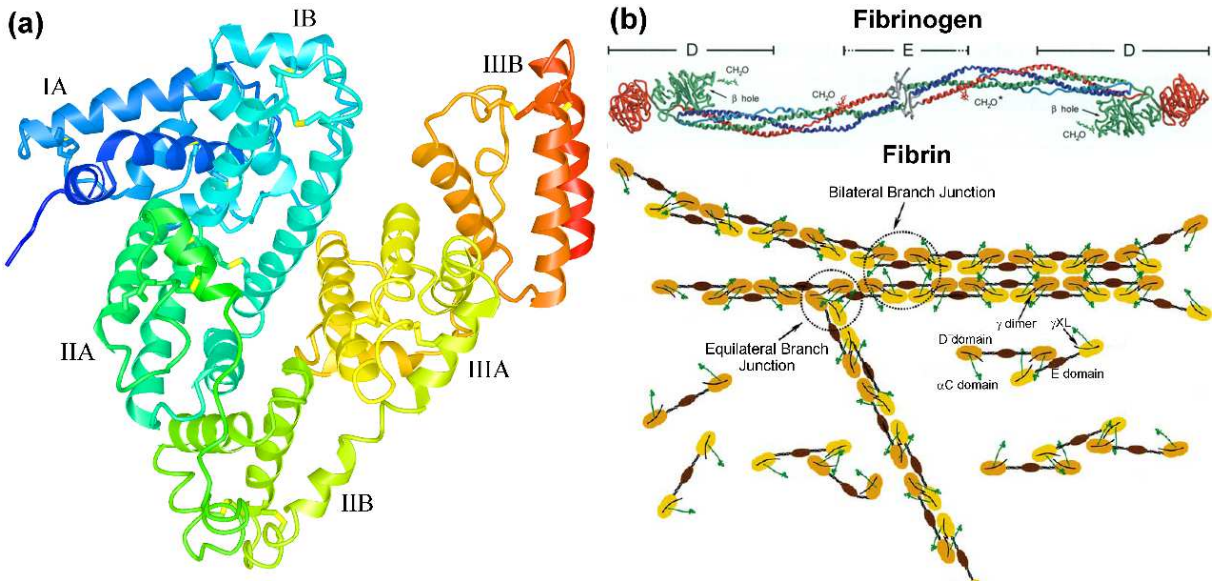

Figure 1.6: (a) Domain division in the BSA structure (PDB 4S5F in NCBI database, [147]), (b) the view of bovine fibrinogen molecule (reproduced with permission from PNAS, Copyright (2000) National Academy of Sciences, U.S.A [148]) and schematic diagram of fibrin assembly and λ chain cross-linking (reproduced with permission from *Wiley,* [149]).

At present, to determine the effect of proteins on Mg degradation, BSA is normally added as simplified protein component to testing medium [150, 151]. On the other hand, fetal bovine serum (FBS) is also used for *in vitro* investigations, especially as supplement for cell culture media [109, 152]. Although the major components of FBS are proteins, its composition is fairly

complex. Besides albumin (BSA), it contains various inorganic ions, for example, Ca^{2+}, and some other important trace compounds, such as antibodies, growth factors, etc.. These compounds and the interaction between organic molecules also can affect the degradation of Mg under certain conditions. They affect not only the degradation rate, but also the composition of degradation products [74, 82]. The reported results about the effect of proteins on Mg degradation are reviewed in Table 1.3. Except the results presented, there are also some studies focussing on the effect of proteins, but the detailed information related to the degradation rate is missing [76, 153]. To get a better comparability for *in vitro* degradation test by using different methods, the degradation rates in different reports are all converted to mm/year [55], since it is the most frequent used unit in the literature. However, it should be noted that different methods used could result in the deviations between different investigations.

As stated by various authors [71, 154], the effect of proteins on Mg degradation is mainly due to the adsorption or binding/chelating of proteins. The adsorption of proteins on surfaces is determined by external parameters (temperature, pH, ionic strength), protein properties (size, structural stability, composition) and surface properties (surface energy, polarity, charge, topography) [155]. The adsorption of proteins on Mg surface is believed to affect the compactness and/or thickness of the degradation layer on Mg surface, subsequently influencing the degradation of Mg [72, 74]. Moreover, the presence of the adsorbed protein layer is important in mediating cellular response to the implant. Proteins like fibronectin, vitronectin, bone morphogenetic proteins and some synthetic peptides, can regulate cell adhesion and subsequent tissue attachment to materials used as implants and this can lead to an increased rate of normal tissue regeneration [156]. Therefore, understanding the adsorption behaviour of protein on Mg during immersion is a necessity for a clear understanding of the influence of protein on the degradation of Mg.

Table 1.3: Overview of proteins effect on Mg degradation during *in vitro* test.

Ref.	Sample dimension	Solution changed	Conditions	Method	Degradation rate (mm/year)								
[71]	12 mm × 4 mm × 3 mm	30 ml (14mL changed per day)	Dynamic (an orbital shaking platform) 37 °C 5% CO_2	Mass loss		HP Mg			AZ31			Mg-1.34Ca-3Zn	
					solution	7 day	14 day	21 day	7 day	14 day	21 day	7 day	14 day	21 day
					In vivo	0.39	0.39	0.221	0.335	0.335	0.223	0.786	1.001	1.001
					EBSS	0.572	0.468	0.382	0.795	0.67	0.546	1.62	1.811	1.573
					MEM	0.728	0.676	0.659	1.291	1.018	1.192	4.718	9.889	10.04
					MEM + 40 g/L BSA	2.185	1.483	1.37	1.937	1.291	0.944	3.288	4.337	2.844
						Mg-0.8Ca			Mg-1Zn			Mg-1Mn		
					solution	7 day	14 day	21 day	7 day	14 day	21 day	7 day	14 day	21 day
					In vivo	0.312	0.43	0.351	0.378	0.227	0.164	0.302	0.34	0.252
					EBSS	0.573	0.521	0.382	0.505	0.429	0.303	0.756	0.504	0.722
					MEM	0.937	0.833	0.764	0.959	0.833	0.824	0.856	0.882	0.504
					MEM + 40 g/L BSA	2.812	1.901	1.545	1.716	1.438	1.615	2.771	2.116	1.612
[74]	-	100 ml / 0.7854 cm^2	Cell culture conditions	Polarization curves		CP Mg								
					solution	1 day		3 day		5 day				
					DMEM	0.11±0.05		0.12±0.05		0.20				
					DMEM+20% FBS	0.12±0.02		0.08		0.08				
[95]	10 mm × 10 mm × 10 mm	20 ml / cm^2	37 °C for HEPES In incubator for CO_2/HCO_3^-	Mass loss		HP Mg-cast								
					solution	7 day		solution		7 day				
					MEM (HEPES buffer)	7.14±0.23		MEM (CO_2/HCO_3^- buffer)		1.58±0.22				
					MEM (HEPES buffer) + 40g/L BSA	7.31±0.46		MEM (CO_2/HCO_3^- buffer) + 40g/L BSA		3.63±0.43				

[82]	Φ 9.5 mm × 2 mm	27.5 mL (15 mL changed every day)	37 °C 5% CO_2 rotated 300 rpm	Mg^{2+} concentration	Pure Mg								
					solution	1 d	2 d	3 d	5 d	7 d	10 d	12 d	14 d
					EBSS	1.084	0.765	0.659	0.65	0.601	0.542	0.521	0.492
					E-MEM	2.168	1.881	1.700	1.492	1.385	1.256	1.206	1.184
					E-MEM + 10% FBS	0.701	0.51	0.446	0.37	0.337	0.287	0.266	0.26

[151]	0.8 mm^2	-	Room conditions	Polarization curves		Pure Mg (99.98%)	AZ31	LAE442
					solution	5 min	5 min	5 min
					PBS	0.18±0.20	0.74±0.27	0.35±0.24
					PBS + 0.1 g/L Albumin	8.06±7.74	0.86±0.14	0.97±0.63
					PBS + 1 g/L Albumin	2.88±1.73	1.00±0.11	1.36±0.72
					PBS + 10 g/L Albumin	0.85±1.24	0.90±0.10	1.50±0.57

[157]	12 mm × 4 mm × 3 mm	30 mL (14 mL changed per day)	Dynamic (an orbital shaking platform) 300 rev/min	Mass loss		Pure Mg(99.99%)			Mg-coated Brushite			Mg-coated Monelite		
					solution	7 day	21 day	28 day	7 day	21 day	28 day	7 day	21 day	28 day
					MEM	1.13±0.03	0.76±0.08	0.62±0.06	1.01±0.27	0.74±0.13	0.60±0.04	0.81±0.22	0.46±0.11	0.39±0.19
					MEM+ 40g/L BSA	2.68±0.39	1.24±0.01	0.95±0.04	0.91±0.16	0.49±0.16	0.45±0.13	0.80±0.15	0.29±0.07	0.26±0.03

[158]	Φ 15 mm × 4 mm	50 mL	37 °C	Polarization curves		Pure Mg-coated PEO			
					solution	PBS	PBS + 1g/L BSA	0.9 wt.% NaCl	0.9 wt.% NaCl + 1g/L BSA
					30 min	3.72E-04	5.85E-05	4.93E-04	1.65E-04

[152]	Φ 12 mm × 2 mm	-	37 °C	Polarization curves		AZ31	AZ91	Mg–1.22Ca
					solution	7 day	7 day	7 day
					DMEM	0.34	0.53	0.55
					DMEM+10%FBS	0.10	0.42	0.90

[159]	10 cm^2	300 mL / cm^2	37 ± 1 °C	Polarization curves	10 min	Mg0.4Ca	Mg0.8Ca	Mg1.34Ca	Mg5Ca	Mg10Ca	Mg16.3Ca	Mg28Ca	AZ31	AZ91
					MEM	0.93	0.75	0.68	0.98	1.88	2.75	3.66	0.59	0.35
					MEM+10 % FBS	0.26	0.41	0.39	0.56	1.73	2.31	2.88	0.21	0.16
[150]	10 mm × 10 mm × 2 mm	-	37 ± 1 °C	mass loss	AZ91									
						SBF		SBF + 1 g/L BSA						
					7 day	3.901±0.091		3.923±0.049						
[160]	10 mm × 10 mm × 4 mm	250 ml (0.9 cm^2)	37 ± 1 °C	Hydrogen evolution	extruded Mg–1.5Ca									
					solution	11 h		24 h	36 h	50 h	53 h	56 h	60 h	70 h
					0.9% NaCl	23.92		13.64	13.66	11.88	11.51	11.19	10.74	9.61
					0.9% NaCl+1g/L BSA	5.79		4.01	3.46	2.98	2.93	2.85	2.78	2.54
					0.9% NaCl+10g/L BSA	3.66		2.50	2.21	1.81	1.75	1.70	1.64	1.47
[154]	disk samples (φ 15 × 3 mm)	25mL (13.75ml changed per day)	Cell culture conditions	Mass loss	Mg–2.1Nd–0.21Zn–0.5Zr alloy									
						Medium 199				Medium 199 + 10% FBS				
					7 day	0.87 ± 0.02				0.78 ± 0.03				
[161]	-	-	37 °C	Hydrogen evolution	M1A Mg alloy									
					solutions	0 h		1 h	2 h	4 h	6 h	12 h	24 h	
					SBF	23.39		18.41	10.62	7.96	5.64	3.32	3.24	
					SBF + 40 g/L BSA	12.94		12.27	11.36	10.29	8.46	6.64	5.56	

Many studies on protein adsorption have been performed on stable (non-degrading) biomaterial surface, for example, titanium (Ti) surface and nanoparticles [162-164]. Thus, it is comparably easy to investigate the effect of surface properties including roughness [165, 166], hydrophobicity [167] and charge [162, 168] on the adsorption of proteins. Protein adsorption and desorption are largely affected by surface condition (wettability, surface change, surface energy), pH, ionic strength. For example, BSA was found to lose more α-helix conformer upon adsorption on CaP surface than Ti and germanium (Ge) surfaces [169]. Ca^{2+} can induce the transition of osteocalcin to α-helix conformation, which promotes the adsorption on bone mineral crystals with certain orientation [170]. However, for degradable magnesium and its alloys, there is an intricate interplay between Mg surface and proteins. Two main processes occur simultaneously during Mg immersion in protein-containing media: Mg degradation (Mg dissolution and products formation) and protein adsorption. Generally, the increases of pH and Mg^{2+} concentration caused by Mg dissolution result in the formation of degradation products covering the Mg surface, such as $Mg(OH)_2$, $MgCO_3$, Mg/Ca-PO_4 [77, 80]. Thus, Mg surface is changing for protein adsorption during immersion, especially during the initial immersion time. All these degradation-induced variations (pH, ionic strength, surface conditions, surface chemistry, and so on.) during immersion add lots of difficulties to understand the adsorption of proteins on degrading Mg surface. Therefore, the adsorption of protein is quite complex process on the Mg implant under physiological conditions, which needs detailed and comprehensive investigations.

On the other hand, the binding/chelating of Mg^{2+} to proteins can promote the Mg dissolution reaction, which is largely correlated to some parameters, such as temperature, pH, protein concentration, Mg^{2+} concentration and protein structure [171]. The studies for other metal surfaces, such as stainless steels, aluminum and titanium, suggest that proteins can interfere with the formation of a passivation layer by complexing with surface oxides [172]. Albumin is the major circulatory protein involved in the handling of Ca^{2+} (Mg^{2+}) in mammals, controlling the ionized or 'biologically active' levels of these metals in the blood. Mg^{2+} is transported by albumin with slightly lower binding affinity compared to Ca^{2+} (K_a (Mg) = 1×10^2 M^{-1}, K_a (Ca) = 1.5×10^2 M^{-1}) [140]. The high binding of Mg^{2+} to ATP, phosphonucleotides and phosphometabolites indicates the importance of other organic molecules to the Mg degradation *in vivo* [6]. Nevertheless, the binding of impurity elements (eg. Fe) to proteins may decrease the degradation of Mg. One recent modelled mechanism of magnesium degradation is the iron impurity-based re-deposition effect [173]. In a further study, the inhibition efficiency of iron-complexing agents was analysed and all used iron complexing agents (CN^-, salicylate, oxalate, SCN^-, 5-Methylsalicylate) efficiently lowered the corrosion rate of Mg [174]. However, the primary iron-binding entities in physiological condition are proteins, such as albumin,

transferrin and fibrinogen. Therefore, the binding/chelating effect of proteins on Mg degradation could be more complex due to the diversity of proteins *in vivo* and the different affinity to different ions caused by the properties of proteins.

The great complexity of organic molecules and the very wide range of proteins (e.g. albumin, fibrinogen, globulins) *in vivo* indicates that the organic molecule behaviour in mixtures is often a result of an overlap of adsorption, exchange, desorption and repulsion processes. Clearly there are interactions between different proteins, for example, the competitive adsorption (known as “Vroman Effect”) or cooperative adsorption between proteins [175, 176]. A typical example for competitive adsorption is that fibrinogen (Fib) absorbed on a biopolymer surface is replaced by high molecular weight kininogen [177]. The co-existence of these proteins can affect the influence of single protein on Mg degradation, therefore also affecting the degradation rate of Mg and/or the degradation products on Mg surface. However, when FBS was used to investigate the effect of proteins on Mg degradation, the complexity of FBS and the interplay between organic molecules did not get enough considerations. Therefore, a better understanding on the influence of protein on the Mg degradation demands deep investigations about the protein performance on Mg surface, the composition of degradation products under physiological conditions and the interactions between proteins and Mg surfaces.

2. Motivation and objectives

More and more complex conditions has been exploited to pursue closest physiological conditions compared to *in vivo*. A proper testing solution, a prerequisite for *in vitro* test, should contain not only comparable inorganic ions to plasma and a good buffering system, but also equivalent organic components. Although the influence of proteins or amino acids has been studied, the conclusion is still ambiguous, even adverse results are shown in different works. Therefore, the motivation of this thesis is to confirm the influence of organic components on the degradation of Mg under cell culture conditions and to investigate the effect of commonly used proteins (BSA, Fib, FBS) in different media under cell culture conditions. The objectives of this research focus on the following questions:

(1) What is the difference between the effect of small organic molecules and macromolecules (protein) on Mg degradation? How do organic molecules affect the degradation rate of Mg and the formation of degradation products?

(2) How do proteins affect the degradation of Mg under different conditions, such as medium composition, ratio of media to sample and static/semi-static conditions? Can any benefits to *in vitro* results be obtained from the addition of proteins?

(3) How to avoid the effect of continuous surface change on the investigation about protein adsorption on Mg surface during immersion? What is the difference of protein adsorption on Mg surface formed in salt solution and on *in vivo*-like Mg surface?

(4) What is the difference between the effect of single protein and protein mixtures on Mg degradation? Is it a corporative or competitive effect for Mg degradation in protein mixtures?

3. Materials and Methods

3.1. Materials

Pure Mg (99.94 %, chemical composition (Table 3.1) was determined by a Spark Analyser (Spectrolab M, Spektro, Germany) used in this thesis was purchased from Magnesium Elektron (Manchester, UK). Rectangular specimens with dimensions of 10 mm × 10 mm × 4 mm were cut out of the ingots. Before use, the specimens were successively wet ground with SiC abrasive paper (Schmitz-Metallographie GmbH, Herzogenrath, Germany) from 800 to 2500 grit, then ultrasonically cleaned for 20 min in N-hexane, 5 min in acetone and 20 min in ethanol (Merck KGaA, Darmstadt, Germany). Finally, the samples were dried in 12-well cell culture plates (Greiner Bio-One, Frickenhausen, Germany) for at least 30 min in air under sterile conditions. To examine the microstructure of Mg used, four samples were polished with oxide polishing suspensions (OPS, Cloeren Technology GmbH, Wegberg, Germany) after grinding, then etched using a picric acid-based etchant (100 mL ethanol, 20 mL distilled water, 6.5 mL acetic acid and 12-15 g picric acid). Typical results are displayed in Fig. 3.1a. The homogeneity of sample surface after grinding was investigated by profilometer as shown in Fig. 3.1b.

Table 3.1: Chemical composition of pure Mg.

Element	Ca	Zn	Fe	Cu	Si	Mn	Ni	Mg
(Wt.%)	0.0004	0.018	0.0044	0.0089	0.0014	0.0021	<0.0002	balance

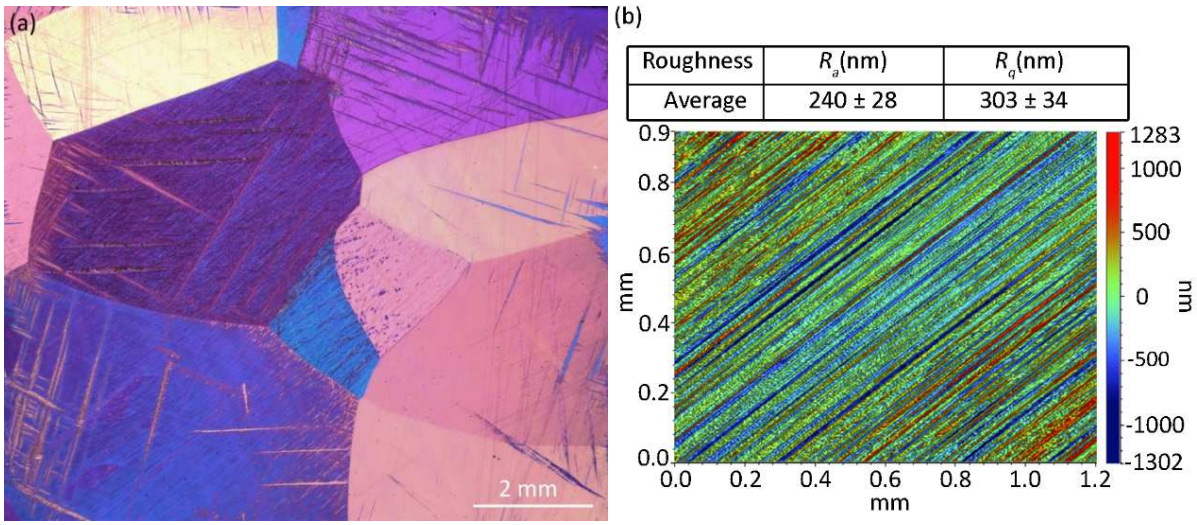

Figure 3.1: (a) Typical microstructure of pure Mg, (b) the surface roughness of samples before immersion tests measured by profilometer (Bruker, Karlsruhe, Germany). At least six samples were checked for the microstructure and surface roughness, at least four positions for each samples were examined for surface roughness (as supplementary published [178]).

3.2. Immersion test

The immersion test used are different based on the experimental objectives. They are described according to the aims of study in this thesis as follows:

Influence of small organic molecules

Hank's balanced salt solution (HBSS, Order-No. 14715, Life Technologies, Darmstadt, Germany) without calcium and magnesium addition (the composition is shown in Table 3.2), was used as a base solution for all immersion media. L-ascorbic acid (L-AA, Sigma-Aldrich Chemie, Steinheim, Germany), L-glutamine (L-Gln, Thermo Fisher, Karlsruhe, Germany), L-alanyl-L-glutamine (L-Ala-L-Gln, Biowest, Darmstadt, Germany) and 10 % fetal bovine serum (FBS, PAA laboratories, Linz, Austria) as a protein component, were added in a concentration comparable to that in two cell culture media, Dulbecco's modified Eagle's medium (DMEM) and Minimum Essential Media Alpha (α-MEM). After these components except FBS were added into HBSS, the media were sterile filtered by bottle top-filters with a pore size of 0.2 µm (Thermo Fisher, Karlsruhe, Germany). Thus, eight immersion media were prepared as following:

A: Base solution (HBSS)
B: HBSS + 50 mg/L L-AA
C: HBSS + 292 mg/L L-Gln
D: HBSS + 862 mg/L L-Ala-L-Gln
E: HBSS + 50 mg/L L-AA + 292 mg/L L-Gln
F: HBSS + 50 mg/L L-AA + 862 mg/L L-Ala-L-Gln
G: HBSS + 50 mg/L L-AA + 292 mg/L L-Gln + 10 % FBS
H: HBSS + 50 mg/L L-AA + 862 mg/L L-Ala-L-Gln + 10 % FBS

Six replicate samples for each time point were immersed in media at a ratio of 5 mL/g (medium/sample) under cell culture conditions (37 °C, 5% CO_2, 20% O_2, 95% rel. humidity) in an incubator (Heraeus BBD 6620, Thermo Fisher Scientific, Schwerte, Germany). The immersion media were changed every 2 to 3 days to present semi-static conditions. At each medium change, changes in pH (Sentron Argus X pH-meter, Fisher Scientific, Schwerte, Germany) and osmolality (Osmomat 030, Gonotec, Berlin, Germany) were measured. pH and osmolality of the media incubated without samples were determined as control.

Influence of proteins

The base immersion media are HBSS, HBSS with calcium (HBSSCa, 1.8 mM $CaCl_2$) and DMEM (Life Technologies, Darmstadt, Germany). 10% FBS was added in HBSS, HBSSCa

and DMEM, respectively, to prepare the media HBSS + 10% FBS, HBSSCa + 10% FBS and DMEM + 10% FBS. The concentration of BSA (Carl ROTH GmbH, Karlsruhe, Germany) was set at a similar concentration (3.4 mg/mL) as 10% FBS to avoid the difference deriving from protein concentration as much as possible. The concentration of fibrinogen (Fib: 2.0-4.5 g/L in plasma, Sigma-Aldrich, Saint Louis, USA) was set to 0.34 mg/mL due to the ten times lower concentration than BSA in plasma (35-50 g/L in plasma): Finally, the media were sterile filtered (0.2 µm pore size, Thermo Fisher, Karlsruhe, Germany). Thus, the following media were prepared to investigate the influence of proteins:

a: HBSS
b: HBSS + 3.4 mg/mL BSA
c: HBSS + 0.34 mg/mL Fib
d: HBSS + 3.4 mg/mL BSA + 0.34 mg/mL Fib
e: HBSS + 10% FBS
f: HBSSCa
g: HBSSCa + 3.4 mg/mL BSA
h: HBSSCa + 0.34 mg/mL Fib
i: HBSSCa + 3.4 mg/mL BSA + 0.34 mg/mL Fib
j: HBSSCa + 10% FBS
k: DMEM
l: DMEM + 3.4 mg/mL BSA
m: DMEM + 0.34 mg/mL Fib
n: DMEM + 3.4 mg/mL BSA + 0.34 mg/mL Fib
o: DMEM + 10% FBS

For **static immersion test**, Fib was not used due to the instability of Fib after one week in media, which means that media c, d, h, i, m and n will not be presented in static tests. Four replicate samples for each time point were immersed in 80 mL media (~30 mL/g) under cell culture conditions (37 °C, 5% CO_2, 20% O_2, 95% rel. humidity). pH (Sentron Argus X pH-meter, Fisher Scientific, Schwerte, Germany) and osmolality (Osmomat 030, Gonotec, Berlin, Germany) were measured every 2 or 3 days. pH and osmolality of the media incubated without samples were determined as control.

As for **semi-static immersion test**, six replicate samples for each time point were immersed in media at a ratio of 5 mL/g (medium/sample) under cell culture conditions. The immersion media were changed every 2 to 3 days to present semi-static conditions. pH and osmolality were determined at every medium-changed time points.

Table 3.2: The composition of Hanks' balanced salt solution without (HBSS) or with calcium (HBSSCa) and Dulbecco's Modified Eagle Medium Glutamax-I (DMEM).

Ingredient	HBSS		HBSSCa		DMEM	
	mg/L	mM	mg/L	mM	mg/L	mM
$CaCl_2$ $2H_2O$	-	-	264	1.80	264	1.80
$Fe(NO_3)_3$ $9H_2O$	-	-	-	-	0.1	2.48e-4
$MgSO_4$ $7H_2O$	-	-	-	-	200	0.81
KCl	400	5.33	400	5.33	400	5.33
KH_2PO_4	60	0.441	60	0.441	-	-
$NaHCO_3$	350	4.17	350	4.17	3700	44.05
NaCl	8000	137.93	8000	137.93	6400	110.34
$NaH_2PO_4 \cdot 2H_2O$	-	-	-	-	141	0.916
Na_2HPO_4	48	0.338	48	0.338	-	-
Vitamins	-	-	-	-	31.6	0.15
Amino acids	-	-	-	-	1852	10.29
D-Glucose (Dextrose)	1000	5.56	1000	5.56	4500	25.00
Phenol red	-	-	-	-	15	0.0399
Sodium pyruvate	-	-	-	-	110	1.00

Degradation rate

Before sterilization, the initial weights of samples (Waagen-Schmitt GmbH, Hamburg, Germany) as well as the initial pH (SENTRON ARGUS X pH-meter, Fisher Scientific, Schwerte, Germany) and osmolality (Osmomat 030, Gonotec, Berlin, Germany) for the immersion media were recorded.

After immersion, samples were cleaned twice with sterile distilled water and dried at 50 °C in air. The degradation products were removed by immersing in chromic acid (180 g/L chromium (VI) oxide in distilled water, VWR International, Darmstadt, Germany) for 20 min at room temperature. Subsequently, samples were cleaned with distilled water and 100% ethanol. After drying, the weights of samples (Waagen-Schmitt GmbH, Hamburg, Germany) were determined again to obtain the mass loss during the immersion. The mean degradation depth (h) of samples in µm was calculated using the following equation:

$$h = \frac{10000 \cdot \Delta m}{A \cdot \rho} = \frac{DR \cdot t}{8.76} \qquad (3.1)$$

where A is the surface area in cm^2, ρ is the density of pure Mg (1.74 g/cm^3), t is immersion time in hours, Δm is the observed mass loss in gram and DR is the degradation rate in mm/year. The mean degradation depth can be transformed into degradation rate (mm/year) by using equation (3.1). The rationale of mean degradation depth used has been discussed in literature [56].

Before the use of chromic acid, the effect of chromic acid on bulk material (pure Mg) was checked by immersing samples in chromic acid for 20 min. No changes in weight of samples before and after immersion suggest that the bulk material cannot be dissolved by chromic acid.

3.3. Concentration of ions and organic molecules

3.3.1. On-line pH

A 24-well Sensor Dish integrated with pre-calibrated pH sensor spots at the bottom of each round well (PreSens Precision Sensing GmbH, Regensburg Germany) was used to monitor the change of pH with the immersion time. The pH values are read out contactless with the SDR SensorDish® Reader through the transparent bottom of the dish. The measurement method is based on non-invasive luminescence detection (see Fig. 3.2). The pH range detected in this system is from five to nine.

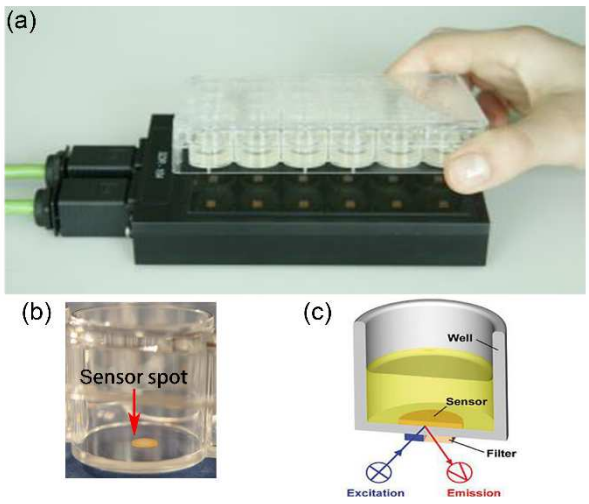

Figure 3.2: Online pH measurement. (a) 24-well sensor Dish and SDR SensorDish® Reader. (b) the pH integrated sensor spot (c) the Illustration of measurement [179] (with the permission of PreSens GmbH, Regensburg, Germany).

3.3.2. Concentration of L-Gln

The concentration of L-Gln in media was determined by using the glutamine colorimetric assay kit (BioVision, Inc., Zürich, Schweiz). The standard curve was prepared by using Gln standard

solutions with a successive concentration from 0 µM to 250 µM. At each time point, 10 µL of media with or without samples (three replicates) were taken out from well plates, then centrifuged at 10000 g (Heraeus Biofuge Pico, Osterode, Germany) for 5 min at 4 ˚C. 2 µL of the supernatant was added to 96-well clear plates with flat bottom. The volume was adjusted to 40 µL/well with ddH_2O. 10 µL Hydrolysis Mix solution was added to each sample well, then the plates were incubated for 30 min at 37 ˚C. Subsequently, 50 µL Reaction Mix solution was added to each sample well and incubated for 60 min at 37 ˚C. Finally, the absorbance at 450 nm was measured with a reference absorbance at 620 nm in Tecan A-5082 microplate reader (Tecan Sunrise TECAN Deutschland GmbH, Crailsheim, Germany). The absorbance of analyte at certain wavenumber satisfies Beer-Lambert law, which can be expressed as following:

$$A = \mathrm{Log}\frac{I_0}{I_t} = \varepsilon\, b\, c \qquad (3.2)$$

where *A* is the measured absorbance, I_0 is the initial light intensity, I_t is the light intensity after it passes through the sample, ε is the wavelength-dependent molar absorptivity coefficient (L/(mol·cm)), *b* is the path length (cm), and c is the analyte concentration (mol/L). Therefore, according to the standard plots (absorbance with different concentration of analyte), the concentration of analyte in solution can be deduced.

3.3.3. Protein concentration

BCA Protein Assay (Pierce Biotechnology, Rockford, USA). is a colorimetric detection based on bicinchoninic acid (BCA) for the quantitation of total protein, which is used to determine the protein concentration in this thesis. This method is a combination between the well-known biuret reaction (the reduction of Cu^{2+} to Cu^{+} by protein in an alkaline medium) and the highly sensitive and selective colorimetric detection for the cuprous cation (Cu^{+}) using bicinchoninic acid. The purple-coloured reaction product of this assay is formed by the chelation of two molecules of BCA with one cuprous ion. This water-soluble complex exhibits a strong absorbance at 562 nm that is a function of protein concentrations. In the present study, the media without samples as control were checked at the same time. 10 µL solutions of media + BSA, media + BSA + Fib and media + FBS were taken out from the plates after certain immersion time, then diluted to 25 µL with distilled water in 96-wells plates. 25 µL solution of media + Fib also was taken out after certain immersion time in a 96-well plate. Subsequently, 200 µL working reagent was added to each well and the plates were mixed thoroughly on a plate shaker for 30 s. Afterwards, the plates were incubated at 37 ˚C for 30 min. Finally, the absorbance at 570 nm was measured on the Tecan microplate reader. The concentration of proteins in solution can be deduced from the standard curves (0-2000 mg/L). Due to the

interference of phenol red with some amino acids, the protein concentration in DMEM cannot be determined by BCA assay.

3.3.4. Small angle X-ray scattering (SAXS)

SAXS belongs to a family of X-ray technique, which can determine the size and shape of macromolecules. The basic mechanism of SAXS is illustrated in Fig. 3.3.

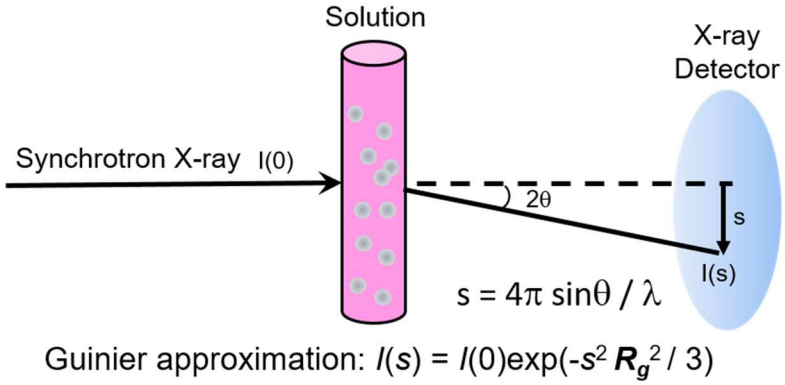

Figure 3.3: Illustration of small angle X-ray scattering. (I(0) indicates the intensity of initial X-ray, s refers to the scattering vector, 2θ refers to scattering angle, λ refers to wavelength, R_g indicates the gyration radius of particle in solution)

The scattering intensity, I(s), derives from the difference in the average electron density of the particle in solution (ρ(r)), e.g. protein molecules, and the bulk solvent ρ(s). It is obtained as a function of the scattering vector (s). According to the shape of scattering curves and scattering intensity, it can be used to deduce the information on molecules, such as size, shape, internal structure and molecular mass. For example, at small scattering vector, the scattering curve (similar size particles) can be used to calculate the gyration radius (Guinier approximation). Furthermore, the comparison between scattering intensity at same concentration and particle size can be used to identify the interaction between molecules.

In this study, small angle X-ray scattering (SAXS) measurements were recorded at the P12 BioSAXS beam-line of the European Molecular Biology Laboratory (EMBL) at the storage ring PETRA III of the Deutsche Elektronen Synchrotron (DESY, Hamburg, Germany) at 20 °C using a Pilatus 2M detector (1475 × 1679 pixels, Dectris, Switzerland) and synchrotron radiation with a wavelength 0.1 nm. The sample-detector distance was 3 m, allowing for measurements in an s-range of 0.03-4.4 nm^{-1}. Twenty diffraction patterns were collected for every sample, each with an exposure time of 0.05 s. To avoid radiation damage by subsequent illuminations, curves showing deviations were discarded. The final scattering curve was obtained using the automated acquisition and analysis by averaging the scattering data collected from different frames [180].

3.4. Characterization of degradation products

3.4.1. X-ray diffraction (XRD)

X-ray diffraction (XRD) is a rapid analytical technique used to determine the atomic and molecular structure of a crystal phase. It is based on the constructive interference of monochromatic X-rays diffracted by the ordered lattice structure of crystalline materials as shown in Fig. 3.4. Bragg's law ($2d \sin\theta = n \lambda$) is used to explain the interference pattern of X-rays scattered by crystals. To identify the products formed and deposited on the surface, the Mg surfaces after different days of immersion without further treatment were examined by X-ray diffraction (XRD), performed on a Bruker D8 Advance (Bruker, Karlsruhe, Germany) in grazing incidence mode or coupled two-theta mode. The generator was set for 40 kV and 40 mA. Data was collected between $2\theta = 10° - 75°$ at 0.01° intervals. The counting time was 0.5 s per point. Data analysis was carried out using analysis software (BrukerEVA and PDF-2 Release 2015 RDB).

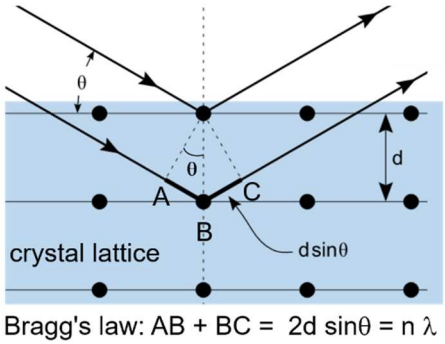

Figure 3.4: Bragg diffraction from a cubic crystal lattice.

3.4.2. Infrared spectroscopy (IR)

Infrared (IR) spectroscopy is one of the most common and widely used spectroscopic techniques, and is very useful in the identification and structure analysis of a variety of substances including both organic and inorganic compounds. It can sensitively determine the functional groups of sample since different functional group absorbs different particular frequency of IR radiation. As shown in Fig. 3.5, once the vibration can causes a change in dipole moment and the energy of the radiation exactly matches the difference in energy levels between the vibrational quantum states, absorption of radiation can lead to the transitions in vibrational energy levels.

Therefore, to characterize the amorphous-state degradation products, the infrared spectra were recorded with a resolution of 2 cm^{-1}, taking 256 scans by using infrared spectroscopy in

reflectance mode (Bruker Hyperion 2000, Ettlingen, Germany). For data evaluation, Bruker OPUS software version 7.5.18 was used.

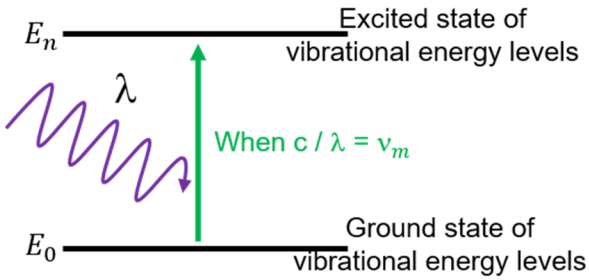

$$E_{radiation} = \Delta E = E_n - E_0 = h\,\nu_m = \frac{h}{2\pi}\sqrt{\frac{k}{\mu}}$$

Figure 3.5: Schematic illustration of infrared spectroscopy. (E_n is the energy level of excited state, E_0 is the energy level of ground state, h is Planck's constant, k is the spring constant for the bond, ν_m is the vibrational frequency, μ is reduced mass)

3.4.3. X-ray photoelectron spectroscopy (XPS)

X-ray Photoelectron Spectroscopy (XPS), one of most widely used surface analysis technique, can be applied to a broad range of materials and provides valuable quantitative and chemical state information for the material surface. Typically, a sample surface is excited by an X-ray, leading to the emission of photoelectrons. The energy of the emitted photoelectron is measured by an electron energy analyser. Thus, the binding energy of the emitted photoelectrons can be determined as shown in Fig. 3.6 [181]:

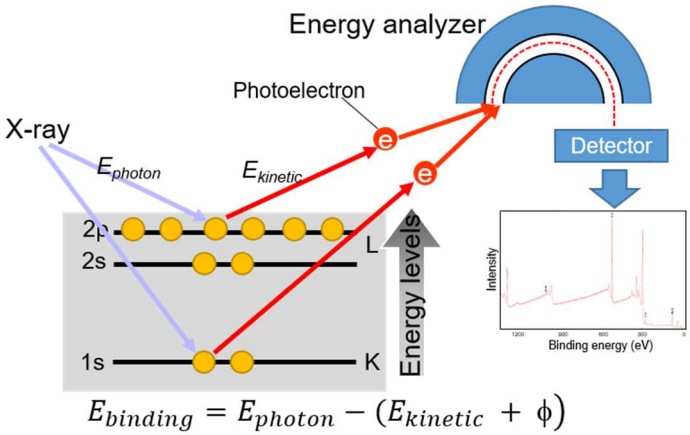

$$E_{binding} = E_{photon} - (E_{kinetic} + \phi)$$

Figure 3.6: The principle of X-ray photoelectron spectroscopy. ($E_{binding}$ is the binding energy (BE) of the photoelectron, E_{photon} is the energy of the used X-ray photons (for Al Kα X-rays, E_{photon} = 1486.7 eV), $E_{kinetic}$ is the kinetic energy of the measured photoelectron and ϕ is the instrumental correction factor dependent on the spectrometer and the material)

Due to different oxidation states and different chemical environments, the binding energies of a certain element level will shift, which relates to the charge distribution of the surrounding

atoms. Therefore, it can be used to determine the elemental identity and chemical state. According to the linear relation between the elemental signal intensity and atomic concentration, the quantity of a detected element can be further determined [181].

XPS measurements were carried out on a KRATOS AXIS Ultra DLD (Kratos Analytical, Manchester, United Kingdom) equipped with a monochromatic Al K_α anode working at 15 kV (225W). For the survey spectra a pass energy of 160 eV was used, while for the region spectra the pass energy was 20 eV. For all of the samples, charge neutralization was necessary to correct the chemical shifts caused by charging. The investigated area was 700 x 300 µm. For depth profiling, Ar etching was performed. The etching rate was 10 nm / min related to Ta_2O_5 (acceleration voltage 3.8 kV with an extraction current of 160 µA). The evaluation and validation of the data were carried out with the software CASA-XPS version 2.3.18. Calibration of the spectra was done by adjusting the C1s signal to 284.5 eV. For deconvolution of the region files, background subtraction (linear or Shirley) was performed before calculation. Element binding energy database used is the NIST Standard Reference Database 20, Version 3.5.

3.4.4. Scanning electron microscopy (SEM) and Energy dispersive X-ray (EDX)

After immersion, to investigate the surface morphologies, samples after drying were directly examined using scanning electron microscopy (SEM, Phenom-World, Eindhoven, Netherlands). SEM in backscattering mode with an accelerating voltage of 15 kV was used to analyse the morphologies.

EDX is an analytical technique used for the elemental analysis or chemical characterization of a sample. A high-energy electron beam is used to eject the electron in an inner shell and create an electron hole. Subsequently, the electron in outer, higher-energy shell fill it and simultaneously the characteristic X-rays are released due to the energy difference between the inner and outer shell, as depicted in Fig. 3.7. The analytical depth can be calculated as following (Castaing's formula) [182]:

$$Z_m = 0.033(E_0^{1.7} - E_c^{1.7})\frac{\mathrm{A}}{\rho\,\mathrm{Z}} \qquad (3.3)$$

Wherer Z_m is the detected depth, E_0 is accelerating voltage (kV), E_c is minimum emission voltage (kV), A is atomic mass, ρ is the density of sample (kg/cm^3) and Z is the atomic number. Therefore, the nominal acceleration depth for Mg is about 3.5 µm under this condition.

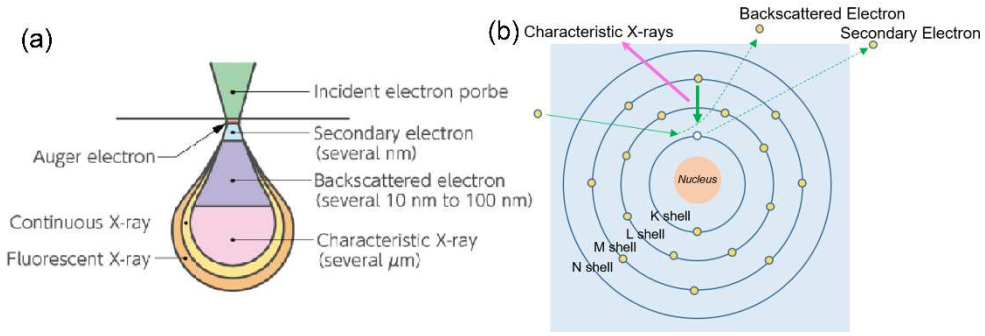

Figure 3.7: (a) Depth of quantum emission and spatial resolution of X-ray characterizations, (b) the generation of secondary electron, backscattered electron and characteristic X-rays [183] (JEOL Ltd, Freising, Germany).

Before the removal of outer precipitates layer, the cross sections of samples were prepared by embedding in resin (Demotec 30, Nidderau, Germany), with the cross sections oriented upwards and subsequently polished with colloidal silica suspension (Cloeren Technology GmbH, Wegberg, Germany) to a mirror-like surface. The chemical element mapping by using a scanning electron microscope (Tescan Vega3 SB, Brno, Czech Republic) equipped with energy dispersive X-ray spectrometer (EDX) was conducted for the resulting cross sections. Element mappings were performed using an accelerating voltage of 15 kV and the resolution was 256 pixels. The diameter of beam was 300-500 nm depending on the beam intensity used. The acquisition time was 80 ms per pixel. The area of the scanned surface depended on the magnification used. The pixel size was about 400 nm × 400 nm. The minimum limit of detection in our experiments was 1000 ppm. The deviation of counting statistics is 3-6 %. The weight percentages of phosphorus (P) or calcium (Ca) in degradation products near the Mg matrix were calculated from the mapping by using Iridium Ultra software (Eumex Instrumentebau GmbH, Heidenrod, Germany).

At least 80 sites of cross section for each sample were measured for the layer thickness from the BSE images of the degradation layer. The thickness of Ca/P-rich layer was measured from the mapping results using Adobe Photoshop CS6 (Adobe Systems Incorporated, San Jose, USA) and at least 10 measurements for each sample were performed.

3.5. Adsorption of proteins

3.5.1. Adsorption of fluorescent proteins during immersion

The adsorption of proteins on Mg surface during immersion was directly performed in Hank's balance salt solution (HBSS) and Dulbecco's modified eagle medium Glutamax-I (DMEM). 15 µg/mL fluorescent BSA or Fib (Alexa Fluor® 594 for BSA, Oregon Green 488 for Fib, Molecular Probes, Inc., Eugene, USA) in HBSS and DMEM were prepared before the immersion test.

Pure Mg samples were immersed in the media as a ratio of 0.2 g/L (sample/medium) under cell culture conditions. Media without samples in well plates (Greiner Bio-One, Kremsmünster, Germany) were conducted as controls. After 1 day of immersion, samples were taken out from the well plates, then cleaned with distilled water and dried at 50 °C in air. Subsequently, the samples were checked by using a fluorescence microscope (Nikon TI Eclipse, Düsseldorf, Germany) using Texas Red filter for BSA (Ex/Em: 590/622 nm) and FITC filter for Fib (Ex/Em: 496/524 nm) to examine the adsorption of proteins on Mg surface. Instrument parameters between samples were not changed to compare the adsorption of same protein except exposure time (as stated in the captions of figures), while the comparison between BSA and Fib was not performable due to the unidentified fluorescent properties, like bleaching time, excitation probability, etc..

Cross sections of samples after 2 days of immersion were prepared by embedding samples vertically into the resin (Demotec 30, Nidderau, Germany), then successively ground by 800#, 1200#, 2400# SiC abrasive paper, and subsequently polished with colloidal silica suspension (Cloeren Technology GmbH, Wegberg, Germany). Finally, the cross sections were analysed using fluorescence microscopy.

3.5.2. Adsorption of fluorescent proteins after immersion

To circumvent the adsorption complexity during immersion, the experiment was performed in two steps to separate the degradation process and the protein adsorption process as much as possible.

a) Immersion process: Mg samples were immersed in different media without proteins for 1 day under cell culture conditions;
b) Adsorption process: after immersion, the samples were cleaned with distilled water, then immersed in solution (water, HBSS or DMEM) with 15 µg/mL fluorescent BSA/Fib for 1 h under cell culture conditions, respectively.

Finally, Mg samples were cleaned with distilled water and dried in air, then examined using fluorescence microscopy.

3.5.3. Adsorption of proteins on possible degradation products

Preparation, characterization of the possible degradation products

The possible degradation products, $CaCO_3$, Mg-PO_4 and Ca-PO_4 were synthesized by using $CaCl_2$ (Fluka Chemie, Buchs, Switzerland), $MgCl_2$ (Merck, Darmstadt, Germany), $NaHCO_3$ (Merck, Darmstadt, Germany) and K_3PO_4 (Fluka Chemie, Buchs, Switzerland). The equivalent

volume of 6 mol/L $CaCl_2$ or $MgCl_2$ was gradually added to 4 mol/L K_3PO_4 to synthesize Ca-PO_4 or Mg-PO_4. $CaCO_3$ was prepared by adding the equivalent volume of 6 mol/L $CaCl_2$ to 6 mol/L $NaHCO_3$. After at least 30 min precipitation, the turbid solutions were centrifuged at 3000 rpm for 5 min (Rotina 420, Hettich, Tuttlingen, Germany) to remove the supernatant. Subsequently, the products were cleaned three times with distilled water, then dried at 70 ˚C. Commercial $MgCO_3$ (Sigma, Steinheim, Germany) was directly used as $MgCO_3$ degradation product.

X-ray diffraction (XRD, Bruker D8 Advance, Karlsruhe, Germany) operating in the reflection mode with Cu-Kα radiation (40 kV, 40 mA) was used to examine the products obtained. It was conducted from 15° - 75° at 0.02° intervals. The counting time was 1 s per points. Data analysis was carried out using analysis software (BrukerEVA and PDF-2 Release 2015 RDB).

Dynamic light scattering (DLS) is a widely used method for determining the size and mode of aggregation of proteins and other biomolecules in solution. A laser is focused on the sample, light scattered by the particles in the solution shows random intensity fluctuations due to the interference of the light scattered by individual molecules (Fig. 3.8a). The average frequency of these fluctuations can be used to measure the moving speed of particle based on the autocorrelation function (ACF, Eq. 3.4). Furthermore, the particle sizes can be deduced using the Stokes–Einstein equation (Eq. 3.6).

$$g(t) = 1 + e^{2Dq^2t} \quad (3.4)$$

$$\mathrm{q} = \frac{4\pi \mathrm{n}}{\lambda} \sin\frac{\theta}{2} \quad (3.5)$$

$$\mathrm{D} = \frac{\mathrm{k_b}T}{3\pi\eta d} \quad (3.6)$$

Where q is the scattering vector, n is refractive index, λ is the wavelength of light, θ is the scattering angle, t is time, D is the diffusion constant, k_b is the Boltzmann constant, *T* is the temperature, η is the viscosity of the solution, *d* is the hydrodynamic radius of particle.

Zeta potential is defined as the potential at the slipping plane, while the potential at the position far from the particle surface, as reference, is defined to zero (Fig. 3.8b). The charged particles or molecules migrates towards an electrode if a field is applied. The moving speed is proportional to the field strength and their zeta potential, which can be determined by the changes of laser frequency after scattering. The zeta potential (Z) can be calculated from the Smoluchowski equation:

$$Z = \frac{\eta}{\varepsilon_0 \varepsilon_r} U \qquad (3.7)$$

Where ε_0 and ε_r are the dielectric constants in vacuo and of the solvent, respectively. *U* is the mobility of particles or molecules in solution.

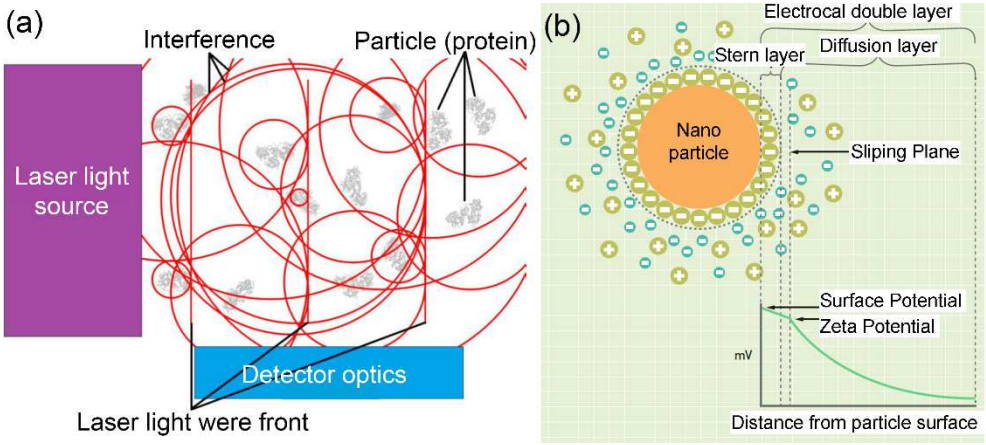

Figure 3.8: (a) Scattering effect from particles (proteins) in solution. Detector optics guide the scattered light to the detector which reads out intensity fluctuations over different time intervals [184] (Xtal Concepts GmbH, Hamburg, Germany). (b) Electrical double layer of the particle surface [185] (Malvern Instruments GmbH, Herrenberg, Germany). When an electric field is applied to charged particles in the suspension, particles move toward an electrode opposite to its surface charge. It leads to the frequency shift of the scattered light, which can be used to determine the mobility and zeta potential of particle.

In this thesis, the prepared degradation products were distributed in distilled water to determine the particle size by using DLS (SpectroSize 300, Xtal Concepts GmbH, Hamburg, Germany). The scattering angle was 90˚. The refractive index and the viscosity of the solvent were set to 1.33 and 1.006 mPa s. Every measurement was repeated three times with 10 - 20 runs at room temperature.

These four different products were distributed in water and 1 mg/mL Fib solution for zeta potential measurements, which was performed with the help of Dr.-Ing. Marion Frant at Institute for Bioprocessing and Analytical Measurement Techniques (IBA, Heiligenstadt, Germany). Three replicates were determined using Zetasizer Nano ZS90 (Malvern Instruments GmbH, Herrenberg, Germany).

Adsorption of proteins on degradation products

The artificial products were distributed on the well plates with distilled water. Subsequently, 2 mL 15 µg/mL fluorescent BSA or Fib in water were added to each wells, then the plates were incubated under cell culture conditions for 1 h. After that, the solution was carefully removed

from the plates. Afterwards, the plates were washed twice with distilled water, then dried at 50 ˚C and analysed by fluorescence microscopy.

The quantitative adsorption of proteins on different artificial products was performed as following: 10 mg artificial products was weighed in a 1.5 mL plastic tube (Carl Roth GmbH, Karlsruhe, Germany), then 1 mL 0.68 mg/mL BSA (Carl Roth GmbH, Karlsruhe, Germany) or Fib (Sigma-Aldrich, Saint Louis, USA) in water was added. Adsorption was performed for 1 hour under cell culture conditions. Afterwards, the solution was centrifuged for 5 min at 8000 rpm (Heraeus Biofuge Pico, Osterode, Germany). Finally, the supernatant was collected to measure the protein concentration by using BCA kit (Pierce Biotechnology, Rockford, USA). The concentrations of BSA and Fib before adsorption also were simultaneously determined. The control was performed in water without protein to determine the mass change before and after 1 h incubation.

3.6. Characteristics of Mg surface after immersion

3.6.1. Contact angle determination

Contact angles is used to quantify the wettability of a solid surface via the Young equation. It reflects the relative strength of the liquid, solid and vapor molecular interaction as shown in Fig. 3.9.

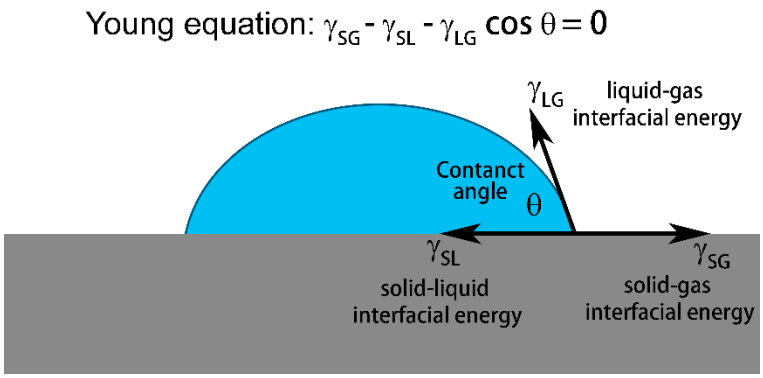

Figure 3.9: Scheme of a liquid drop on a surface showing the quantities in the Young equation.

Contact angles of Mg samples before and after immersion in HBSS and DMEM with or without protein adsorption were determined using a drop shape analyzer (DSA100, Krüss GmbH, Hamburg, Germany) at room temperature to evaluate the hydrophobicity of Mg surfaces. For each drop (5 µL) of deionized water, a sequence of contact angle was recorded by the Advance software (Krüss GmbH, Hamburg, Germany) for 35 s starting from the moment of the drop deposition. Finally, the contact angle at 30 s was used.

3.6.2. Surface topography

The Mg surface conditions before and after 1, 6 and 24 h of immersion in HBSS and DMEM were characterized using scanning electron microscopy (SEM, Phenom-World, Eindhoven, Netherlands) and profilometry (Bruker Nano GmbH, Tucson, USA). SEM was used in backscattering mode with an accelerating voltage of 15 kV. Three samples and at least four positions for each samples were checked for the surface topography and roughness by using profilometer at vertical scanning interferometry (VSI) mode (Fig. 3.10). Under VSI mode, the vertical resolution is about 1-5 nm for each objective, the maximum vertical range or surface variations can be up to 10 mm. The roughness of samples surface can be expressed as following:

The average deviation of the surface (S_a): $$S_a = \frac{1}{A}\iint Z\,dx\,dy \quad (3.8)$$

The root-mean-square deviation of the surface (S_q): $$S_q = \sqrt{\frac{1}{A}\iint Z^2\,dx\,dy} \quad (3.9)$$

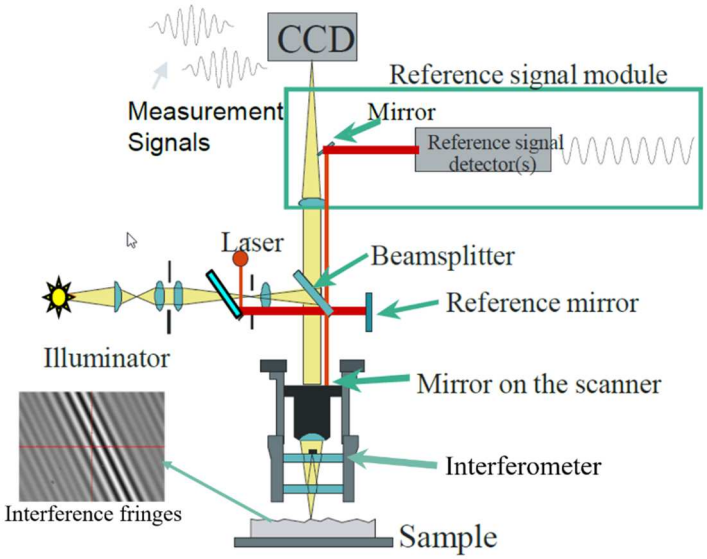

Figure 3.10: Basic white light interferometry scheme with Bruker's self-calibration HeNe laser. Interference microscope combines an interferometer and microscope into one instrument. The interferometer divides a beam of light into two beams and then recombines them to create an interference pattern. Interference will be constructive at some points, destructive at others, forming an interferogram. The imaging lens images the interferogram onto the CCD camera [186]. (Bruker Nano GmbH, Tucson, USA)

3.7. Thermodynamical calculation

To understand the formation of different degradation products in different media, the critical Mg^{2+} or Ca^{2+} concentration for different products ($Mg(OH)_2$, $MgCO_3$, $MgCO_3$ $3H_2O$,

$Mg_5(CO_3)_4(OH)_2{\cdot}4H_2O$, $Mg_3(PO_4)_2$ $8H_2O$, $CaCO_3$, $Ca_5(PO_4)_3(OH)$) was calculated according to the products solubility. At 37 ˚C, the solubility constants of different degradation products are listed as follows [77]:

$Mg^{2+}+2OH^- \rightarrow Mg(OH)_2$ $K_{sp}(Mg(OH)_2)= [Mg^{2+}]\,[OH^-]^2=5.62\times10^{-12}$ (3.10)

$Mg^{2+}+CO_3^{2-} \rightarrow MgCO_3$ $K_{sp}(MgCO_3)=[Mg^{2+}]\,[CO_3^{2-}]=3.09\times10^{-6}$ (3.11)

$3Mg^{2+}+2PO_4^{3-}+8H_2O \rightarrow Mg_3(PO_4)_2\,8H_2O$ $K_{sp}(Mg_3(PO_4)_2)=[Mg^{2+}]^3[PO_4^{3-}]^2=2.48\times10^{-28}$ (3.12)

$Mg^{2+}+CO_3^{2-}+3H_2O \rightarrow MgCO_3{\cdot}3H_2O$ $K_{sp}(MgCO_3\ 3H_2O)=[Mg^{2+}]\,[CO_3^{2-}]=3.24\times10^{-5}$ (3.13)

$5Mg^{2+}+5OH^-+4CO_3^{2-}+4H_2O \rightarrow Mg_5(CO_3)_4(OH)_2{\cdot}4H_2O$

$K_{sp}(Mg_5(CO_3)_4(OH)_2{\cdot}4H_2O)=[Mg^{2+}]^5\,[CO_3^{2-}]^4\,[OH^-]^2=3.73\times10^{-32}$ (3.14)

$Ca^{2+}+ CO_3^{2-} \rightarrow CaCO_3$ $K_{sp}(CaCO_3)= [Ca^{2+}]\,[CO_3^{2-}] = 3.63\times10^{-9}$ (3.15)

$5Ca^{2+}+3PO_4^{3-}+OH^- \rightarrow Ca_5(PO_4)_3(OH)$

$K_{sp}(Ca_5(PO_4)_3(OH))= K_{sp}(HA)= [Ca^{2+}]^5\,[PO_4^{3-}]^3\,[OH^-]=1.70\times10^{-59}$ (3.16)

For simplicity, the activity coefficients for all species are taken as unity. Hydroxyapatite, $Ca_5(PO_4)_3(OH)$, was chosen as reference for Ca-P salts formed in HBSSCa and DMEM. With regard to $Mg(OH)_2$, the critical Mg^{2+} concentration can be calcaulated as following:

$$C_{critical}(Mg^{2+})_{Mg(OH)_2} = \frac{K_{sp}(Mg(OH)_2)}{[OH^-]^2} = \frac{K_{sp}(Mg(OH)_2)\,[H^+]^2}{[K(H_2O)]^2} \quad (3.17)$$

Where $K(H_2O)$, the dissociation constant of water is 2.45×10^{-14} when the temperature is 37˚C [77].

In terms of Mg-CO_3 products,

$$C_{total}(CO_3^{2-}) = [H_2CO_3] + [HCO_3^-] + [CO_3^{2-}] + [CO_2] \quad (3.18)$$

$$K_{\alpha1}(H_2CO_3) = \frac{[H^+]\,[HCO_3^-]}{[H_2CO_3]} \quad (3.19)$$

$$K_{\alpha2}(HCO_3^-) = \frac{[H^+]\,[CO_3^{2-}]}{[HCO_3^-]} \quad (3.20)$$

where $K_{\alpha1}$ and $K_{\alpha2}$ are the dissociation constants of H_2CO_3 and HCO_3^- as 1.59×10^{-4} and 5.62×10^{-11}, respectively [61]. Here, it should be noted that the concentration of CO_2 was kept

about 5% in the incubator and the equilibrium solubility is 170 mM [72]. This is the reason why Eq. (3.18) contains a part of $[CO_2]$. The concentration of free CO_3^{2-} is obtained by the combination of Eqs. (3.18-20):

$$[CO_3^{2-}] = \frac{C_{total}(CO_3^{2-})\ K_{\alpha1}\ K_{\alpha2}}{[H^+]^2 + [H^+]\ K_{\alpha1} + K_{\alpha1}\ K_{\alpha2}} \quad (3.21)$$

Therefore, the critical Mg^{2+} concentration for $MgCO_3$, nesquehonite and hydromagenesite can be calculated:

$$C_{critical}(Mg^{2+})_{MgCO_3} = \frac{K_{sp}(MgCO_3)}{[CO_3^{2-}]} = \frac{K_{sp}(MgCO_3)\{[H^+]^2 + [H^+]K_{\alpha1} + K_{\alpha1}\ K_{\alpha2}\}}{C_{total}(CO_3^{2-})K_{\alpha1}K_{\alpha2}} \quad (3.22)$$

$$C_{critical}(Mg^{2+})_{MgCO_3\ 3H_2O} = \frac{K_{sp}(MgCO_3 3H_2O)}{[CO_3^{2-}]} = \frac{K_{sp}(MgCO_3 3H_2O)\{[H^+]^2 + [H^+]K_{\alpha1} + K_{\alpha1}\ K_{\alpha2}\}}{C_{total}(CO_3^{2-})K_{\alpha1}K_{\alpha2}} \quad (3.23)$$

$$C_{max}(Mg^{2+})_{Mg_5(CO_3)_4(OH)_2\ 4H_2O} = \sqrt[5]{\frac{K_{sp}(Mg_5(CO_3)_4(OH)_2\ 4H_2O)}{[CO_3^{2-}]^4\ [OH^-]^2}}$$

$$= \sqrt[5]{\frac{K_{sp}(Mg_5(CO_3)_4(OH)_2\ 4H_2O)\{[H^+]^2 + [H^+]K_{\alpha1} + K_{\alpha1}\ K_{\alpha2}\}^4 [H^+]^2}{\left(C_{total}(CO_3^{2-})K_{\alpha1}K_{\alpha2}\right)^4\ [K(H_2O)]^2}} \quad (3.24)$$

Similarly, the following equation can be deduced to calculate the concentration of PO_4^{3-} in solution:

$$[PO_4^{3-}] = \frac{C_{total}(PO_4^{3-})K_{\alpha1}K_{\alpha2}K_{\alpha3}}{[H^+]^3 + [H^+]^2K_{\alpha1} + [H^+]K_{\alpha1}K_{\alpha2} + K_{\alpha1}K_{\alpha2}K_{\alpha3}} \quad (3.25)$$

Where, $K_{\alpha1}$, $K_{\alpha2}$ and $K_{\alpha3}$ are the dissociation constants of H_3PO_4, $H_2PO_4^-$, and HPO_4^{2-} as 5.68×10^{-3}, 6.84×10^{-8} and 6.61×10^{-13}, respectively [187]. Hence, the critical Mg^{2+} concentration for $Mg_3(PO_4)_2\ 8H_2O$ can be calculated:

$$C_{max}(Mg^{2+})_{Mg_3(PO_4)_2\ 8H_2O} = \sqrt[3]{\frac{K_{sp}(Mg_3(PO_4)_2\ 8H_2O)}{[PO_4^{3-}]^2}}$$

$$= \sqrt[3]{\frac{K_{sp}(Mg_3(PO_4)_2\ 8H_2O)\ ([H^+]^3 + [H^+]^2K_{\alpha1} + [H^+]\ K_{\alpha1}K_{\alpha2} + K_{\alpha1}K_{\alpha2}K_{\alpha3})^2}{\left(C_{total}(PO_4^{3-})K_{\alpha1}K_{\alpha2}K_{\alpha3}\right)^2}} \quad (3.26)$$

When Ca^{2+} is present in media, the critical Ca^{2+} concentration for $CaCO_3$ and hydroxyapatite can be deduced by the following equations:

$$C_{critical}(Ca^{2+})_{CaCO_3} = \frac{K_{sp}(CaCO_3)}{[CO_3^{2-}]} = \frac{K_{sp}(CaCO_3)\{[H^+]^2+[H^+]K_{\alpha1}+K_{\alpha1}K_{\alpha2}\}}{C_{total}(CO_3^{2-})K_{\alpha1}K_{\alpha2}} \quad (3.27)$$

$$C_{max}(Ca^{2+})_{HA} = \sqrt[5]{\frac{K_{sp}(HA)}{[PO_4^{3-}]^3\,[OH^-]}}$$

$$= \sqrt[5]{\frac{K_{sp}(HA)\{[H^+]^3+[H^+]^2K_{\alpha1}+[H^+]K_{\alpha1}K_{\alpha2}+K_{\alpha1}K_{\alpha2}K_{\alpha3}\}^3\,[H^+]}{(C_{total}(PO_4^{3-})K_{\alpha1}K_{\alpha2}K_{\alpha3})^3\,K(H_2O)}} \quad (3.28)$$

3.8. Statistical analysis

The data were analysed and plotted using the software Origin 9.0 (Originlab Corporation, Wellesley Hills, USA). Standard analysis comparing more than two treatments was done by one-way analysis of variance (ANOVA) on ranks with Dunn's multiple comparison post hoc tests. Significance level: (*): $p<0.05$, (**): $p<0.01$. EDX mappings were organized by using Adobe Photoshop CS6 (Adobe Systems Incorporated, San Jose, USA).

4. Results

4.1. Effects of small organic molecules on Mg degradation

Degradation rate, pH, osmolality and layer thickness

The mean degradation depths of pure Mg after 3, 7 and 14 days of exposure in different media are depicted in Fig. 4.1. After 3 days of immersion, there was no significant difference between the mean degradation depths in different media. However, after a relatively long immersion (14 days), the samples immersed in media with organic components showed a higher degradation depth than the control (in HBSS), especially for those in media with more than one kind of organic components.

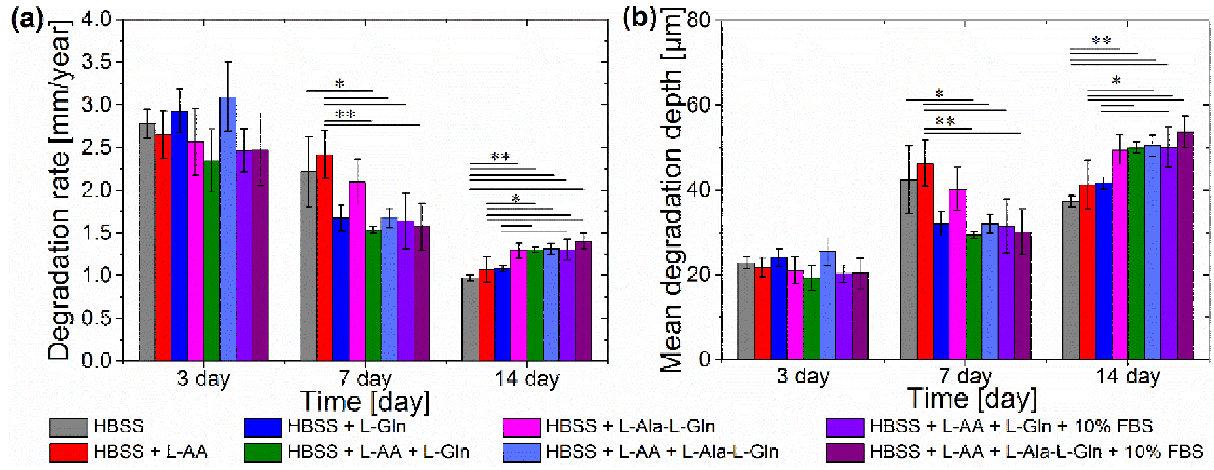

Figure 4.1: Degradation rates (a) and mean degradation depths (b) of pure Mg after immersion for 3, 7 and 14 days in different media under cell culture conditions. (One-way ANOVA, Dunn's test, Significance level: (*): $p<0.05$, (**): $p<0.01$)

The changes in pH and osmolality of the degradation media were measured after each change of media, as shown in Fig. 4.2. As expected, both the pH and the osmolality increased irrespective of the used media compared to those without samples. The increase in pH was generally higher for HBSS than other media, while the increase in osmolality showed an adverse trend, especially for the media with more than one kind of organic components. The osmolality of all media generally decreased with incubation time, suggesting the decrease of degradation rates with immersion time.

Generally, the thickness of the degradation layer tended to increase with the incubation time (Fig. 4.2c). Single organic component, like L-AA, L-Gln, L-Ala-L-Gln, led to the thickening of degradation layer. In contrast, when more than one kind of organic components was present, the layer thickness sharply decreased compared to that formed in HBSS.

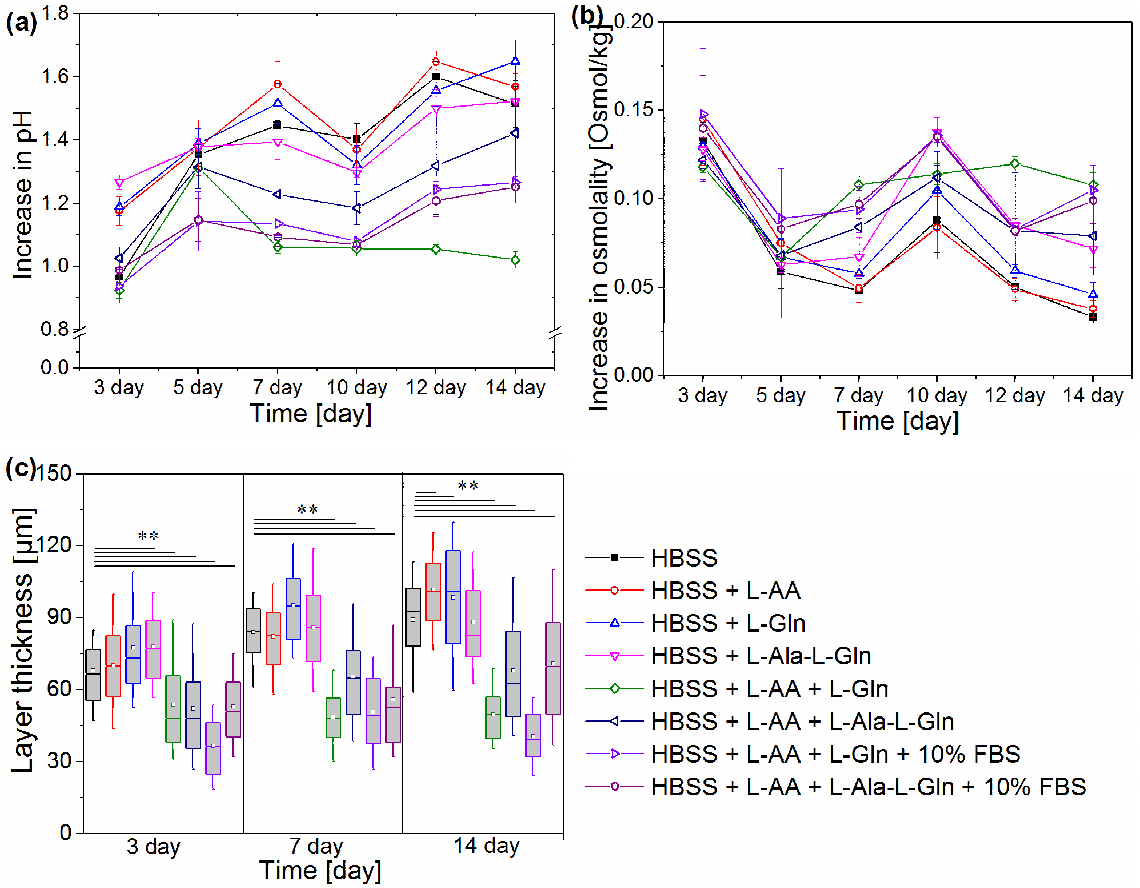

Figure 4.2: Changes in pH (a) and osmolality (b) after different days of incubation under cell culture conditions in different media, Box and Whisker plot of the layer thickness (c) after different incubation time in different media. (The boxes (bottom to top) show the 25th percentile, median and 75th percentile. The whiskers mark the 10th and 90th percentiles, the rectangular points in the box are average values, significance level: (*): $p<0.05$, (**): $p<0.01$)

The concentration of L-Gln during immersion

To verify the participation of L-Gln in the formation of degradation products, the concentration of L-Gln was measured during incubation as shown in Fig. 4.3b. Since L-Gln is not stable during incubation and it could deaminate with the increase of pH, pH of media were also determined during the incubation (Fig. 4.3a). The range of the on-line pH device (pH: 5~9) limited the determination of pH, which led to a vacancy during the first several hours of immersion. However, it could be seen that the pH value reached a comparably stable value after about 20 hours of immersion. The concentrations of L-Gln were also measured when pH was adjusted to 8.5, 9.5 and 12 without sample (Fig. 4.3b), it was stable at around 1.4 mM, which indicated after 20 hours of immersion the deamination of L-Gln had little influence on the concentration of L-Gln. However, the concentration of L-Gln with samples decreased with further incubation (as indicated by the grey background in Fig. 4.3b), suggesting the participation of L-Gln in the process of degradation by adsorption or other ways.

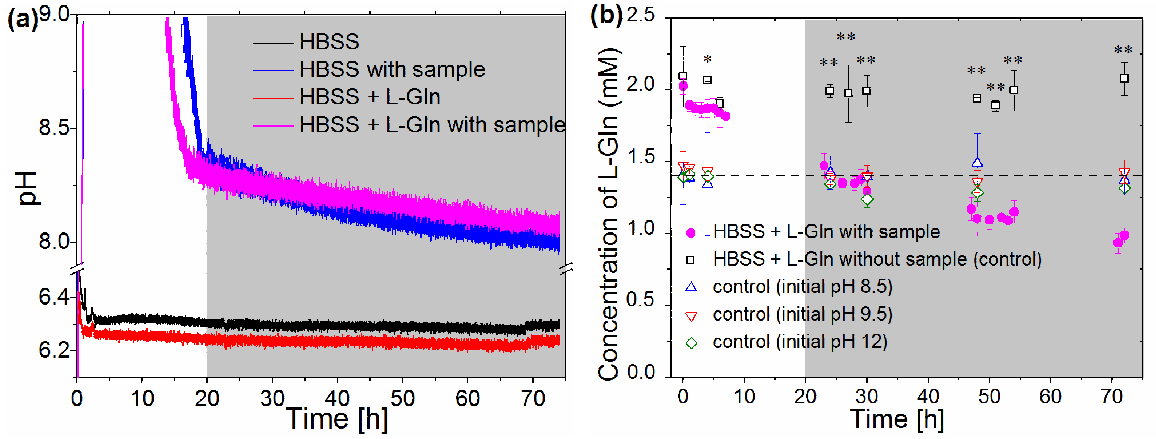

Figure 4.3: The changes of pH (a) and the concentration of L-Gln (b) during the immersion. The absence of data during the initial immersion resulted from the range of on-line pH device (measurement range: pH 5 - 9), when pH is higher than 9, it can not be determined by the device. Significance level: (*): $p<0.05$, (**): $p<0.01$. The grey background indicates the stable pH region.

Surface morphology

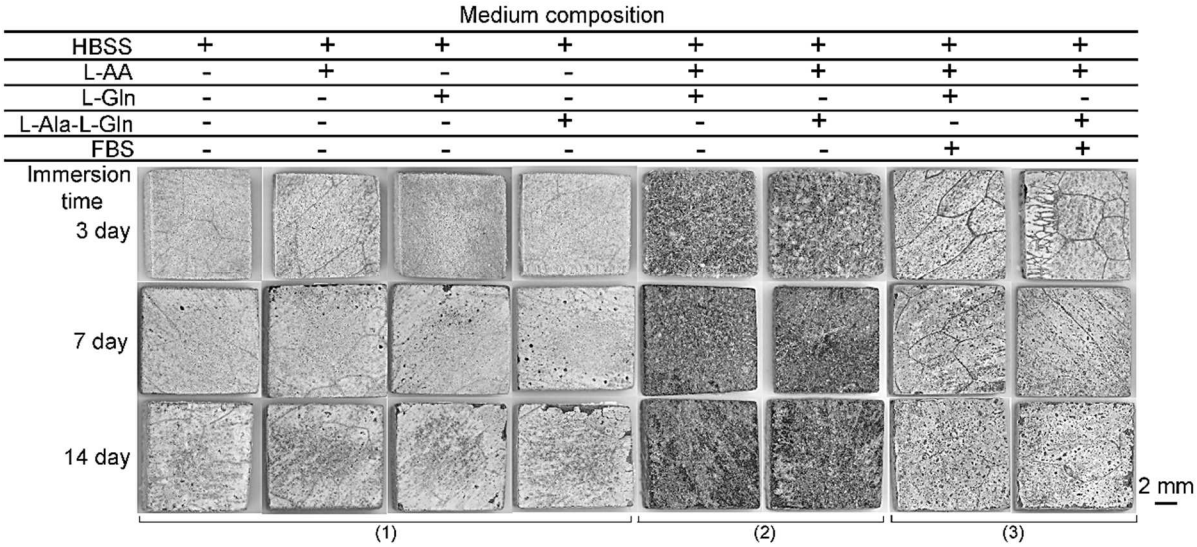

Figure 4.4 Optical images of samples after immersion in different media for different time. The compositions of media are listed in the above table, + refers to the existence of the component in medium, - refers to the absence of the component in medium. (1) refers to the surfaces in HBSS or HBSS with one kind of organic component, (2) refers to the surfaces in HBSS with two kinds of organic components, (3) refers to the surfaces in HBSS with three kinds of organic components.

All samples after immersion showed a blackish surface with some white precipitates, as shown in the optical images (Fig. 4.4). Two kinds of precipitates with different morphologies can be determined. A detailed comparison of the sample surfaces after degradation is shown in Fig. 4.5. From the SEM images (corresponding to the optical images), the white precipitates in HBSS and HBSS with one kind of organic components showed a conglomerate of very thin platelets. When

two kinds of organic components were added in HBSS, a well-formed needle-like precipitate layer was present on the surface. However, the needles gradually diminished with immersion time, indicating that the needles were not stable under this condition. The addition of FBS had further influence on the morphology of the precipitates on the surface. The detailed morphologies are shown in the images with a higher magnification (Fig. 4.5).

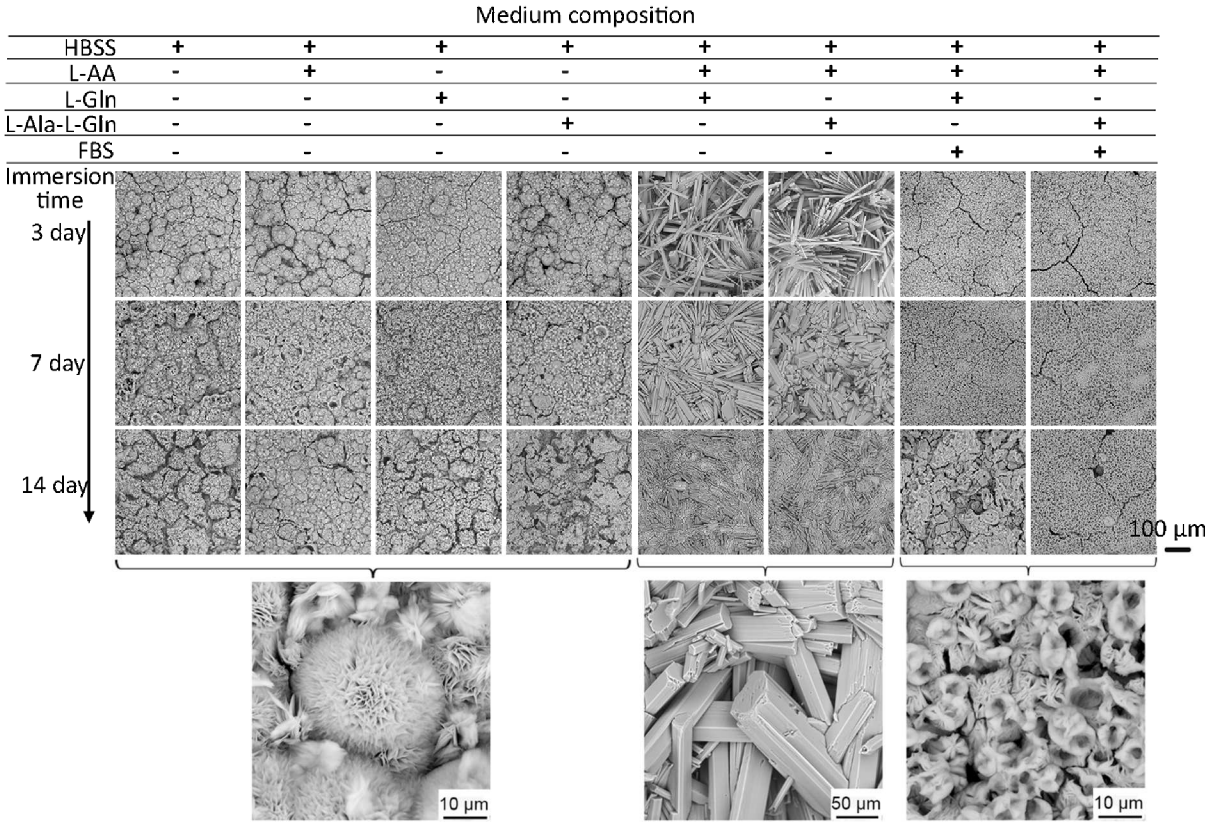

Figure 4.5: SEM images (corresponding to Fig. 4.4) of samples immersed in different media for different time.

Composition of degradation products

Since the samples with the same morphology had a reproducible spectrum, typical spectra of the degradation layer with different morphology were selected to present the XRD results. As shown in Fig. 4.6a, the results revealed that hydromagnesite (reference card 00-070-1177) and dypingite (reference card 00-29-0857 and 00-23-1218) were the main components of the conglomerate composed of thin platelets, while the well-formed needles were nesquehonite (reference card 00-020-0669). The precipitates formed in HBSS containing FBS were also identified as nesquehonite, although the morphology of precipitates changed after the addition of FBS (Fig. 4.5). However, after the removal of the “outer” precipitates, the morphologies of the “inner” degradation layers formed in different media showed little difference (SEM images in Fig. 4.6a). In addition, only several weak peaks from Mg were examined from the XRD patterns, suggesting the amorphous state or the nanocrystals of the “inner” degradation products.

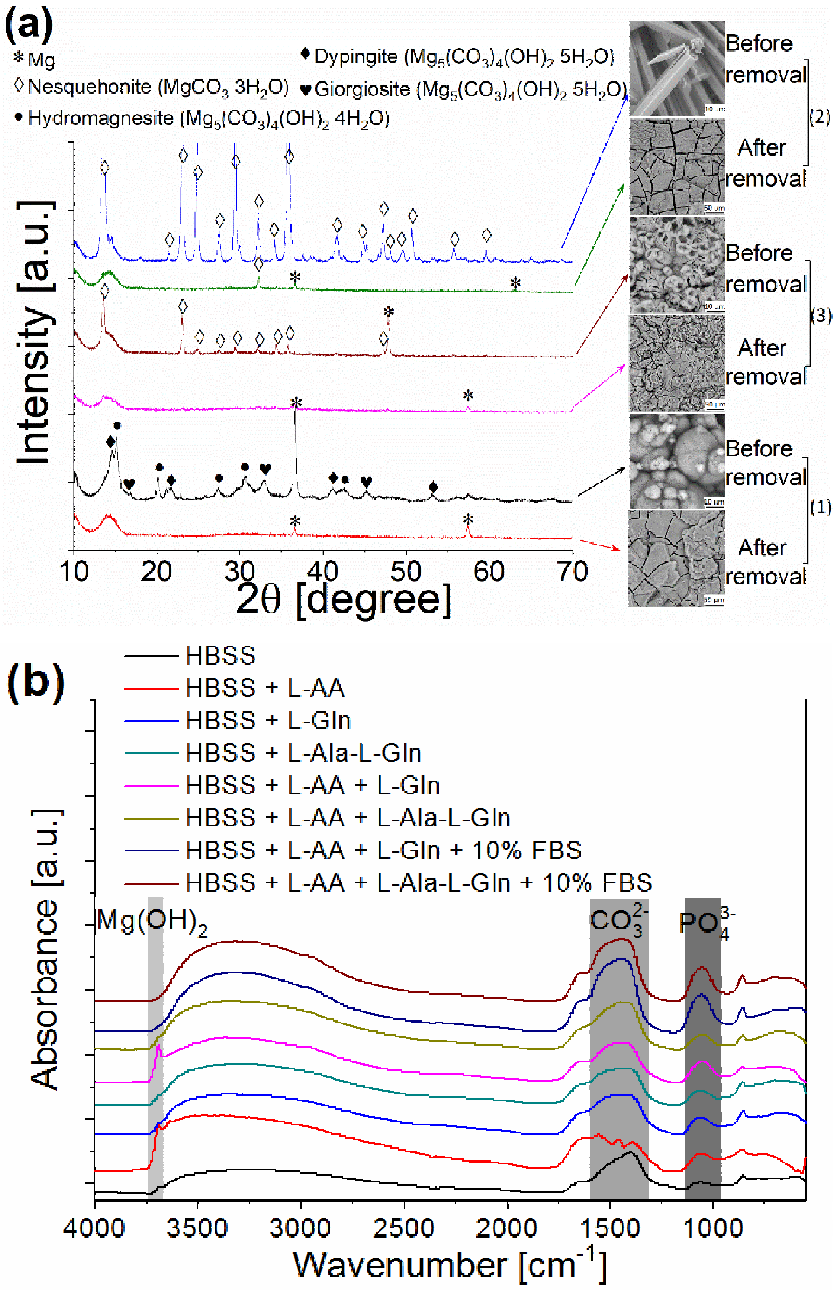

Figure 4.6: (a) XRD patterns of samples with different morphologies before and after the removal of white precipitates (1) refers to the surfaces in HBSS or HBSS with one kind of organic components, (2) refers to the surfaces in HBSS with two kinds of organic component, (3) refers to the surfaces in HBSS with three kinds of organic components. (b) IR reflection spectra of the "inner" degradation layers on Mg after 14 days of exposure in different media.

To give an insight into the composition of the "inner" degradation layer, IR reflection spectra were conducted for the samples after the removal of the "outer" precipitates by adhesive tape. The spectra from the surface of the "inner" degradation layer formed in different media gave similar information, indicating similar components of all "inner" degradation layers. The spectra of samples in different media are all provided in Fig. 4.6b. The band at 860 cm^{-1} is assigned to the

carbonate bending vibration [188] and the band around 1050 cm^{-1} is associated with the asymmetric stretching of phosphate [189], while strong IR signals in the range of 1400-1550 cm^{-1} arise from the anti-symmetrical stretching of CO_3^{2-} and/or amide II of organic components [72, 190]. The shoulder at 1640 cm^{-1} is ascribed to an OH-bending mode of water and/or amide I of organic molecules [116]. The broad band centred near 3500 cm^{-1} is attributed to the stretching vibration of the hydroxyl group. This broad band stems mainly from strong H bonding of water inside the "inner" degradation products, which absorbed on the degradation products or embedded in interstitial spaces of degradation products [111]. Moreover, a weak sharp band at 3698 cm^{-1} is related to the free hydroxyl group, indicating the presence of $Mg(OH)_2$ in the "inner" layer [188]. Therefore, it can be confirmed that the "inner" degradation products were mainly magnesium carbonate, phosphate and magnesium hydroxide. As previously proposed [73], MgO most probably is also present. The non-detection of MgO in our results is due to the high signal to noise ratio below 600 cm^{-1}, while Mg-O vibrational modes give rise to bands below 560 cm^{-1} [116].

Chemical element mapping

To validate the variations in the chemical composition of the Mg surface immersed in different solutions, chemical element mapping was conducted for the cross sections of degradation layers before the removal of crystalline precipitates. The distributions of elements, carbon (C), oxygen (O), phosphorous (P), magnesium (Mg) and calcium (Ca) were probed for all samples after immersion (Ca only existed on the degradation layer formed in the media with FBS). The detected amount of S, Na and Cl was negligible for all samples (< 0.5 wt.%), hence the corresponding mappings are not presented in Fig. 4.7. The contrast and brightness of figures were adjusted to visualize the qualitative difference.

To highlight the most important points, element mappings of the degradation layers with different morphologies were selected to present the results (Fig. 4.7). As expected, the existence of C, O and Mg in the degradation layer supports that carbonate was one of the degradation products as revealed by both XRD and IR reflection spectra. Due to the similarity of the compositions between the "outer" precipitates and the "inner" degradation layer, it was hard to distinguish the boundary between these two layers. However, there was an obvious difference for the distribution of P in degradation products near Mg matrix. The existence of P indicated the formation of phosphate in the degradation layer. For the samples incubated in media with FBS, a thin P/Ca-rich layer was formed after 3 days of incubation, indicating the formation of a more compact layer for Mg against the attack of aggressive ions in media with FBS [83]. The distribution of Ca was in accordance with that of P for the samples immersed in media with FBS, indicating the formation of Ca-P salts.

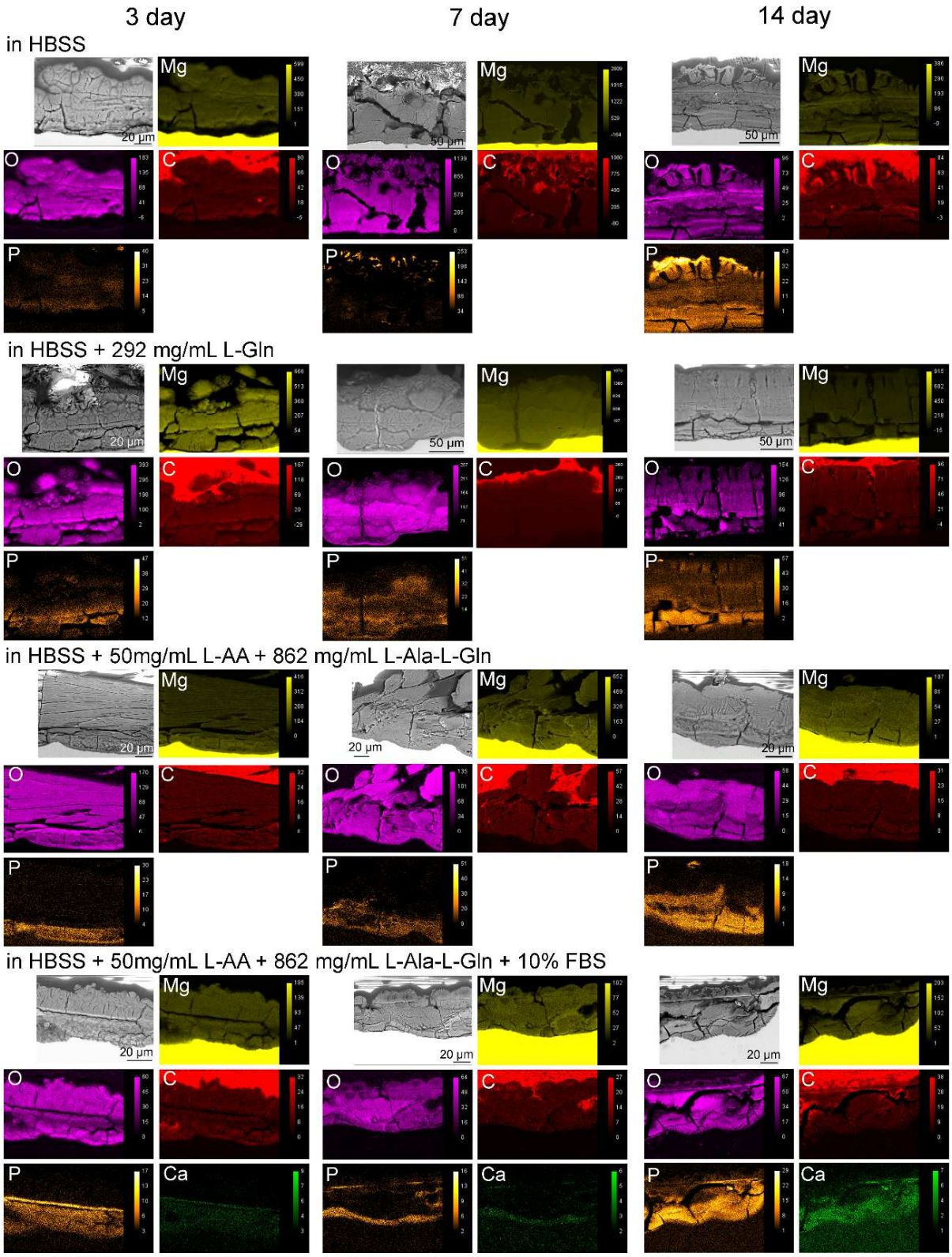

Figure 4.7: Backscattered electron (BSE) images and chemical element mappings of Mg samples exposed to HBSS with different organic components for different days.

The weight percentage of P in the degradation products near the Mg matrix was analysed according to the chemical element mapping to get the quantitative difference of the chemical

compositions of the degradation layer. As shown in Fig. 4.8, after the addition of organic components, the contents of P in the degradation products significantly increased, especially for those media with more than one kind of organic components. Moreover, the values also rose with immersion time. However, it should be noted that the content of P is quite low (< 6 wt.%) in the degradation products.

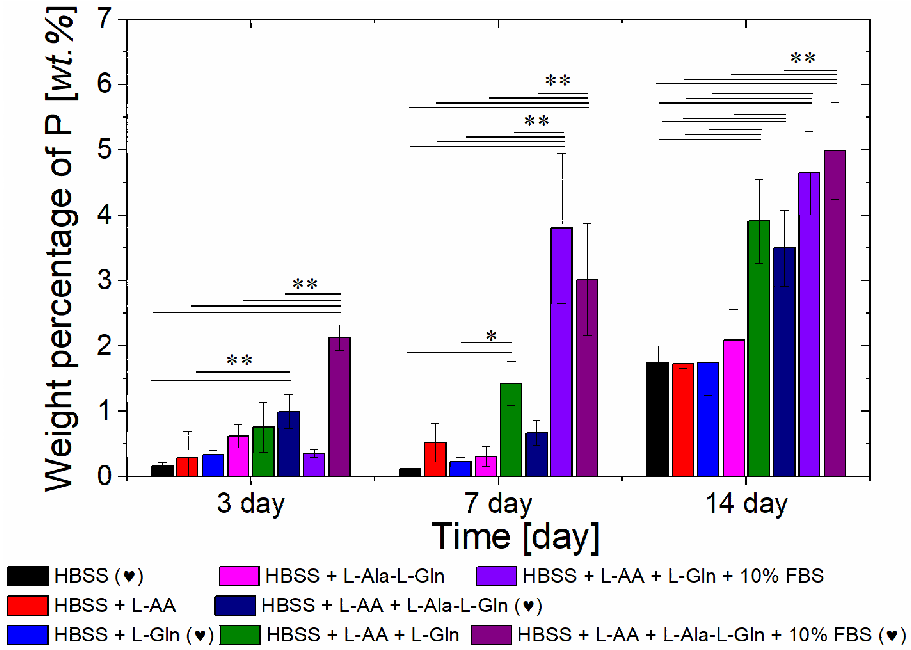

Figure 4.8: Weight percentage of P in degradation products near the Mg matrix formed in different media. (One-way ANOVA, Dunn's test, Significance level: (*): p<0.05, (**): p<0.01. ♥ refers to the mapping results in Fig. 4.7)

4.2. Effect of proteins on Mg degradation

4.2.1. Static conditions

Degradation rate, pH, osmolality

The degradation rates and mean degradation depths of pure Mg in different media under static conditions are displayed in Fig. 4.9. The results showed that Mg degraded much slower in HBSSCa and DMEM than in HBSS. The addition of BSA and FBS into HBSS and DMEM significantly decreased the degradation rate of Mg during immersion. Moreover, FBS showed a stronger degradation inhibition effect on Mg degradation than BSA, indicating the inhibitory effect of other components in FBS. However, no significant decrease is visible in HBSSCa when either BSA or FBS is present, suggesting the weak influence of protein on Mg degradation in this medium.

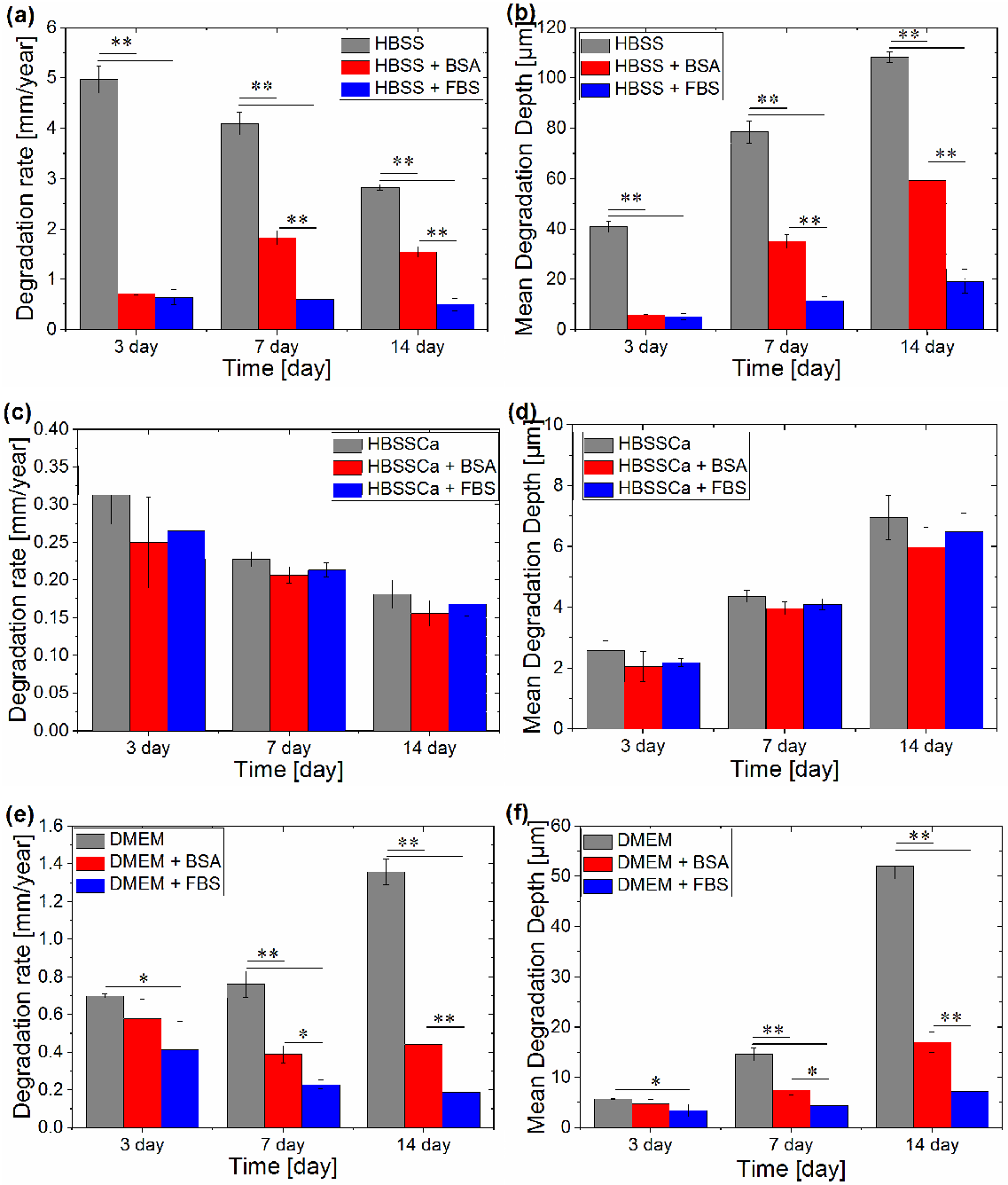

Figure 4.9: Degradation rate and mean degradation depth of pure Mg in HBSS-based (a, b), HBSSCa-based (c, d) and DMEM-based (e, f) media after different immersion time under static conditions. (One-way ANOVA, Dunn's test, Significance level: (*): $p<0.05$, (**): $p<0.01$)

The increases of pH and osmolality of media during immersion are shown in Fig. 4.10. Generally, both pH and osmolality increased irrespective of media used. In HBSS, pH significantly increased by about 1.4 after 1 day of immersion, and then remained stable. In comparison, when proteins were present in HBSS, pH gradually increased during the first 2-3 days of immersion, especially in HBSS + 10% FBS. This can be ascribed to the faster degradation of pure Mg in HBSS than in HBSS + BSA and HBSS + FBS and the buffering ability of proteins (carboxyl-group and amino

group). In HBSSCa-based media, pH gradually increased with immersion time, indicating the continuous degradation of Mg during immersion. No significant difference can be observed between HBSSCa, HBSSCa + BSA and HBSSCa + FBS, except a slightly lower pH increase in HBSSCa + FBS. In DMEM, the increase of pH was much lower than HBSS and HBSSCa. BSA and FBS further inhibited the increase of pH.

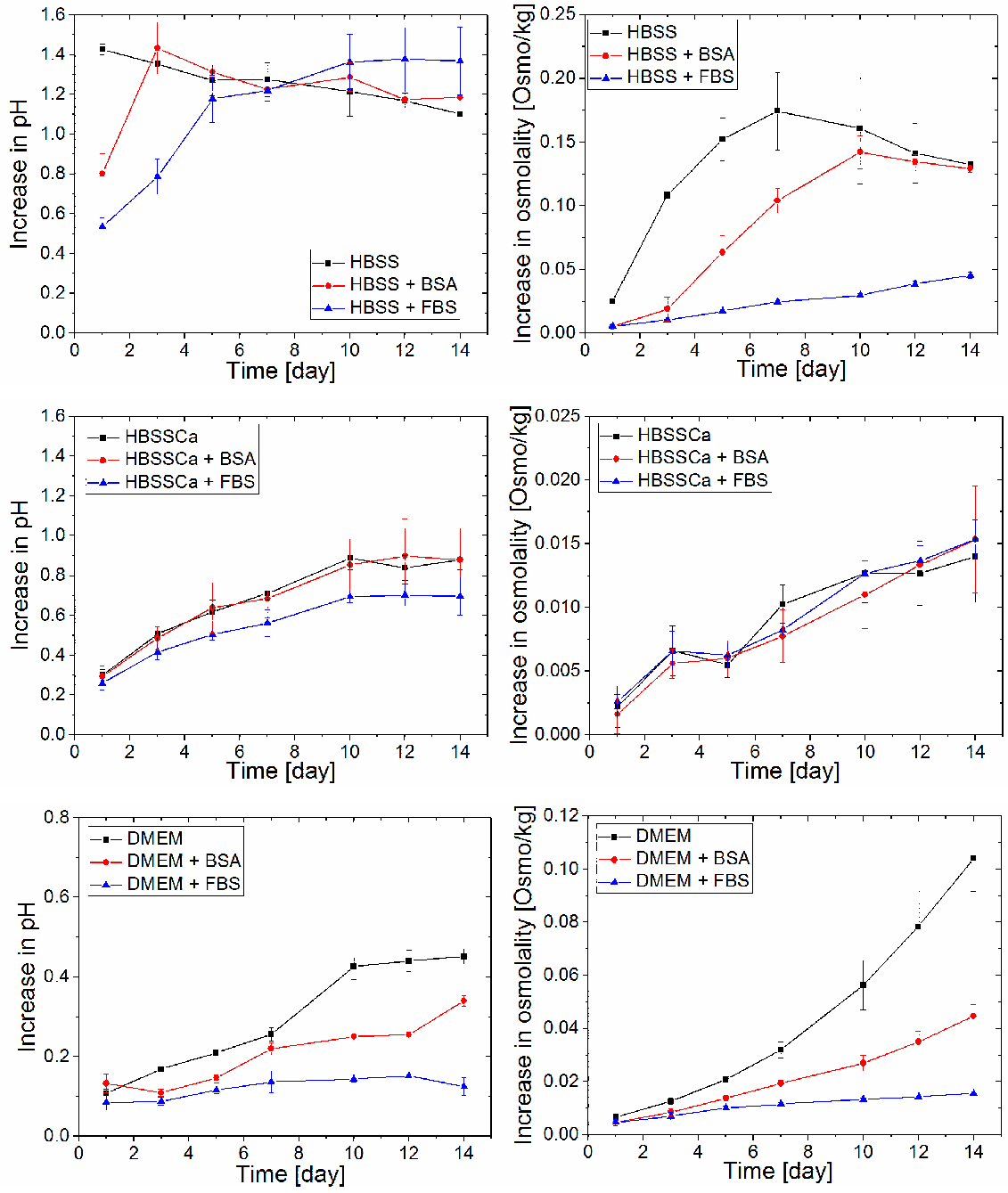

Figure 4.10: Increases in pH and osmolality of various media when Mg was immersed under static conditions.

The increase of media osmolality showed a similar tendency to the change of pH. Fast and obvious increase of osmolality was observed in HBSS, followed by HBSS + BSA, then it slowly

decreased. This should result from the fast degradation of Mg and the formation of precipitates (as shown in the surface morphology, Fig. 4. 12). In HBSSCa-based media, the increase of osmolality is quite small and it showed no difference between in presence or absence of proteins. The addition of proteins to DMEM led to a lower osmolality, which was more significant for FBS than BSA.

Surface morphology

The optical images for samples immersed in different media are taken after different immersion time to present the overall degradation surface, as shown in Fig. 4.11. During the initial immersion (3 day), all samples showed a blackish surface. It became white in HBSS-based and DMEM-based media with further immersion. Moreover, some white precipitates were formed on Mg surface in HBSS-based media. However, in HBSSCa-based media, some bright dots were formed on blackish surface, and they spreaded over the whole surface after 14 days of immersion.

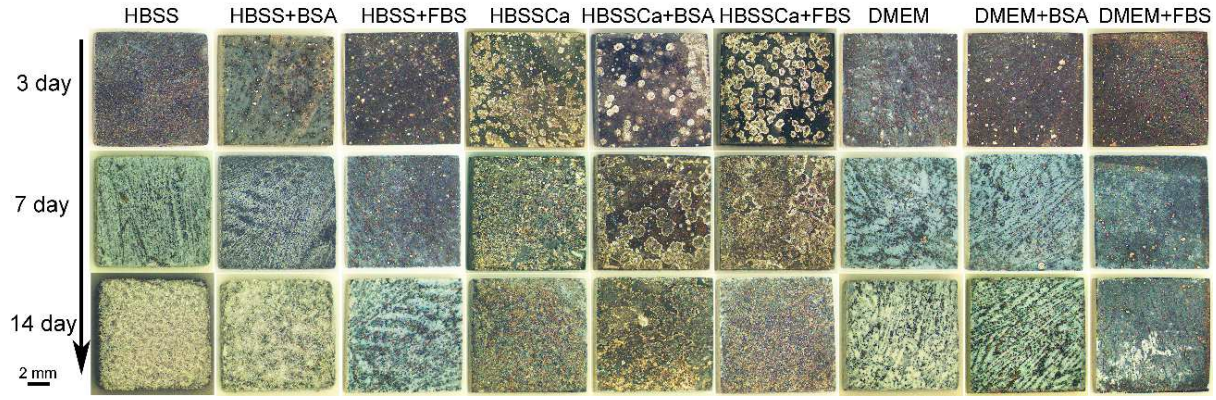

Figure 4.11: Optical images of pure Mg after immersion in different media for 3, 7 and 14 days under static conditions.

Sample morphologies after immersion in different media for different time are displayed in Fig. 4.12. In HBSS, the breakage of degradation layer can be observed after 3 and 7 days of immersion, with a decrease of the content of P in degradation layer over immersion time as shown in EDX results (Fig. 4.12). Afterwards, a conglomerate of very thin platelets was formed on Mg surface. In HBSS + BSA, the degradation layer was also broken after 7 days of immersion accompanied by the decrease of P from 13.1 wt.% to 7.5 wt.%, then needle-like precipitates were formed on Mg surface. However, the degradation layer formed in HBSS + FBS and the wt.% of P and Ca were stable during 14 days of *immersion*. The addition of proteins (BSA or FBS) seems to increase the wt.% of P (and Ca in the case of HBSS + FBS) in degradation products and to prevent the degradation layer from breakage.

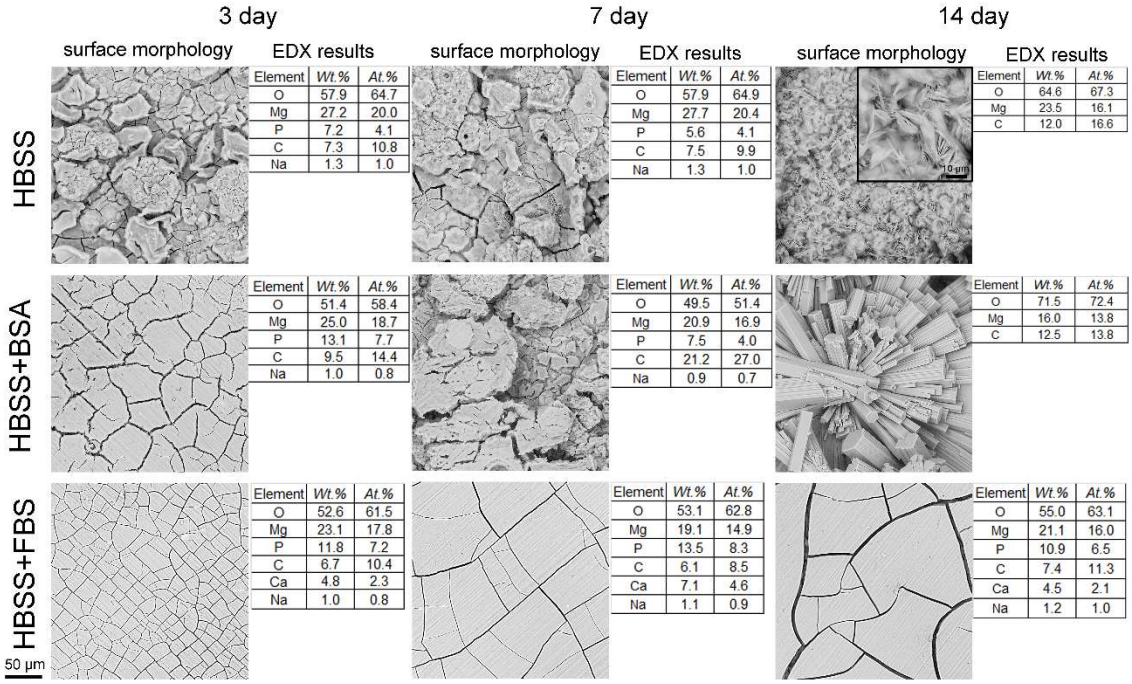

Figure 4.12: SEM images and the corresponding EDX results for the samples immersed in different medium after 3, 7 and 14 days of immersion under static conditions. (EDX results are the average values obtained from at least 6 points analysis)

In HBSSCa-based media, normal morphology (Fig. 4.13a) after immersion can be observed except some localised degradation (Fig. 4.13b and c). Some large particles (Fig. 4.13b) were formed on Mg surface with high contents of P and Ca, indicating the formation of Ca-P salts. The top of the degradation layer seemed to dissolve or break during immersion (Fig. 4.13c) with a lower wt.% of P and Ca (point E) compared with the normal degradation positions (point D). Meanwhile, some small white particles were formed on these positions with a higher wt.% of P and Ca (point F), suggesting the formation of Ca-P particles on these positions. Additionally, the peeling off of the top degradation layer was found (Fig. 4.13d) and a higher wt% of Ca and P were found in the top degradation layer. For the normal positions, average EDX results were shown in Table 4.1. It revealed a higher content of P and Ca in degradation layer in the presence of BSA or FBS compared to that in HBSSCa. Moreover, the content of P and Ca seemed to decrease with immersion time in HBSSCa and HBSSCa + BSA, while the content of Ca increased in the degradation layer for samples immersed in HBSSCa + FBS.

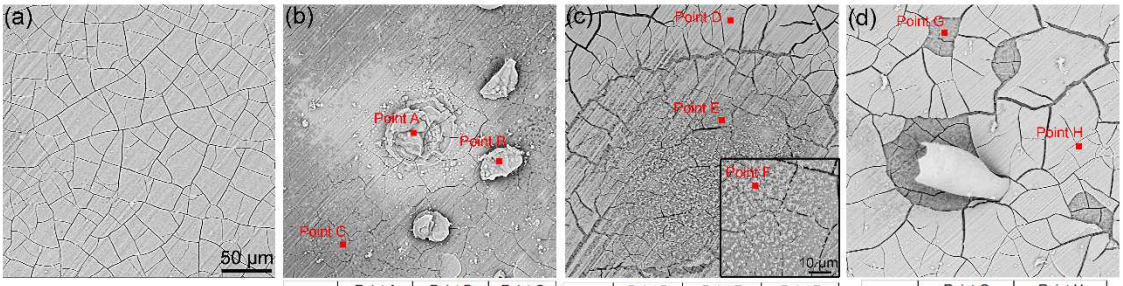

	Point A		Point B		Point C	
Element	*Wt.%*	*At.%*	*Wt.%*	*At.%*	*Wt.%*	*At.%*
O	55.7	66.6	50.1	62.7	54.5	62.9
Mg	10.5	6.6	11.8	9.8	30.4	23.1
P	10.7	8.3	10.6	6.8	5.0	3.0
C	6.3	10.0	5.8	9.7	5.8	9.0
Ca	15.4	7.3	21.0	10.5	3.1	1.4
Na	1.5	1.2	0.4	0.2	-	-
Cl	-	-	0.3	0.3	1.1	0.6

	Point D		Point E		Point F	
Element	*Wt.%*	*At.%*	*Wt.%*	*At.%*	*Wt.%*	*At.%*
O	49.0	58.7	47.0	52.7	44.3	52.5
Mg	14.2	11.2	22.2	16.4	19.2	15.0
P	14.1	8.7	7.9	4.6	11.1	6.8
C	9.3	14.8	15.0	22.5	12.3	19.5
Ca	12.7	6.1	7.2	3.2	12.0	5.7
Na	0.7	0.6	0.7	0.6	-	-
Cl	-	-	-	-	1.1	0.6

	Point G		Point H	
Element	*Wt.%*	*At.%*	*Wt.%*	*At.%*
O	53.4	60.3	43.6	50.8
Mg	27.2	20.2	16.2	12.4
P	6.1	3.5	12.8	7.7
C	9.4	14.2	14.8	22.9
Ca	3.9	1.8	12.1	5.6
Na	-	-	0.6	0.5

Figure 4.13: SEM images and EDX results for the samples immersed in HBSSCa-based media under static conditions. (EDX results are the average values obtained from at least 3 points analysis)

Table 4.1: Average EDX results (wt.%, at least 6 points analysis) for degradation surface of the samples immersed in different media after 3, 7 and 14 days of immersion.

Medium	time	Element (wt.%)						
		O	Mg	P	C	Ca	Na	Cl
HBSSCa	3 d	53.5 ± 2.6	28.9 ± 3.4	6.1 ± 1.7	7.6 ± 0.6	3.0 ± 0.7		0.9 ± 0.4
	7 d	53.1 ± 1.9	26.0 ± 2.1	6.5 ± 2.0	7.3 ± 0.4	4.3 ± 1.1	0.8 ± 0.1	2.0 ± 0.6
	14 d	54.1 ± 4.8	28.6 ± 5.9	4.3 ± 0.6	8.0 ± 0.8	3.6 ± 1.2	0.8 ± 0.2	0.6 ± 0.3
HBSSCa + BSA	3 d	48.6 ± 1.1	12.8 ± 1.1	14.6 ± 0.7	9.3 ± 0.9	14.7 ± 0.9	-	-
	7 d	50.5 ± 0.5	17.9 ± 1.1	12.4 ± 1.3	9.5 ± 1.1	9.0 ± 1.0	0.7± 0.1	
	14 d	46.2 ± 3.4	21.6 ± 5.6	8.7 ± 1.6	14.2 ± 3.3	7.7 ± 2.2	0.8 ± 0.2	0.8 ± 0.5
HBSSCa + FBS	3 d	49.2 ± 1.5	21.8 ± 0.9	13.2 ± 1.1	8.4 ± 0.5	7.1 ± 0.8	0.3 ± 0.1	-
	7 d	45.6 ± 3.5	19.5 ± 3.2	10.2 ± 1.0	13.1 ± 1.4	10.4 ± 1.6	0.7 ± 0.1	-
	14 d	45.2 ± 2.1	15.7 ± 1.1	10.8 ± 1.9	15.4 ± 0.8	11.7 ± 0.5	0.8 ± 0.2	0.3 ±0.1
DMEM	3 d	50.9 ± 1.7	13.1 ± 1.0	12.8 ± 1.2	8.1 ± 0.3	14.2 ± 1.5	0.9 ± 0.2	-
	7 d	50.6 ± 2.0	12.3 ± 0.6	11.8 ± 1.1	7.6 ± 0.4	13.7 ± 1.5	1.0 ± 0.5	-
	14 d	53.0 ± 2.3	12.7 ± 0.6	10.1 ± 1.0	8.2 ± 0.6	13.1 ± 1.3	0.9 ± 0.2	-
DMEM + BSA	3 d	54.5 ± 1.6	20.9 ± 1.0	8.8 ± 0.8	8.4 ± 0.6	6.3 ± 0.7	1.0 ± 0.2	-
	7 d	52.7 ± 1.8	18.0 ± 1.4	10.4 ± 0.9	7.9 ± 0.4	9.9 ± 1.8	1.1 ± 0.2	-
	14 d	54.6 ± 1.8	16.5 ± 2.0	11:9 ± 1.3	8.7 ± 0.7	10.8 ± 1.8	1.2 ± 0.2	-
DMEM + FBS	3 d	54.8 ± 1.6	21.9 ± 1.3	9.2 ± 0.7	8.1 ± 0.4	5.2 ± 0.6	1.0 ± 0.1	-
	7 d	51.3 ± 1.4	15.3 ± 2.0	12.6 ± 1.1	8.3 ± 0.6	11.6 ± 1.7	0.9 ± 0.2	-
	14 d	51.7 ± 1.3	15.2 ± 0.4	13.2 ± 1.0	7.8 ± 0.3	11.2 ± 0.9	0.8 ± 0.1	-

In DMEM-based media, the surface morphologies of all samples after immersion were similar to Fig. 4.13a. Therefore, only EDX results are exhibited in Table 4.1. Surprisingly, it showed higher contents of P and Ca in DMEM than in DMEM + BSA/FBS, especially after 3 days of immersion. Nevertheless, the contents of P and Ca decreased with immersion time in DMEM, while increased in DMEM + BSA/FBS. Moreover, higher content of Ca than P were observed for samples immersed in DMEM, but the content of Ca was generally lower than that of P in DMEM + BSA/FBS and HBSSCa-based media.

Determination of crystalline precipitates

The precipitates formed on Mg surface were determined by XRD (Fig. 4.14). It showed similar results as before. The conglomerate of very thin platelets formed in HBSS is mainly hydromagnesite ($Mg(CO_3)_4(OH)_2$ $4H_2O$), while the needle-like precipitates formed in HBSS + BSA is nesquehonite ($MgCO_3$ $3H_2O$). Besides the diffraction peaks of Mg, no crystalline peak is visible for samples immersed in HBSS + FBS. Similar XRD patterns were found for samples in HBSSCa-based and DMEM-based media, indicating amorphous or nanocrystaline products on these sample surfaces.

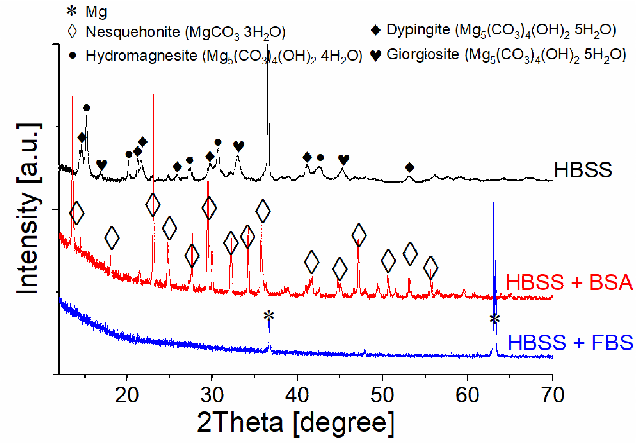

Figure 4.14: XRD patterns for samples immersed in different media after 14 days of immersion.

Chemical element mapping

The element distribution in degradation layer formed in HBSS-based media are displayed in Fig. 4.15. Generally, O and P were rich and C was present in degradation layer, indicating the formation of phosphate and carbonate in the degradation layer. Furthermore, P-rich products were mainly formed near Mg matrix in HBSS, but a much lower content of P was observed when precipitates were formed after 14 days of immersion. When proteins (BSA or FBS) were present, P mainly distributed in the top of degradation layer, which was broken in HBSS + BSA, but remained stable in HBSS + FBS. Ca, derived from FBS, was also rich in the top of degradation layer in HBSS + FBS, indicating the formation of Ca-P salts. The P-rich top layer seems to be of great importance to the degradation behaviour of Mg.

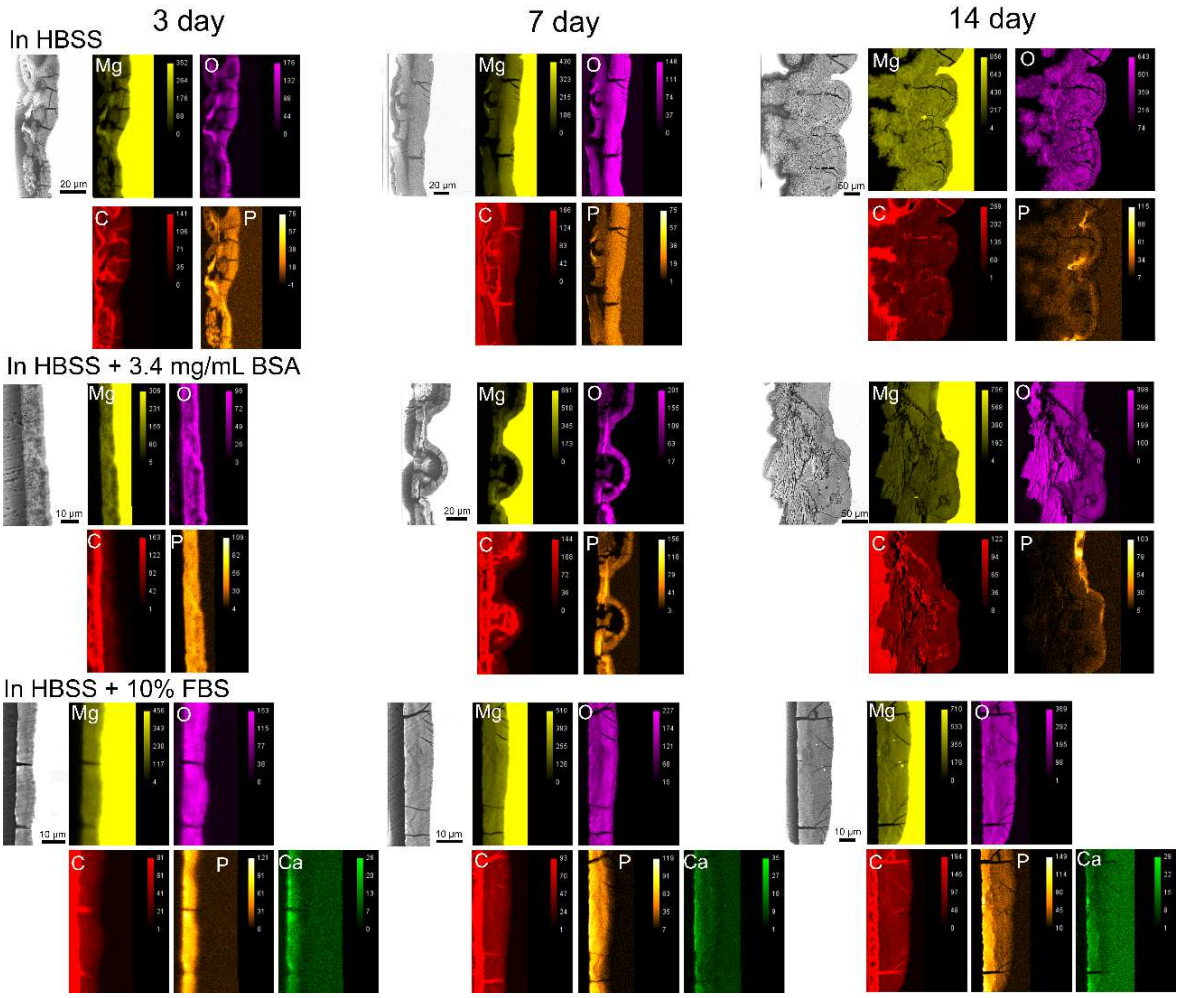

Figure 4.15: BSE images and chemical element mappings of Mg samples exposed to HBSS, HBSS + BSA and HBSS + FBS for different days.

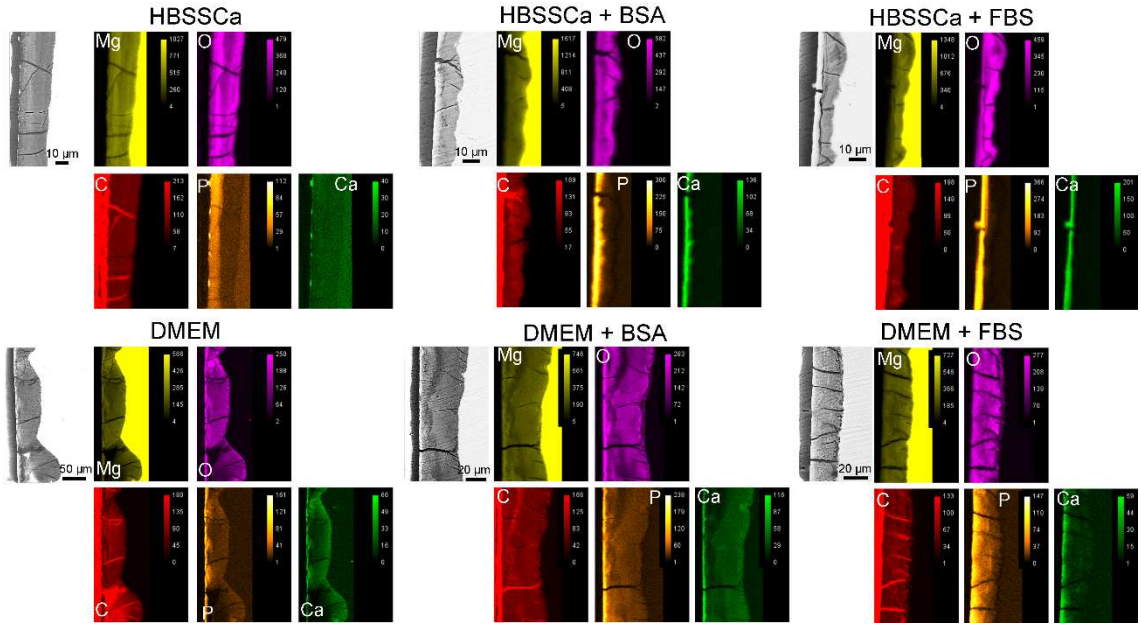

Figure 4.16: BSE images and chemical element mappings of Mg samples exposed to HBSS-based and DMEM-based media under static conditions for 14 days.

Due to the similar distribution patterns of elements in degradation layers formed in HBSSCa-based and DMEM-based media, only the element mappings of Mg samples after 14 days of immersion in different media were displayed in Fig. 4.16. Generally, the results showed a P/Ca-rich top layer and an inner oxide layer. In HBSS-based media, almost no Ca and P were present in the inner layers, while a low content of P/Ca existed in the inner layers in DMEM-based media. Moreover, the distinct boundary between these two layers is visible in HBSSCa-based media, especially in HBSS + BSA/FBS. Whereas, this boundary was vague in DMEM-based media, especially in DMEM + FBS. It suggests that the P/Ca-rich layer might be more dense in HBSSCa than in DMEM, thus preventing the diffusion of phosphate and calcium ions into the degradation layer. This fact may also be responsible for the lower degradation rate of Mg in HBSSCa-based media compared to DMEM-based media.

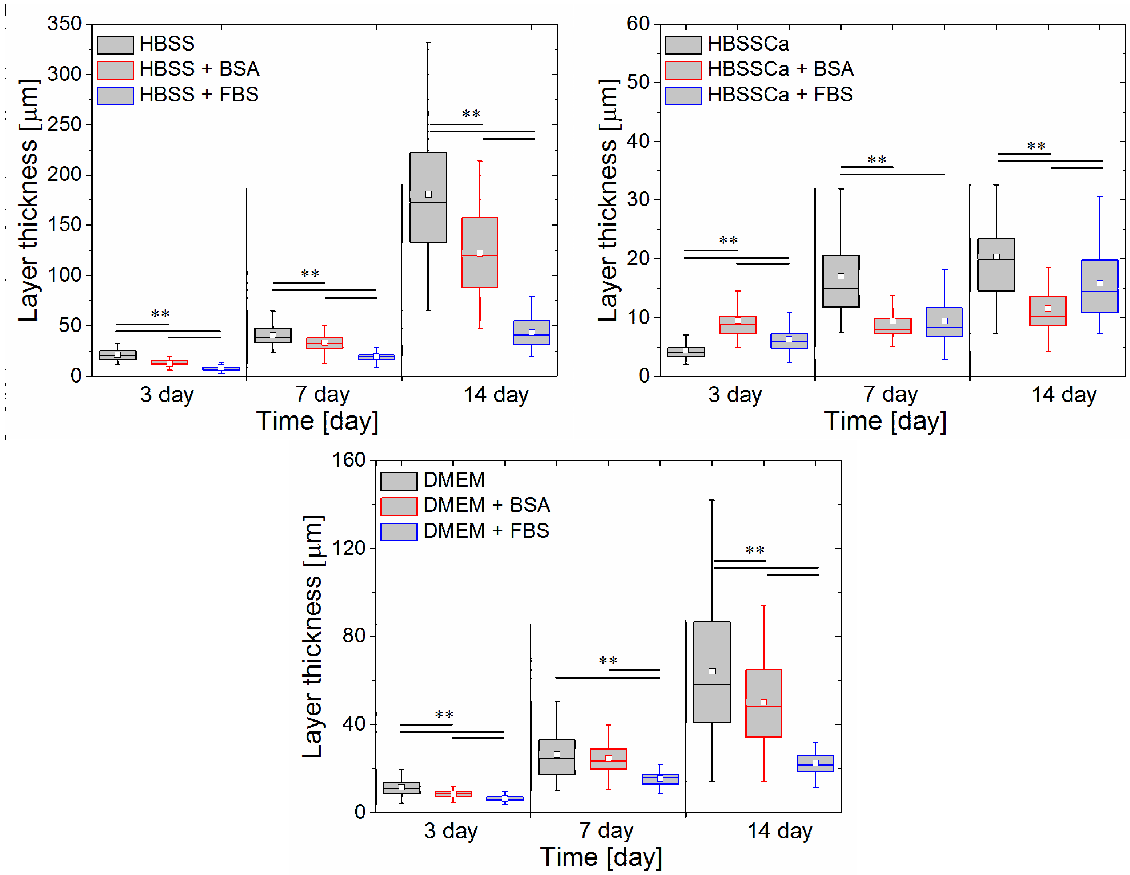

Figure 4.17: Thickness of degradation layer formed in different media after various immersion time. (The solid line indicates significant difference, One-way ANOVA, Dunn's test, Significance level: (*): $p < 0.05$, (**): $p < 0.01$)

The thickness of degradation layer formed in different media after different immersion time are depicted in Fig. 4.17. In consistence with the previous results, it revealed an increase of degradation layer thickness with immersion time due to the continuous degradation of Mg. In HBSS-based and DMEM-based media, the degradation layer was thinner when proteins were

present, which is in agreement with the degradation depth as shown in Fig. 4.9. The formation of precipitates on Mg surface in HBSS and HBSS + BSA after 14 days of immersion seemed to largely increase the layer thickness. However, in HBSSCa media, the addition of proteins resulted in thicker degradation layers after 3 days of immersion, while the layers were thinner after further immersion in the presence of proteins, which might result from the precipitation of Ca-P salts and the growth of the inner layer.

The weight percentages of Ca and P in degradation layer were calculated according to the chemical mapping results. As depicted in Fig. 4.18, wt.% of P (and Ca) gradually decreased in HBSS-based media and HBSSCa, while those values for P and Ca remained stable in HBSSCa with protein and DMEM-based media. This might result from the transformation of products on Mg surface during immersion. Moreover, the presence of proteins generally led to higher contents of P and Ca in degradation layer.

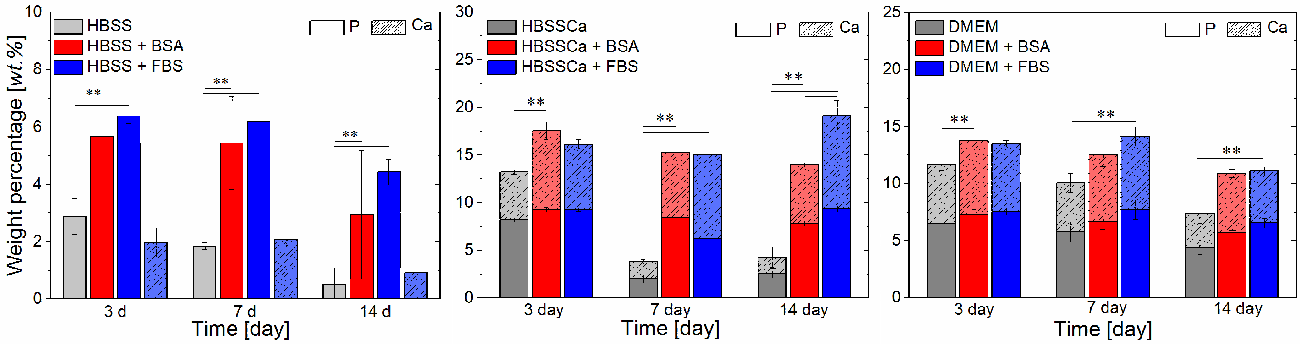

Figure 4.18: Weight percentages of Ca and P in degradation layer formed in different media after different immersion time. The solid line indicates significant difference for P/Ca content, One-way ANOVA, Dunn's test, Significance level: (*): $p < 0.05$, (**): $p < 0.01$. No significant difference of P content between DMEM and DMEM + BSA after 3 days of immersion.

4.2.2. Semi-static conditions

Mean degradation depth, pH, osmolality

As shown in Fig. 4.19, degradation rates and mean degradation depths of pure Mg were calculated after 3, 7 and 14 days of immersion in HBSS, HBSSCa and DMEM with and without BSA, Fib or FBS. As expected, the addition of Ca ions to HBSS decreased the degradation of Mg after 3 days of immersion and Mg degraded significantly faster in HBSS than in DMEM. In HBSSCa, proteins significantly reduced the degradation of Mg, especially when Fib was present. The addition of BSA / Fib / FBS to HBSS or DMEM also led to a lower degradation depth after 3 and 7 days of exposure, suggesting lower degradation rates of Mg when BSA/Fib/FBS was present in the medium during the short-term immersion. After 14 days of immersion, BSA exhibited little effect on Mg degradation in both HBSS and DMEM. However, FBS promoted the

degradation of Mg in HBSS, but showed an adverse effect in DMEM. More importantly, when BSA and Fib were simultaneously present in HBSS or DMEM, the mean degradation depth increased compared with that in HBSS or DMEM with BSA or Fib alone.

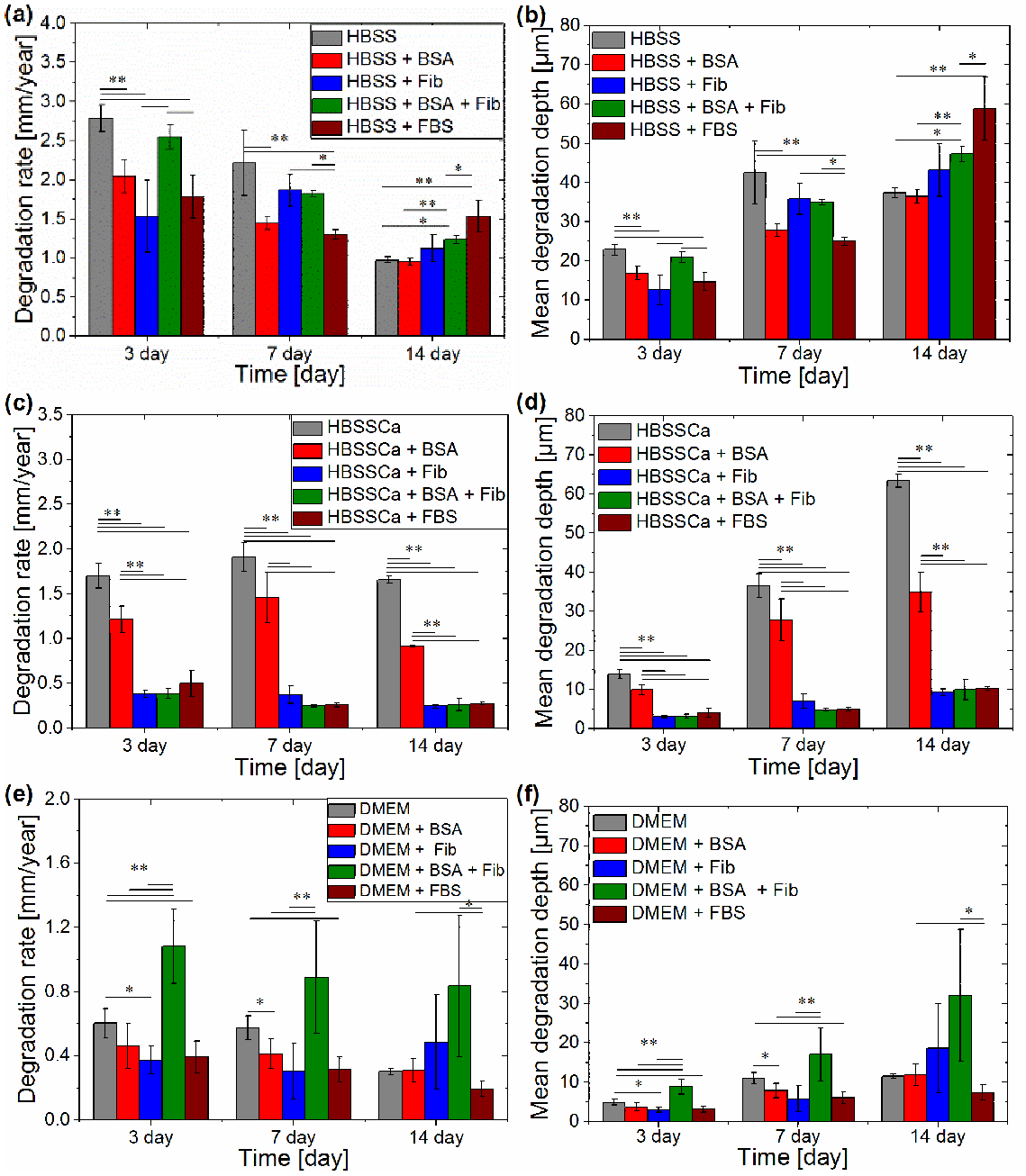

Figure 4.19: Degradation rates and mean degradation depths of pure Mg in HBSS-based (a, b), HBSSCa-based (c, d) and DMEM-based (e, f) media after different immersion time. (Significant differences are depicted by the solid line, Significance level: (*): $p < 0.05$, (**): $p < 0.01$).

The changes in pH and osmolality of media are displayed in Fig. 4.20. In HBSS-based media, changes in pH slightly increased with immersion time, and the addition of proteins led to a higher pH compared with the control (HBSS) after 3 days of immersion. In HBSSCa-based media, changes of pH for the control (HBSSCa) remained stable, while the addition of proteins resulted

in a decrease of pH with immersion time. A similar decreasing trend of pH could also be found in DMEM-based media. Moreover, the addition of proteins to DMEM resulted in a lower pH during immersion except in DMEM + BSA + Fib. The changes in osmolality of media decreased with immersion time irrespective of media compositions, indicating a stable degradation rate of Mg. The addition of proteins resulted in a higher osmolality in HBSS, while they had an adverse effect on the osmolality in HBSSCa and DMEM except in DMEM + BSA + Fib.

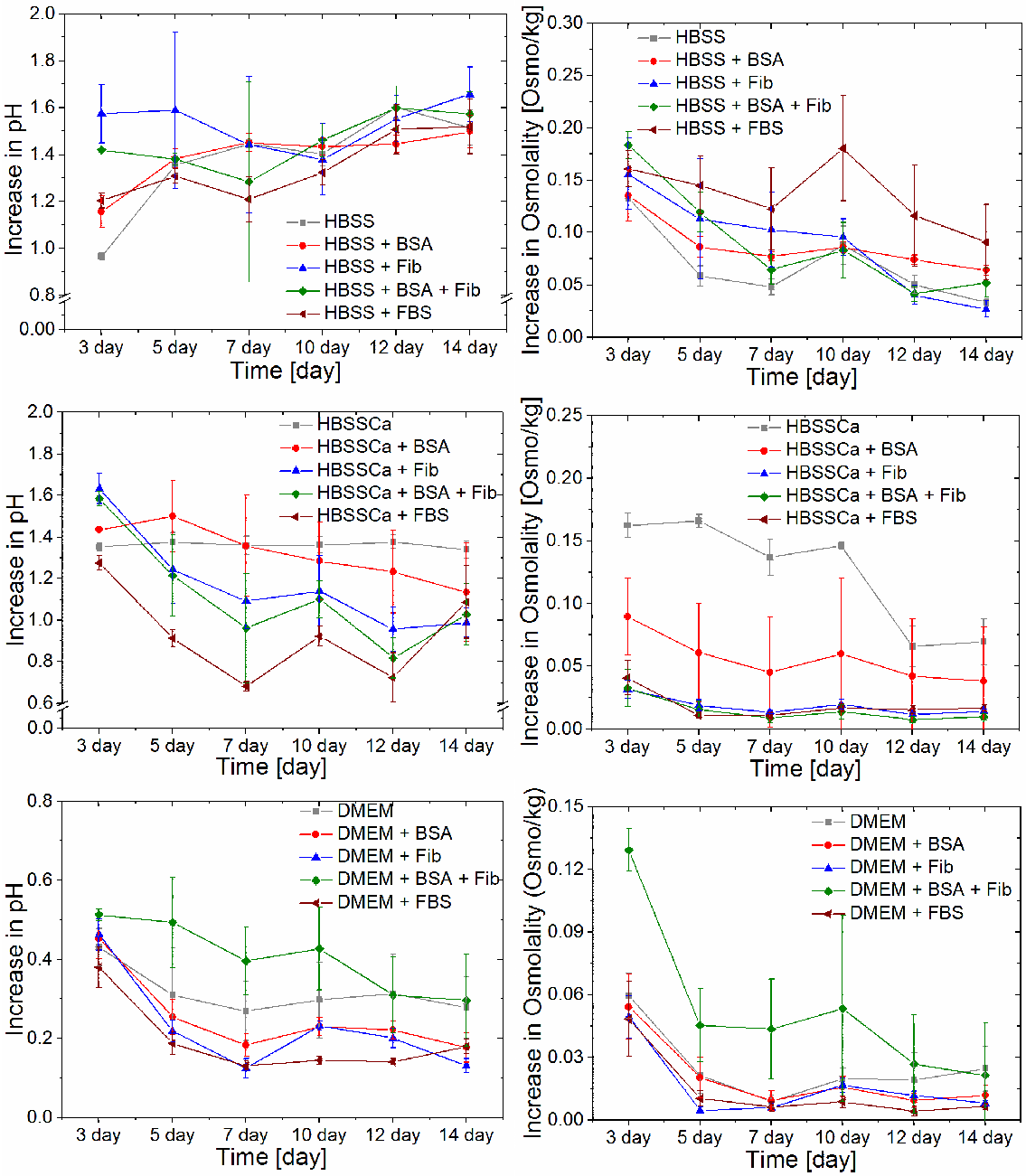

Figure 4.20: Changes in pH (a) and osmolality (b) for pure Mg in different media after different immersion time.

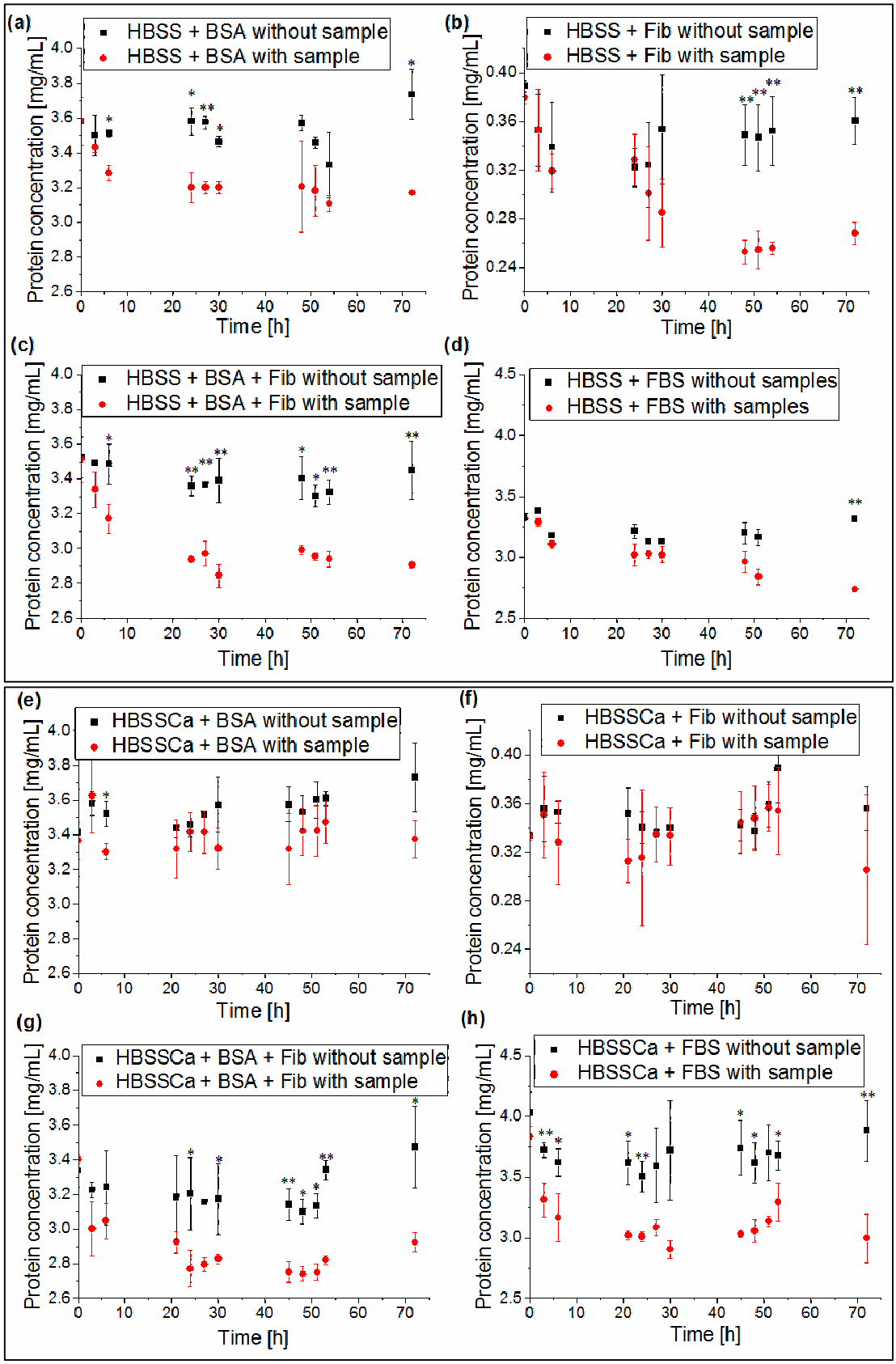

Figure 4.21: Concentration of proteins in media + 3.4 mg/mL BSA (a, e), media + 0.34 mg/mL Fib (b, f), media + 3.4 mg/mL BSA + 0.34 mg/mL Fib (c, g) and media + 10% FBS (d, h) during immersion under cell culture conditions (One-way ANOVA, Dunn's test, Significance level: (*): $p < 0.05$, (**): $p < 0.01$)

Protein concentration during immersion

To examine the adsorption of proteins during immersion, the concentration of proteins in HBSS-based and HBSSCa-based media were monitored during 3 days of immersion. As shown in Fig. 4.21, the initial concentrations of proteins were similar in HBSS + BSA and HBSS + FBS (3.3-3.7 mg/mL). Compared with the controls (media without sample), the concentration of proteins gradually decreased with immersion time in HBSS-based media, HBSSCa + BSA + Fib and HBSSCa + FBS, while the significant decreases of protein concentration were not visible in HBSS + BSA / Fib, indicating that different interaction between proteins and Mg surface took place in HBSS and HBSSCa. The decrease of protein concentration demonstrated the participation of proteins in the Mg degradation process by adsorption or other ways.

SAXS results

SAXS for BSA and Fib in different media was performed to check their interaction in media. As shown in Fig. 4.22, the results showed that BSA is stable in HBSS and HBSSCa, but the gyration radius decreased in DMEM (R_g(HBSS) = 3.71 ± 0.004 nm, R_g(HBSSCa) = 3.72 ± 0.006 nm, R_g(DMEM) = 3.17 ± 0.004 nm), indicating the influence of small organic molecules on BSA conformation in DMEM. In the case of Fib, the higher scattering intensity at low s in the presence of Ca^{2+} indicates that Ca^{2+} largely increased the aggregation, while the aggregation was weaker in DMEM than in HBSSCa, but still stronger than in HBSS, indicating small organic molecules in DMEM depress the aggregation of Fib. The comparison between media + BSA + Fib showed that interaction between BSA and Fib resulted in the increase of scattering in HBSS and HBSSCa compared to DMEM, which possibly results from the conformation change of proteins or the formation of BSA/Fib complexes in HBSS and HBSSCa.

Comparing the fitted average scattering (according to the scattering in media +BSA and media +Fib) with the obtained scattering in BSA and Fib containing media, it can be observed that BSA and Fib showed slight higher scattering intensity compared to the fitted average in HBSS, indicating the possible synergistic interaction between BSA and Fib in HBSS. However, in HBSSCa and DMEM, the scattering intensity of the BSA and Fib mixture is lower than the average scattering, which may be due to the decomposition of Fib complexes in media + BSA + Fib. This indicates that the presence of BSA and small organic molecules decreases the aggregation of Fib, which is possibly caused by their net negative charge in media at pH = ~7 (> isoelectric point) [140, 143, 191]. This also might be the reason that the reported phenomenon that the decreased fluidity of solution is appreciably less in the presence of serum proteins than in purified solutions of Fib [192].

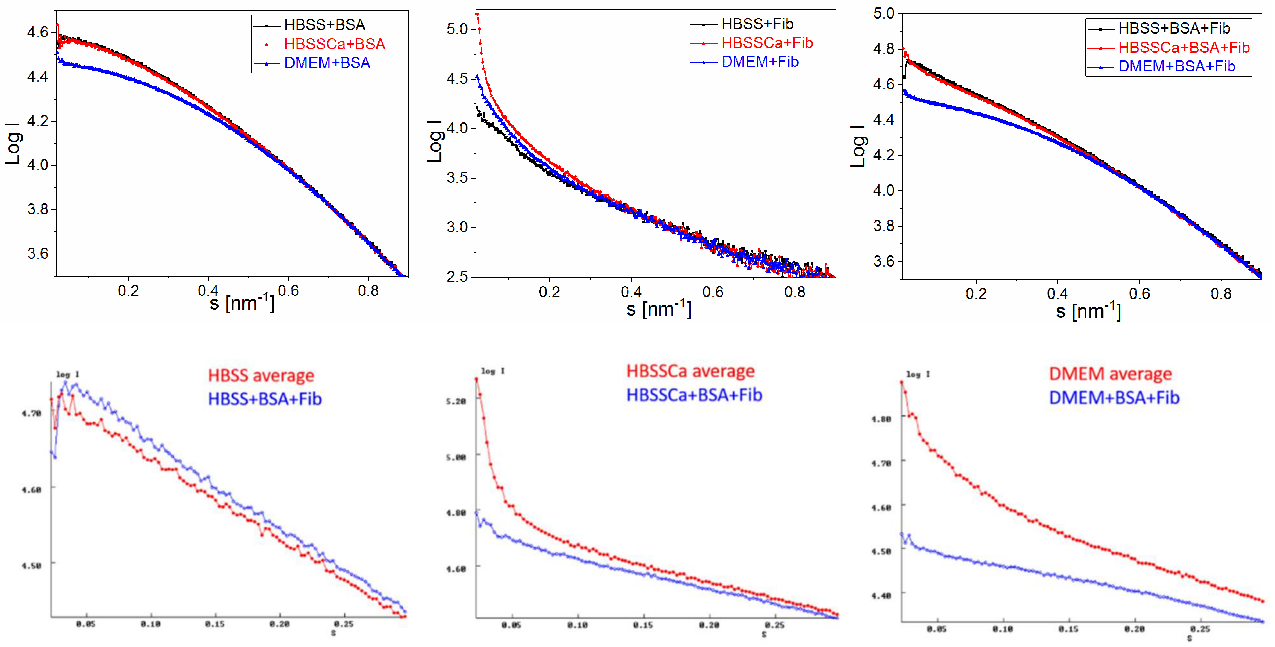

Figure 4.22: Small angle X-ray scattering (SAXS) curves for BSA and Fib in different media (upper row), and the comparison between the fitted average scattering of BSA and Fib in media and the scattering in medium + BSA + Fib (lower row).

Surface morphology

The surface morphologies of samples after immersion in different media are shown in Fig. 4.23 and 4.24. In HBSS, macroscopic white precipitates were formed on the surface as a conglomerate of very thin platelets. The addition of BSA led to the formation of needle-like precipitates and both of these two kinds of precipitates (conglomerate of thin platelets and needle-like precipitates) were formed on Mg surface in HBSS + Fib. In comparison, only conglomerates of thin platelets were formed in HBSS + BSA + Fib and there were only few precipitates on the surface in HBSS + FBS. Moreover, the precipitates changed with exposure time, especially for the needle-like precipitates. In HBSSCa-based media (Fig. 6), the flocculent precipitates were formed in HBSSCa after 7 days of immersion, while granular precipitates were visible on Mg surface in HBSSCa + BSA and HBSSCa + Fib. No obvious formation of precipitates could be observed on the sample surfaces in HBSSCa + BSA + Fib and HBSSCa + FBS. Similar results were also gained in DMEM-based media, showing little morphology difference induced by the addition of proteins and little changes with immersion time, so SEM images of samples immersed in DMEM-based media are not shown here.

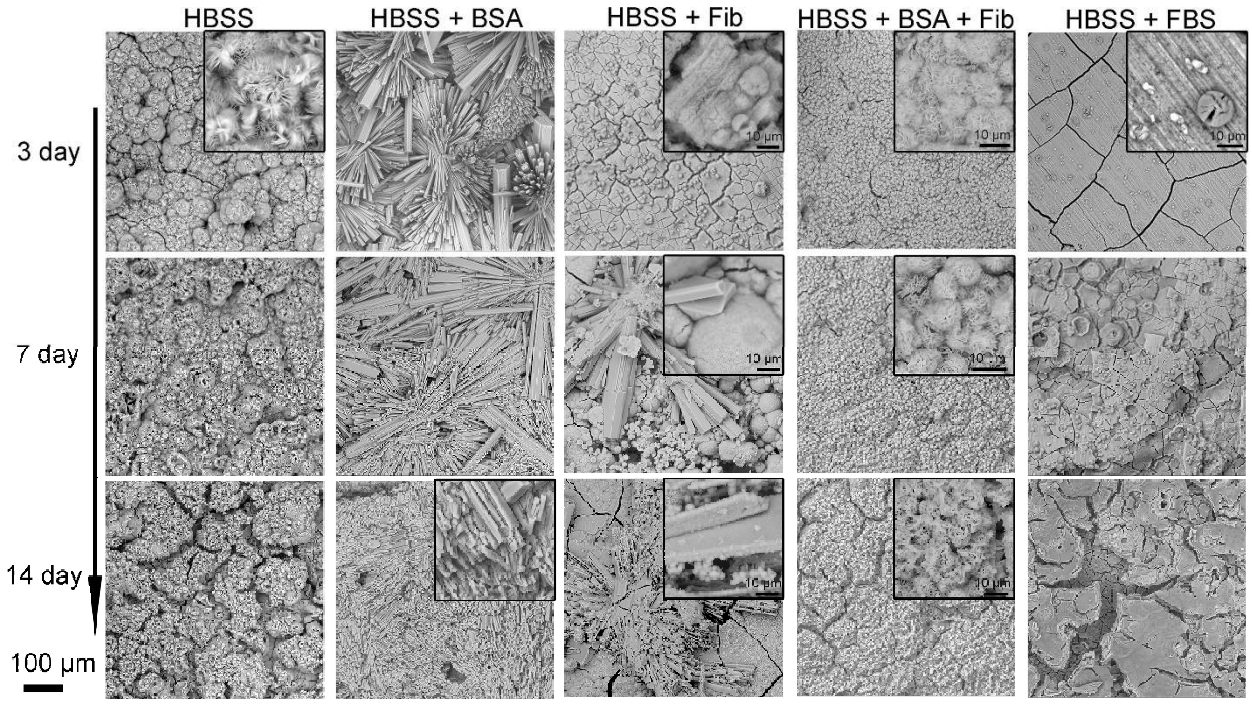

Figure 4.23: SEM images of samples after different immersion times in HBSS-based media.

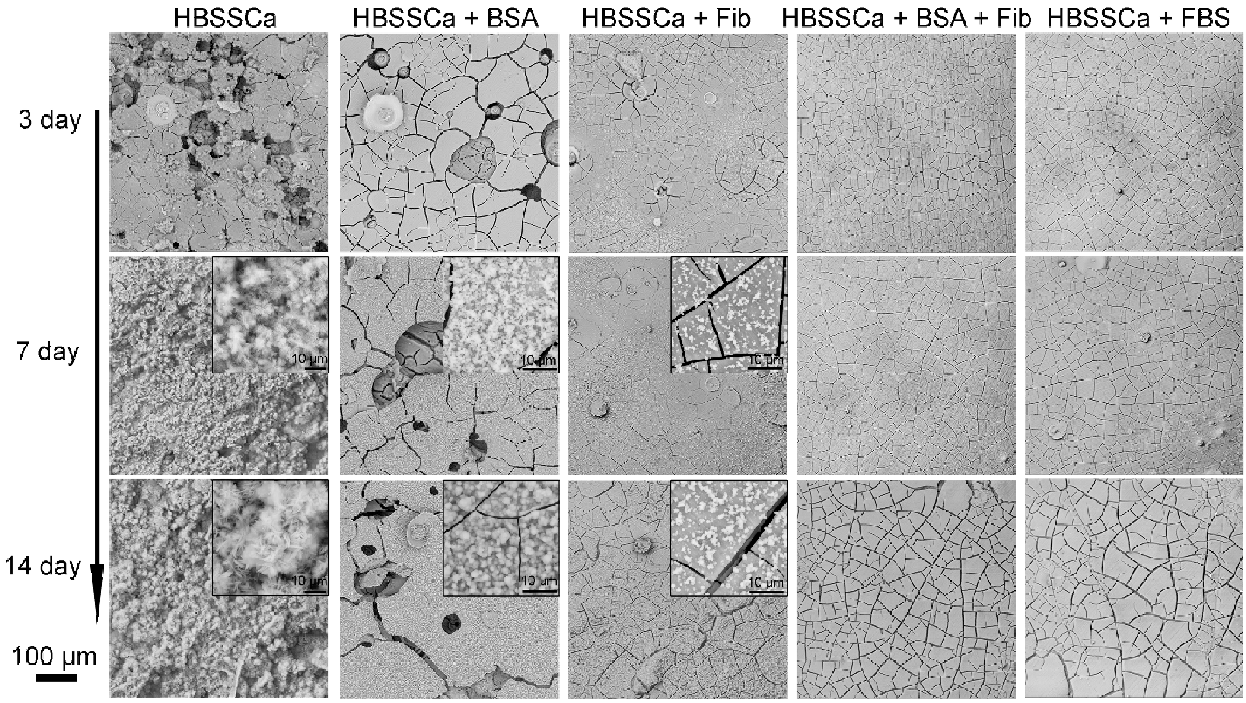

Figure 4.24: SEM images of samples after different immersion times in HBSSCa-based media.

Characterization of degradation products

XRD results (Fig. 4.25) revealed that the conglomerates of very thin platelets formed in HBSS-based media and the flocculent precipitates formed in HBSSCa were mainly composed of hydromagnesite and dypingite, while the needle-like precipitates formed in HBSS + BSA were

well-formed nesquehonite, which is in accordance with the above results (Figs. 4.6 and 4.14). The precipitates formed in HBSS + BSA + Fib contained not only nesquehonite, but also hydromagnesite and dypingite. However, the XRD patterns of samples in the other of media only gave the Mg diffraction peaks as shown in the spectrum obtained from DMEM.

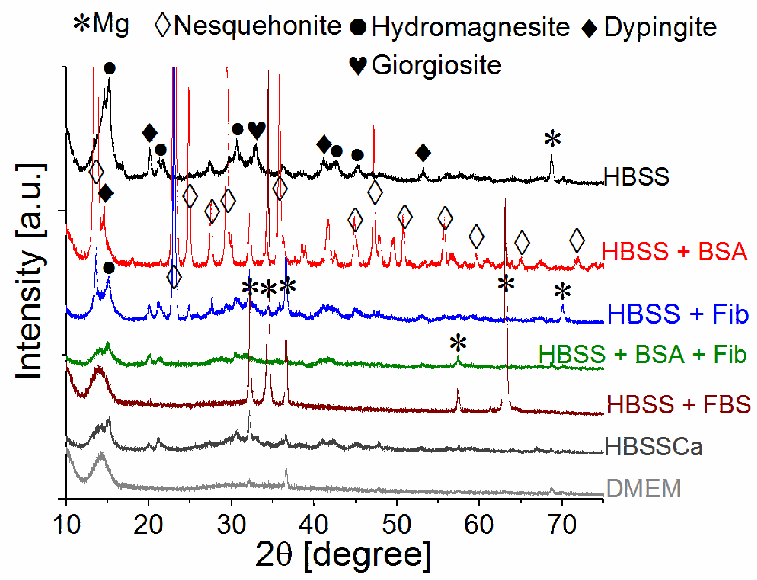

Figure 4.25: XRD patterns of Mg samples after immersion in different media

IR reflection spectra were obtained for the samples immersed in HBSS + FBS, HBSSCa + protein and DMEM-based media. Only the range from 2200 cm^{-1} to 550 cm^{-1} was depicted in Fig. 4.26 a and b, since the major information is located in this range. The band near 1646 cm^{-1} is attributed to the OH-bending of absorbed water and/or the amide I of organic molecules absorbed on Mg surface [116]. The broad band from 1600 cm^{-1} to 1300 cm^{-1} is a result of the overlap between the anti-symmetrical CO_3^{2-} stretching and the band II/III/VI stretching of organic molecules [72]. Compared with the spectra from BSA and Fib, the bands from proteins can be observed for protein-containing media, indicating the adsorption of proteins on Mg surface. The bands from the asymmetric stretching of phosphate obviously shifted from 1182 cm^{-1} and 1093 cm^{-1} in DMEM to around 1134 cm^{-1} in DMEM with proteins [193]. This shift of bands from phosphate in HBSSCa with proteins indicated the possible different conformation or compositions of Ca/Mg-PO_4 when protein is present. The band at 861 cm^{-1} is assigned to the CO_3^{2-} bending vibration [188]. Therefore, it can be concluded that the degradation products are mainly composed of Mg/Ca-PO_4, Ca/$MgCO_3$ and absorbed organic components in HBSSCa and DMEM. As previously proposed [73], $Mg(OH)_2$ and MgO are also possible products, but they were not detected herein. This could be due to the fact that only the outmost surface was detected and the high signal to noise ratio in the low wavenumber range.

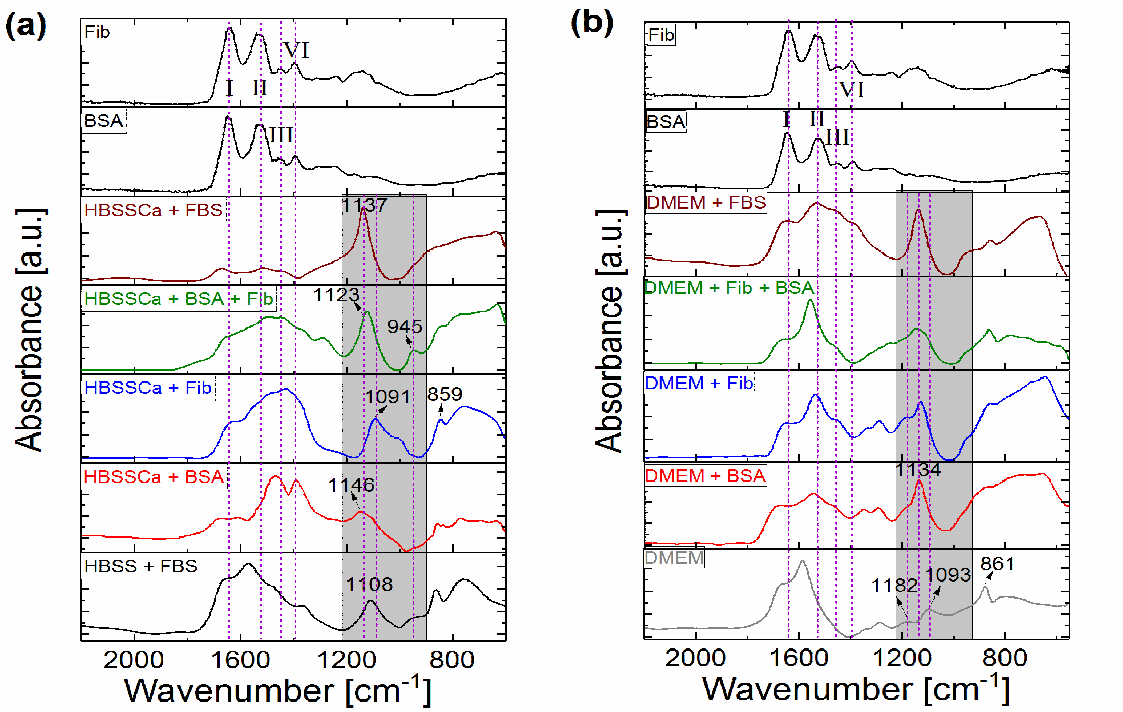

Figure 4.26: IR spectra of Mg samples after immersion in different media (the bands marked by grey background result from vibration of phosphate).

X-ray Photoelectron Spectroscopy (XPS) at different depths were performed for samples immersed in HBSSCa with proteins after 14 days of immersion to examine the composition of the degradation layer. As shown in Fig. 4.27, except the outmost surface (no etching), the composition of degradation layer showed a certain tendency over the etching depths. The content of elements in degradation layer formed in HBSSCa + BSA was stable within the etching depth and the ratio of Ca/P remains around 1. However, the increase of Mg and the decrease of P, Ca and C could be observed for HBSSCa + Fib / HBSSCa + BSA + Fib / HBSSCa + FBS, especially within 45 min of etching time. Higher contents of P and Ca in HBSSCa + Fib, HBSS + BSA + Fib and HBSSCa + FBS than in HBSSCa + BSA were accordant with the higher degradation rate in HBSSCa + BSA than in the other groups. Furthermore, the ratio of Ca/P in HBSSCa + BSA + Fib (< 1) was different from that in HBSS + BSA and HBSSCa + Fib (~1), which might be related to the effect of the interaction between BSA and Fib on the formation of degradation products. In HBSSCa + FBS, the ratio of Ca/P was around 1 in the top of layer, but decreases to <1 with etching depths. The depth files of C and N indicated the presence of proteins in the degradation layer, which largely decreased to near zero with the etching time extended, proving that proteins only adsorbed on the top of degradation layer. Due to the non-conductivity of degradation products formed in HBSSCa-based media, surface charging could not be totally compensated during measurement, which led to the shift of XPS peaks. Therefore, detailed reliable analysis of the results is impossible.

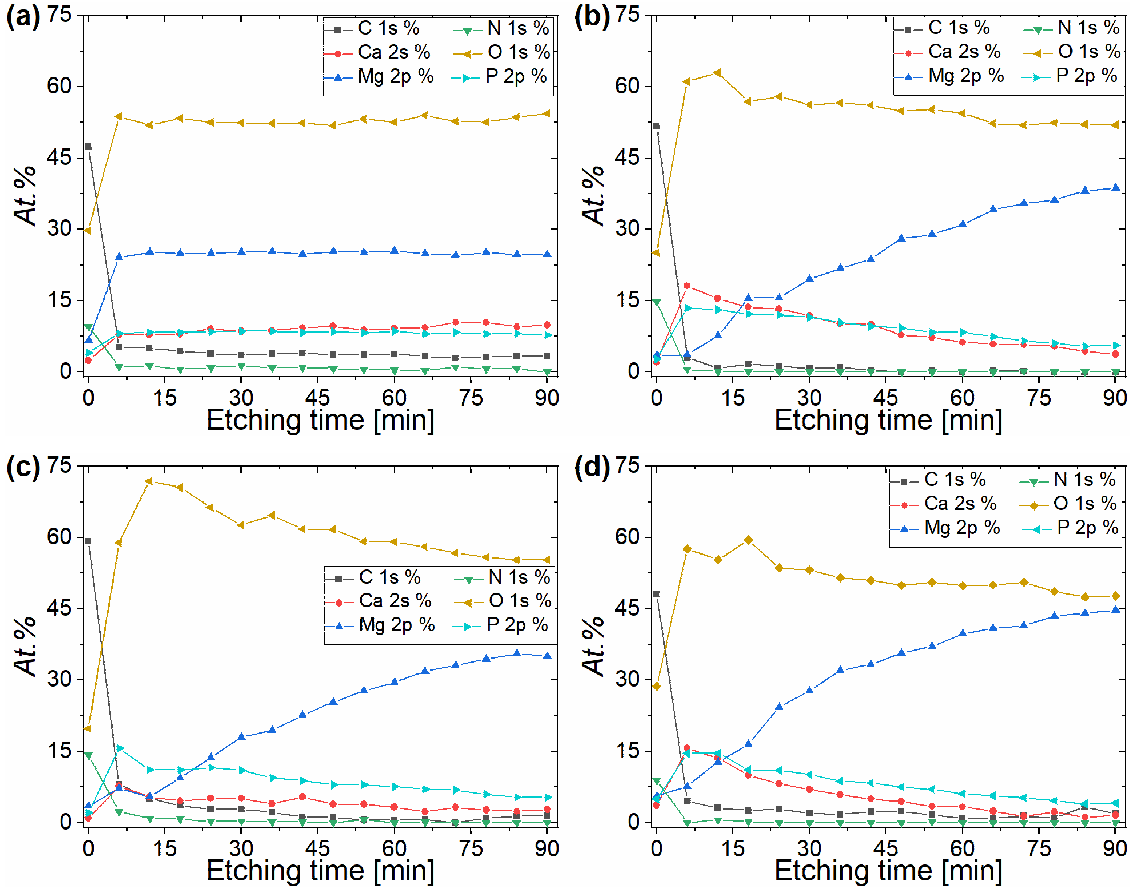

Figure 4.27: The compositions of degradation products obtained by XPS at different depth in HBSSCa + BSA (a), HBSSCa + Fib (b), HBSSCa + BSA + Fib (c) and HBSSCa + FBS (d) after 14 days of immersion.

Typical XPS region spectra from DMEM-based media are depicted in Fig. 4.28. Obviously, the spectra of C1s, O1s and N1s before etching from DMEM were different from DMEM + BSA and DMEM + FBS. Because the only reason for the existence of N is from organic molecules, the existence of N for samples in DMEM indicated the adsorption of small organic molecules on Mg surface, which is in agreement with the results in Fig. 4.3. The peaks at the highest binding energy of C 1s in DMEM simply exhibited as shoulder in DMEM + BSA / FBS, which resulted from the different composition of organic molecules (-COOH/-COOR) and carbonate in the top of the degradation layer. Similarly, a shoulder at the high binding energy of N1s could be observed in DMEM + BSA/FBS, which is caused by the protonated amino groups [194]. It indicates the different surface properties (e.g. surface charge) when proteins are present. The shape of O1s spectra from DMEM was totally different from that of DMEM + BSA/FBS, which can be mainly ascribed to the composition of the top degradation layer, such as, phosphate, carbonate, $Mg(OH)_2$ and MgO. The details can be directly observed in the following deconvoluted spectra in Fig. 4.30.

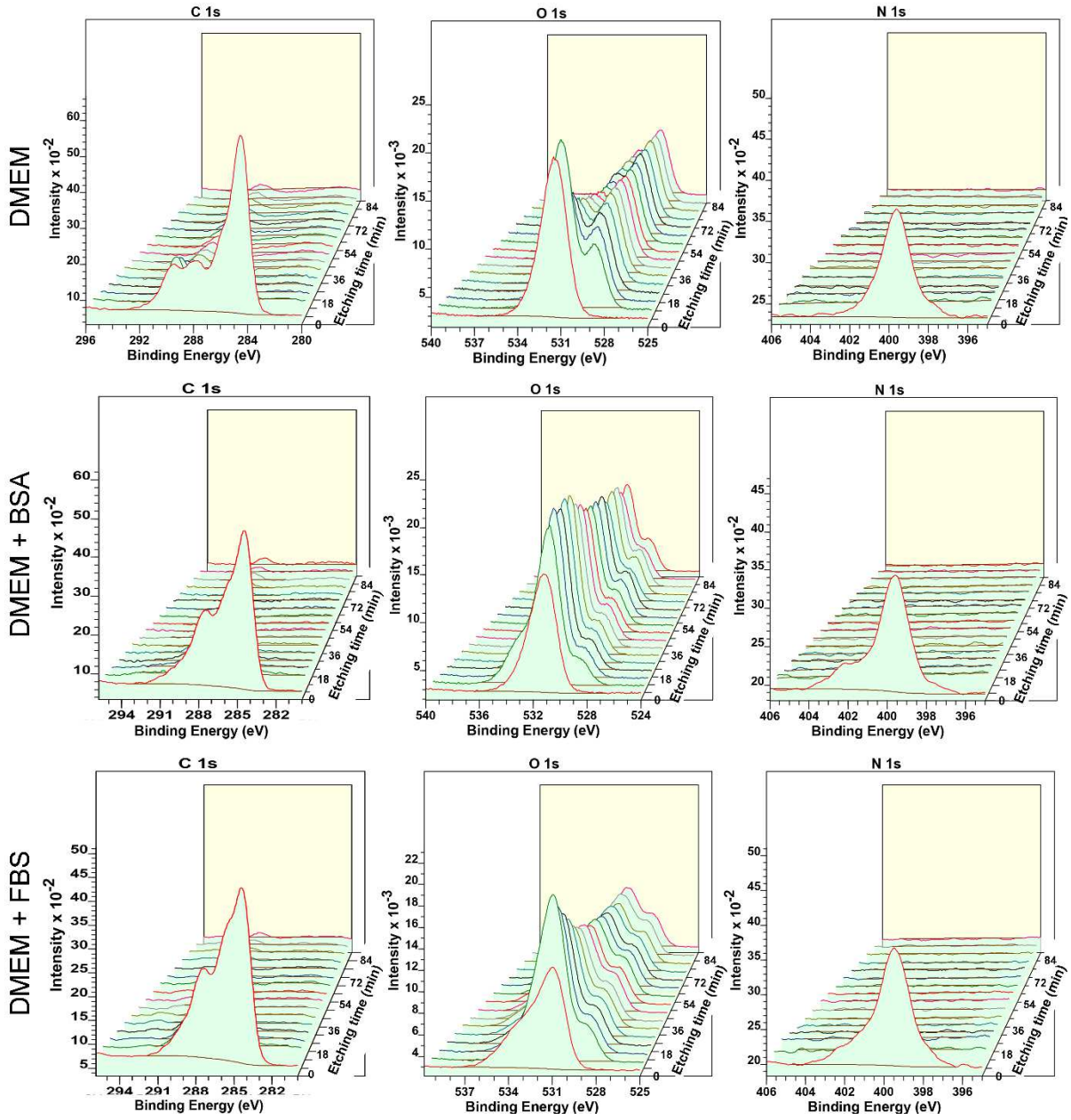

Figure 4.28: The high-resolution C1s, O1s and N1s XPS depth profiles of degradation products formed in DMEM (a), DMEM + BSA (b) and DMEM + FBS (c) after 14 days of immersion

The change of element contents over etching time in DMEM-based media are displayed in Fig. 4.29. Obviously, the contents of P and Ca were considerably higher in DMEM + BSA / FBS than in DMEM, indicating that proteins can promote the formation of Ca-P salts. The at.% of Mg increased with increasing etching time for all the cases and was higher in DMEM than in DMEM + BSA / FBS. The at.% of O in the degradation layer hardly changed with etching time in the range of 50-60%. The ratio of Ca/P obviously was lower in DMEM + BSA / FBS than in DMEM (~1), possibly caused by the existence of Mg-PO_4. Due to the complex composition of degradation products and the amorphous states, it is hard to distinguish the exact products on the surface.

The at.% of N was less than 0.3 % after etching for all the samples, indicating the organic molecules mainly adsorbed on the top of the Mg surface in DMEM, which was similar as in HBSSCa. On the other hand, it also suggests that the content of C derives from the carbonate when etching is applied. Higher at % of C can be found in DMEM than in DMEM + BSA / FBS within 20 min of etching, demonstrating more carbonate in the top of degradation products in DMEM.

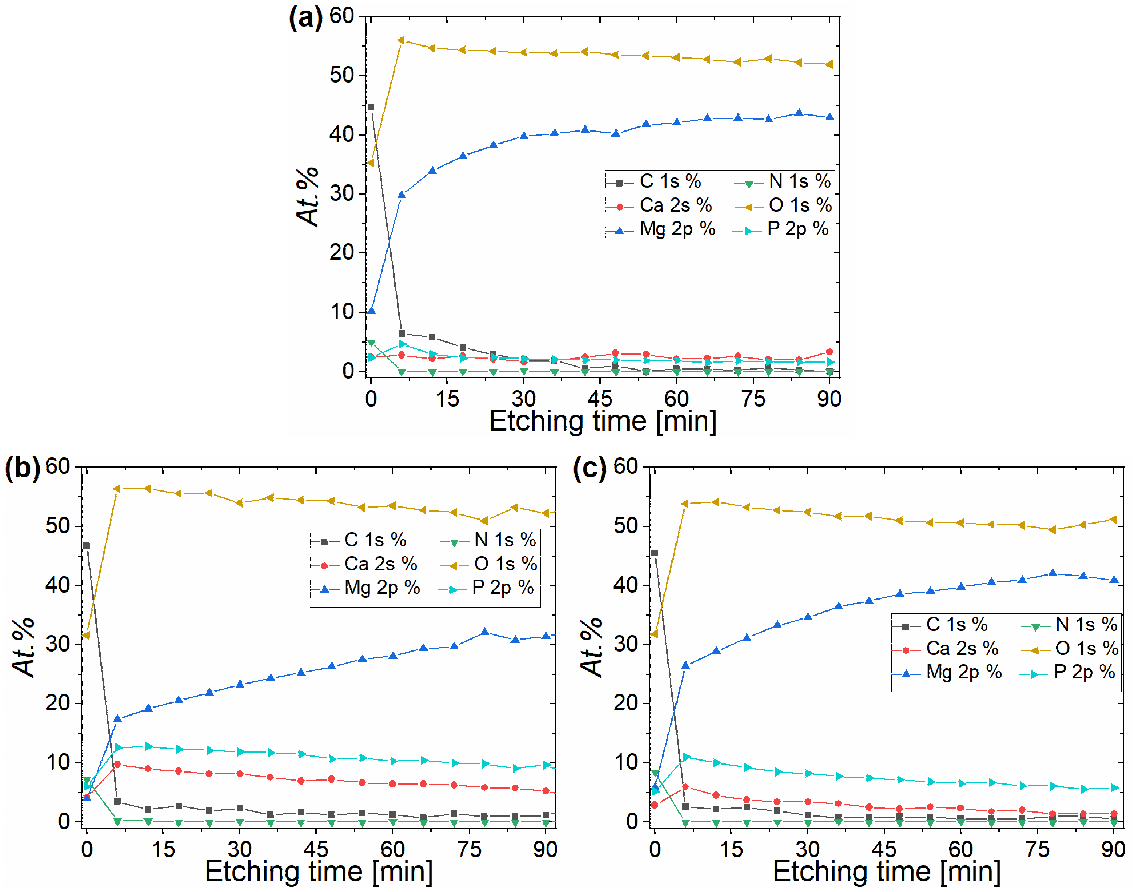

Figure 4.29: The distribution of degradation products obtained by XPS at different depth in DMEM (a), DMEM + BSA (b) and DMEM + FBS (c) after 14 days of immersion.

The region spectra of C1s, O1s, P2p and Mg2p at different depths for samples were analysed according to the NIST Standard Reference Database. Herein, typical example from the region spectra of O1s for samples immersed in DMEM, DMEM + BSA and DMEM + FBS are depicted in Fig. 4.30. The high-resolution O1s XPS spectra of the degradation products revealed three components at a lower binding energy (marked as 'b') and a middle binding energy (marked as 'a') with a higher binding energy shoulder. The peak marked as 'b' can be interpreted as oxygen in the form of MgO and $Mg(OH)_2$, which always overlaps in the range of 528.8-530.8 eV. The peak 'a' at 531.0-532.4 eV corresponds to phosphate containing PO_4^{3-}, HPO_3^{2-} and $H_2PO_4^-$, while the shoulder at higher binding energy (532.1-533.2 eV) can be attributed to carbonate. The

results revealed that O from phosphate decreased in the inner layer in DMEM, while it still dominated in DMEM + BSA / FBS. Correspondingly, the content of O from MgO and $Mg(OH)_2$ significantly increased to be the main peaks for the inner products in DMEM, and also gradually increased in DMEM +BSA /FBS. This agrees well with the results that Ca-P salts are formed in the top of $Mg(OH)_2$ and carbonates in DMEM [79].

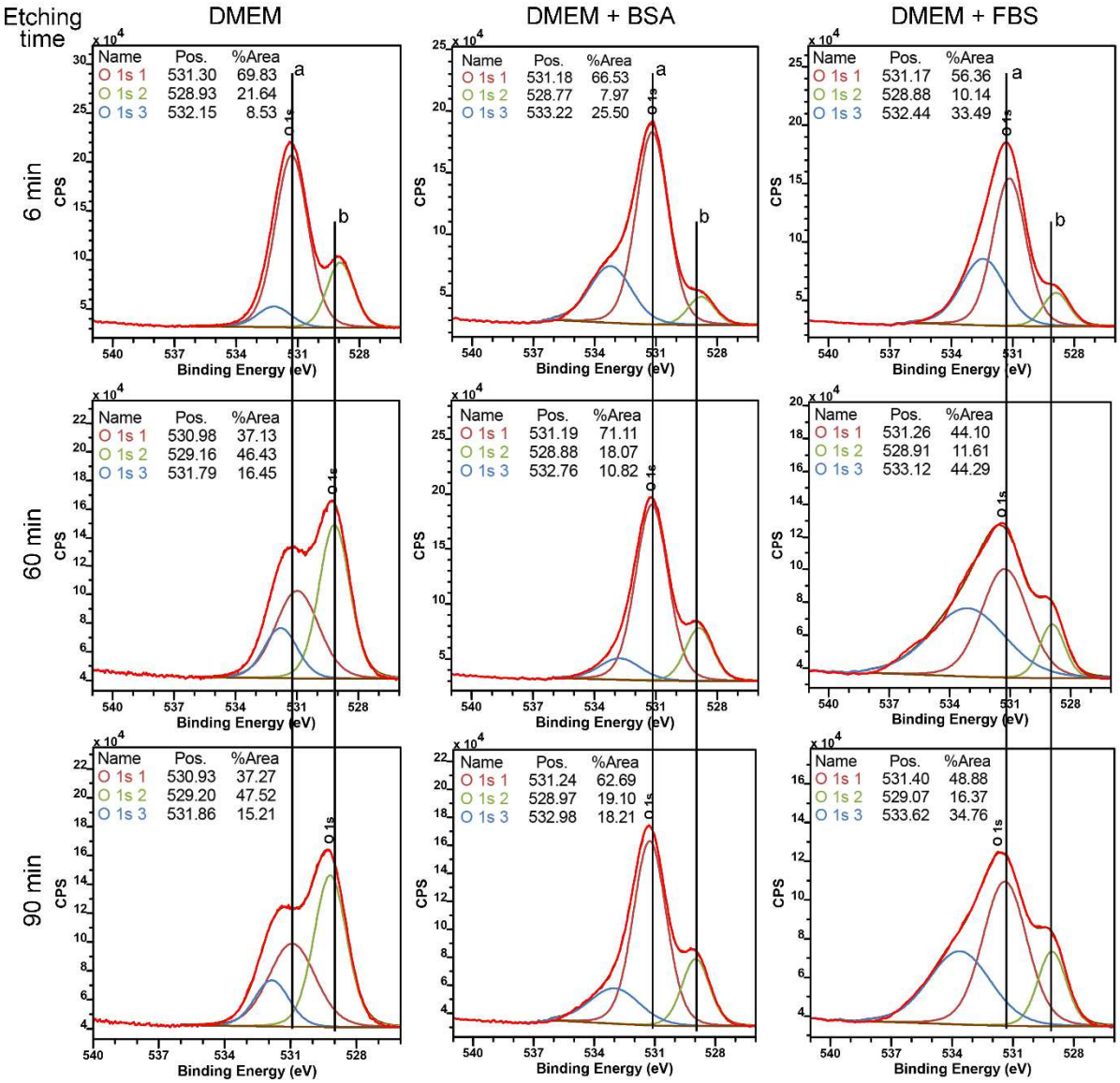

Figure 4.30: O1s XPS region spectra of samples immersed in DMEM, DMEM + BSA and DMEM + FBS for 14 days.

Degradation layer analysis

To analyse the variations of element distribution in degradation products, chemical element mappings were performed for samples after different immersion time in different media. The amount of Na, Cl and S were negligible for all samples. The distribution of elements in degradation layer formed in different media are provided in Fig. 4.31-33. Ca was not present in HBSS and

HBSS + BSA / Fib / BSA + Fib. As expected, O mainly distributed in degradation layer, while C existed mainly in the resin. The obvious differences came from the distributions of P and Ca. In HBSS and HBSS + BSA / Fib / BSA + Fib, the existence of P in degradation layer indicated the formation of Mg-PO_4 during immersion. A Ca/P-rich layer could be observed for the degradation layer formed in HBSSCa-based and DMEM-based media, which is in agreement with the results obtained under static conditions. Furthermore, the addition of proteins generally resulted in the thickening of the Ca/P-rich outmost layer, which is in agreement with the XPS results. However, when BSA and Fib were simultaneously present in DMEM, the formation of Ca-P salts in degradation layer was largely inhibited.

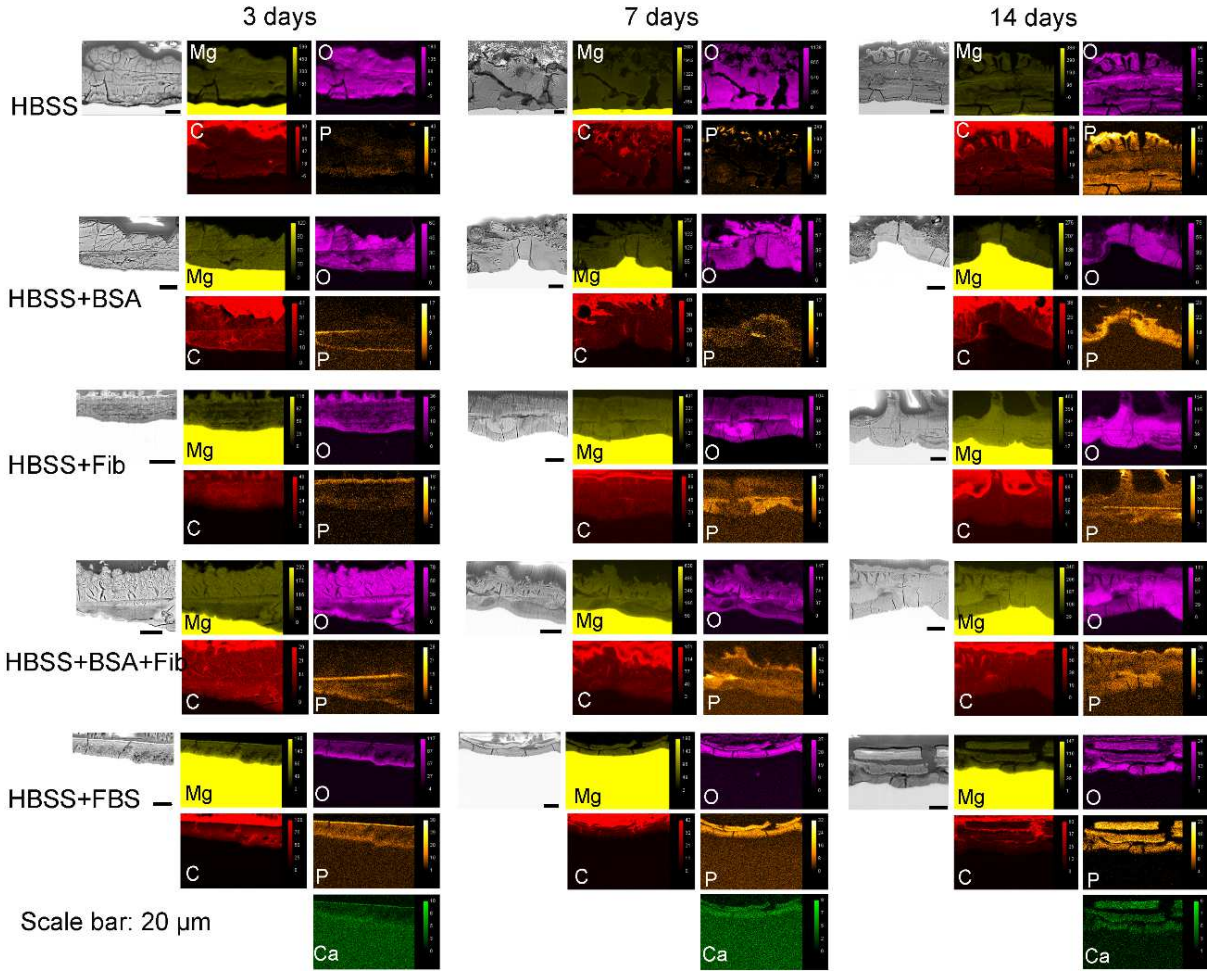

Figure 4.31: Element mapping of degradation layer formed in HBSS with and without proteins after different immersion time.

The thicknesses of degradation layers are displayed in Fig. 4.34. As a general trend, the thickness increased with immersion time except in HBSS + BSA. Additionaly, the degradation layer formed in HBSS-based media was much thicker than that formed in HBSSCa-based and DMEM-based media, especially during the first 7 days of immersion. The addition of proteins to media resulted in thinner degradation layers except in DMEM + BSA + Fib.

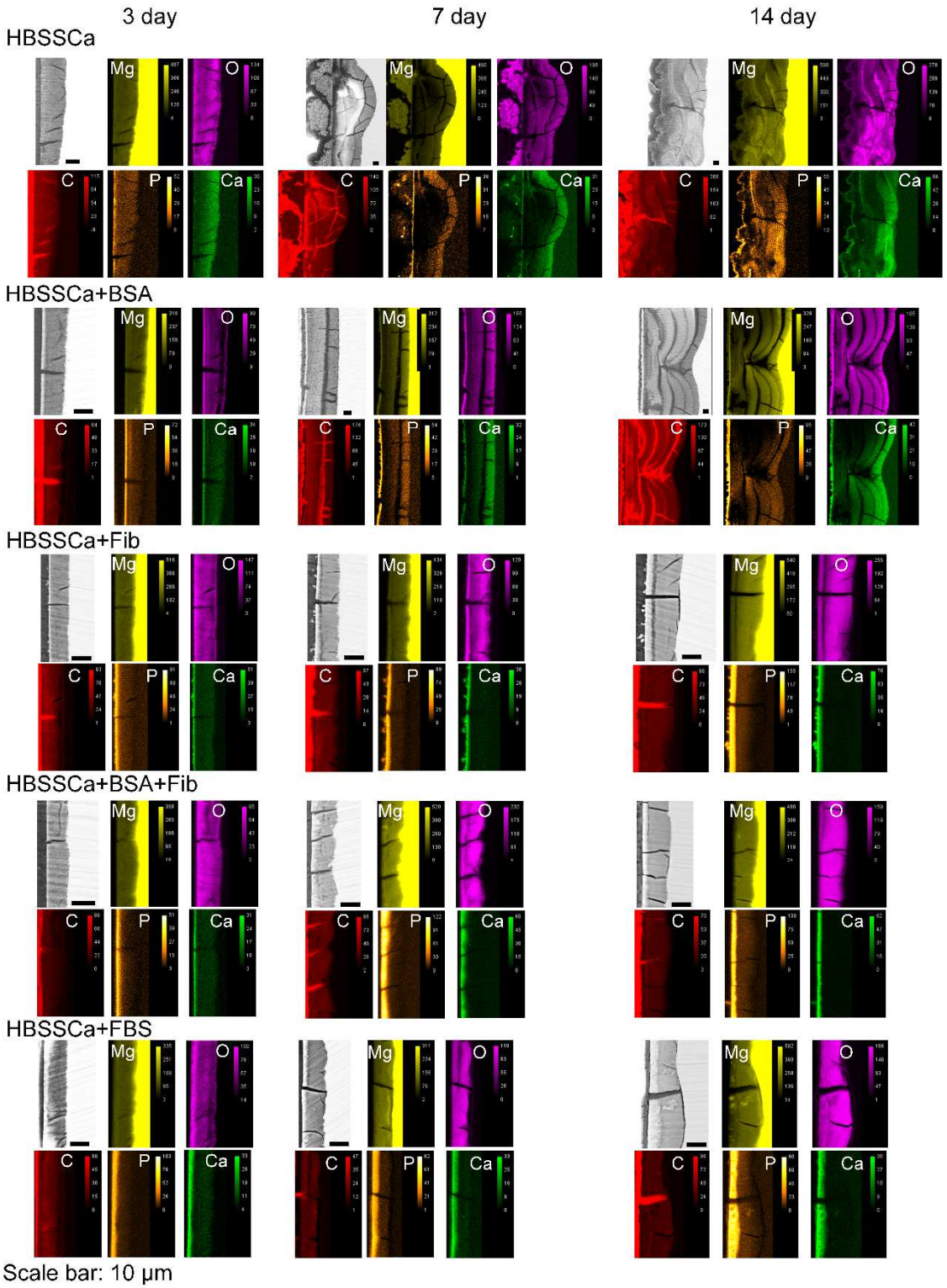

Figure 4.32: Element mapping of degradation layer formed in HBSSCa with and without proteins after different immersion time.

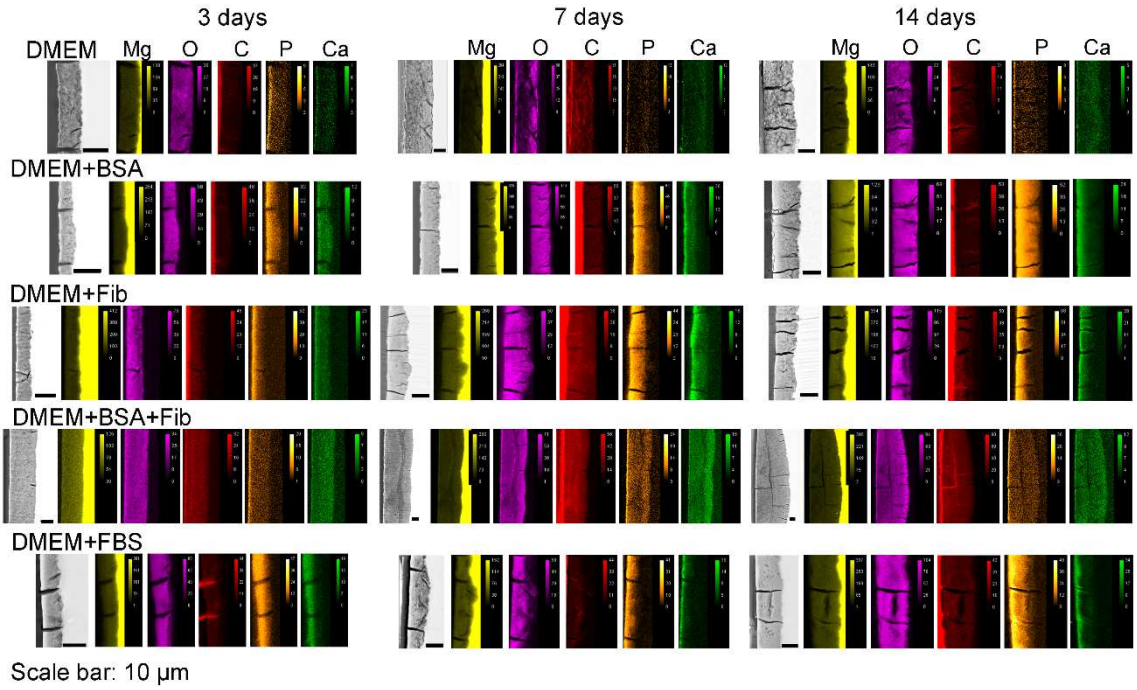

Figure 4.33: Element mapping of degradation layer formed in DMEM with and without proteins after different immersion time.

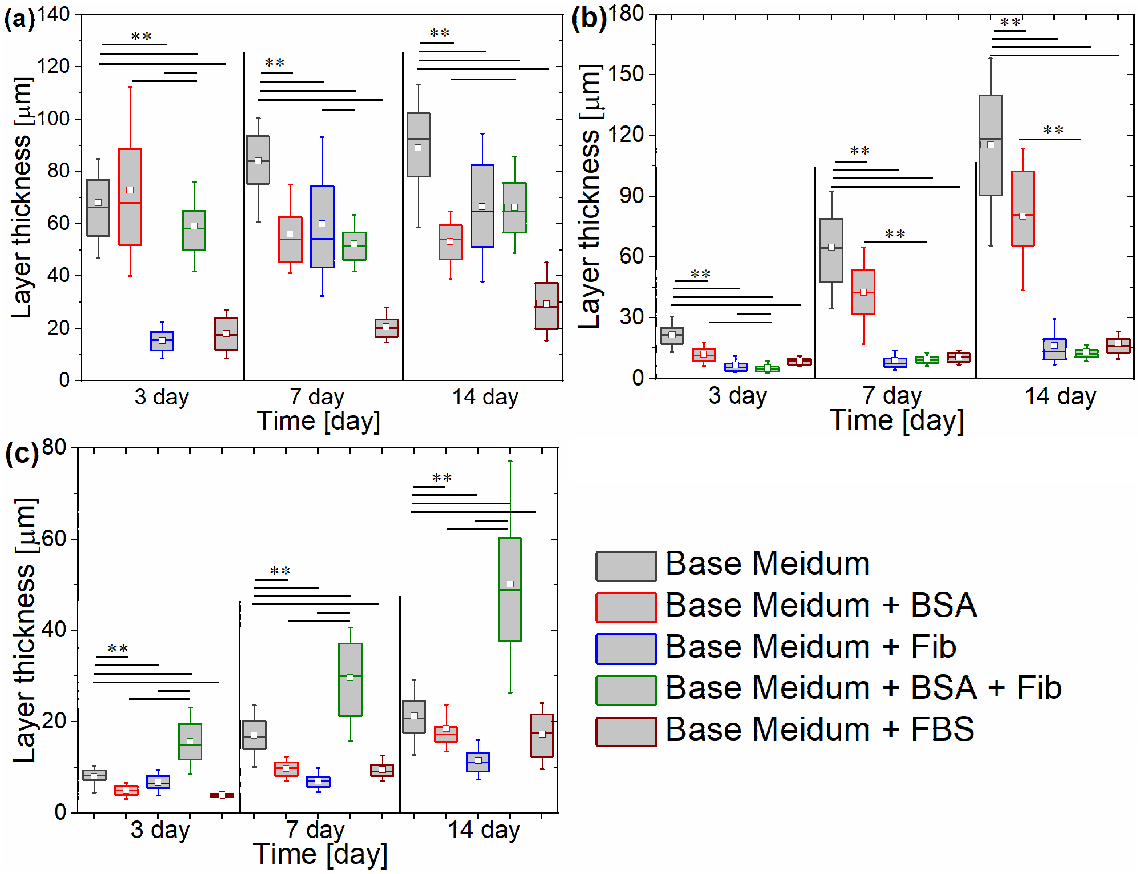

Figure 4.34: Thickness of degradation layer formed in HBSS-based (a), HBSSCa-based (b) and DMEM-based (c) media after different immersion time. (The solid line indicates significant difference, One-way ANOVA, Dunn's test, Significance level: (*): $p < 0.05$, (**): $p < 0.01$)

The weight percentages of Ca and P in the degradation layer were calculated according to the chemical mapping results. As depicted in Fig. 4.35, the wt.% of Ca and P increased with immersion time irrespective of media composition due to the fresh media provided at intervals and the progression of Mg degradation. Generally, higher contents of Ca and P existed in degradation layer formed in DMEM and HBSSCa than in HBSS, which resulted from the higher concentration of PO_4^{3-} or Ca^{2+} in HBSSCa and DMEM. Moreover, the addition of proteins also evidently promoted the increase of the wt.% of Ca and P in degradation layer. The presence of FBS generally resulted in a higher content of Ca and P in degradation layer than BSA, especially during the initial immersion time. The wt.% of Ca and P formed in HBSSCa + BSA + Fib was higher than that in HBSSCa + BSA. However, in DMEM-based media, it showed an adverse result that the content of Ca and P was much lower in degradation layer formed in DMEM + BSA + Fib than in DMEM + BSA and DMEM + Fib.

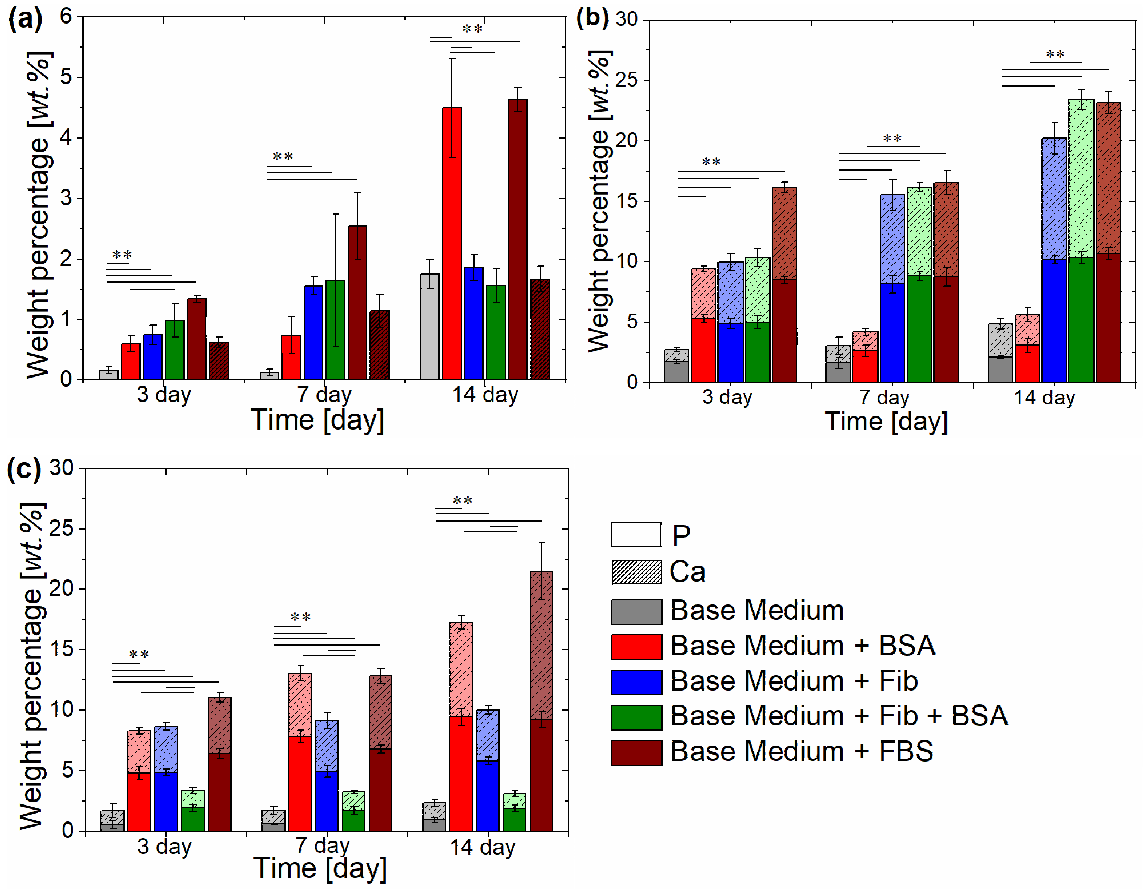

Figure 4.35: Weight percentages of Ca and P in degradation layer formed in HBSS-based (a), HBSSCa-based (b) and DMEM-based (c) media after different immersion time. The solid line indicates significant difference for P/Ca content, One-way ANOVA, Dunn's test, Significance level: (*): $p < 0.05$, (**): $p < 0.01$. No significant difference of Ca content between HBSSCa and HBSSCa + BSA after 7 days of immersion, and between DMEM and DMEM + BSA + Fib after 3 and 7 days of immersion.

Furthermore, the thickness of Ca/P-rich layer in the top of degradation layer formed in HBSSCa-based and DMEM-based media were estimated as shown in Fig. 4.36. Generally, the thickness of this Ca/P-rich layer increased when proteins were present in media. In HBSSCa, co-existence of BSA and Fib resulted in a comparable thickness of the Ca/P-rich layer to that formed in HBSSCa + BSA or Fib, while in DMEM the thickness of this Ca/P-rich layer significantly decreased when both BSA and Fib were present compared with that in DMEM + BSA or Fib.

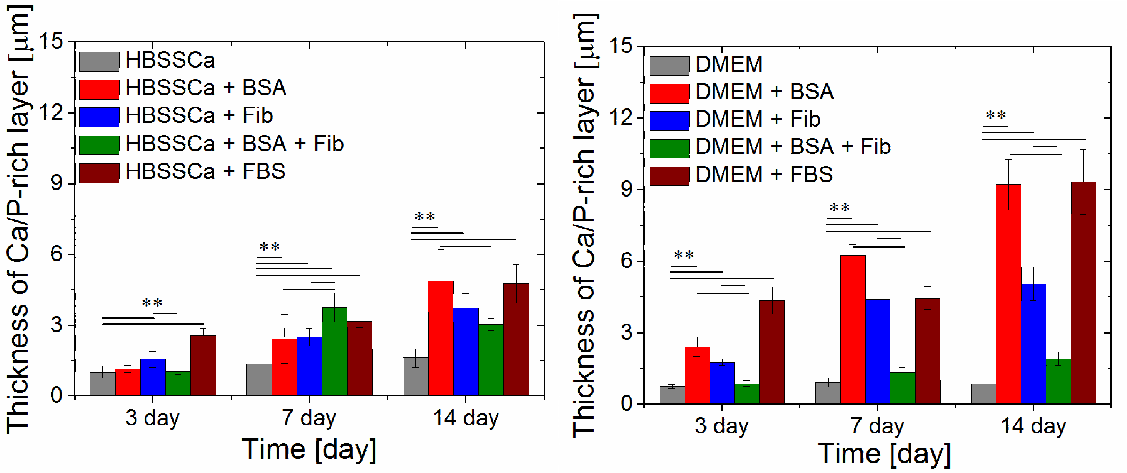

Figure 4.36: Thickness of Ca/P-rich outmost layer formed in HBSSCa-based and DMEM-based media. The solid line indicates significant difference, One-way ANOVA, Dunn's test, Significance level: (*): $p < 0.05$, (**): $p < 0.01$.

4.2.3. Protein adsorption

Adsorption of fluorescent proteins during immersion

The adsorption of fluorescent BSA and Fib on Mg surfaces during immersion are shown in Fig. 4.37. The results revealed that both BSA and Fib successfully adsorbed on Mg surface in HBSS and DMEM, while almost no adsorption could be observed on tissue culture plastic (the controls). No autofluorescence was visible for Mg samples during the immersion (results not shown). The adsorption of BSA and Fib increased with immersion time in HBSS, while no difference was observed for protein adsorption in DMEM. After 24 h of immersion, BSA and Fib exhibited significantly stronger and more uniform adsorption on Mg surface in HBSS than in DMEM, and only some spots showed an obvious adsorption in DMEM.

The cross sections of samples are presented in in Fig. 4.38. In HBSS, stronger and more uniform adsorption of proteins on the degradation layer was observed compared to DMEM. Moreover, proteins adsorbed mainly on the top of the degradation layer, and little on the inner products in DMEM, especially for BSA.

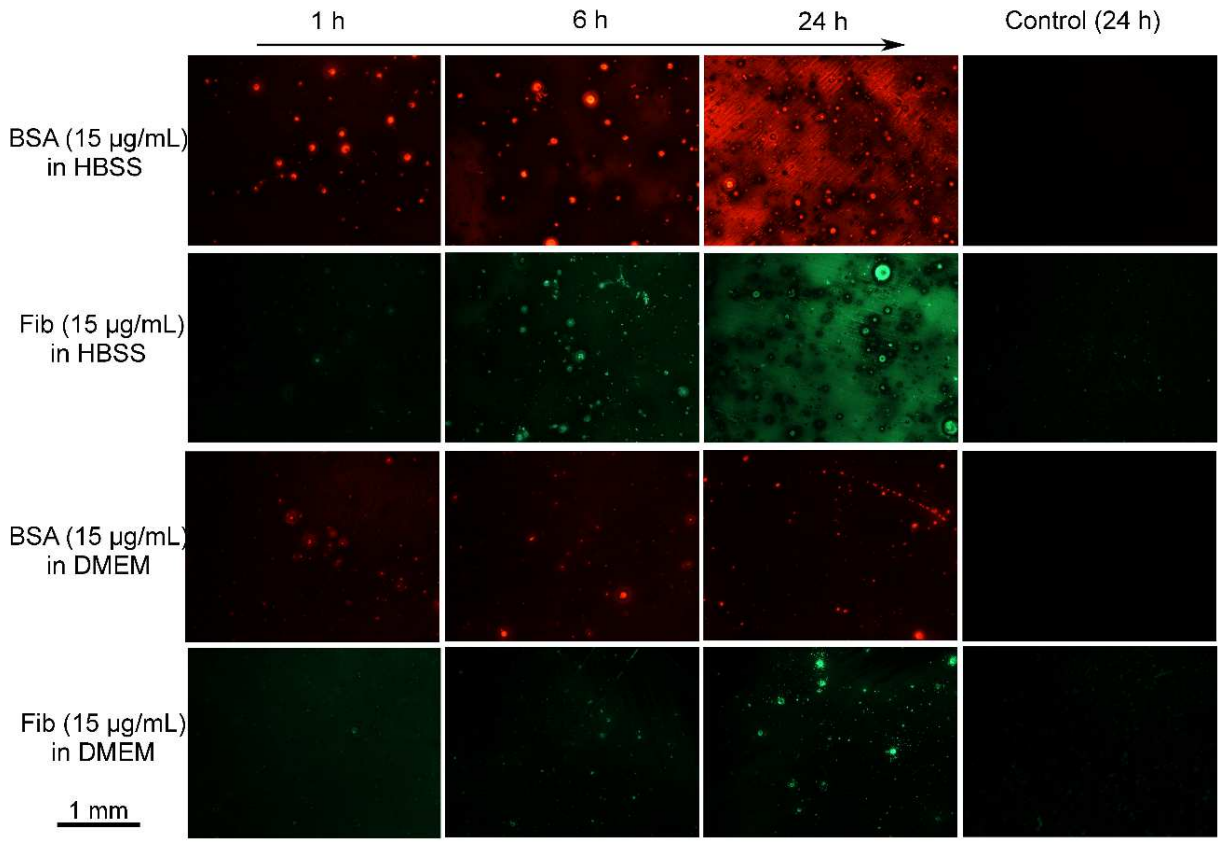

Figure 4.37: The adsorption of fluorescent BSA and Fib on pure Mg during immersion in HBSS and DMEM (exposure time during imaging: 1.5 s). Higher brightness of images indicates more adsorption of proteins on surface due to the same parameters used during imaging.

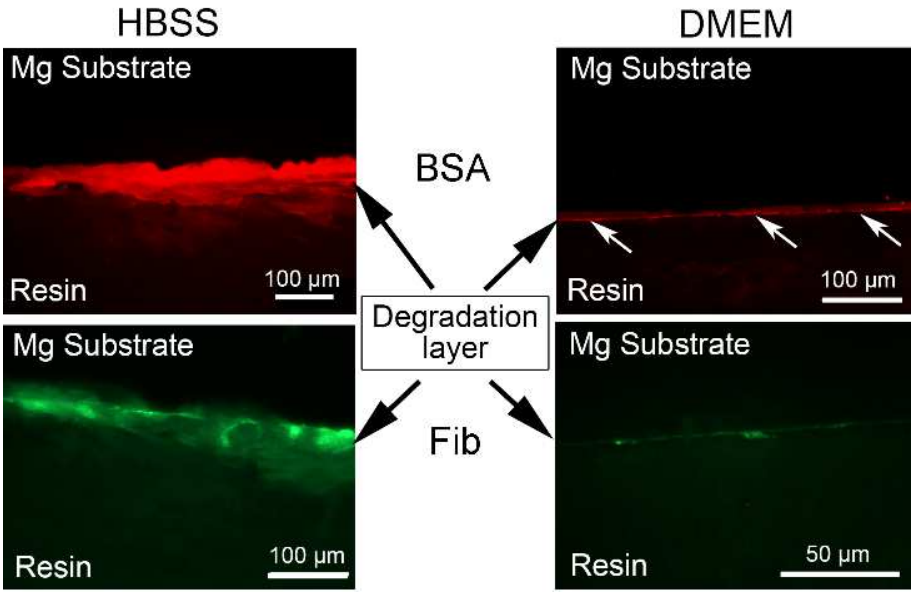

Figure 4.38: Cross sections of samples after 2 days of immersion in media with fluorescent BSA or Fib. In HBSS with fluorescent BSA or Fib (left, exposure time during imaging: 0.5 s) and in DMEM with fluorescent BSA or Fib (right, exposure time during imaging: 1.5 s). White arrows refer to the outmost layer formed in DMEM.

Adsorption of fluorescent proteins after immersion

To simplify the analysis of protein adsorption during Mg immersion, the process was separated into two steps (immersion and adsorption) to check the effect of surface conditions on protein adsorption. Firstly, the effect of immersion solutions and adsorption solutions on protein adsorption on corroded Mg surface was performed. As shown in Fig. 4.39, the Mg surface formed in HBSS exhibited more adsorption for BSA and Fib than that formed in DMEM irrespective of adsorption solutions used. Three kinds of adsorption solutions (water, HBSS and DMEM) resulted in a slight difference for the adsorption of protein on Mg surfaces formed in the same immersion solution. This difference could be caused by the change of surface during adsorption process.

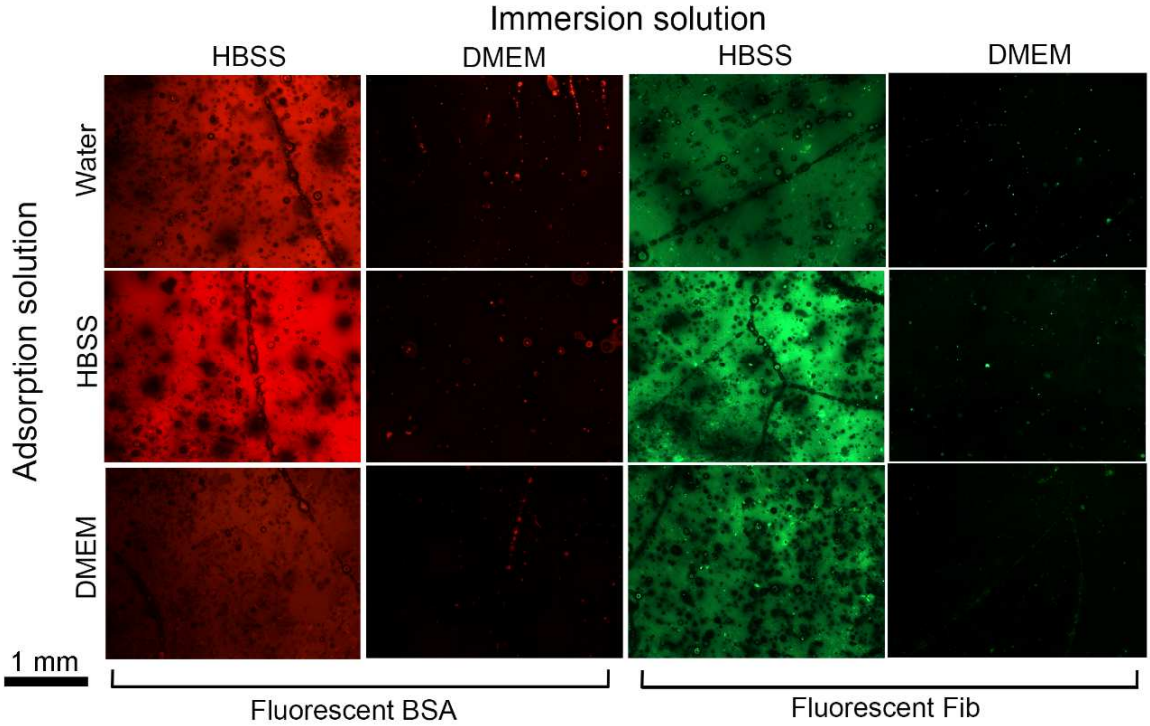

Figure 4.39: The adsorption of fluorescent BSA or Fib on the corroded Mg surface after immersion in different solutions for 1 day (exposure time during imaging: 1.5 s).

To identify which components are mainly responsible for the difference of corroded Mg surfaces formed in HBSS and DMEM, different immersion solutions were prepared for protein adsorption after immersion according to the media composition. As shown in Fig. 4.40, the addition of $MgSO_4$, $NaHCO_3$ or L-alanyl-L-glutamine (L-Ala-L-Gln) alone to immersion media (HBSS) resulted in changes of the surface, for example the formation of needle-like precipitates, but no attenuated adsorption of BSA and Fib was observed. However, when $CaCl_2$ was present, the adsorption of BSA and Fib on the corroded Mg surface was largely reduced. When $MgSO_4$, $NaHCO_3$ or organic components (L-Ala-L-Gln or glucose) were added to the immersion media in the presence of $CaCl_2$, the adsorption of BSA and Fib was still restrained. As expected, when the composition of immersion solution is approaching that of DMEM (Fig. 4.39), the adsorption of proteins on the

corroded Mg surface was reduced. Moreover, the effect of adsorption solution on protein adsorption was also examined by using the same immersion solution (HBSS) but different adsorption solutions. The results showed similar adsorption (Fig. 4.41), which further highlighted the importance of Mg surface formed in different media upon protein adsorption.

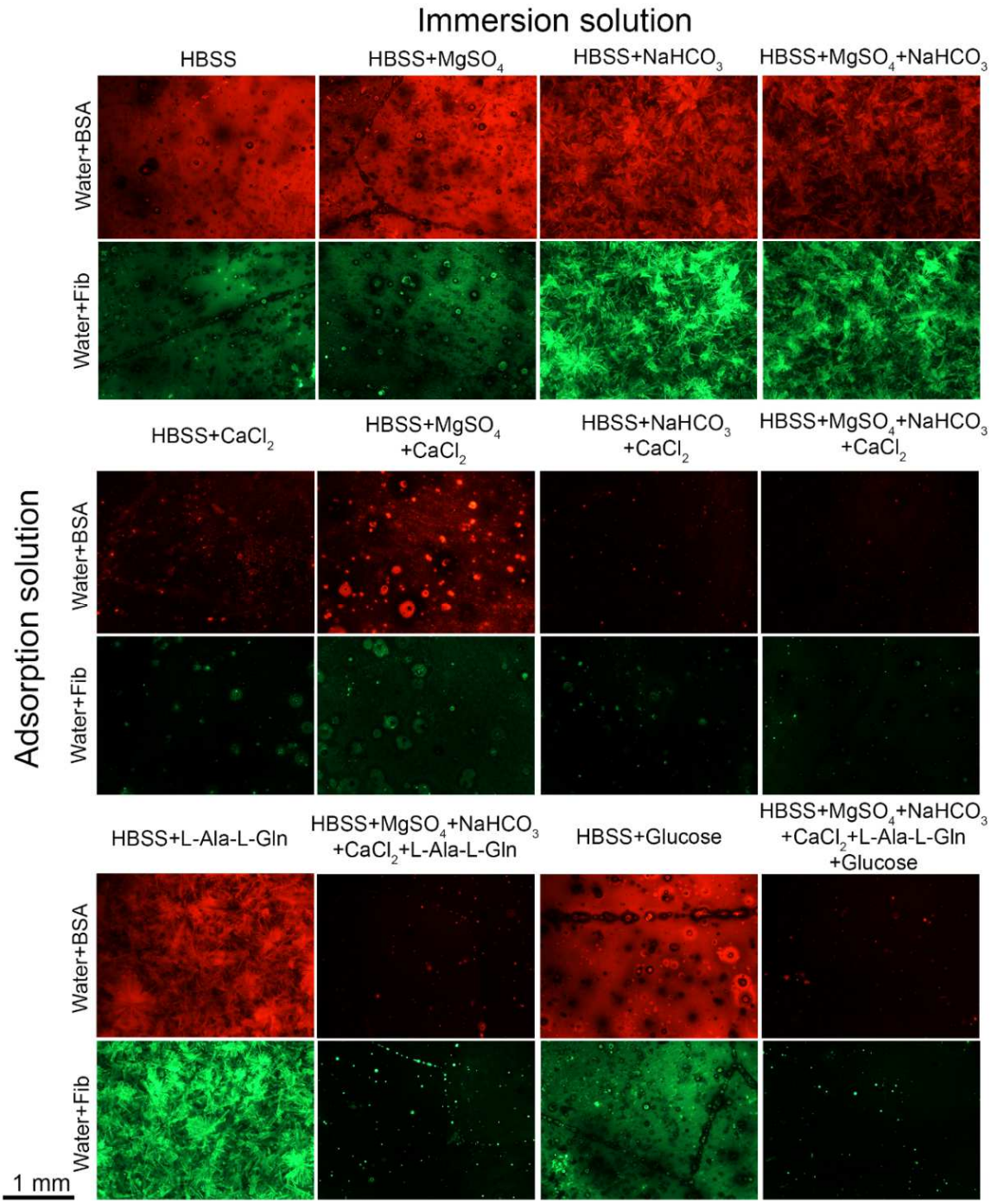

Figure 4.40: Fluorescent micrographs of pure Mg after immersion in different solutions for 1 day, then stained in water with 15 µg/mL fluorescent BSA or Fib for 1 h in incubator (exposure time during imaging: 1.5 s). The concentration used was 0.81 mM for $MgSO_4$, 1.80 mM for $CaCl_2$, 39.88 mM for $NaHCO_3$, 4 mM for L-alanyl-L-glutamine (L-Ala-L-Gln) and 19.44 mM for glucose. The results for DMEM can be found in Fig. 4.39.

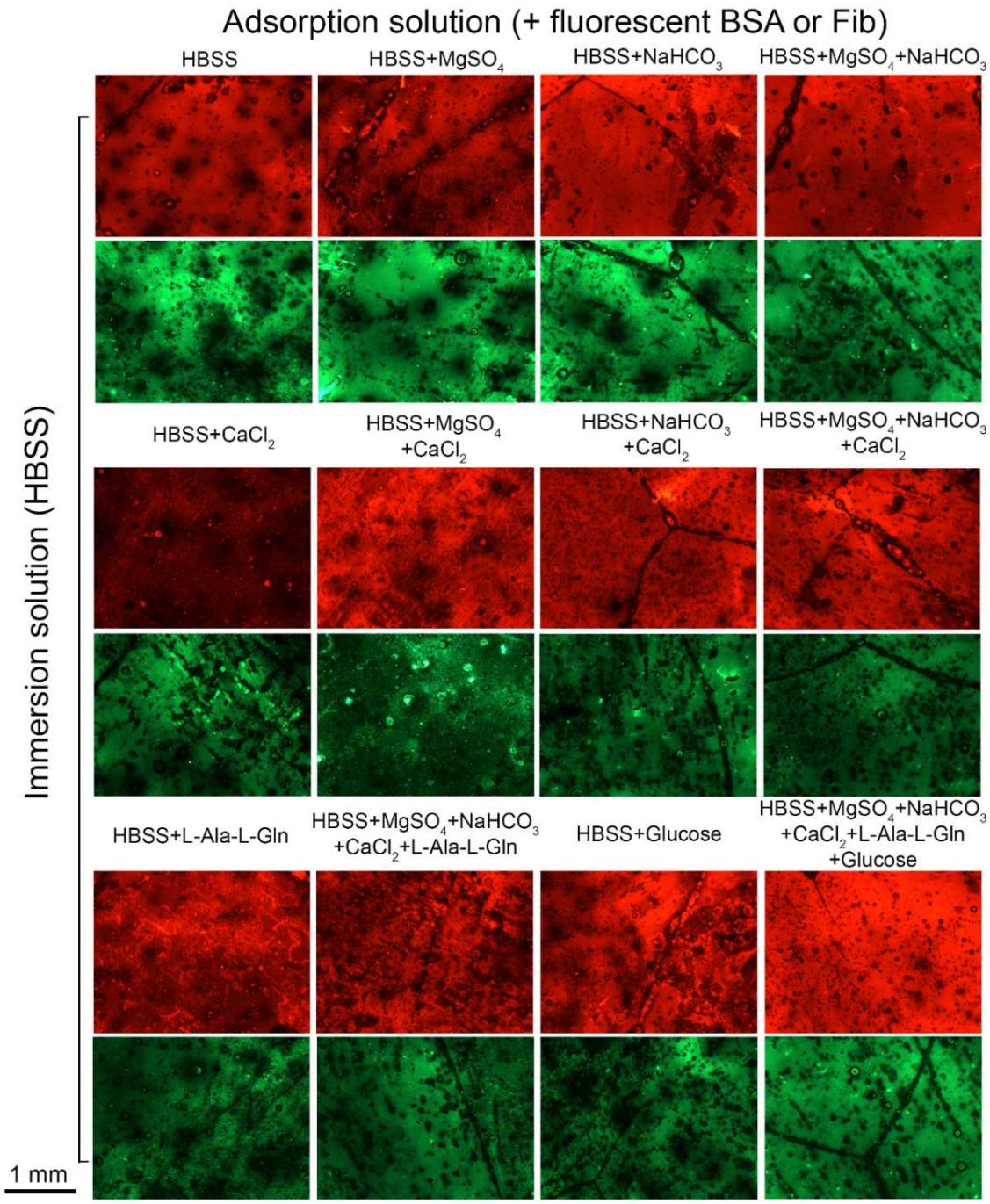

Figure 4.41: Fluorescent micrographs of pure Mg after immersed in HBSS for 1 day, then stained in different adsorption solutions with 15 µg/mL fluorescent BSA or Fib for 1 h in incubator (exposure time during imaging: 1.5s). The concentration used was 0.81 mM for $MgSO_4$, 1.80 mM for $CaCl_2$, 39.88 mM for $NaHCO_3$, 4 mM for L-alanyl-L-glutamine (L-Ala-L-Gln) and 19.44 mM for glucose.

Adsorption of proteins on possible degradation products

The possible degradation products formed in HBSS and DMEM were synthesized and characterized in an attempt to examine the effect of surface chemistry on protein adsorption. As shown in Fig. 4.42, the synthesized $CaCO_3$, Ca-PO_4 and Mg-PO_4 are calcite (PDF 01-083-1762), apatite (PDF 01-070-0793, PDF 01-088-2169), and $Mg_3(PO_4)_2$ xH_2O (PDF 01-073-6719, PDF 00-

035-0329), respectively. The size of these four artificial products was in the range of 0.8-1.6 µm (Fig. 4.43 b).

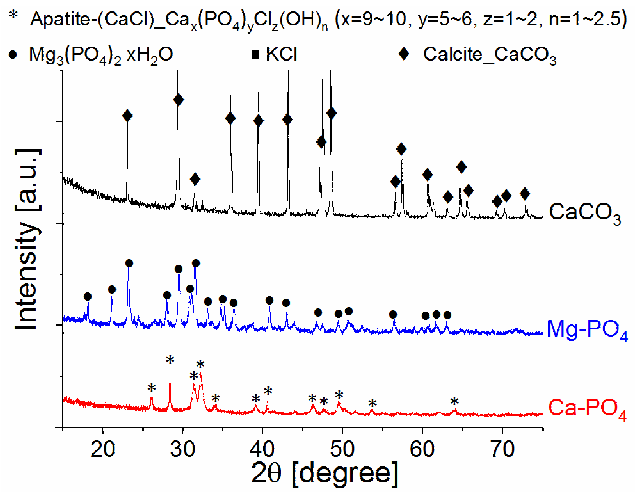

Figure 4.42: XRD patterns for different products prepared by precipitating method

The adsorption of fluorescent BSA and Fib on these four different products are displayed in Fig. 4.43. It showed that BSA and Fib had higher adsorption intensity on $MgCO_3$ and Mg-PO_4 compared to $CaCO_3$ and Ca-PO_4. The quantitative adsorption is depicted in Fig. 4.43b, which confirmed the results exhibited in Fig. 4.43 a. Generally, Fib showed a higher adsorption on the products than BSA, except on $CaCO_3$.

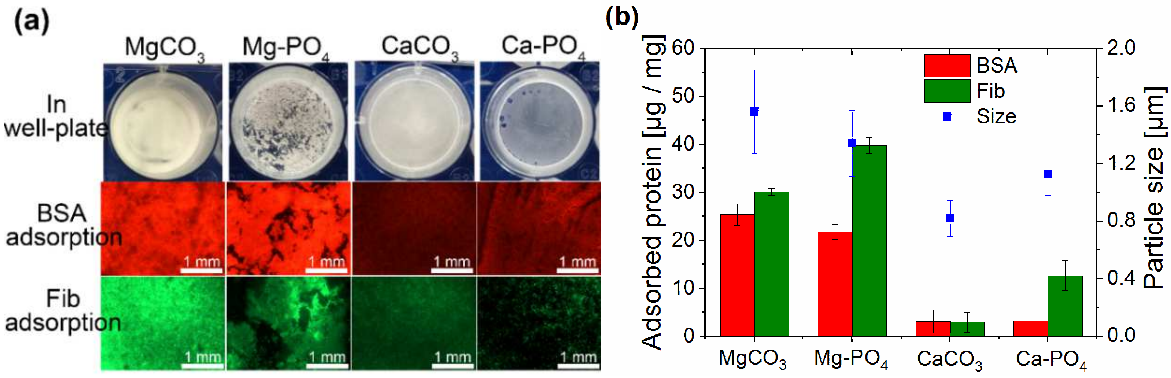

Figure 4.43: (a) Fluorescent BSA and Fib adsorption (15 µg/mL in water) on different degradation products in 12-well plates, (b) The adsorbed amount of BSA and Fib on different products and the size of the salts.

4.2.4. Factors for protein adsorption

pH and Osmolality

pH and osmolality during Mg immersion in protein-containing media are depicted in Fig. 4.44. pH in HBSS + protein rapidly increased to around 9.0 after 6 hours of immersion, while it remained stable at about 8.0 after 1 h of immersion in DMEM with protein. This was caused by the faster

degradation of Mg in HBSS and the higher buffering capacity of DMEM. The higher pH of DMEM (~ 7.7) than HBSS (~ 7.1) in the controls resulted from the higher concentration of HCO_3^- in DMEM. Similarly, osmolality of media also increased with the immersion time. Faster increase of osmolality was visible for HBSS + proteins compared to DMEM + protein. However, it still showed lower values in HBSS with protein compared with DMEM + protein during 24 h of immersion

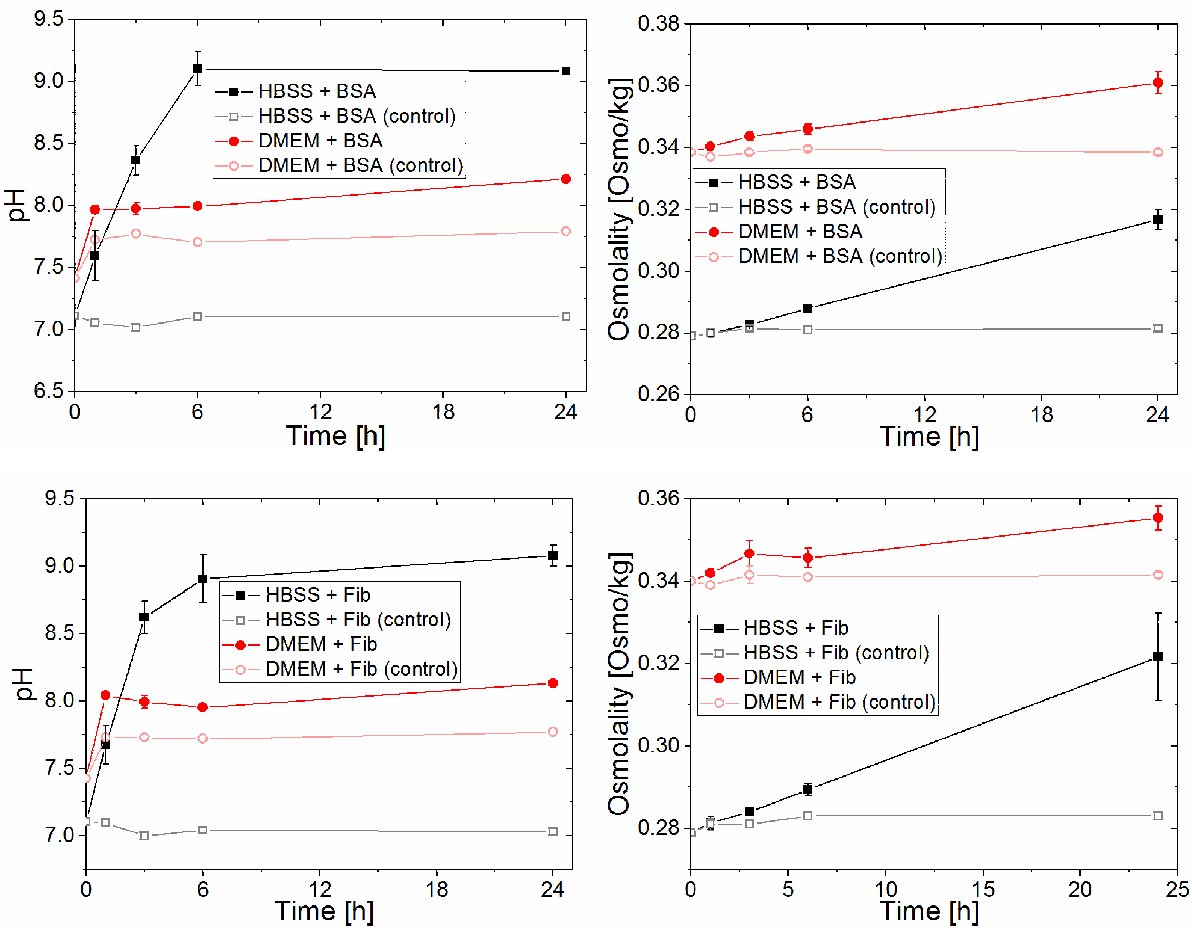

Figure 4.44: pH and osmolality of media during immersion in HBSS and DMEM with 15 µg/mL BSA or Fib.

Degradation rate

The degradation rates of pure Mg in HBSS and DMEM with and without proteins are presented in Fig. 4.45. Proteins resulted in a significant decrease of the degradation rate from 4.46 mm/year in HBSS to 1.09 mm/year (BSA) and 1.23 mm/year (Fib). In DMEM, the degradation rates were generally lower and only the addition of Fib led to a significant decrease compared with the control. The large protein-induced decrease of degradation rate in HBSS might be related to the higher adsorption of proteins on Mg surface during immersion.

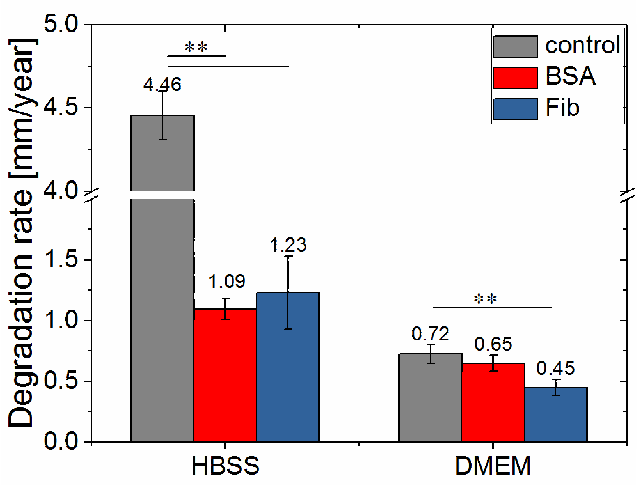

Figure 4.45: Degradation rate of pure Mg after immersion for 24 hours in HBSS and DMEM in the absence or presence of 15 µg/mL BSA or 15 µg/mL Fib. (One-way ANOVA, Dunn's test, Significance level: (*): $p < 0.05$, (**): $p < 0.01$)

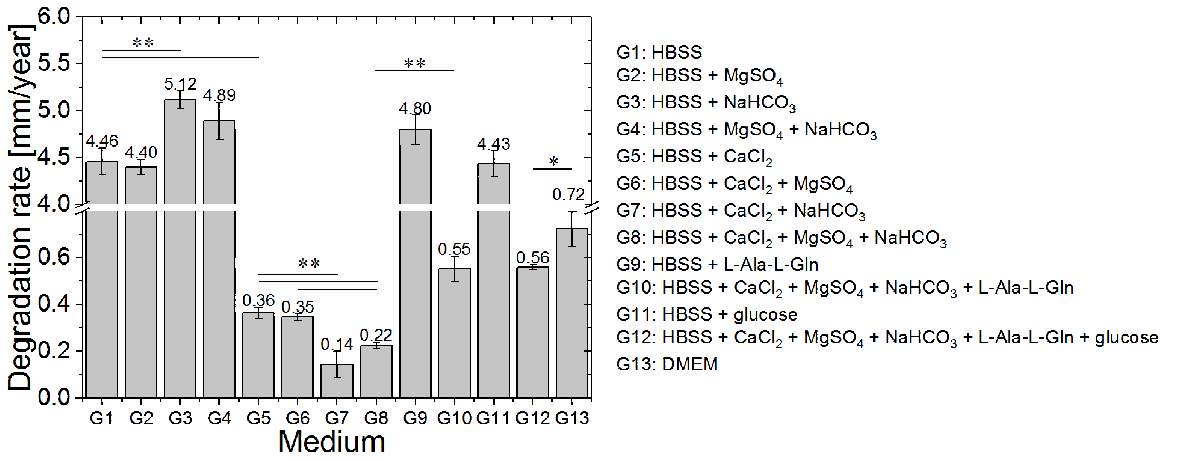

Figure 4.46: Degradation rate of Mg in different media after 24 h of immersion under cell culture conditions. The concentration used was 0.81 mM for $MgSO_4$, 1.80 mM for $CaCl_2$, 39.88 mM for $NaHCO_3$, 4 mM for L-alanyl-L-glutamine (L-Ala-L-Gln) and 19.44 mM for glucose. (One-way ANOVA, Dunn's test, Significance level: (*): $p < 0.05$, (**): $p < 0.01$)

The degradation rates of Mg after 24 h of immersion in different media are presented in Fig. 4.46. As expected, Mg degraded faster in HBSS than in DMEM. The addition of $MgSO_4$ alone showed little effect on Mg degradation, while the degradation rate significantly increased when $NaHCO_3$ was added alone or together with $MgSO_4$. More importantly, the degradation of Mg evidently decreased when $CaCl_2$ was present in media irrespective of other components. The further addition of L-Ala-L-Gln (medium G10) increased the degradation rate of Mg compared to medium G8. By comparing the degradation rate in medium G8 with that in DMEM (medium G13), it can be concluded that small organic molecules in DMEM promoted the degradation of Mg, which is in agreement with the previous results [71, 178]. The degradation rate correlated well with the

protein adsorption on corroded Mg surface, that is, faster degradation led to higher protein adsorption on the corroded Mg surface.

Surface wettability

To determine the hydrophobicity of the corroded Mg surface immersed in different media, contact angle measurements were performed after 24 h of immersion in HBSS and DMEM. It showed that the contact angle of bare Mg was 32.7 ± 3.5˚, while smaller contact angles were observed after 24 h of immersion in HBSS (not detectable) and DMEM (24.8 ± 4.8˚), indicating the increased hydrophilicity of Mg surface after immersion, especially in HBSS. However, after BSA / Fib adsorption for 1 h, the contact angles increased to 60.9 ± 2.1˚ / 27.6 ± 4.6˚ (HBSS) and 77.0 ± 3.3˚ / 44.1 ± 10.1˚ (DMEM). The different degree of contact angles from BSA and Fib might be related to the protein conformation on Mg surface.

Surface roughness

To follow the changes of surface conditions during immersion, surface roughness and protein adsorption after immersion in HBSS and DMEM were characterized as shown in Fig. 4.47. In HBSS, the surface showed little change after 1 h of exposure, and a rather thin and intact degradation layer was formed. After 6 h of immersion, precipitates formed, two different layers were visible from the cross section of the degradation layer and surface roughness (R_a / R_q) increased by a factor of about 2.5. After 24 h, the previously observed zonation of the degradation layer had developed to one loose degradation layer. Surface roughness changed from nanometer to micrometer scale. Simultaneously, the adsorption of BSA and Fib also obviously increased with immersion time. In contrast, the surface morphologies formed in DMEM exhibited little difference in the course of 24 h of immersion, as well as the surface roughness (R_a: 200 - 400 nm). The degradation layer seemed to remain robust and intact during 24 h of immersion, especially for the outermost layer (as marked by red arrows in Fig. 4.47). Accordingly, BSA and Fib showed weak adsorption on Mg surface within 24 h of immersion in DMEM except some spots.

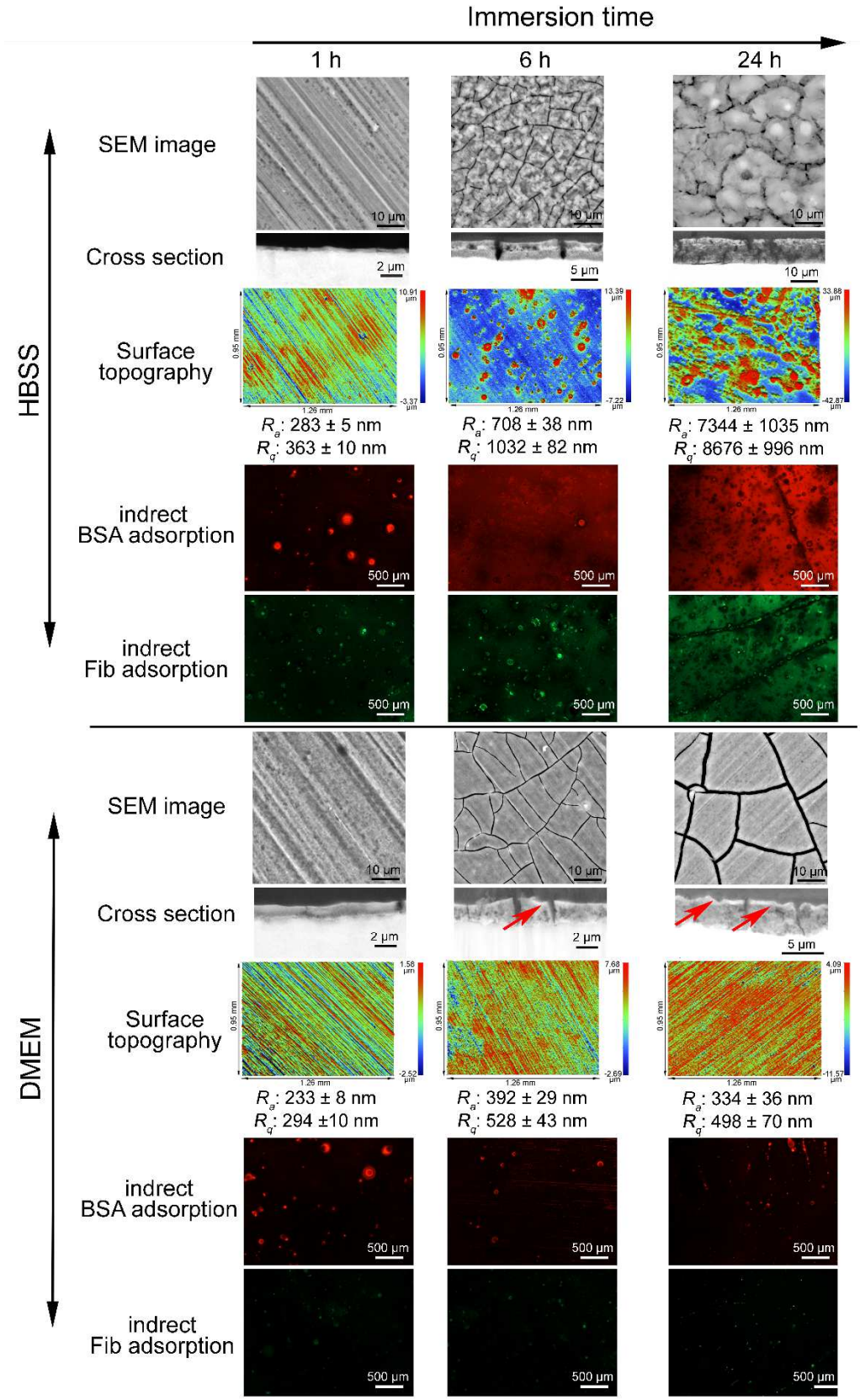

Figure 4.47: Surface morphology, roughness and indirect protein adsorption in HBSS and DMEM after different immersion time. Adsorption solution is water with 15 µg/mL fluorescent BSA or Fib, exposure time: 1.5 s. The red arrows in the SEM pictures of cross section refer to the intact outmost layer formed in DMEM.

Zeta potential

The zeta potentials of different products were analysed to illustrate the electrostatic interaction between proteins and products. As shown in Fig. 4.48, $CaCO_3$ showed the most negative potential in water (-26 mV), whereas the most positive potential was determined for $MgCO_3$ (~10 mV). This indicated an electrostatic attraction between proteins and $MgCO_3$, but an electrostatic repulsion between proteins and $CaCO_3$, due to the negative charge of BSA and Fib at pH > 6 [140, 143, 191]. Moreover, zeta potentials of Ca-PO_4 (~3 mV) and Mg-PO_4 (~ -3 mV) were close to zero. In 1 mg/mL Fib solution, all products showed negative potentials (-15 ~ -20 mV), indicating the change of surface charge caused by protein adsorption on their surfaces.

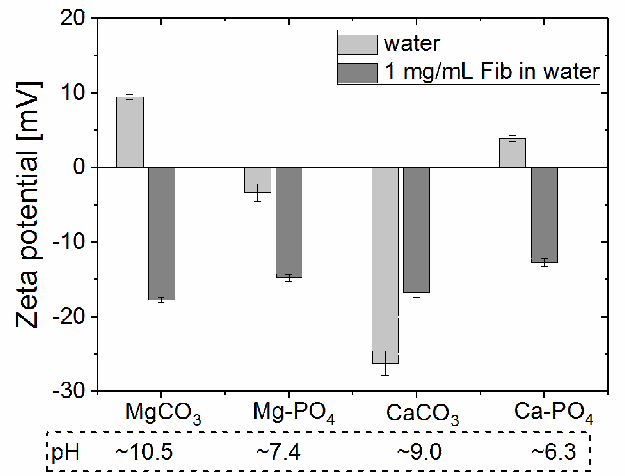

Figure 4.48: Zeta potentials of different degradation products in different solutions (water, 1 mg/mL Fib in water)

5. Discussion

5.1. Mg degradation

In general, when Mg is immersed into aqueous solution, it dissolves into solution as Mg^{2+} and hydrogen is evolved according to the following reactions (eq. 5.1).

$$Mg + 2H_2O \rightarrow Mg^{2+} + 2OH^- + H_2 \uparrow \quad (5.1)$$

Along with the dissolution of Mg, the pH of solution and the concentration of Mg^{2+} near the surface increase, resulting in the formation of degradation products on the surface. The critical Mg^{2+} concentrations for different products in HBSS, HBSSCa and DMEM have been calculated according to the products solubility (Section 3.7.), as shown in Fig. 5.1.

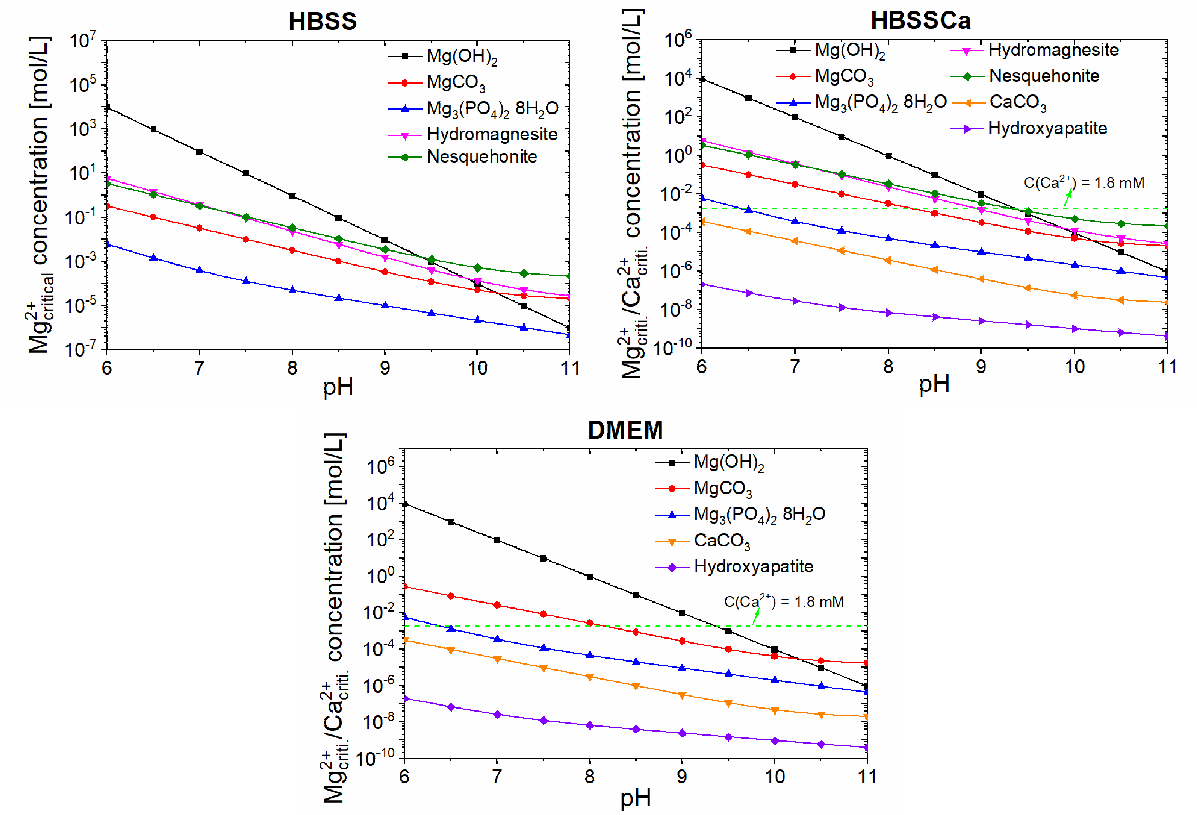

Figure 5.1: The critical Mg^{2+} / Ca^{2+} concentrations for the different products in HBSS, HBSSCa and DMEM with the increase of pH.

Due to the high pH (especially in HBSS) and high Mg^{2+} concentration close to Mg surface caused by the dissolution of Mg, according to the compositions of medium, several components as degradation products can be formed on the surface: $Mg(OH)_2$, $MgCO_3$, $Mg_3(PO_4)_2$, $CaCO_3$ and Ca-P salts [73, 77, 111].

$$Mg^{2+} + 2\ OH^{-} \rightarrow Mg(OH)_2 \quad (5.2)$$

$$Mg^{2+} + CO_3^{2-} \rightarrow MgCO_3 \quad (5.3)$$

$$3\ Mg^{2+} + 2\ PO_4^{3-} + 8\ H_2O \rightarrow Mg_3(PO_4)_2 \cdot 8H_2O \quad (5.4)$$

$$Ca^{2+} + CO_3^{2-} \rightarrow CaCO_3 \quad (5.5)$$

$$x\ Mg^{2+} + y\ Ca^{2+} + z\ PO_4^{3-} + n\ CO_3^{2-} \rightarrow Mg_xCa_y(PO_4)_z(CO_3)_n \quad (5.6)$$

Due to the absence of Ca^{2+}, $Mg_3(PO_4)_2$, $Mg(OH)_2$ and $MgCO_3$ are the main products formed in HBSS. According to the thermodynamical solubility calculations (as shown in Fig. 5.1), $CaCO_3$ and Ca-P salts can be formed in HBSSCa and DMEM before the formation of $MgCO_3$ and crystalline precipitates, which is in accordance with the result that a Ca/P-rich layer is formed in the top of degradation layer.

The continuous degradation of Mg leads to the increase of Mg^{2+} concentration and pH in media, eventually resulting in the saturation of Mg^{2+} for different salts (nesquehonite and hydromagnesite etc.). Therefore, some precipitates also deposit on the surface from the solution to form the “outer” white, loosely bound precipitates layer. In our study, two different precipitates are dominantly formed on the surface, i.e. hydromagnesite ($Mg_5(CO_3)_4(OH)_2\ 4H_2O$) and nesquehonite ($MgCO_3\ 3H_2O$), as shown in Fig. 4.5. Nesquehonite can be formed in three ways: (I) directly precipitated from solution (eq. 5.7), (II) hydrated from magnesite (eq. 5.8) or (III) transformed from hydromagnesite when the CO_2 pressure becomes sufficiently high (eq. 5.9) [188, 195].

$$Mg^{2+} + CO_3^{2-} + 3H_2O \rightarrow MgCO_3 \cdot 3H_2O \quad (5.7)$$

$$MgCO_3 + 3\ H_2O \rightarrow MgCO_3 \cdot 3H_2O \quad (5.8)$$

$$Mg_5(CO_3)_4(OH)_2 \cdot 4H_2O + CO_2 + 10\ H_2O \rightarrow 5\ MgCO_3 \cdot 3H_2O \quad (5.9)$$

Similarly, a number of possible formation pathways have been reported for hydromagnesite, for example, direct precipitation from solution (eq. 5.10). At high CO_2 pressure (about 10^{-5}-10^{-1} atm), magnesite can be hydrated to hydromagnesite along with the increase of water vapour pressure (eq. 5.11) [188]. At high water vapour pressure (about $10^{-2.8}$ ~ $10^{-1.5}$ atm), with the increase of CO_2 pressure, magnesium hydroxide can be converted into hydromagnesite (eq. 5.12) [188]. It can also be formed by dehydration of nesquehonite (eq. 5.13) [188].

$$5\ Mg^{2+} + 5\ OH^{-} + 4\ CO_3^{2-} + 4\ H_2O \rightarrow Mg_5(CO_3)_4(OH)_2{\cdot}4H_2O \quad (5.10)$$

$$5\ MgCO_3 + 5H_2O \rightarrow Mg_5(CO_3)_4(OH)_2{\cdot}4H_2O + CO_2 \quad (5.11)$$

$$5\ Mg(OH)_2 + 4\ CO_2 \rightarrow Mg_5(CO_3)_4(OH)_2{\cdot}4H_2O \quad (5.12)$$

$$5\ MgCO_3{\cdot}3H_2O \rightarrow Mg_5(CO_3)_4(OH)_2{\cdot}4H_2O + CO_2 + 10\ H_2O \quad (5.13)$$

Based on the conditions used in this study, the precipitates are possibly formed as the equations (5.7, 5.8, 5.10, 5.11, 5.13) indicated. Additionally, the type of the “outer” loosely bound precipitates (nesquehonite or hydromageniste) may affect the thickness of degradation layer. When nesqueshonite deposits on the surface, the degradation layer is significantly thinner than that formed by hydromagnesite precipitates (Fig. 4.2 c).

Organic molecules do not directly participate in the formation of degradation products, but affect the equilibriums of product formation. According to the results obtained, the obvious effects of organic molecules on the ‘outer’ crystalline precipitates and Ca/P-rich layer can be found, which are related to the binding/chelating and/or the adsorption of organic molecules and the interaction between organic molecules, which will be discussed in the following.

5.2. Effect of organic molecules on Ca/P-rich layer

Two situations for the degradation layer can be found in this study: i) the P-rich layer is close to the Mg matrix, covered by crystalline precipitates, which normally refers to the breakage of degradation layer and high degradation rate (> 1 mm/year), ii) the Ca/P-rich products distribute in the top of degradation layer, which are usually formed in the presence of Ca^{2+} in media without the breakage of the top Ca/P-rich layer, generally corresponding to a lower degradation rate (< 1 mm/year).

Although the degradation rate of Mg determines the degradation layer formed on Mg surface, in turn the layer regulates the diffusion processes during Mg degradation and promotes the passivation of Mg. Therefore, whether the top of degradation layer is broken or not can largely affect the degradation rate of Mg. As shown in Fig. 5.2, it is not surprising that the breakage of the degradation layer corresponds to higher degradation rate of Mg, while the intact layer refers to slower degradation of Mg in media, revealing the importance of the integrity of degradation layer to Mg degradation. In turn, faster degradation of Mg leads to thicker degradation layers, which results in the breakage of the layer due to the increasing internal pressure in the degradation layer and the fast hydrogen evolution.

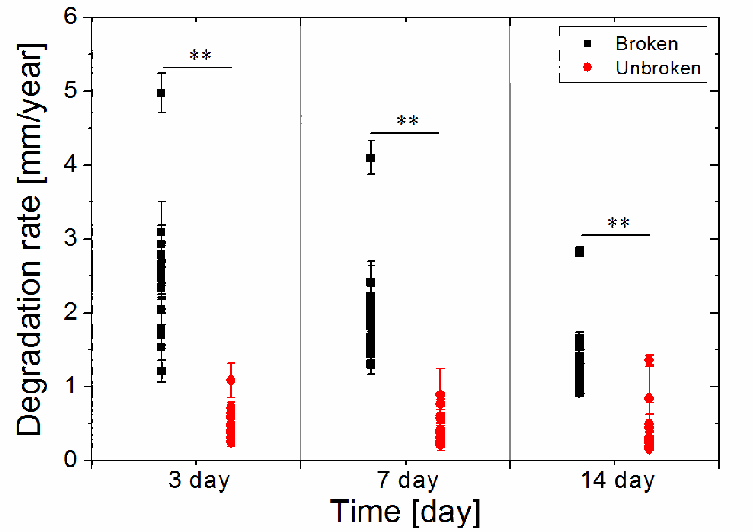

Figure 5.2: Degradation rate of pure Mg in different media with a broken or unbroken top degradation layer.(One-way ANOVA, Dunn's test, Significance level: (*): p<0.05, (**): p<0.01)

In the case of the broken top degradation layer, the addition of organic molecules (e.g. small organic molecules or proteins in HBSS) generally leads to a high content of phosphorous in the degradation products (Fig. 4.8), suggesting that organic molecules promote the formation of phosphates in the "inner" degradation layer, which may inhibit the degradation of Mg. It was reported that some amino-functionalized materials were chosen as phosphate adsorbents to remove phosphate from aqueous solutions by electrostatic attraction and the adsorption capacity was almost unaffected by the presence of competitive ions but changed with pH and temperature [196-200]. Moreover, it has been found that the absorbed amino acids on surfaces can promote hydroxyapatite mineralization by attracting Ca^{2+} and PO_4^{3-} and increasing the local supersaturation [201]. These are possible explanations for the increased content of phosphate in the "inner" degradation layer formed in media containing organics.

When Ca^{2+} is present, the Ca-P salts will be firstly formed in the top of Mg surface as shown in Fig. 5.1, leading to an *in vivo*-like degradation layer. It is in agreement with the reported results that outer Ca/P-rich layer is always formed separately from the inner degradation layer ($Mg(OH)_2$, (Mg,Ca)-CO_3) [79, 80, 94, 202]. In most cases, no crystalline precipitates are formed on the surface due to the slow degradation. Furthermore, this top Ca/P-rich layer is believed to significantly slow down the degradation rate of Mg [80]. As indicated in Fig. 5.3, the relationship between the degradation rate and the content of Ca + P / the thickness of top Ca-P rich layer are presented, respectively. In general, the higher content of Ca-P and the thicker Ca/P-rich layer correspond to lower degradation rate, which is in accordance with the reported results [80]. This could be the reason for the lower degradation rate in HBSSCa compared to HBSS under static conditions.

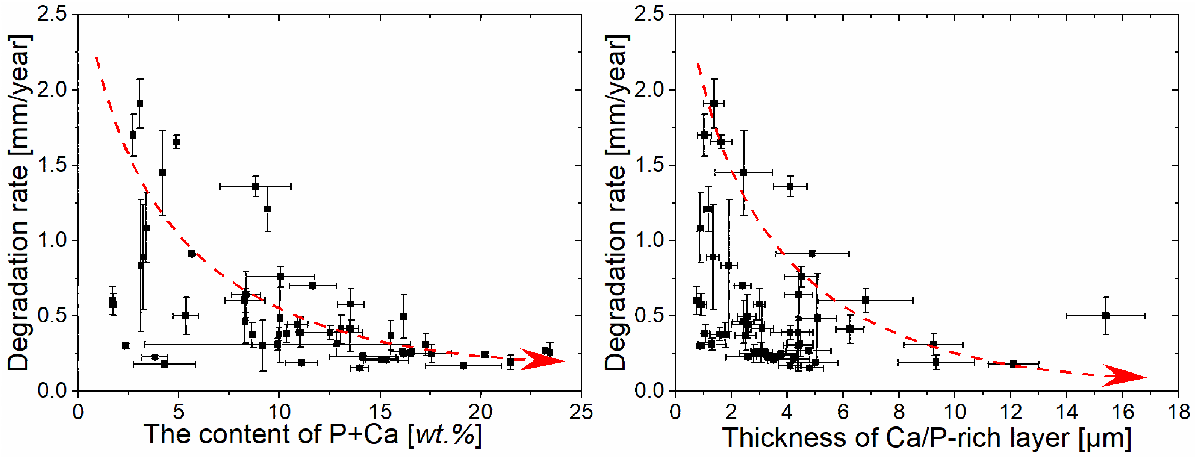

Figure 5.3: Relationship between degradation rate and the top Ca/P-rich layer formed in media during immersion. (Red dash arrow refers to the general change of degradation rate as the content of wt.% Ca+P or the thickness of Ca/P-rich layer increases)

Under static conditions, some Ca-P particles are formed on the positions where localised dissolution of the top layer happens in HBSSCa-based media (Fig. 4.13), which is caused by the locally increased pH at these sites and the sufficient amount of Ca^{2+} and PO_4^{3-} in solution. However, the average wt.% of P and Ca decrease in HBSSCa-based media and DMEM with immersion time except wt.% of Ca in HBSSCa + FBS (Table 4.1), indicating the instability of Ca-P products on Mg surface. Correspondingly, the degradation rate of Mg in HBSSCa increases after 21 days of immersion (data not shown), which further highlights the relationship between the top Ca/P-rich layer and Mg degradation. In contrast, the wt.% of Ca and P in the top of Ca/P layer increased over time under semi-static conditions. This difference can be ascribed to the different conditions during immersion, such as total ions concentration, media change and pH.

As reflected in Fig. 4.15 and 4.31, proteins (BSA or FBS) stabilize the degradation layer and prolong the protection duration irrespective of static or semi-static conditions, accompanying by relatively slow degradation rate. Furthermore, the addition of proteins, especially FBS, to HBSSCa or DMEM increases the contents of Ca and P in the top layer regardless of conditions used, which is verified by EDX (Figs. 4.18 and 4.35) and XPS results (Fig. 4.29). This could be one reason for the protein-induced decrease of degradation rate under physiological conditions. The promoted formation of Ca-P salts in immersion media may be related to the complex biomineralization process. Generally, collagen fibrils provide a framework known as extracellular matrix (ECM), which determines the ultimate structure and orientation of hydroxyapatite (HA). A set of negatively charged phosphorylated non-collagenous proteins can attract Ca^{2+} and PO_4^{3-} ions through their charged amino acid (AA) residues and increase the local supersaturation to form the nuclei with a critical size, which can develop into HA

crystals [201, 203, 204]. Therefore, the electrostatic interaction between adsorbed proteins and Ca^{2+}/PO_4^{3-} could be the reason for the promoted Ca-P salt formation on Mg surface, indicating the importance of the interaction between Ca^{2+}, PO_4^{3+} ions and adsorbed proteins for HA precipitation. Additionally, the existence of Ca^{2+} and PO_4^{3-} in FBS can also promote the formation of phosphate in the degradation layer. However, other adverse results were reported that FBS led to a low content of P and Ca in the degradation products on Mg surfaces [74, 154]. This discrepancy possibly derives from the different testing environments and detection parameters used, such as protein concentration and detection depth.

5.3. Effect of organic molecules on crystalline precipitates

In this study, crystalline precipitates are formed at relatively high degradation rate (> 1 mm/year under semi-static conditions) or after relatively long-time immersion (under static conditions due to the accumulation of Mg^{2+}). Hydromagensite is only found in HBSS or HBSS with single small organic component, while the addition of two or more kinds of small organic components and the addition of proteins to HBSS leads to the formation of nesquehonite. It is obvious that the precipitates are formed faster under semi-static conditions (3 day) than under static conditions (14 day). This is due to the low medium volume used under semi-static conditions, leading to a higher osmolality during the initial days of immersion than under static conditions. It can also be verified by the variation trends of pH and osmolality during immersion (Figs. 4.10 and 4.20).

The formation of different precipitates results from pH, free Mg^{2+} concentration and possible influence of organic molecules on the nucleation and/or growth of products. The changes in pH do not only depend on the buffering of HCO_3^-/CO_2. The addition of small organic components, especially when at least two kinds of small organic components are added, results in a lower pH than in HBSS during the immersion. This may be related to the buffering capacity of the carboxyl-groups and amino-groups of organic molecules, since the pH values are still lower than that of HBSS even after 14 days of incubation when the degradation rates of Mg in the organic-containing media are already higher than that of the control (Fig. 4.1). However, in all the cases with precipitates formation, pH is in the range of 8.0-8.5, suggesting little effect of pH on the priority of products formation (hydromagnesite and nesquehonite), as indicated by the thermodynamic calculation (Fig. 5.1).

On the other hand, Mg^{2+} concentration in the solution can be reflected by the osmolality of media. The obvious feature for the media containing organic components is the higher osmolality compared to that in HBSS solution under semi-static conditions (Fig. 4.2 b and 4.20). It can be explained by the binding/chelating effect of ions to organic molecules [72, 205-

207]. When organic molecules are present in media, a part of Mg^{2+} is bound to them as shown in eq. 5.14.

$$C\ (\text{total } Mg^{2+}) = C\ (\text{bound } Mg^{2+}) + C\ (\text{free } Mg^{2+}) \quad (5.14)$$

In blood plasma, approximately 45% of Mg^{2+} is complexed by albumin [140]. Mg^{2+} competes with Ca^{2+} for the binding sites in serum albumin, but with a lower binding affinity ($K_a(Ca^{2+})$ = 1.5×10^3 M^{-1}, $K_a(Mg^{2+})$ = 1×10^2 M^{-1}) [140, 208]. At least three binding sites of albumin for Ca^{2+}/Mg^{2+} have been identified and they possess variable affinity and binding capacity [140, 209]. Moreover, the binding of Ca^{2+}/Mg^{2+} to albumin is getting much higher with increasing ion concentration and increasing pH above the physiological level due to the increased net negative charge of protein and conformation change [171, 209-211]. Therefore, the binding of Mg^{2+} to organic molecules affect the free Mg^{2+} concentration in media, thereby possibly leading to the formation of different crystalline precipitates.

Additionally, as shown in Fig. 5.1, in view of thermodynamics, hydromagnesite should be formed prior to nesquehonite with increasing free Mg^{2+} concentration in the range of pH 8-9. However, under semi-static conditions only nesquehonite is observed in two kinds of organic molecules and protein-containing media. Moreover, under static conditions, in HBSS + BSA, only crystalline nesquehonite is formed with the increase of osmolality at a relatively stable pH. The possible explanation is that the presence of organic molecules may also affect the nucleation of products or the kinetics of products formation process [201].

Under semi-static conditions, the media are changed every 2 or 3 days, which results in fresh media with low osmolality and low pH after the change of media. This condition leads to the dissolution or transformation of nesquehonite, resulting in the change of morphology with immersion time (Fig. 4.5), because the solubility and stability of nesquehonite is related to the concentration of Mg^{2+} and pH [212, 213]. It has also been demonstrated that nesquehonite, as the precursor of hydromagnesite, can decompose to hydromagnesite with the formation of some intermediate hydrate phases, such as, dypingite and protohydromagnesite [195, 214], which were also identified on Mg surface in HBSS under flow conditions (data not shown). The transformation between these carbonates is tightly related to the fluctuation of some parameters, e.g. pH， Mg^{2+} concentration, temperature, etc. [215]. The processes of precipitation are quite complex, since the family of magnesium carbonates consists of a variety of compounds and they can be transformed into each other under certain conditions [214, 216, 217]. Therefore, a slight change of parameters in the immersion experiment setups in other studies might lead to the formation of other members of this family.

5.4. Ion binding of proteins

Besides the decreased free Mg^{2+} concentration due to the binding/chelating of Mg^{2+} to organic molecules, the binding/chelating is also believed to promote the dissolution of Mg due to the equilibrium shift of Mg dissolution reaction (eq. 1). However, organic molecules generally have binding effect for lots of species, such as Ca^{2+}, Zn^{2+} or Fe^{3+}. As revealed in Fig. 4.19, the addition of Ca^{2+} to HBSS largely enhances the corrosion inhibition of proteins to Mg degradation under semi-static conditions, suggesting the synergistic effect of proteins and Ca^{2+}, especially for Fib and FBS. This may be related to the high affinity of proteins to Ca^{2+} [208, 210]. Ca^{2+} is required as a catalyst during the course of polymerization conversion process from fibrinogen to fibrin, while it also protects the Fib molecules against thermal denaturation due to the stabilization of a more compact structure [218]. Furthermore, the addition of Ca^{2+} can change the zeta potential of degradation products, thereby affecting the electrostatic interaction between proteins and degradation products. For example, the zeta potential of hydroxyapatite increases as Ca^{2+} concentration increases [168]. Additionally, the presence of Ca^{2+} results in the different compositions of degradation products and different surface charge, thereby affecting protein adsorption on Mg surface (Fig. 4.40).

Besides Mg^{2+} and Ca^{2+}, impurities, e.g. Fe^{3+}, dissolved from Mg matrix, can also be bound to organic molecules. Transferrin (~80 kDa, pI: ~5.2-6.4), existing in FBS, is an iron-binding blood plasma glycoprotein with two specific high-affinity sites for reversible Fe ion binding [219-221]. The binding of Fe ions to transferrin can decrease Mg degradation due to the limitation of the Fe re-deposition on Mg surface. The Fe re-deposition is largely promote Mg degradation and has been modelled as a corrosion mechanism [173]. The inhibition efficiency of iron-complexing agents has been analysed for *in vitro* degradation of Mg alloys and strong Fe ion complexing agents can efficiently decrease the corrosion rate of Mg [174]. Similar cases can also be applicable to other impurity ions, e.g. Ni^{2+}, Cu^{2+} etc.. The different structure and conformation result in different binding affinity of proteins to kinds of ions. Therefore, the binding/chelating ability of proteins to different ions (Mg^{2+}, Fe^{3+}, etc.) can contribute to the different influence of proteins on Mg degradation by affecting the stability of degradation layer and the galvanic corrosion between Mg matrix and impurities.

5.5. Adsorption of organic molecules

Besides the effect of binding/chelating of organic molecules, adsorption of organic molecules may not only promote the formation of Ca/P-rich layer, but also affect the properties of degradation layer, e.g. compactness [74].

5.5.1. Small organic molecules

To verify the participation of small organic molecules in the process of Mg degradation, the concentration of L-Gln in medium was determined with immersion time. pH can largely affect the stability of L-Gln, thereby leading to the decrease of L-Gln concentration. Therefore, the concentrations of L-Gln at different pH were also determined as references. As revealed by Fig. 4.3, after 20 hours of immersion, the pH of media reaches a stable value at around 8.4. Whereas, at higher pH (9.5 or 12), the concentration of L-Gln still remains at about 1.5 mM. Therefore, the decrease of L-Gln concentration after 20 hours of immersion (Fig. 4.3b) indicates the participation of L-Gln in the degradation process by adsorption or other ways. L-ascorbic acid (L-AA) and amino acids have already been evaluated as corrosion inhibitors for Mg alloys, Al alloys or steel due to their adsorption on material surfaces [131-133, 135]. These results are in agreement with the decrease of L-Gln concentration with immersion time (Fig. 4.3).The adsorption of small organic molecules can also be verified by the XPS results in DMEM (Fig. 4.28). Moreover, the adsorption of organic molecules can affect the growth direction of crystals [222], thereby affecting the morphology of precipitates on the surface. This could be one possible reason for the change of the morphology of nesquehonite when FBS is present in media.

5.5.2. Proteins

Due to the wide availability and high abundance of proteins in living systems, these molecules deserve special attention, especially for their adsorption. The adsorption of proteins is dramatically affected by the surrounding environments, protein properties and surface properties [155]. It suggests that an *in vivo*-like surface is of outmost importance to predict the protein adsorption on Mg surface under *in vivo* conditions. In the present study, HBSS and DMEM were chose to present the typical *in vitro* medium and *in vivo*-like medium for protein adsorption, respectively. The adsorption of BSA and Fib on Mg surface during immersion was directly investigated by using fluorescent proteins. Both BSA and Fib showed a higher adsorption on Mg surface in HBSS than in DMEM during immersion, suggesting less adsorption of proteins on *in vivo*-like degradation surface. There are two kinds of possible reasons for the different adsorption of protein in HBSS and DMEM: (i) surrounding environment (pH, ionic strength, etc.), and (ii) surface properties (wettability, charges, etc.).

Surrounding environment

Firstly, the surrounding circumstances during immersion were considered and investigated. These, including temperature, pH and ionic strength, have a decisive influence on the adsorption behaviour of proteins. Since the temperature used in this thesis is 37 ˚C, it is reasonable to assume that the temperature during immersion has no contribution to the

different adsorption of proteins on Mg surface in different media. In general, maximum adsorption of BSA and Fib is observed near their isoelectric points (pI) (~4.8 for BSA, ~5.8 for Fib) [223-225], and high pH is favourable for the desorption of proteins [226]. Nevertheless, increasing ionic strength seems to enhance the adsorption of protein within a certain concentration range [223, 225], which possibly correlates with the ability to stabilize or destabilize the native conformation of proteins [155]. In this study, a higher pH and a lower osmolality in HBSS than in DMEM during the 24 h of immersion are determined, while the adsorption of proteins (BSA, Fib) shows little difference after 1 h of immersion in HBSS and DMEM, but stronger in HBSS than in DMEM after 6 h of immersion (Fig. 4.44). This indicates that the surrounding environments containing temperature, pH and ionic strength are not the dominant factors for the different adsorption of BSA and Fib on Mg surface during immersion in HBSS and DMEM.

Surface properties

Due to the little influence of surrounding environments, the surface properties seem to be more important for protein adsorption. However, it is nearly impossible to determine the surface properties during Mg immersion. Therefore, the corroded Mg surface are prepared by immersing Mg samples in different media without proteins for 24 h. Although higher degradation rate is obtained in the absence of proteins during immersion (Fig. 4.45), protein adsorption shows similar trend over time on Mg surface during immersion (Fig. 4.37) and after immersion (Fig. 4.47), indicating that the Mg surface after immersion is an appropriate model for studying the adsorption of protein on Mg surface during immersion.

The little effect of adsorption solutions on protein adsorption on the corroded Mg surface (Fig. 4.39 and Fig. 4.41) further verifies the limited influence of surrounding environments on protein adsorption. Concerning the possible differences of surface properties, important parameters including surface roughness, wettability and surface charge have been considered in this thesis, since the interactions between proteins and surface mainly result from hydrophobic/hydrophilic interaction, hydrogen bonding, and electrostatic interaction [155].

Surface topography

The increasing surface roughness in HBSS leads to a higher adsorption of BSA and Fib, while in DMEM, the adsorption of BSA and Fib remains weak accompanied by a low surface roughness during 24 h of immersion (Fig. 4.47). This is consistent with other studies, revealing that the adsorption of BSA and Fib on Ti surface increased as surface roughness increased, especially from nanometer to micrometer range, due to the increase of actual surface area [163]. Similar results were also shown for lysozyme on polyether sulfone (PES) surface [227]

and Fib on tantalum films [165]. Moreover, surface topography can also affect the conformation of adsorbed proteins, which is critical to the absorbed quantity, density and rate of protein. For instance, less fibrinogen adsorption on surfaces with a roughness of 11 nm compared to other surfaces was observed [228], and Fib loses secondary structure to a greater extent when adsorbing onto high curvature surfaces [145]. Protein adsorption shows large response to nano-topography (< 100 nm) [229], whereas here the surface roughness is larger than 200 nm or even reaches to micrometer scale after immersion. Although in this thesis it is hard to obtain the information about protein conformation due to the complex surface conditions, a general conclusion can be drawn that the increase of surface roughness results in larger surface area, thereby providing more adsorption sites for proteins. It indicates the increasing surface roughness in HBSS could be one of the reasons for the higher adsorption of proteins compared to in DMEM due to the larger actual surface area.

Additionally, the compactness of the degradation layer also affects the amount of absorbed proteins on the corroded Mg surface. It is observed that a denser degradation layer is formed in DMEM compared to HBSS, especially for the outmost layer. As discussed above, the outmost Ca/P-rich layer formed in DMEM reduces the degradation rate of Mg. Hence, it would appear that the loose layer formed in HBSS enables proteins to adsorb in the whole degradation layer, while the adsorption of proteins mainly focuses on the top of degradation layer in DMEM as reflected by the XPS results (Fig. 4.38 and 4.29).

Surface hydrophobicity

The surface wettability is an important factor for protein adsorption on biomaterial surfaces. Generally, proteins tend to adsorb more effectively on hydrophobic surfaces, and the contact angle of 60˚ - 65˚ can be viewed as a criterion for distinguishing the hydrophobic force between proteins and surface [167, 230]. The immersion of Mg gives rather hydrophilic surfaces (contact angle < 30°) in both HBSS and DMEM, indicating similar hydrophobic/hydrophilic interaction between proteins and Mg surfaces formed in HBSS and DMEM. After protein adsorption, the increase of contact angles indicates that BSA and Fib predominantly expose the hydrophilic amino acid residues toward the corroded Mg surface.

Surface chemistry and charge

As shown in Figs. 4.15 and 4.16, the existence of Ca^{2+} in DMEM can lead to the formation of top Ca/P-rich layer, while they would not form on Mg surface in HBSS. Therefore, $MgCO_3$ and Mg-PO_4 can represent the surface chemistry formed in HBSS [178], while $CaCO_3$ and Ca-PO_4 are the main products of the Ca/P-rich outmost layer in DMEM [73]. As simple model for surface chemistry formed in HBSS and DMEM, four possible degradation products ($MgCO_3$,

$CaCO_3$, Mg-PO_4 and Ca-PO_4) were prepared and examined in this thesis. Higher amount of BSA and Fib absorption on $MgCO_3$ and Mg-PO_4 compared to $CaCO_3$ and Ca-PO_4 (Fig. 4.43) is in agreement with the protein adsorption on the corroded Mg surface obtained in HBSS compared to that in DMEM. The different amount of absorbed proteins on these products could be mainly ascribed to the electrostatic interactions between proteins and degradation products. The charge-dominated adsorption for proteins has been reported for BSA on Al_2O_3 surface [162] and Fib on TiO_2 and hydroxyapatite [231]. The lower isoelectric points (pI) of BSA (~ 4.8) and Fib (~5.8) than medium pH (>7) [140, 143, 191], indicate the negative net charge of proteins during the adsorption process. Consequently, the positive zeta potential of products ($MgCO_3$) indicates the electrostatic attraction between protein and products, while the negative zeta potential ($CaCO_3$) suggests the electrostatic repulsion between protein and products. It is consistent with the largest amount of adsorbed proteins on $MgCO_3$, but the lowest on $CaCO_3$ (Fig. 4.43 b). The disagreement between zeta potential and the absorbed amount of protein for Ca-PO_4 and Mg-PO_4 could be ascribed to the different surface areas exposed to media, which relates to the particle size, density and molecular weight of the products. Moreover, the zeta potentials (~ -15 mV) are comparable for all degradation products in water containing 1 mg/mL Fib, which is caused by the adsorption of negatively charged Fib. Thus, the different electrostatic interaction between proteins and surface products could be another possible reason for the different adsorption of proteins on Mg surface in HBSS and DMEM.

Further study was performed for the corroded Mg surface in HBSS with successive additions of different compounds according to the composition of DMEM (Fig. 4.40). The addition of $CaCl_2$ largely decreased the degradation rate of Mg irrespective of other components, proteins correspondingly showed weak adsorption. The protein adsorption is in accordance with the degradation rate of Mg. Based on the above discussion, this can be caused by the formation of more compact degradation layer and the formation of Ca-containing products on Mg surface. They trigger the changes of surface properties including roughness and surface charge, thereby eliciting the weak adsorption of proteins on Mg surface after immersion in $CaCl_2$-containing media.

5.6. Small molecules vs. macromolecules

In this study, different organic molecules are used to investigate their effect on Mg degradation. According to the comparison, it shows that larger influence of proteins on degradation rate of Mg in HBSS than small organic molecules can be observed (Figs. 4.1 and 4.19), especially after 3 days of immersion. Furthermore, a big difference of degradation products can be observed for small organic molecules and macromolecules (proteins), especially for the

degradation precipitates (nesquehonite or hydromagnesite), indicating a stronger influence of macromolecules than small organic molecules on Mg degradation. This is also reflected by the large changes of osmolality in HBSS with protein during immersion (Figs. 4.2 and 4.20). Additionally, the formation of Ca/P-rich layer is more obvious in DMEM than in DMEM + proteins, indicating the stronger ability of proteins to promote the formation of Ca-P salts. The possible reasons for the larger influence of proteins on Mg degradation are their large molecule size and high concentration.

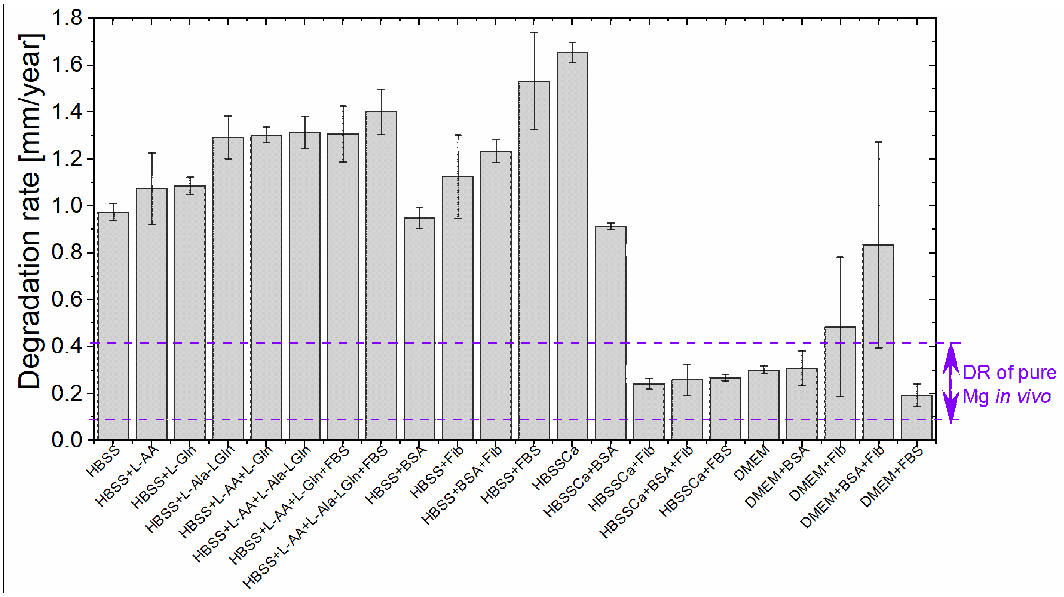

Figure 5.4: Degradation rate (DR) of pure Mg in different media after 14 days of immersion under semi-static conditions. (Dash line marked area refers to the range of DR of pure Mg *in vivo* from literature [59, 71, 79]).

In this thesis, Fib generally shows larger influence on Mg degradation than BSA (Fig. 5.4), which is related to the binding/chelating and adsorption ability. As found, more Fib adsorbs on the possible degradation products than BSA (Fig. 4.43b), indicating different affinity of proteins to the same surface [232]. Similar results have been reported on Ti surface [163]. A possible reason may be the different charge repulsion between BSA/Fib and the surface. The isoelectric point of BSA (~4.8 [140, 191]) is lower than Fib (~5.8 [143, 191]), indicating a more negative net charge of BSA than Fib at the same pH. Thus, the charge repulsion between BSA and negatively charged products is higher, leading to the lower BSA adsorption on the products. Another explanation for the different adsorbed amount of proteins may be the different physical properties of BSA and Fib. For example, the molecular size can affect adsorption of proteins due to the possibly different protein-surface interaction and adsorption sites [233]. Moreover, albumin has a substantial iron-binding capacity due to the high concentration *in vivo*, but weak binding affinity [234], while Fib has a function as acute phase

protein and is essential for iron regulation [235, 236]. Thus, as discussed above, the different binding ability between Fib and BSA to impurity ions possibly contributes to the different influence of Fib and BSA on Mg degradation. Additionally, the large influence of Fib on Mg degradation may be from its physicochemical properties. Fib decreases the fluidity of solution [192] and the surface tension [237, 238]. It has a low dilatational modulus at the air-water interface compared with other proteins, which suggests the formation of a surface network [238]. It can explain the observed phenomenon during immersion that bubbles are always limited to the Mg surface in media with the addition of Fib, indicating that Fib can hinder or suppress the mass transfer process in the media. This could be another reason for the different influence of Fib and BSA on Mg degradation.

5.7. Single organic molecule vs. organic molecule mixture

Due to the presence of a wide range of organic molecules *in vivo*, only one kind of organic molecules (eg. BSA) is not sufficient to represent the influence of organic molecules on Mg degradation. Therefore, the organic molecules mixtures are also presented in this thesis.

The mixture of small organic components shows slightly larger influence on degradation of pure Mg than single small organic molecules (Fig. 4.1). It is also verified by the faster degradation of Mg in small organic molecule mixtures than single small organic molecules during 24 hours of immersion (G8, G10 and G13 in Fig. 4.46). Moreover, the mixture of small organic molecules results in the formation of different precipitates on Mg surface after 3 days of immersion, indicating a larger effect of the mixture of the organic components on the formation of crystalline precipitates than single organic components.

In organic molecule mixtures, the organic molecules may interact with each other, which leads to contrary or similar results in different base media. One of typical examples is the faster degradation rate when both BSA and Fib are present in DMEM (Fig. 5.4). As reflected by SAXS results, the existence of the small organic molecules in DMEM reduces the aggregation of Fib and this aggregation is further decreased by the addition of BSA to HBSSCa or DMEM. It may be caused by the charge repulsion between the negative charged organic molecules, like BSA and Fib. Another already discovered fact caused by the interaction between Fib and serum proteins is that the effect of Fib in decreasing the fluidity of water is appreciably weaker in the presence of serum proteins than in purified solutions of Fib [192]. It might be related to the observed phenomena during immersion that bubbles are always limited to the Mg surface in media with the addition of Fib alone, but released from Mg surface in media + BSA +Fib. Additionally, the competitive adsorption between organic molecules has been widely reported, like the adsorption between Fib, albumin, and immunoglobulin (IgG) on surface (e.g. glass and

polyethylene) in diluted plasma [239, 240]. Also, the cooperative adsorption has been reported between different proteins [176]. Therefore, the effect of the organic molecule mixtures on Mg degradation is a result of the overlap of protein adsorption, binding/chelating effect and interactions between each other.

Another typical example for the different influence of single organic molecules and organic mixtures is the slower degradation of Mg in media with FBS than in media with BSA. It is well known that FBS not only contains BSA, but also other proteins (e.g. immunoglobulins and transferrin), vitamins, amino acids and growth factors [241]. The different effect between FBS and BSA can also be found from the literature as show in Fig. 5.5a. It shows positive efficiency when FBS is added to testing medium, indicating a decrease of the degradation rate of Mg. However, except the coated Mg (PEO coating or Ca-P salts coating), negative efficiencies are found for the addition of BSA to testing media, suggesting the acceleration of Mg degradation. In this thesis, both BSA and FBS lead to positive inhibition efficiency except two group under semi-static conditions after relatively long-term immersion (Fig. 5.5b). Moreover, in most cases, FBS results in higher inhibition efficiency than BSA, indicating the roles of other organic molecules in FBS in Mg degradation. It can also be confirmed by the stronger buffering capacity of FBS to the formation of crystalline precipitate than BSA (Fig. 4.23). The different inhibition efficiency of BSA between the presented data and data from literature may be ascribed to the different protein concentration, test duration, medium composition and conditions used.

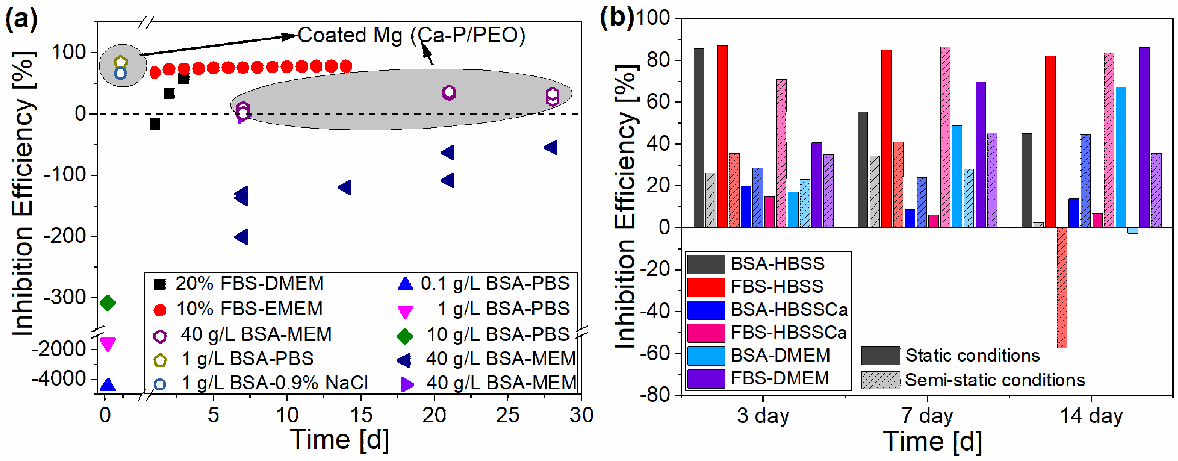

Figure 5.5: Inhibition efficiency of BSA and FBS for pure Mg compiled from literature [74, 82, 95, 151, 157, 158] (a), and inhibition efficiency of BSA and FBS for pure Mg in this thesis (b). The corrosion inhibition efficiency (η) of proteins for Mg degradation was calculated as the equation: $\eta = (DR_{np} - DR_p) / DR_{np} \times 100\% = (i_{np} - i_p) / i_p \times 100\% = (R_p - R_{np}) / R_p \times 100\%$, where DR_p and DR_{np}, i_p and i_{np}, R_p and R_{np} are degradation rate, corrosion current density, polarization resistance of Mg in medium with and without proteins, respectively.

Degradation rates obtained in HBSS irrespective of organic molecules are much higher than those observed *in vivo* [59, 71, 79] (Fig. 5.4), indicating that HBSS is not an appropriate simulated physiological fluid, as indicated by the formation of precipitates which are not found *in vivo*. Ca^{2+} is highly important for Mg degradation due to the formation of Ca-containing products. Both single protein and the mixtures of protein largely reduced the degradation rate of Mg in HBSSCa, leading to comparable degradation rate to *in vivo*. Moreover, *in vivo*-like degradation layer, outmost Ca/P-rich layer with inner $Mg(OH)_2$ and (Mg,Ca)-CO_3 layer, indicates a similar degradation mechanism as occurring *in vivo*. As indicated by Fig. 4.46, the mixture of small organic molecules in DMEM promotes the dissolution of Mg. Moreover, they also affect the performance of proteins (eg. Fib) in DMEM. Although the inclusion of more organic molecules presents more complex situation for Mg degradation, the degradation rate and degradation layer formed in these media reveal more physiological conditions, especially when FBS is present.

5.8. Effect of immersion conditions on Mg degradation

Effect of medium volume

Normally, a high ratio of medium volume to sample is proposed to avoid the excessive alkalinisation of the medium during immersion, and it has been shown to promote the degradation of Mg due to the acceleration of diffusion processes [55]. However, a medium-dependent effect of the ratio of medium volume to sample on Mg degradation can be observed. As revealed by SEM morphologies in Fig. 5.6, the degradation rates of Mg are related to the integrity of degradation layer during immersion, which is in accordance with the previous discussion. In HBSS and DMEM-based media, high medium-sample ratio results in fast degradation, which is in agreement with the literature [55, 94]. However, the existence of Ca^{2+} obviously leads to lower degradation rate at high ratio of medium volume to sample, suggesting the importance of Ca^{2+} to the integrity of degradation layer on Mg surface. The fast degradation of Mg in HBSSCa-media at low medium-sample ratio may be caused by the low amount of Ca^{2+} due to the low media volume used. Herein, the result highlights the importance of medium composition when the effect of medium to sample ratio on Mg degradation is considered. It should be noted that, from simple salt solution (HBSS) to complex medium (DMEM), the difference between degradation rates caused by the medium volume largely reduces, which results from the relatively stable degradation layer in more physiological medium.

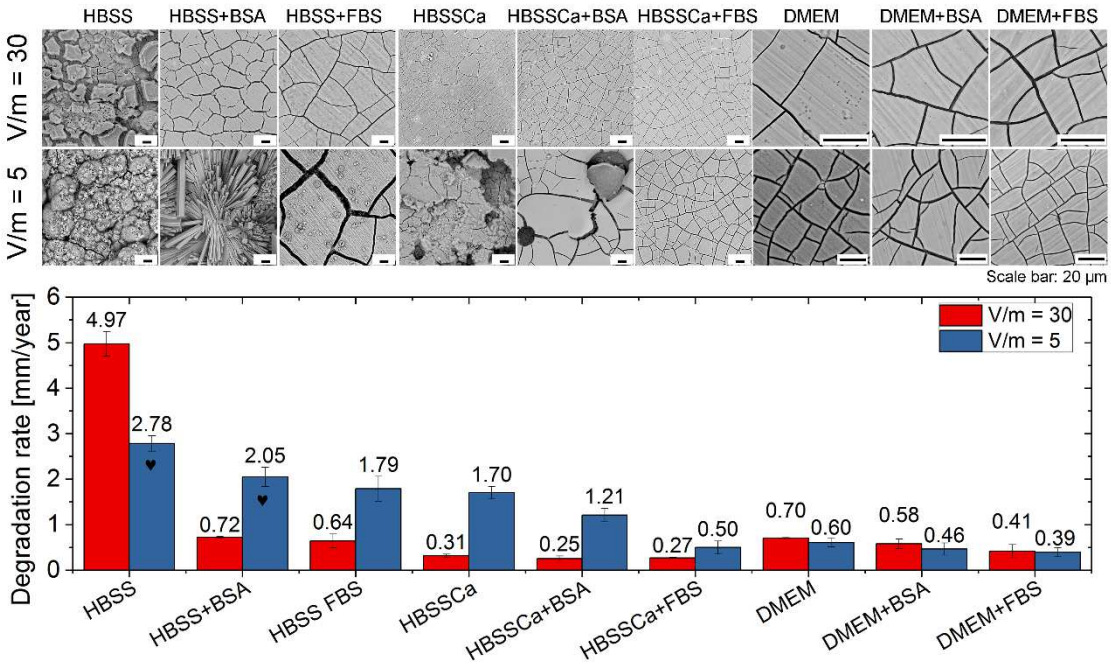

Figure 5.6: Degradation rate of pure Mg after 3 days of immersion in different media at different ratio of medium volume to sample weight. (V/m in mL/g, ♥ indicates the formation of crystalline precipitates on Mg surface)

Effect of static vs semi-static conditions

Semi-static conditions are often used to predict the degradation of Mg *in vitro* [66, 71, 77, 82, 111], which is believed to be more 'realistic' than static conditions, since the immersion medium is refreshed after certain intervals. After 14 days of immersion, in total 21 mL media is used for each sample under semi-static conditions, showing an equal medium to sample ratio compared to static conditions (20 mL/sample). Therefore, the degradation rates of pure Mg after 14 days of immersion under static and semi-static conditions are compared in Fig. 5.7. This comparison also showed a medium-dependent influence of conditions on Mg degradation. Obviously, the degradation rate of Mg is related to the integrity of degradation layer formed on Mg surface during immersion. As for similar states of degradation layer under different conditions (broken in HBSS and HBSS + BSA or unbroken in DMEM-based media), higher degradation rates can be observed under static conditions than under semi-static conditions. This seems to be accordant with the reported result of higher degradation rate of Mg *in vitro* than *in vivo*. However, for other media (HBSS + FBS and HBSSCa-based media), the degradation rate of Mg is higher under semi-static conditions (broken layer) than static conditions (unbroken layer), further highlighting the importance of the integrity of the top Ca/P-rich layer.

Furthermore, the inhibition efficiency of proteins under different conditions are compared in Fig. 5.5b. The result shows higher inhibition efficiency of proteins for Mg degradation under

static conditions than under semi-static conditions in HBSS and DMEM, while an adverse result can be observed in HBSSCa, suggesting the importance of medium compositions and quasidynamic conditions to the effect of proteins on Mg degradation. Therefore, more physiological conditions should be used when the effect of physiological parameters on Mg degradation is studied.

Although the effects of both medium volume and testing conditions are medium-dependent, the addition of organic molecules obviously reduces the difference of degradation rate caused by immersion conditions (medium volume and static or semi-static conditions), especially for FBS. It revealed that the difference of Mg degradation caused by different conditions can be weakened by the addition of organic molecules, which enables the results to be more comparable.

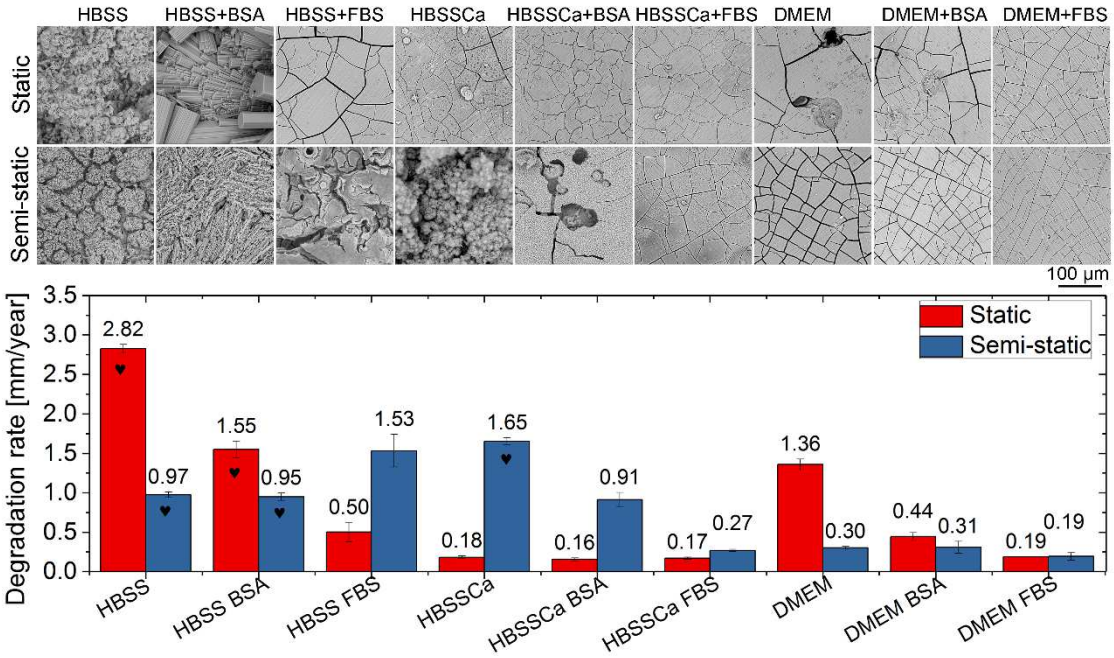

Figure 5.7: Degradation rate of pure Mg after 14 days of immersion in different media under static (20 mL/sample) or semi-static conditions (21 mL/sample). (♥ indicates the formation of crystalline precipitates on Mg surface)

Combining the above discussion, the effect of organic molecules on Mg degradation is largely related to the mobility and characteristics of organic molecules. The adsorbed/bound proteins on Mg surface can promote Ca-P formation by attracting Ca^{2+} and PO_4^{3-} ions and increasing the local supersaturation, thereby influencing the degradation rate of Mg via regulating the degradation layer. Whereas, organic molecules in media are able to inhibit product precipitation and their further growth by chelating or binding effect, for example, their effect on the formation of crystalline precipitates. In turn, the degradation of Mg results in different

surface characteristics, which further determines the adsorption of proteins. The interaction between organic molecules in organic mixtures and the testing conditions used further affect the performance of organic molecules. Finally, a schematic model for Mg degradation in organic molecule-containing media is depicted in Fig. 5.8.

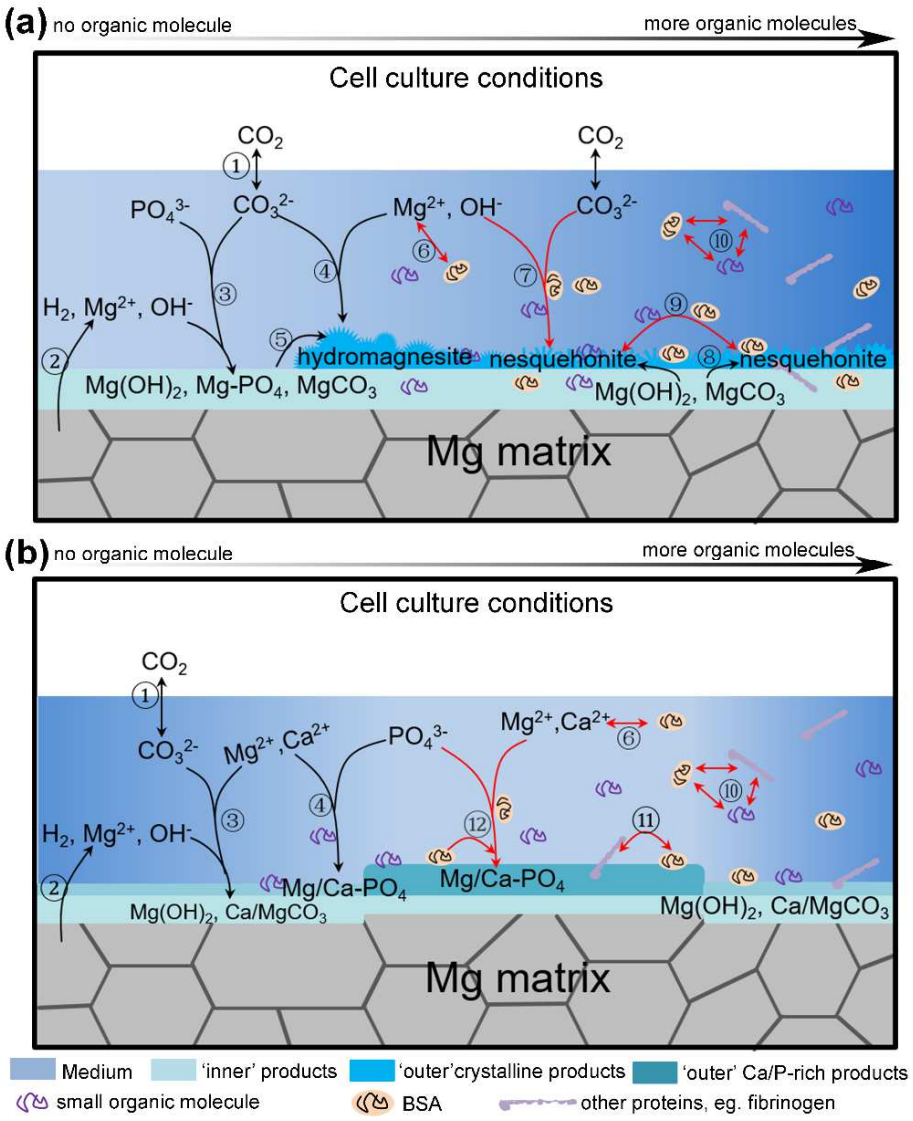

Figure 5.8: Schematic illustration of the effect of organic molecules on pure Mg degradation with high degradation rate (a) and relative low degradation rate (b). The deeper colour of media indicates the higher osmolality of media, and the deeper colour of 'outer' Ca/P-rich layer indicates the higher content of Ca and P. Other proteins refer not only to Fib, but also to e.g. immunoglobulins or transferrin. Small organic molecules refer to vitamins and amino acids. The red arrows indicate the influence of organic molecules on the corresponding process. ①: the reaction equilibrium of CO_2/HCO_3^{2-} buffering system. ②: the dissolution of Mg accompanying by the releases of Mg^{2+}, OH^- and H_2. ③: the formation of 'inner' degradation products containing $Mg(OH)_2$, $Mg\text{-}PO_4$, $Mg/CaCO_3$. ④: the formation of outer products (crystalline precipitates in Fig.

5.8a or Ca/P-rich products in Fig. 5.8b). ⑤: the transformation of $Mg(OH)_2$ / $MgCO_3$ to crystalline hydromagnesite. ⑥: the interaction between organic molecules and ions (eg. Mg^{2+}, Ca^{2+}, Fe^{3+}). ⑦ and ⑧ refers to the formation of crystalline nesquehonite. ⑨: the influence of organic molecules on the morphology of nesquehonite. ⑩: the interaction between organic molecules in media. ⑪: the adsorption of organic molecules on Mg surface and their interaction each other on Mg surface. ⑫: the formation of Ca-P products induced by proteins on Mg surface during immersion.

6. Summary and conclusion

In the present thesis, the effects of small organic molecules and macromolecule (proteins) on Mg degradation are investigated under static or semi-static cell culture conditions. The degradation of Mg during immersion is studied by analysing the degradation rate, the formation of degradation products and the performance of organic molecules.

The results show that the presence of small organic molecules promotes the degradation of Mg after relatively long-term immersion, while proteins generally decrease the degradation of Mg in the presence of Ca^{2+}. Moreover, the organic components play an important role in the formation of degradation products. Organic molecules prefer the precipitation of nesquehonite than hydromagnesite in the “outer” layer in HBSS and largely promote the formation of Ca/P-rich products in HBSSCa and DMEM. The promoted formation of Ca-P salts on Mg surface largely reduces the degradation rate of Mg, indicating the importance of organic molecules to surface biomineralization and tissue regeneration *in vivo*. Furthermore, the addition of organic molecules to *in vitro* test media (HBSSCa and DMEM) leads to *in vivo*-like degradation rate and degradation layer during immersion, revealing similar degradation mechanism or patterns of Mg to *in vivo*. Therefore, the addition of organic components to test medium for *in vitro* characterization is recommend to obtain reliable results comparable to *in vivo* tests.

The utilization of different media shows a media-dependent effect of proteins on Mg degradation. For example, Ca^{2+} largely enhances the inhibition effect of proteins on Mg degradation under semi-static conditions. Moreover, the effect of proteins on Mg degradation varies with the conditions used (static or semi-static), which is mostly related to the integrity of degradation layer. More importantly, the difference of Mg degradation caused by the testing conditions, such as medium compositions, the medium-sample ratio and the static or semi-static immersion, can be weakened by the addition of proteins, especially for FBS, indicating more comparable results when proteins are present in immersion medium.

The Mg surface after immersion can be used as an appropriate model to study the adsorption of proteins on Mg surface during immersion. The degradation layer formed in DMEM, presenting an *in vivo*-like surface, owns lower surface roughness and more negative surface charge than that formed in HBSS, which results in lower adsorption of proteins on Mg surface in DMEM than in HBSS. This demonstrates that surface properties (roughness, chemistry, surface charge, and so on) are more important for protein adsorption on Mg surface compared with the surrounding environment (e.g. pH, ionic strength), which possibly further affect the cell behaviour on Mg surface.

The mixtures of organic components, especially for FBS, exhibit larger effect than single organic component on Mg surface, and present more *in vivo*-like conditions. The effect of protein mixtures on Mg degradation is the results of an overlap of protein adsorption, binding/chelating to different ions (e.g. Mg^{2+}, Ca^{2+}, Fe^{3+}) and interactions between organic molecules. Therefore, the interaction between organic molecules should be seriously considered when more organic molecules are presented in media.

Further investigations about the interaction between organic molecules, the interaction between protein and Mg surface, and the cell behaviour on Mg surface would be very helpful to understand the degradation of Mg *in vivo*.

References

[1] F. Witte, N. Hort, C. Vogt, S. Cohen, K.U. Kainer, R. Willumeit, F. Feyerabend, Degradable biomaterials based on magnesium corrosion, Current opinion in solid state and materials science, 12 (2008) 63-72.
[2] B. Luthringer, F. Feyerabend, R. Willumeit-Römer, Magnesium-based implants: a mini-review, Magnesium. Res., 27 (2014) 142-154.
[3] S. Agarwal, J. Curtin, B. Duffy, S. Jaiswal, Biodegradable magnesium alloys for orthopaedic applications: A review on corrosion, biocompatibility and surface modifications, Mat. Sci. Eng. C-Mater. Biol. Appl., 68 (2016) 948-963.
[4] M.P. Staiger, A.M. Pietak, J. Huadmai, G. Dias, Magnesium and its alloys as orthopedic biomaterials: a review, Biomaterials, 27 (2006) 1728-1734.
[5] J. Velazguez, A. Jimenez, B. Chomon, T. Villa, Magnesium supplementation and bone turnover, Nutr. Rev, 57 (1999) 227.
[6] A.M. Romani, Cellular magnesium homeostasis, Arch. Biochem. Biophys., 512 (2011) 1-23.
[7] A. Hartwig, Role of magnesium in genomic stability, Mutation Research/Fundamental and Molecular Mechanisms of Mutagenesis, 475 (2001) 113-121.
[8] J. Vormann, Magnesium: nutrition and metabolism, Molecular aspects of medicine, 24 (2003) 27-37.
[9] G.A. Quamme, Renal magnesium handling: new insights in understanding old problems, Kidney Int., 52 (1997) 1180-1195.
[10] J.R. Purvis, A. Movahed, Magnesium disorders and cardiovascular diseases, Clin. Cardiol., 15 (1992) 556-568.
[11] N.-E.L. Saris, E. Mervaala, H. Karppanen, J.A. Khawaja, A. Lewenstam, Magnesium: an update on physiological, clinical and analytical aspects, Clin. Chim. Acta, 294 (2000) 1-26.
[12] P.A. Revell, E. Damien, X. Zhang, P. Evans, C.R. Howlett, The effect of magnesium ions on bone bonding to hydroxyapatite coating on titanium alloy implants, in: Key Engineering Materials, Trans Tech Publ, 2004, pp. 447-450.
[13] H. Zreiqat, C. Howlett, A. Zannettino, P. Evans, G. Schulze-Tanzil, C. Knabe, M. Shakibaei, Mechanisms of magnesium-stimulated adhesion of osteoblastic cells to commonly used orthopaedic implants, J. Biomed. Mater. Res. A, 62 (2002) 175-184.
[14] F. Witte, The history of biodegradable magnesium implants: a review, Acta Biomater., 6 (2010) 1680-1692.
[15] P. Wilflingseder, R. Martin, C. Papp, Magnesium seeds in the treatment of lymph-and haemangiomata, Chirurgia plastica, 6 (1981) 105-116.
[16] N. Kirkland, J. Lespagnol, N. Birbilis, M. Staiger, A survey of bio-corrosion rates of magnesium alloys, Corrosion Science, 52 (2010) 287-291.
[17] J. Wang, J. Tang, P. Zhang, Y. Li, J. Wang, Y. Lai, L. Qin, Surface modification of magnesium alloys developed for bioabsorbable orthopedic implants: a general review, Journal of Biomedical Materials Research Part B: Applied Biomaterials, 100 (2012) 1691-1701.
[18] Y. Chen, Z. Xu, C. Smith, J. Sankar, Recent advances on the development of magnesium alloys for biodegradable implants, Acta Biomater., 10 (2014) 4561-4573.
[19] Y. Zheng, X. Gu, F. Witte, Biodegradable metals, Materials Science and Engineering: R: Reports, 77 (2014) 1-34.
[20] A.H. Martinez Sanchez, B.J. Luthringer, F. Feyerabend, R. Willumeit, Mg and Mg alloys: how comparable are in vitro and in vivo corrosion rates? A review, Acta Biomater., 13 (2015) 16-31.
[21] D. Zhao, F. Witte, F. Lu, J. Wang, J. Li, L. Qin, Current status on clinical applications of magnesium-based orthopaedic implants: A review from clinical translational perspective, Biomaterials, 112 (2017) 287-302.
[22] M. Haude, R. Erbel, P. Erne, S. Verheye, H. Degen, D. Böse, P. Vermeersch, I. Wijnbergen, N. Weissman, F. Prati, Safety and performance of the drug-eluting absorbable metal scaffold (DREAMS) in patients with de-novo coronary lesions: 12 month results of the prospective, multicentre, first-in-man BIOSOLVE-I trial, The Lancet, 381 (2013) 836-844.
[23] M. Haude, H. Ince, A. Abizaid, R. Toelg, P.A. Lemos, C. von Birgelen, E.H. Christiansen, W. Wijns, F.-J. Neumann, C. Kaiser, Sustained safety and performance of the second-generation drug-eluting absorbable metal scaffold in patients with de novo coronary lesions: 12-month clinical results and angiographic findings of the BIOSOLVE-II first-in-man trial, Eur. Heart J., 37 (2016) 2701-2709.
[24] M. Haude, H. Ince, A. Abizaid, R. Toelg, P.A. Lemos, C. von Birgelen, E.H. Christiansen, W. Wijns, F.-J. Neumann, C. Kaiser, Safety and performance of the second-generation drug-eluting

absorbable metal scaffold in patients with de-novo coronary artery lesions (BIOSOLVE-II): 6 month results of a prospective, multicentre, non-randomised, first-in-man trial, The Lancet, 387 (2016) 31-39.
[25] R. Erbel, C. Di Mario, J. Bartunek, J. Bonnier, B. de Bruyne, F.R. Eberli, P. Erne, M. Haude, B. Heublein, M. Horrigan, Temporary scaffolding of coronary arteries with bioabsorbable magnesium stents: a prospective, non-randomised multicentre trial, The Lancet, 369 (2007) 1869-1875.
[26] H. Windhagen, K. Radtke, A. Weizbauer, J. Diekmann, Y. Noll, U. Kreimeyer, R. Schavan, C. Stukenborg-Colsman, H. Waizy, Biodegradable magnesium-based screw clinically equivalent to titanium screw in hallux valgus surgery: short term results of the first prospective, randomized, controlled clinical pilot study, Biomedical engineering online, 12 (2013) 62.
[27] J.-W. Lee, H.-S. Han, K.-J. Han, J. Park, H. Jeon, M.-R. Ok, H.-K. Seok, J.-P. Ahn, K.E. Lee, D.-H. Lee, Long-term clinical study and multiscale analysis of in vivo biodegradation mechanism of Mg alloy, Proceedings of the National Academy of Sciences, 113 (2016) 716-721.
[28] D. Zhao, S. Huang, F. Lu, B. Wang, L. Yang, L. Qin, K. Yang, Y. Li, W. Li, W. Wang, Vascularized bone grafting fixed by biodegradable magnesium screw for treating osteonecrosis of the femoral head, Biomaterials, 81 (2016) 84-92.
[29] J. Wang, C.E. Smith, J. Sankar, Y. Yun, N. Huang, Absorbable magnesium-based stent: physiological factors to consider for in vitro degradation assessments, Regenerative Biomaterials, 2 (2015) 59-69.
[30] F. Feyerabend, J. Fischer, J. Holtz, F. Witte, R. Willumeit, H. Drücker, C. Vogt, N. Hort, Evaluation of short-term effects of rare earth and other elements used in magnesium alloys on primary cells and cell lines, Acta Biomater., 6 (2010) 1834-1842.
[31] F. Witte, H. Ulrich, C. Palm, E. Willbold, Biodegradable magnesium scaffolds: Part II: Peri-implant bone remodeling, J. Biomed. Mater. Res. A, 81 (2007) 757-765.
[32] N. Ahmad Agha, R. Willumeit-Romer, D. Laipple, B. Luthringer, F. Feyerabend, The Degradation Interface of Magnesium Based Alloys in Direct Contact with Human Primary Osteoblast Cells, PLoS One, 11 (2016) e0157874.
[33] L. Wu, F. Feyerabend, A.F. Schilling, R. Willumeit-Römer, B.J. Luthringer, Effects of extracellular magnesium extract on the proliferation and differentiation of human osteoblasts and osteoclasts in coculture, Acta Biomater., 27 (2015) 294-304.
[34] A. Loos, R. Rohde, A. Haverich, S. Barlach, In vitro and in vivo biocompatibility testing of absorbable metal stents, in: Macromol. Symp., Wiley Online Library, 2007, pp. 103-108.
[35] H. Waizy, J.-M. Seitz, J. Reifenrath, A. Weizbauer, F.-W. Bach, A. Meyer-Lindenberg, B. Denkena, H. Windhagen, Biodegradable magnesium implants for orthopedic applications, J. Mater. Sci., 48 (2013) 39-50.
[36] C. Legrand, J. Bour, C. Jacob, J. Capiaumont, A. Martial, A. Marc, M. Wudtke, G. Kretzmer, C. Demangel, D. Duval, Lactate dehydrogenase (LDH) activity of the number of dead cells in the medium of cultured eukaryotic cells as marker, J. Biotechnol., 25 (1992) 231-243.
[37] C. Liu, P. Wan, L.L. Tan, K. Wang, K. Yang, Preclinical investigation of an innovative magnesium-based bone graft substitute for potential orthopaedic applications, Journal of Orthopaedic Translation, 2 (2014) 139-148.
[38] R. Willumeit, A. Möhring, F. Feyerabend, Optimization of cell adhesion on mg based implant materials by pre-incubation under cell culture conditions, International journal of molecular sciences, 15 (2014) 7639-7650.
[39] I. Johnson, D. Perchy, H. Liu, In vitro evaluation of the surface effects on magnesium-yttrium alloy degradation and mesenchymal stem cell adhesion, J Biomed Mater Res A, 100 (2012) 477-485.
[40] T.Y. Nguyen, A.F. Cipriano, R.G. Guan, Z.Y. Zhao, H.N. Liu, In vitro interactions of blood, platelet, and fibroblast with biodegradable magnesium-zinc-strontium alloys, J. Biomed. Mater. Res. A, 103 (2015) 2974-2986.
[41] J. Fischer, D. Pröfrock, N. Hort, R. Willumeit, F. Feyerabend, Improved cytotoxicity testing of magnesium materials, Materials Science and Engineering: B, 176 (2011) 830-834.
[42] Q. Wang, L. Tan, W. Xu, B. Zhang, K. Yang, Dynamic behaviors of a Ca–P coated AZ31B magnesium alloy during in vitro and in vivo degradations, Materials Science and Engineering: B, 176 (2011) 1718-1726.
[43] T.A. Huehnerschulte, N. Angrisani, D. Rittershaus, D. Bormann, H. Windhagen, A. Meyer-Lindenberg, In vivo corrosion of two novel magnesium alloys ZEK100 and AX30 and their mechanical suitability as biodegradable implants, Materials, 4 (2011) 1144-1167.
[44] A. Krause, N. Von der Höh, D. Bormann, C. Krause, F.-W. Bach, H. Windhagen, A. Meyer-Lindenberg, Degradation behaviour and mechanical properties of magnesium implants in rabbit tibiae, J. Mater. Sci., 45 (2010) 624.

[45] M. Thomann, C. Krause, D. Bormann, N. Von der Höh, H. Windhagen, A. Meyer-Lindenberg, Comparison of the resorbable magnesium. alloys LAE442 und MgCa0. 8 concerning their mechanical properties, their progress of degradation and the bone-implant-contact after 12 months implantation duration in a rabbit model, Materialwiss. Werkst., 40 (2009) 82-87.
[46] J.M. Seitz, U. Bormann, K. Collier, E. Wulf, R. Eifler, F.W. Bach, Application of a bioactive coating on resorbable, neodymium containing magnesium alloys, and analyses of their effects on the in vitro degradation behavior in a simulated body fluid, Adv. Eng. Mater., 14 (2012).
[47] A. Drynda, T. Hassel, R. Hoehn, A. Perz, F.W. Bach, M. Peuster, Development and biocompatibility of a novel corrodible fluoride-coated magnesium-calcium alloy with improved degradation kinetics and adequate mechanical properties for cardiovascular applications, J. Biomed. Mater. Res. A, 93 (2010) 763-775.
[48] A. Weizbauer, C. Modrejewski, S. Behrens, H. Klein, P. Helmecke, J.-M. Seitz, H. Windhagen, K. Möhwald, J. Reifenrath, H. Waizy, Comparative in vitro study and biomechanical testing of two different magnesium alloys, J. Biomater. Appl., 28 (2014) 1264-1273.
[49] S. Zhang, X. Zhang, C. Zhao, J. Li, Y. Song, C. Xie, H. Tao, Y. Zhang, Y. He, Y. Jiang, Research on an Mg–Zn alloy as a degradable biomaterial, Acta Biomater., 6 (2010) 626-640.
[50] M.B. Kannan, L. Orr, In vitro mechanical integrity of hydroxyapatite coated magnesium alloy, Biomed. Mater., 6 (2011) 045003.
[51] C. Rössig, N. Angrisani, P. Helmecke, S. Besdo, J.-M. Seitz, B. Welke, N. Fedchenko, H. Kock, J. Reifenrath, In vivo evaluation of a magnesium-based degradable intramedullary nailing system in a sheep model, Acta Biomater., 25 (2015) 369-383.
[52] M.B. Kannan, R.S. Raman, In vitro degradation and mechanical integrity of calcium-containing magnesium alloys in modified-simulated body fluid, Biomaterials, 29 (2008) 2306-2314.
[53] S. Jafari, R.K. Singh Raman, C.H.J. Davies, Corrosion fatigue of a magnesium alloy in modified simulated body fluid, Eng. Fract. Mech., 137 (2015) 2-11.
[54] L. Choudhary, R.S. Raman, Mechanical integrity of magnesium alloys in a physiological environment: Slow strain rate testing based study, Eng. Fract. Mech., 103 (2013) 94-102.
[55] N.T. Kirkland, N. Birbilis, M.P. Staiger, Assessing the corrosion of biodegradable magnesium implants: a critical review of current methodologies and their limitations, Acta Biomater., 8 (2012) 925-936.
[56] E.P.S. Nidadavolu, F. Feyerabend, T. Ebel, R. Willumeit-Römer, M. Dahms, On the Determination of Magnesium Degradation Rates under Physiological Conditions, Materials, 9 (2016) 627-737.
[57] M. Dahms, D. Höche, N. Ahmad Agha, F. Feyerabend, R. Willumeit-Römer, A simple model for long-time degradation of magnesium under physiological conditions, Materials and Corrosion, 69 (2018) 191-196.
[58] J. Reifenrath, N. Angrisani, N. Erdmann, A. Lucas, H. Waizy, J.M. Seitz, A. Bondarenko, A. Meyer-Lindenberg, Degrading magnesium screws ZEK100: biomechanical testing, degradation analysis and soft-tissue biocompatibility in a rabbit model, Biomed. Mater., 8 (2013) 045012.
[59] A. Myrissa, N.A. Agha, Y. Lu, E. Martinelli, J. Eichler, G. Szakács, C. Kleinhans, R. Willumeit-Römer, U. Schäfer, A.-M. Weinberg, In vitro and in vivo comparison of binary Mg alloys and pure Mg, Mat. Sci. Eng. C-Mater. Biol. Appl., 61 (2016) 865-874.
[60] F. Witte, V. Kaese, H. Haferkamp, E. Switzer, A. Meyer-Lindenberg, C. Wirth, H. Windhagen, In vivo corrosion of four magnesium alloys and the associated bone response, Biomaterials, 26 (2005) 3557-3563.
[61] N.I.Z. Abidin, A.D. Atrens, D. Martin, A. Atrens, Corrosion of high purity Mg, Mg2Zn0. 2Mn, ZE41 and AZ91 in Hank's solution at 37 C, Corrosion Science, 53 (2011) 3542-3556.
[62] G. Song, Control of biodegradation of biocompatable magnesium alloys, Corros. Sci., 49 (2007) 1696-1701.
[63] E. Willbold, A. Kaya, R. Kaya, F. Beckmann, F. Witte, Corrosion of magnesium alloy AZ31 screws is dependent on the implantation site, Materials Science and Engineering: B, 176 (2011) 1835-1840.
[64] B.R. Sunil, T.S. Kumar, U. Chakkingal, V. Nandakumar, M. Doble, V.D. Prasad, M. Raghunath, In vitro and in vivo studies of biodegradable fine grained AZ31 magnesium alloy produced by equal channel angular pressing, Mat. Sci. Eng. C-Mater. Biol. Appl., 59 (2016) 356-367.
[65] Biological evaluation of medical devices, in: Part 5: Tests for in vitro cytotoxicity, International Organization for Standardization, 2009.
[66] J. Gonzalez, R.Q. Hou, E.P. Nidadavolu, R. Willumeit-Römer, F. Feyerabend, Magnesium degradation under physiological conditions–Best practice, Bioactive Materials, 3 (2018) 174-185.
[67] A. Internasional, Standard Practice for Laboratory Immersion Corrosion Testing of Metals, in, ASTM Internasional, United State, 2004.

[68] I.O.f. Standardization, Guidance for absorbable implants, in: Cardiovascular biological evaluation of medical devices, International Organization for Standardization, 2014.
[69] M.P. Staiger, F. Feyerabend, R. Willumeit, C.S. Sfeir, Y.F. Zheng, S. Virtanen, W.D. Müeller, A. Atrens, M. Peuster, P.N. Kumta, D. Mantovani, F. Witte, Summary of the panel discussions at the 2nd Symposium on Biodegradable Metals, Maratea, Italy, 2010, Materials Science and Engineering: B, 176 (2011) 1596-1599.
[70] F. Witte, J. Fischer, J. Nellesen, H.-A. Crostack, V. Kaese, A. Pisch, F. Beckmann, H. Windhagen, In vitro and in vivo corrosion measurements of magnesium alloys, Biomaterials, 27 (2006) 1013-1018.
[71] J. Walker, S. Shadanbaz, N.T. Kirkland, E. Stace, T. Woodfield, M.P. Staiger, G.J. Dias, Magnesium alloys: predicting in vivo corrosion with in vitro immersion testing, J Biomed Mater Res B Appl Biomater, 100 (2012) 1134-1141.
[72] R. Willumeit, J. Fischer, F. Feyerabend, N. Hort, U. Bismayer, S. Heidrich, B. Mihailova, Chemical surface alteration of biodegradable magnesium exposed to corrosion media, Acta Biomater., 7 (2011) 2704-2715.
[73] D. Tie, F. Feyerabend, N. Hort, R. Willumeit, D. Hoeche, XPS studies of magnesium surfaces after exposure to Dulbecco's Modified Eagle Medium, Hank's buffered salt solution, and simulated body fluid, Adv. Eng. Mater., 12 (2010) B699-B704.
[74] V. Wagener, S. Virtanen, Protective layer formation on magnesium in cell culture medium, Mat. Sci. Eng. C-Mater. Biol. Appl., 63 (2016) 341-351.
[75] K. Anselme, Osteoblast adhesion on biomaterials, Biomaterials, 21 (2000) 667-681.
[76] R. Rettig, S. Virtanen, Composition of corrosion layers on a magnesium rare-earth alloy in simulated body fluids, J. Biomed. Mater. Res. A, 88 (2009) 359-369.
[77] M. Kieke, F. Feyerabend, J. Lemaitre, P. Behrens, R. Willumeit-Römer, Degradation rates and products of pure magnesium exposed to different aqueous media under physiological conditions, BioNanoMaterials, 17 (2016) 131-143.
[78] R. Harrison, D. Maradze, S. Lyons, Y.F. Zheng, Y. Liu, Corrosion of magnesium and magnesium-calcium alloy in biologically-simulated environment, Prog. Nat. Sci.-Mater., 24 (2014) 539-546.
[79] I. Marco, A. Myrissa, E. Martinelli, F. Feyerabend, R. Willumeit-Römer, A. Weinberg, O. Van der Biest, In vivo and in vitro degradation comparison of pure Mg, Mg-10Gd and Mg-2Ag: a short term study, Eur. Cells Mater., 33 (2017) 90-104.
[80] I. Marco, F. Feyerabend, R. Willumeit-Römer, O. Van der Biest, Degradation testing of Mg alloys in Dulbecco's modified eagle medium: Influence of medium sterilization, Mat. Sci. Eng. C-Mater. Biol. Appl., (2016).
[81] P.K. Bowen, J. Drelich, J. Goldman, Magnesium in the murine artery: Probing the products of corrosion, Acta Biomater., 10 (2014) 1475-1483.
[82] A. Yamamoto, S. Hiromoto, Effect of inorganic salts, amino acids and proteins on the degradation of pure magnesium in vitro, Mat. Sci. Eng. C-Mater. Biol. Appl., 29 (2009) 1559-1568.
[83] Y. Jang, B. Collins, J. Sankar, Y. Yun, Effect of biologically relevant ions on the corrosion products formed on alloy AZ31B: an improved understanding of magnesium corrosion, Acta Biomater., 9 (2013) 8761-8770.
[84] A. Guyton, Overview of the circulation, and medical physics of pressure, flow, and resistance, Textbook of medical physiology, (1991).
[85] J.E. Hall, Textbook of medical physiology, in, Elsevier Saunders, 2006.
[86] Y. Zhang, B. Hinton, G. Wallace, X. Liu, M. Forsyth, On corrosion behaviour of magnesium alloy AZ31 in simulated body fluids and influence of ionic liquid pretreatments, Corrosion engineering, science and technology, 47 (2012) 374-382.
[87] B. Liu, Y.F. Zheng, Effects of alloying elements (Mn, Co, Al, W, Sn, B, C and S) on biodegradability and in vitro biocompatibility of pure iron, Acta Biomater., 7 (2011) 1407-1420.
[88] J. Wang, V. Giridharan, V. Shanov, Z. Xu, B. Collins, L. White, Y. Jang, J. Sankar, N. Huang, Y. Yun, Flow-induced corrosion behavior of absorbable magnesium-based stents, Acta Biomater., 10 (2014) 5213-5223.
[89] J. Grogan, D. Gastaldi, M. Castelletti, F. Migliavacca, G. Dubini, P. McHugh, A novel flow chamber for biodegradable alloy assessment in physiologically realistic environments, Rev. Sci. Instrum., 84 (2013) 094301.
[90] S. Johnston, Z. Shi, A. Atrens, The influence of pH on the corrosion rate of high-purity Mg, AZ91 and ZE41 in bicarbonate buffered Hanks' solution, Corros. Sci., 101 (2015) 182-192.
[91] A.P.M. Saad, N. Jasmawati, M.N. Harun, M.R.A. Kadir, H. Nur, H. Hermawan, A. Syahrom, Dynamic degradation of porous magnesium under a simulated environment of human cancellous bone, Corros. Sci., 112 (2016) 495-506.

[92] J. Levesque, H. Hermawan, D. Dube, D. Mantovani, Design of a pseudo-physiological test bench specific to the development of biodegradable metallic biomaterials, Acta Biomater., 4 (2008) 284-295.
[93] N. Li, C. Guo, Y. Wu, Y. Zheng, L. Ruan, Comparative study on corrosion behaviour of pure Mg and WE43 alloy in static, stirring and flowing Hank's solution, Corrosion Engineering, Science and Technology, 47 (2012) 346-351.
[94] L. Yang, E. Zhang, Biocorrosion behavior of magnesium alloy in different simulated fluids for biomedical application, Materials Science and Engineering: C, 29 (2009) 1691-1696.
[95] N.T. Kirkland, J. Waterman, N. Birbilis, G. Dias, T.B. Woodfield, R.M. Hartshorn, M.P. Staiger, Buffer-regulated biocorrosion of pure magnesium, J. Mater. Sci. Mater. Med., 23 (2012) 283-291.
[96] T. Kokubo, H. Takadama, How useful is SBF in predicting in vivo bone bioactivity?, Biomaterials, 27 (2006) 2907-2915.
[97] I. Marco, F. Feyerabend, R. Willumeit-Römer, O. Van der Biest, Influence of testing environment on the degradation behavior of magnesium alloys for bioabsorbable implants, in: TMS 2015, 144th Annual Meeting & Exhibition, John Wiley & Sons, Inc., 2015, pp. 497-506.
[98] X.B. Chen, D.R. Nisbet, R.W. Li, P.N. Smith, T.B. Abbott, M.A. Easton, D.H. Zhang, N. Birbilis, Controlling initial biodegradation of magnesium by a biocompatible strontium phosphate conversion coating, Acta Biomaterialia, 10 (2014) 1463-1474.
[99] F. Feyerabend, H. Drucker, D. Laipple, C. Vogt, M. Stekker, N. Hort, R. Willumeit, Ion release from magnesium materials in physiological solutions under different oxygen tensions, J Mater Sci Mater Med, 23 (2012) 9-24.
[100] A.C. Hänzi, I. Gerber, M. Schinhammer, J.F. Löffler, P.J. Uggowitzer, On the in vitro and in vivo degradation performance and biological response of new biodegradable Mg–Y–Zn alloys, Acta biomaterialia, 6 (2010) 1824-1833.
[101] P. Shi, W.F. Ng, M.H. Wong, F.T. Cheng, Improvement of corrosion resistance of pure magnesium in Hanks' solution by microarc oxidation with sol–gel TiO2 sealing, J. Alloy. Compd., 469 (2009) 286-292.
[102] N.I.Z. Abidin, B. Rolfe, H. Owen, J. Malisano, D. Martin, J. Hofstetter, P.J. Uggowitzer, A. Atrens, The in vivo and in vitro corrosion of high-purity magnesium and magnesium alloys WZ21 and AZ91, Corrosion Science, 75 (2013) 354-366.
[103] Y. Xin, P.K. Chu, Influence of Tris in simulated body fluid on degradation behavior of pure magnesium, Materials Chemistry and Physics, 124 (2010) 33-35.
[104] R. Walter, M.B. Kannan, In-vitro degradation behaviour of WE54 magnesium alloy in simulated body fluid, Mater. Lett., 65 (2011) 748-750.
[105] M. Schinhammer, J. Hofstetter, C. Wegmann, F. Moszner, J.F. Löffler, P.J. Uggowitzer, On the immersion testing of degradable implant materials in simulated body fluid: active pH regulation using CO2, Advanced Engineering Materials, 15 (2013) 434-441.
[106] Y. Xin, T. Hu, P.K. Chu, Degradation behaviour of pure magnesium in simulated body fluids with different concentrations of HCO3-, Corros. Sci., 53 (2011) 1522-1528.
[107] B. Hadzima, M. Mhaede, F. Pastorek, Electrochemical characteristics of calcium-phosphatized AZ31 magnesium alloy in 0.9% NaCl solution, Journal of Materials Science: Materials in Medicine, 25 (2014) 1227-1237.
[108] D. Zhao, T. Wang, X. Guo, J. Kuhlmann, A. Doepke, Z. Dong, V.N. Shanov, W.R. Heineman, Monitoring biodegradation of magnesium implants with sensors, JOM, 68 (2016) 1204-1208.
[109] L. Yang, N. Hort, R. Willumeit, F. Feyerabend, Effects of corrosion environment and proteins on magnesium corrosion, Corrosion Engineering, Science and Technology, 47 (2012) 335-339.
[110] A. Oyane, H.M. Kim, T. Furuya, T. Kokubo, T. Miyazaki, T. Nakamura, Preparation and assessment of revised simulated body fluids, J. Biomed. Mater. Res. A, 65 (2003) 188-195.
[111] N.A. Agha, F. Feyerabend, B. Mihailova, S. Heidrich, U. Bismayer, R. Willumeit-Romer, Magnesium degradation influenced by buffering salts in concentrations typical of in vitro and in vivo models, Mater Sci Eng C Mater Biol Appl, 58 (2016) 817-825.
[112] G. Song, A. Atrens, D. St John, X. Wu, J. Nairn, The anodic dissolution of magnesium in chloride and sulphate solutions, Corros. Sci., 39 (1997) 1981-2004.
[113] M.-C. Zhao, M. Liu, G.-L. Song, A. Atrens, Influence of pH and chloride ion concentration on the corrosion of Mg alloy ZE41, Corros. Sci., 50 (2008) 3168-3178.
[114] R. Ambat, N.N. Aung, W. Zhou, Studies on the influence of chloride ion and pH on the corrosion and electrochemical behaviour of AZ91D magnesium alloy, J. Appl. Electrochem., 30 (2000) 865-874.

[115] F.E.-T. Heakal, A. Fekry, M. Fatayerji, Influence of halides on the dissolution and passivation behavior of AZ91D magnesium alloy in aqueous solutions, Electrochim. Acta, 54 (2009) 1545-1557.
[116] Y. Xin, K. Huo, H. Tao, G. Tang, P.K. Chu, Influence of aggressive ions on the degradation behavior of biomedical magnesium alloy in physiological environment, Acta Biomater., 4 (2008) 2008-2015.
[117] N.E. Good, G.D. Winget, W. Winter, T.N. Connolly, S. Izawa, R.M. Singh, Hydrogen ion buffers for biological research, Biochemistry-us., 5 (1966) 467-477.
[118] C. Schille, M. Braun, H.P. Wendel, L. Scheideler, N. Hort, H.P. Reichel, E. Schweizer, J. Geis-Gerstorfer, Corrosion of experimental magnesium alloys in blood and PBS: A gravimetric and microscopic evaluation, Materials Science and Engineering: B, 176 (2011) 1797-1801.
[119] S. Naddaf Dezfuli, Z. Huan, J.M.C. Mol, M.A. Leeflang, J. Chang, J. Zhou, Influence of HEPES buffer on the local pH and formation of surface layer during in vitro degradation tests of magnesium in DMEM, Progress in Natural Science: Materials International, 24 (2014) 531-538.
[120] M.B. Kannan, H. Khakbaz, A. Yamamoto, Understanding the influence of HEPES buffer concentration on the biodegradation of pure magnesium: An electrochemical study, Mater. Chem. Phys., 197 (2017) 47-56.
[121] C. Shipman, Evaluation of 4-(2-hydroxyethyl)-1-piperazineëthanesulfonic acid (HEPES) as a tissue culture buffer, Exp. Biol. Med., 130 (1969) 305-310.
[122] K. Törne, A. Örnberg, J. Weissenrieder, The influence of buffer system and biological fluids on the degradation of magnesium, Journal of Biomedical Materials Research Part B: Applied Biomaterials, 105 (2017) 1490-1502.
[123] Y. Xin, T. Hu, P.K. Chu, Influence of Test Solutions on In Vitro Studies of Biomedical Magnesium Alloys, J. Electrochem. Soc., 157 (2010) C238.
[124] L.-Y. Cui, Y. Hu, R.-C. Zeng, Y.-X. Yang, D.-D. Sun, S.-Q. Li, F. Zhang, E.-H. Han, New insights into the effect of Tris-HCl and Tris on corrosion of magnesium alloy in presence of bicarbonate, sulfate, hydrogen phosphate and dihydrogen phosphate ions, J. Mater. Sci. Technol., 33 (2017) 971-986.
[125] Z. Li, G.-L. Song, S. Song, Effect of bicarbonate on biodegradation behaviour of pure magnesium in a simulated body fluid, Electrochim. Acta, 115 (2014) 56-65.
[126] G. Gstraunthaler, T. Lindl, Zell-und Gewebekultur, in, Springer, 2013.
[127] P. Astrup, O.S. Andersen, K. Jørgensen, K. Engel, The acid-base metabolism. A new approach, Lancet, (1960) 1035-1339.
[128] R. Lindström, L.-G. Johansson, G.E. Thompson, P. Skeldon, J.-E. Svensson, Corrosion of magnesium in humid air, Corros. Sci., 46 (2004) 1141-1158.
[129] K. Barouni, L. Bazzi, R. Salghi, M. Mihit, B. Hammouti, A. Albourine, S. El Issami, Some amino acids as corrosion inhibitors for copper in nitric acid solution, Mater. Lett., 62 (2008) 3325-3327.
[130] W.A. Badawy, K.M. Ismail, A.M. Fathi, Corrosion control of Cu–Ni alloys in neutral chloride solutions by amino acids, Electrochim. Acta, 51 (2006) 4182-4189.
[131] H. Ashassi-Sorkhabi, M.R. Majidi, K. Seyyedi, Investigation of inhibition effect of some amino acids against steel corrosion in HCl solution, Appl. Surf. Sci., 225 (2004) 176-185.
[132] H. Ashassi-Sorkhabi, Z. Ghasemi, D. Seifzadeh, The inhibition effect of some amino acids towards the corrosion of aluminum in 1M HCl+1M H2SO4 solution, Appl. Surf. Sci., 249 (2005) 408-418.
[133] E. Ferreira, C. Giacomelli, F. Giacomelli, A. Spinelli, Evaluation of the inhibitor effect of L-ascorbic acid on the corrosion of mild steel, Mater. Chem. Phys., 83 (2004) 129-134.
[134] R.S. Gonçalves, L.D. Mello, Electrochemical investigation of ascorbic acid adsorption on low-carbon steel in 0.50 M Na 2 SO 4 solutions, Corros. Sci., 43 (2001) 457-470.
[135] N.H. Helal, W.A. Badawy, Environmentally safe corrosion inhibition of Mg–Al–Zn alloy in chloride free neutral solutions by amino acids, Electrochim. Acta, 56 (2011) 6581-6587.
[136] Y. Wang, L.-Y. Cui, R.-C. Zeng, S.-Q. Li, Y.-H. Zou, E.-H. Han, In Vitro Degradation of Pure Magnesium—The Effects of Glucose and/or Amino Acid, Materials, 10 (2017) 725.
[137] G. Ellison, J.V. Straumfjord, J. Hummel, Buffer capacities of human blood and plasma, Clin. Chem., 4 (1958) 452-461.
[138] C. Wrotnowski, The future of plasma proteins, Genet. Eng. News, 18 (1998).
[139] J.N. Adkins, S.M. Varnum, K.J. Auberry, R.J. Moore, N.H. Angell, R.D. Smith, D.L. Springer, J.G. Pounds, Toward a human blood serum proteome analysis by multidimensional separation coupled with mass spectrometry, Molecular & Cellular Proteomics, 1 (2002) 947-955.
[140] K.A. Majorek, P.J. Porebski, A. Dayal, M.D. Zimmerman, K. Jablonska, A.J. Stewart, M. Chruszcz, W. Minor, Structural and immunologic characterization of bovine, horse, and rabbit serum albumins, Mol. Immunol., 52 (2012) 174-182.

[141] J. Figge, T. Rossing, V. Fencl, The role of serum proteins in acid-base equilibria, The Journal of laboratory and clinical medicine, 117 (1991) 453-467.
[142] R.F. Ritchie, O. Navolotskaia, Serum proteins in clinical medicine, American Association for Clinical Chemistry, 1996.
[143] A. Bratek-Skicki, P. Żeliszewska, J.M. Ruso, Fibrinogen: a journey into biotechnology, Soft matter, 12 (2016) 8639-8653.
[144] Z.E. Allouni, N.R. Gjerdet, M.R. Cimpan, P.J. Høl, The effect of blood protein adsorption on cellular uptake of anatase TiO2 nanoparticles, International journal of nanomedicine, 10 (2015) 687.
[145] P. Roach, D. Farrar, C.C. Perry, Surface tailoring for controlled protein adsorption: effect of topography at the nanometer scale and chemistry, J. Am. Chem. Soc., 128 (2006) 3939-3945.
[146] F. Putnam, The plasma proteins, Elsevier, 2012.
[147] A. Bujacz, Structures of bovine, equine and leporine serum albumin, Acta Crystallographica Section D: Biological Crystallography, 68 (2012) 1278-1289.
[148] J.H. Brown, N. Volkmann, G. Jun, A.H. Henschen-Edman, C. Cohen, The crystal structure of modified bovine fibrinogen, Proceedings of the National Academy of Sciences, 97 (2000) 85-90.
[149] M. Mosesson, Fibrinogen γ chain functions, Journal of Thrombosis and Haemostasis, 1 (2003) 231-238.
[150] C. Liu, Y. Xin, X. Tian, P.K. Chu, Degradation susceptibility of surgical magnesium alloy in artificial biological fluid containing albumin, J. Mater. Res., 22 (2007) 1806-1814.
[151] W.D. Mueller, M. Fernández Lorenzo de Mele, M.L. Nascimento, M. Zeddies, Degradation of magnesium and its alloys: dependence on the composition of the synthetic biological media, J. Biomed. Mater. Res. A, 90 (2009) 487-495.
[152] X. Gu, Y. Zheng, L. Chen, Influence of artificial biological fluid composition on the biocorrosion of potential orthopedic Mg–Ca, AZ31, AZ91 alloys, Biomed. Mater., 4 (2009) 065011.
[153] R. Rettig, S. Virtanen, Time-dependent electrochemical characterization of the corrosion of a magnesium rare-earth alloy in simulated body fluids, J. Biomed. Mater. Res. A, 85 (2008) 167-175.
[154] J. Zhang, N. Kong, Y. Shi, J. Niu, L. Mao, H. Li, M. Xiong, G. Yuan, Influence of proteins and cells on in vitro corrosion of Mg–Nd–Zn–Zr alloy, Corros. Sci., 85 (2014) 477-481.
[155] M. Rabe, D. Verdes, S. Seeger, Understanding protein adsorption phenomena at solid surfaces, Adv. Colloid Interfac, 162 (2011) 87-106.
[156] C.J. Wilson, R.E. Clegg, D.I. Leavesley, M.J. Pearcy, Mediation of biomaterial–cell interactions by adsorbed proteins: a review, Tissue Eng., 11 (2005) 1-18.
[157] S. Shadanbaz, J. Walker, T.B. Woodfield, M.P. Staiger, G.J. Dias, Monetite and brushite coated magnesium: in vivo and in vitro models for degradation analysis, J. Mater. Sci. M., 25 (2014) 173-183.
[158] P. Wan, X. Lin, L. Tan, L. Li, W. Li, K. Yang, Influence of albumin and inorganic ions on electrochemical corrosion behavior of plasma electrolytic oxidation coated magnesium for surgical implants, Appl. Surf. Sci., 282 (2013) 186-194.
[159] N.T. Kirkland, N. Birbilis, J. Walker, T. Woodfield, G.J. Dias, M.P. Staiger, In-vitro dissolution of magnesium–calcium binary alloys: Clarifying the unique role of calcium additions in bioresorbable magnesium implant alloys, Journal of Biomedical Materials Research Part B: Applied Biomaterials, 95 (2010) 91-100.
[160] C.L. Liu, Y.J. Wang, R.C. Zeng, X.M. Zhang, W.J. Huang, P.K. Chu, In vitro corrosion degradation behaviour of Mg–Ca alloy in the presence of albumin, Corros. Sci., 52 (2010) 3341-3347.
[161] Y. Wang, C.S. Lim, C.V. Lim, M.S. Yong, E.K. Teo, L.N. Moh, In vitro degradation behavior of M1A magnesium alloy in protein-containing simulated body fluid, Mat. Sci. Eng. C-Mater. Biol. Appl., 31 (2011) 579-587.
[162] K. Rezwan, L.P. Meier, M. Rezwan, J. Vörös, M. Textor, L.J. Gauckler, Bovine serum albumin adsorption onto colloidal Al2O3 particles: a new model based on zeta potential and UV− Vis measurements, Langmuir., 20 (2004) 10055-10061.
[163] K. Cai, J. Bossert, K.D. Jandt, Does the nanometre scale topography of titanium influence protein adsorption and cell proliferation?, Colloid. Surface. B, 49 (2006) 136-144.
[164] B.E. Givens, Z. Xu, J. Fiegel, V.H. Grassian, Bovine Serum Albumin Adsorption on SiO 2 and TiO 2 Nanoparticle Surfaces at Circumneutral and Acidic pH: A Tale of Two Nano-Bio Surface Interactions, J. Colloid Interf. Sci, 493 (2017) 334-341.
[165] K. Rechendorff, M.B. Hovgaard, M. Foss, V. Zhdanov, F. Besenbacher, Enhancement of protein adsorption induced by surface roughness, Langmuir., 22 (2006) 10885-10888.
[166] M.B. Hovgaard, K. Rechendorff, J. Chevallier, M. Foss, F. Besenbacher, Fibronectin adsorption on tantalum: the influence of nanoroughness, J. Phys. Chem. B, 112 (2008) 8241-8249.

[167] L.-C. Xu, C.A. Siedlecki, Effects of surface wettability and contact time on protein adhesion to biomaterial surfaces, Biomaterials, 28 (2007) 3273-3283.
[168] G. Yin, Z. Liu, J. Zhan, F. Ding, N. Yuan, Impacts of the surface charge property on protein adsorption on hydroxyapatite, Chem. Eng. J., 87 (2002) 181-186.
[169] H. Zeng, K.K. Chittur, W.R. Lacefield, Analysis of bovine serum albumin adsorption on calcium phosphate and titanium surfaces, Biomaterials, 20 (1999) 377-384.
[170] P. Hauschka, Osteocalcin: the vitamin K-dependent Ca2+-binding protein of bone matrix, Pathophysiology of Haemostasis and Thrombosis, 16 (1986) 258-272.
[171] U. Kragh-Hansen, H. Vorum, Quantitative analyses of the interaction between calcium ions and human serum albumin, Clin. Chem., 39 (1993) 202-208.
[172] G. Clark, D. Williams, The effects of proteins on metallic corrosion, J. Biomed. Mater. Res., 16 (1982) 125-134.
[173] D. Höche, C. Blawert, S.V. Lamaka, N. Scharnagl, C. Mendis, M.L. Zheludkevich, The effect of iron re-deposition on the corrosion of impurity-containing magnesium, Phys. Chem. Chem. Phys., 18 (2016) 1279-1291.
[174] S.V. Lamaka, D. Höche, R.P. Petrauskas, C. Blawert, M.L. Zheludkevich, A new concept for corrosion inhibition of magnesium: Suppression of iron re-deposition, Electrochem. Commun., 62 (2016) 5-8.
[175] J. Andrade, V. Hlady, Protein adsorption and materials biocompatibility: a tutorial review and suggested hypotheses, in: Biopolymers/Non-Exclusion HPLC, Springer, 1986, pp. 1-63.
[176] M. Rabe, D. Verdes, J. Zimmermann, S. Seeger, Surface organization and cooperativity during nonspecific protein adsorption events, J. Phys. Chem. B, 112 (2008) 13971-13980.
[177] L. Vroman, A. Adams, G. Fischer, P. Munoz, Interaction of high molecular weight kininogen, factor XII, and fibrinogen in plasma at interfaces, Blood, 55 (1980) 156-159.
[178] R.-Q. Hou, N. Scharnagl, F. Feyerabend, R. Willumeit-Römer, Exploring the effects of organic molecules on the degradation of magnesium under cell culture conditions, Corros. Sci., 132 (2018) 35-45.
[179] PreSens, SensorDishes® & SensorVials, Instuction Manual, in, pp. https://www.presens.de/.
[180] C.E. Blanchet, A. Spilotros, F. Schwemmer, M.A. Graewert, A. Kikhney, C.M. Jeffries, D. Franke, D. Mark, R. Zengerle, F. Cipriani, Versatile sample environments and automation for biological solution X-ray scattering experiments at the P12 beamline (PETRA III, DESY), J. Appl. Crystallogr., 48 (2015) 431-443.
[181] A.M. Venezia, X-ray photoelectron spectroscopy (XPS) for catalysts characterization, Catal. Today, 77 (2003) 359-370.
[182] J.I. Goldstein, D.E. Newbury, J.R. Michael, N.W. Ritchie, J.H.J. Scott, D.C. Joy, Scanning electron microscopy and X-ray microanalysis, Springer, 2017.
[183] J. Ltd, Energy table for EDS analysis, in, pp. https://www.jeol.co.jp/en/.
[184] X. Concepts, User Manual for SpectroSize 300/300 FT, in, pp. http://xtal-concepts.com/index.php/en/Spectrozize-300.html.
[185] M. Instruments, ZETASIZER NANO Series Performance, Simplicity, Versatility, in, pp. https://www.malvernpanalytical.com/en/search?q=Zetasizer+Nano+ZS90.
[186] B. Nano, Correlating Advanced 3D Optical Profiling Surface Measurements to Traceable Standards, in, pp. https://www.bruker.com/products/surface-and-dimensional-analysis/3d-optical-microscopes/products-3d-optical-microscopes.html.
[187] P. Koutsoukos, Z. Amjad, M. Tomson, G. Nancollas, Crystallization of calcium phosphates. A constant composition study, J. Am. Chem. Soc., 102 (1980) 1553-1557.
[188] M. Jönsson, D. Persson, D. Thierry, Corrosion product formation during NaCl induced atmospheric corrosion of magnesium alloy AZ91D, Corros. Sci., 49 (2007) 1540-1558.
[189] Y. Yu, X. Fei, J. Tian, L. Xu, X. Wang, Y. Wang, Self-assembled enzyme–inorganic hybrid nanoflowers and their application to enzyme purification, Colloids and Surfaces B: Biointerfaces, 130 (2015) 299-304.
[190] P.-L. Jiang, R.-Q. Hou, C.-D. Chen, L. Sun, S.-G. Dong, J.-S. Pan, C.-J. Lin, Controllable Degradation of Medical Magnesium by Electrodeposited Composite Films of Mussel Adhesive Protein (Mefp-1) and Chitosan, J. Colloid Interf. Sci, 478 (2016) 246–255.
[191] A. Marucco, I. Fenoglio, F. Turci, B. Fubini, Interaction of fibrinogen and albumin with titanium dioxide nanoparticles of different crystalline phases, in: Journal of Physics: Conference Series, IOP Publishing, 2013, pp. 012014.
[192] E.C. Bingham, R.R. Roepke, The rheology of the blood. II. The effect of fibrinogen on the fluidity of blood plasma, J. Am. Chem. Soc., 64 (1942) 1204-1206.

[193] W. Jastrzębski, M. Sitarz, M. Rokita, K. Bułat, Infrared spectroscopy of different phosphates structures, Spectrochimica Acta Part A: Molecular and Biomolecular Spectroscopy, 79 (2011) 722-727.
[194] A. Shchukarev, M. Ransjö, Z.i. Mladenović, To build or not to build: the interface of bone graft substitute materials in biological media from the view point of the cells, in: Biomaterials Science and Engineering, InTech, 2011.
[195] J.T. Kloprogge, W.N. Martens, L. Nothdurft, L.V. Duong, G.E. Webb, Low temperature synthesis and characterization of nesquehonite, J. Mater. Sci. Lett., 22 (2003) 825-829.
[196] R. Saad, K. Belkacemi, S. Hamoudi, Adsorption of phosphate and nitrate anions on ammonium-functionalized MCM-48: Effects of experimental conditions, J. Colloid Interf. Sci, 311 (2007) 375-381.
[197] H.Y. Shen, Z.J. Wang, A. Zhou, J.L. Chen, M.Q. Hu, X.Y. Dong, Q.H. Xia, Adsorption of phosphate onto amine functionalized nano-sized magnetic polymer adsorbents: mechanism and magnetic effects, RSC Adv., 5 (2015) 22080-22090.
[198] Y. Zhang, X. Xi, S. Xu, J. Zhou, J. Zhou, Q. Xu, H. Shen, Adsorption studies on phosphate by amino-functionalized nano-size composite materials, Acta Chim. Sinica., 70 (2012) 1839-1846.
[199] J.K. Kang, J.H. Kim, S.B. Kim, S.H. Lee, J.W. Choi, C.G. Lee, Ammonium-functionalized mesoporous silica MCM-41 for phosphate removal from aqueous solutions, Desalin. Water Treat., 57 (2016) 10839-10849.
[200] Z.F. Ren, X. Xu, X. Wang, B.Y. Gao, Q.Y. Yue, W. Song, L. Zhang, H.T. Wang, FTIR, Raman, and XPS analysis during phosphate, nitrate and Cr(VI) removal by amine cross-linking biosorbent, J. Colloid Interf. Sci, 468 (2016) 313-323.
[201] M. Tavafoghi, M. Cerruti, The role of amino acids in hydroxyapatite mineralization, J. R. Soc. Interface, 13 (2016) 20160462.
[202] Y. Zong, G. Yuan, X. Zhang, L. Mao, J. Niu, W. Ding, Comparison of biodegradable behaviors of AZ31 and Mg–Nd–Zn–Zr alloys in Hank's physiological solution, Materials Science and Engineering: B, 177 (2012) 395-401.
[203] A. George, A. Veis, Phosphorylated proteins and control over apatite nucleation, crystal growth, and inhibition, Chem. Rev., 108 (2008) 4670-4693.
[204] W.J. Landis, R. Jacquet, Association of calcium and phosphate ions with collagen in the mineralization of vertebrate tissues, Calcified. Tissue Int, 93 (2013) 329-337.
[205] R.E. Cian, A.G. Garzón, D.B. Ancona, L.C. Guerrero, S.R. Drago, Chelating Properties of Peptides from Red Seaweed Pyropia columbina and Its Effect on Iron Bio-Accessibility, Plant Food Hum. Nutr., 71 (2016) 96-101.
[206] C. Orme, A. Noy, A. Wierzbicki, M. McBride, M. Grantham, H. Teng, P. Dove, J. DeYoreo, Formation of chiral morphologies through selective binding of amino acids to calcite surface steps, Nature, 411 (2001) 775-779.
[207] M. Seddigh, A.H. Khoshgoftarmanesh, S. Ghasemi, The effectiveness of seed priming with synthetic zinc-amino acid chelates in comparison with soil-applied ZnSO4 in improving yield and zinc availability of wheat grain, J. Plant Nutr., 39 (2016) 417-427.
[208] K. Pedersen, Binding of calcium to serum albumin III. Influence of ionic strength and ionic medium, Scand. J. Clin. Lab. Inv., 29 (1972) 427-432.
[209] A. Besarab, A. DeGuzman, J.W. Swanson, Effect of albumin and free calcium concentrations on calcium binding in vitro, J. Clin. Pathol., 34 (1981) 1361-1367.
[210] R. Frye, H. Lees, G. Rechnitz, Magnesium-albumin binding measurements using ion-selective membrane electrodes, Clin. Biochem., 7 (1974) 258-270.
[211] Y.C. Guillaume, C. Guinchard, A. Berthelot, Affinity chromatography study of magnesium and calcium binding to human serum albumin: pH and temperature variations, Talanta, 53 (2000) 561-569.
[212] M. Dong, W. Cheng, Z. Li, G.P. Demopoulos, Solubility and stability of nesquehonite ($MgCO_3 \cdot 3H_2O$) in NaCl, KCl, $MgCl_2$, and NH_4Cl solutions, J. Chem. Eng. Data, 53 (2008) 2586-2593.
[213] M. Dong, Z. Li, J. Mi, G.P. Demopoulos, Solubility and stability of nesquehonite ($MgCO_3 \cdot 3H_2O$) in mixed NaCl+ $MgCl_2$, NH_4Cl+ $MgCl_2$, LiCl, and LiCl+ $MgCl_2$ solutions, J. Chem. Eng. Data, 54 (2009) 3002-3007.
[214] P.J. Davies, B. Bubela, The transformation of nesquehonite into hydromagnesite, Chem. Geol., 12 (1973) 289-300.
[215] A.P.A. dos Anjos, A. Sifeddine, C.J. Sanders, S.R. Patchineelam, Synthesis of magnesite at low temperature, Carbonate. Evaporite., 26 (2011) 213-215.

[216] Z. Zhang, Y. Zheng, Y. Ni, Z. Liu, J. Chen, X. Liang, Temperature-and pH-dependent morphology and FT-IR analysis of magnesium carbonate hydrates, J. Phys. Chem. B, 110 (2006) 12969-12973.
[217] J. Canterford, G. Tsambourakis, B. Lambert, Some observations on the properties of dypingite, Mg5 (CO3) 4 (OH) 2· 5H2O, and related minerals, Mineral. Mag., 48 (1984) 437-442.
[218] G. Marguerie, G. Chagniel, M. Suscillon, The binding of calcium to bovine fibrinogen, Biochimica et Biophysica Acta (BBA)-Protein Structure, 490 (1977) 94-103.
[219] D.G. Makey, U.S. Seal, The detection of four molecular forms of human transferrin during the iron binding process, Biochimica et Biophysica Acta (BBA)-Protein Structure, 453 (1976) 250-256.
[220] E. Betgovargez, V. Knudson, M.H. Simonian, Characterization of proteins in the human serum proteome, Journal of biomolecular techniques: JBT, 16 (2005) 306.
[221] A.G. Hovanessian, Z.L. Awdeh, Gel Isoelectric Focusing of Human-Serum Transferrin, The FEBS Journal, 68 (1976) 333-338.
[222] P.K. Yan, B. Wang, Y.J. Gao, Study on synthesis of the high aspect ratios nesquehonite whiskers, in: Adv. Mater. Res., Trans Tech Publ, 2011, pp. 1118-1122.
[223] K.L. Jones, C.R. O'Melia, Protein and humic acid adsorption onto hydrophilic membrane surfaces: effects of pH and ionic strength, J. Membrane. Sci., 165 (2000) 31-46.
[224] S. Demanèche, J.-P. Chapel, L.J. Monrozier, H. Quiquampoix, Dissimilar pH-dependent adsorption features of bovine serum albumin and α-chymotrypsin on mica probed by AFM, Colloid. Surface. B, 70 (2009) 226-231.
[225] T.S. Tsapikouni, Y.F. Missirlis, pH and ionic strength effect on single fibrinogen molecule adsorption on mica studied with AFM, Colloid. Surface. B, 57 (2007) 89-96.
[226] T. Furuike, T. Chaochai, D. Komoto, H. Tamura, Adsorption and Desorption Behaviors of Bovine Serum Albumin on Gelatin/Chitosan Sponge, J. Mater. Sci. Chem. Eng., 5 (2017) 109.
[227] M. Han, A. Sethuraman, R.S. Kane, G. Belfort, Nanometer-scale roughness having little effect on the amount or structure of adsorbed protein, Langmuir., 19 (2003) 9868-9872.
[228] M. Lord, B. Cousins, P. Doherty, J. Whitelock, A. Simmons, R. Williams, B. Milthorpe, The effect of silica nanoparticulate coatings on serum protein adsorption and cellular response, Biomaterials, 27 (2006) 4856-4862.
[229] M.S. Lord, M. Foss, F. Besenbacher, Influence of nanoscale surface topography on protein adsorption and cellular response, Nano Today, 5 (2010) 66-78.
[230] L. Hao, J. Lawrence, The adsorption of human serum albumin (HSA) on CO 2 laser modified magnesia partially stabilised zirconia (MgO-PSZ), Colloid. Surface. B, 34 (2004) 87-94.
[231] C. Yongli, Z. Xiufang, G. Yandao, Z. Nanming, Z. Tingying, S. Xinqi, Conformational changes of fibrinogen adsorption onto hydroxyapatite and titanium oxide nanoparticles, J. Colloid Interf. Sci, 214 (1999) 38-45.
[232] P. Roach, D. Farrar, C.C. Perry, Interpretation of protein adsorption: surface-induced conformational changes, J. Am. Chem. Soc., 127 (2005) 8168-8173.
[233] G.B. Sigal, M. Mrksich, G.M. Whitesides, Effect of surface wettability on the adsorption of proteins and detergents, J. Am. Chem. Soc., 120 (1998) 3464-3473.
[234] A. Loban, R. Kime, H. Powers, Iron-binding antioxidant potential of plasma albumin, Clinical science (London, England: 1979), 93 (1997) 445-451.
[235] A.S. Borges, T.J. Divers, T. Stokol, O.H. Mohammed, Serum iron and plasma fibrinogen concentrations as indicators of systemic inflammatory diseases in horses, J. Vet. Intern. Med., 21 (2007) 489-494.
[236] K. Orino, Functional binding analysis of human fibrinogen as an iron-and heme-binding protein, Biometals, 26 (2013) 789-794.
[237] E.M. Hernández, E.I. Franses, Adsorption and surface tension of fibrinogen at the air/water interface, Colloids and Surfaces A: Physicochemical and Engineering Aspects, 214 (2003) 249-262.
[238] N. Hassan, J. Maldonado-Valderrama, A.P. Gunning, V.J. Morris, J.M. Ruso, Surface characterization and AFM Imaging of mixed fibrinogen− surfactant films, The Journal of Physical Chemistry B, 115 (2011) 6304-6311.
[239] J. Brash, P. Ten Hove, Effect of plasma dilution on adsorption of fibrinogen to solid surfaces, Thromb. Haemostasis., 51 (1984) 326-330.
[240] J. Huang, Y. Yue, C. Zheng, Vroman effect of plasma protein adsorption to biomaterials surfaces, Journal of biomedical engineering, 16 (1999) 371-376.
[241] M. Johnson, Fetal Bovine Serum, Materials and Methods, (2012) https://www.labome.com/method/Fetal-Bovine-Serum.html.

Appendix

1. Figures

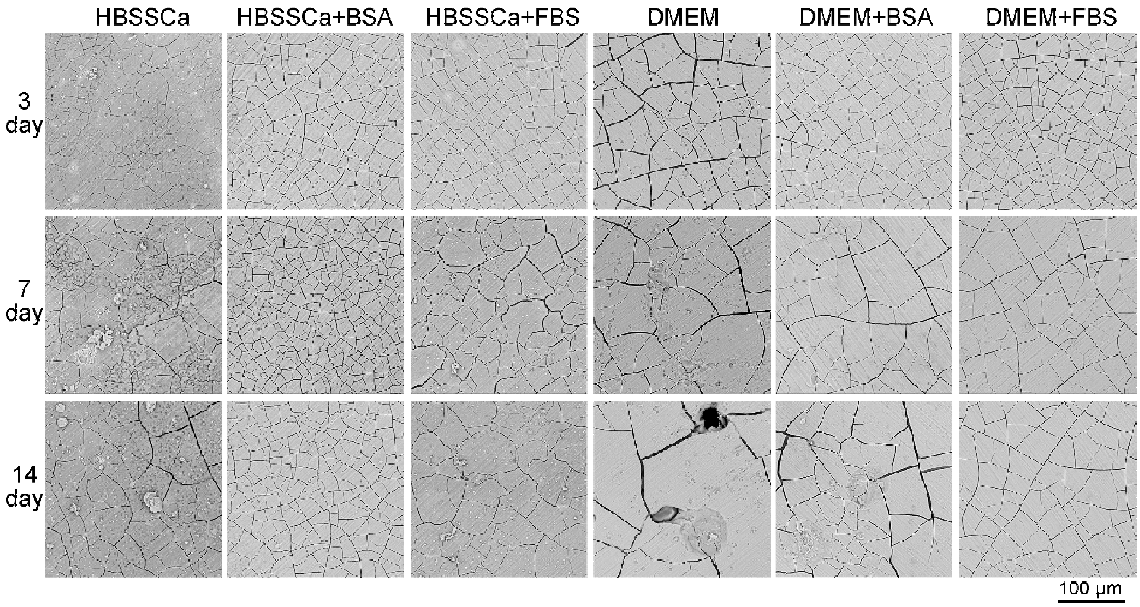

Figure s1: SEM images of pure Mg immersed in HBSSCa and DMEM under static conditions.

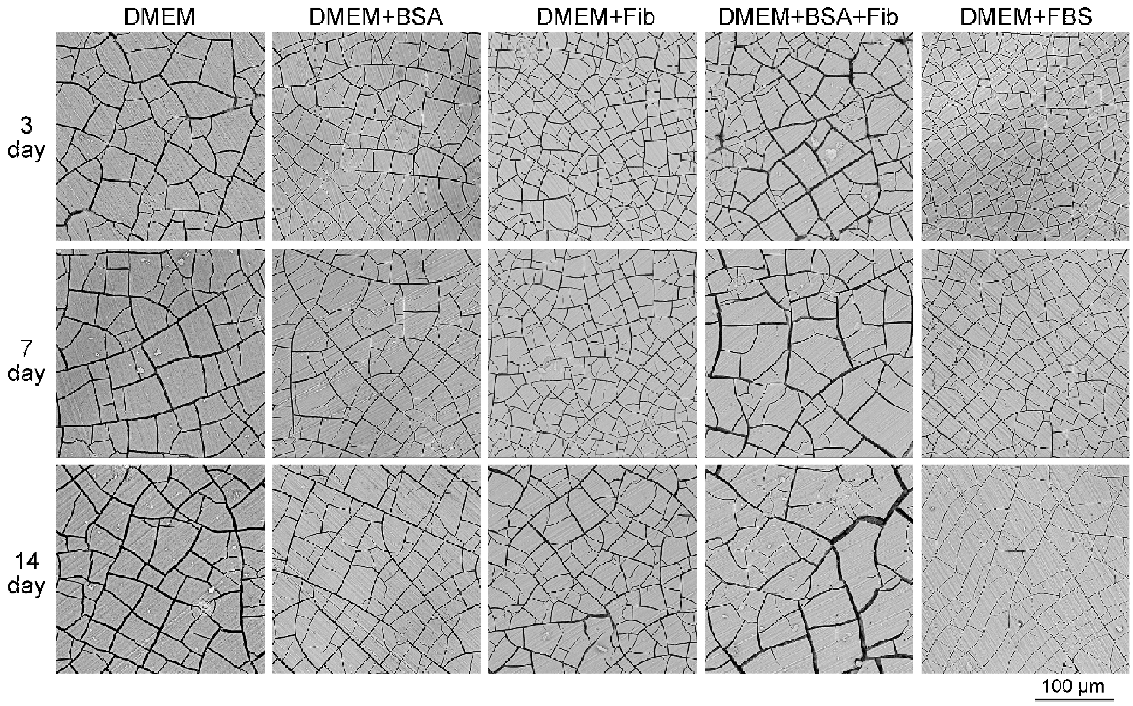

Figure s2: SEM images of pure Mg immersed in DMEM under semi-static conditions.

2. Abbreviations

Ag	Silver
Al	Aluminum
at. %	Atomic percentage
ATP	Adenosinetriphosphate
BCA	Bicinchoninic acid
BSA	Bovine serum albumin
C	Carbon
Ca	Calcium
$CaCl_2$	Calcium chloride
$CaCO_3$	Calcium carbonate
Ce	Cerium
Cl	Chloride
CO_2	Carbon dioxide
CO_3^{2-}	Carbonate ion
Cu	Copper
DAPI	4′,6-diamidino-2-phenylindole
DLS	Dynamic light scattering
DMEM	Dulbecco′s Modified Eagle′s Medium GlutaMAX™
DNA	Deoxyribonucleic acid
DR / CR	Degradation rate / Corrosion rate
Dy	Dysprosium
e.g.	*exempli gratia*
EBSS	Earle's Balanced Salt Solution
EDX	Energy dispersive X-ray spectroscopy
FBS	Fetal bovine serum
Fe	Iron
Fib	Fibrinogen
Gd	Gadolinium
H_2	Hydrogen
H_2O	Water
HBSS	Hank’s balanced salt solution without magnesium and calcium
HBSSCa	Hank’s balanced salt solution with calcium
HCO_3^-	Bicarbonate ion
HEPES	4-(2-hydroxyethyl)-1-piperazineethanesulfonic acid
IR	Infrared microspectroscopy
K_3PO_4	Potassium phosphate
La	Lathanum
L-AA	L-ascorbic acid
L-Ala-L-Gln	L-alanyl-L-glutamine
LDH	Lactate dehydrogenase
L-Gln	L-glutamine
MEM	Minimum Essential Medium

Mg	Magnesium
$Mg(OH)_2$	Magnesium hydroxide
$Mg_3(PO_4)_2$	Magnesium phosphate
$Mg_5(CO_3)_4(OH)_2 \cdot 4H_2O$	Hydromagnesite
$MgCl_2$	Magnesium chloride
$MgCO_3$	Magnesium carbonate
$MgCO_3 \bullet 3H_2O$	Nesquehonite
$MgSO_4$	Magnesium sulphate
Mn	Manganese
MTT	3-(4,5-Dimethylthiazol-2-yl)-2,5-diphenyltetrazoliumbromid
NaCl	Sodium chloride
$NaHCO_3$	Sodium bicarbonate
Nd	Neodymium
Ni	Nickel
O	Oxygen
O_2	Oxygen gas
OH^-	Hydroxide ion
P	Phosphorous
PBS	Phosphate buffered saline
PO_4^{3-}	Phosphate ion
R_a	The arithmetic average roughness
R_g	Gyration radius
RNA	Ribonucleic acid
R_q	The root mean squared roughness
S	Sulphur
SAXS	Small angle X-ray scattering
SBF	Simulated body fluid
SCC	Stress corrosion cracking
SEM	Scanning electron microscopy
Si	Silicon
SO_4^{2-}	Sulphate ion
Sr	Strontium
SSRT	Slow strain rate test
Ti	Titanium
wt.%	Weight percentage
XPS	X-ray photoelectron spectroscopy
XRD	X-ray diffraction
XTT	2,3-Bis-(2-Methoxy-4-Nitro-5-Sulfophenyl)-2H-Tetrazolium-5-Carboxanilide
Y	Yttrium
Zn	Zinc
Zr	Zirconium

Acknowledgements

Firstly, I would like to express my sincere appreciation to my supervisor, Prof. Regine Wilumeit-Römer for giving me the opportunity to study at Helmholtz-Zentrum Geesthacht and for her guidance and continuous support for my PhD study. Her rigorous consideration and highly enthusiasm on the academic research inspire me to think more for my work, this has really benefited me.

I am sincerely grateful to my direct supervisor, Dr. Frank Feyerabend, for his patient, encouraging and careful instruction during my PhD studying and the kind help with my thesis writing. I also wish to thanks Dr. Thomas Ebel and Dr. Bérengère J. C. Luthringer - Feyerabend for their support for my experiments and many useful advises during my studying.

My regards also to Dr. Carsten Blawert, Dr. Sviatlana Lamaka, Dr. Daniel Höche and Dr. Dietmar Letzig for the general discussion about my results and their valuable suggestions and comments. I also appreciate Dr. Nico Scharnagl for the IR and XPS performance and discussions about these results, Dr. Vasyl M. Haramus for the help and discussion for the SAXS result, Dr. Heike Helmholz for AAS measurements and discussions about protein properties, Dr. Marion Frant for the surface charge measuements and Dr. Joachim Koll for the contact angle measurements. Many thanks for their kind helps for my experiments. The technical support and assistance from Monika Luczak, Gert Wiese, Anke Schuster and Gabriele Salamon are acknowledged. Dr. Björn Wiese gave me a great help for the sample preparation. My thanks also goes to Jorge Gonzalez, Banglong Fu, Eshwara P. S. Nidadavolu, Jochen Harmuth, Peng Xu, Yiming Jin, Lei Xu and Marcjanna Gawlik for their warm help in my experiments and life. I would also like to thank all colleagues, lab technicians and friends for providing me with a good working environment and a nice time.

The China Scholarship Council (CSC) and my supervisor, Prof. Regine Wilumeit-Römer, are acknowledged for their financial supports in my PhD studying at HZG.

Finally, but also very importantly, I would like to thanks my parents and my sisters for their selfless and continuous support for my study. I also very thanks my wife, Pingli Jiang, for her help and contribution to my life and work. Without their understanding, support and encouragement, I could not do what I want to do and get through my PhD study.

Lists of publications and conferences

Papers:

1. **R.Q. Hou**, N. Scharnagl, F. Feyerabend, R. Willumeit-Römer, Exploring the effects of organic molecules on the degradation of magnesium under cell culture conditions, Corr. Sci., 132 (2018) 35-45. DOI: *10.1016/j.corsci.2017.12.023*
2. J. Gonzalez, **R.Q. Hou**, E.P. Nidadavolu, R. Willumeit-Römer, F. Feyerabend, Magnesium degradation under physiological conditions–Best practice, Bioactive Materials, 3 (2018) 174-185. DOI: *10.1016/j.bioactmat.2018.01.003*
3. **R.Q. Hou**, R. Willumeit-Römer, V. M. Haramus, M. Frant, J. Koll, F. Feyerabend, Adsorption of proteins on degradable magnesium - which factors are relevant? ACS Appl. Mater. Inter. 10 (2018) 42175-42185. DOI: *10.1021/acsami.8b17507*.
4. **R.Q. Hou**, N. Scharnagl, F. Feyerabend, R. Willumeit-Römer, Different effects of single proteins vs. protein mixtures on magnesium degradation under cell culture conditions, Acta Biomater. In press. DOI: *10.1016/j.actbio.2019.02.013*.
5. **R.Q. Hou,** J. Victoria-Hernandez, F. Feyerabend, R. Willumeit-Römer, B. Luthringer-Feyerabend, S. Yi , D. Letzig, The *in vitro* degradation and mechanical integrity of rolled MgZnCa alloy as implanted plates, **Submiited.**
6. Z.D. Liu*, **R.Q. Hou***, B. Luthringer-Feyerabend, V. M. Haramus, R. Willumeit-Römer, F. Feyerabend, Degradation of magnesium-silver alloys and their mineralization behaviour in the presence of HUCPV cells and primary human osteoblasts, **in preparation.** (*: **equal contribution)**
7. **R.Q. Hou**, F. Feyerabend, R. Willumeit-Römer, Effect of proteins on Mg degradation under static vs. dynamic conditions, **In preparation**.

Conference:

1. **R.Q. Hou**, F. Feyerabend, R. Willumeit-Römer, Exploring the effects of organic components on the degradation of magnesium in vitro under physiological conditions, 4th Euro BioMAT - European Symposium and Exhibition on Biomaterials and Related Areas, May 2017, Weimar, Germany.
2. **R.Q. Hou**, F. Feyerabend, R. Willumeit-Römer, Effects of bovine serum albumin (BSA) and fetal bovine serum (FBS) on Mg degradation under cell culture conditions, The 9th International Symposium on Biodegradable Metals, Sep. 2017, Bertinoro, Italy.
3. **R.Q. Hou**, F. Feyerabend, R. Willumeit-Römer, Adsorption of proteins on degrading magnesium surface, The 10th International Symposium on Biodegradable Metals, Aug. 2018, University of Oxford, United Kingdom.

Curriculum Vitae

PERSONAL DATA:

Name: Ruiqing Hou **Place of birth**: Shaanxi, China

Gender: Male **Nationality**: Chinese

Email: ruiqing.hou@hzg.de; hourq8910@163.com;

EDUCATIONAL BACKGROUND:

2015.09-present PhD study at Institute of Materials Research, Helmholtz-Zentrum Geesthacht and Christian-Albrecht-University (CAU) Kiel, Germany

Thesis: The effect of organic molecules on the magnesium degradation

2011.09-2014.06 Master study in Applied Chemistry (Electrochemistry), College of Chemistry and Chemical Engineering, Xiamen University

Thesis: Study of corrosion behaviour of Mg-Ca alloys in physiological saline solution and its corrosion control by mussel adhesive protein

2007.09-2011.07 Bachelor of Agriculture in Plant Science and Technology, Department of Agriculture, Northwest A&F University

Thesis: Cloning and sequence analysis of γ–gliadin genes from Dasypyrum villosum TA2127

RESEARCH EXPERIENCE:

2015.09-present PhD study in Material Science, Department of material Design and Characterisation, Institute of Materials Research, Helmholtz-Zentrum Geesthacht

2014.07-2015.07 Research assistant at College of Chemistry and Chemical Engineering, Xiamen University

2011.09-2014.06 Graduate Research in Applied Chemistry (Electrochemistry), College of Chemistry and Chemical Engineering, Xiamen University

2007.09-2011.07 Bachelor study in Plant Science and Technology, Department of Agriculture, Northwest A&F University